

---

*Least-Squares Finite Element Methods for Coupled  
Generalized Newtonian Stokes-Darcy Flow*

---

Von der Fakultät für Mathematik und Physik  
der Gottfried Wilhelm Leibniz Universität Hannover  
zur Erlangung des Grades  
Doktor der Naturwissenschaften  
Dr. rer. nat.  
genehmigte Dissertation  
von

Dipl.-Math. Steffen Münzenmaier

geboren am 18.06.1980 in Hamburg

2012

Referent: Prof. Dr. Gerhard Starke, Gottfried Wilhelm Leibniz Universität Hannover  
Korreferent: Prof. Dr. Joachim Escher, Gottfried Wilhelm Leibniz Universität Hannover  
Korreferent: Prof. Dr. Chad Westphal, Wabash College  
Tag der Promotion: 23. Juli 2012

## Abstract

The coupled problem for a generalized Newtonian Stokes flow in one domain and a generalized Newtonian Darcy flow in a porous medium is studied in this work. Both flows are treated as a first order system in a stress-velocity formulation for the Stokes problem and a volumetric flux-hydraulic potential formulation for the Darcy problem. The coupling along an interface is done by using the well known Beavers-Joseph-Saffman interface condition. A least-squares finite element method is used for the numerical approximation of the solution. It is shown that under some assumptions on the viscosity the least-squares functional corresponding to the nonlinear first order system is an efficient and reliable error estimator which allows for adaptive refinement of the triangulations. The adaptive refinement is examined in several numerical examples where boundary singularities are present. Due to the nonlinearity of the problem a Gauß-Newton method is used to iteratively solve the problem. It is shown that the variational problems arising in the Gauß-Newton method are well-posed. The performance of the Gauß-Newton method is analyzed for several examples.

**Keywords:** Least-Squares finite element method, non-Newtonian fluids, Beavers-Joseph-Saffman condition, a-posteriori error estimator, adaptive refinement, Gauß-Newton method



## Kurzzusammenfassung

In dieser Arbeit wird ein gekoppeltes Problem für eine *generalized Newtonian* Stokes Strömung und eine *generalized Newtonian* Darcy Strömung in einem porösen Medium betrachtet. Beide Probleme werden als System erster Ordnung in einer Spannungs-Geschwindigkeitsformulierung für das Stokes Problem und einer volumetrischer Fluss-hydraulisches Potential Formulierung für das Darcy Problem betrachtet. Die Kopplung über das Interface erfolgt über die Beavers-Joseph-Saffman Bedingung. Es wird eine Least-Squares Finite-Elemente-Methode zur numerischen Approximation der Lösung verwendet. In dieser Arbeit wird, unter Annahmen an die Viskosität, gezeigt, dass das zu dem nichtlinearen Problem gehörende Least-Squares-Funktional ein effizienter und verlässlicher Fehlerschätzer ist. Dies erlaubt die Verwendung von Verfahren zur adaptiven Verfeinerung der Triangulierungen. Die adaptive Verfeinerung wird in mehreren Beispielen untersucht bei denen Randsingularitäten auftreten. Wegen der Nichtlinearität des Problems wird ein Gauß-Newton Verfahren zur iterativen Lösung des Problems verwendet. Es wird gezeigt, dass die Variationsprobleme, die bei dem Gauß-Newton Verfahren auftreten, wohlgestellt sind. Das Verhalten des Gauß-Newton Verfahrens wird für mehrere Beispiele untersucht.

**Schlagworte:** Least-Squares Finite-Element-Methode, nichtnewtonsche Fluide, Beavers-Joseph-Saffman Bedingung, a-posteriori Fehlerschätzer, adaptive Verfeinerung, Gauß-Newton Verfahren



# Contents

<b>1</b>	<b>Introduction</b>	<b>9</b>
<b>2</b>	<b>Basics of LSFEM</b>	<b>11</b>
2.1	Least-Squares Finite Element Methods . . . . .	11
2.2	The Hilbert Spaces $H^{div}(\Omega)$ and $H^1(\Omega)$ . . . . .	14
2.2.1	Important Inequalities . . . . .	15
2.3	FE-Spaces . . . . .	16
2.3.1	Approximations of $H^1(\Omega)$ . . . . .	16
2.3.2	Approximations of $H^{div}(\Omega)$ . . . . .	17
<b>3</b>	<b>Least-Squares Formulation of the Separate Problems</b>	<b>19</b>
3.1	Stokes Flow . . . . .	19
3.1.1	The Least-Squares Functional as an Error Estimator . . . . .	22
3.1.2	The Linearized Problem . . . . .	33
3.1.3	Numerical Examples . . . . .	37
3.2	Darcy Flow . . . . .	59
3.2.1	The Least-Squares Functional as an Error Estimator . . . . .	60
3.2.2	The Linearized Problem . . . . .	64
3.2.3	Numerical Examples . . . . .	65
<b>4</b>	<b>The Coupled Problem</b>	<b>77</b>
4.1	The Least-Squares Functional . . . . .	78
4.1.1	The Least-Squares Functional as an Error Estimator . . . . .	79
4.1.2	The Linearized Problem . . . . .	85
4.2	Numerical Examples . . . . .	87
4.2.1	Example I . . . . .	89
4.2.2	Example II . . . . .	107
4.3	Performance of the Gauß-Newton Method . . . . .	120
<b>5</b>	<b>Outlook/Conclusion</b>	<b>129</b>
5.1	Outlook . . . . .	129
5.1.1	Free Boundary Problems . . . . .	129
5.1.2	Viscosity Models . . . . .	129
5.1.3	Conservation of Mass . . . . .	130
5.1.4	Convergence of Gauss-Newton Methods . . . . .	130
5.2	Conclusion . . . . .	130
	<b>Bibliography</b>	<b>131</b>





# Chapter 1

## Introduction

This work is about the numerical analysis of a fluid flow coupled with a porous media flow. The mathematical formulation of these problems is given by a Stokes formulation for the fluid flow and a Darcy formulation for the flow through the porous medium coupled along an interface. The interface is assumed to be non-moving.

There are several applications for coupled Stokes/Darcy flows. Considering Newtonian flows these models can be used to simulate groundwater flow in karst aquifers [CGH<sup>+</sup>10] or the interaction between surface and groundwater flows [LSY02]. The coupling of generalized Newtonian Stokes/Darcy flows arises in industrial filtration processes [EJS09, HWNW06] where the lifespan of the filters is determined by the hydrostatic pressure gradient. Further examples include the simulation of blood flow through arteries and the transport of plasma through the artery walls [SWH<sup>+</sup>06, CBBH08]. Though the flow is often approximated as a Newtonian fluid blood exhibits a non-Newtonian behavior which is studied in [CB05, MK10].

The coupling along the interface is done by assuming continuity of flux and balance of forces. Another component of the coupling is given by the Beavers-Joseph-Saffman condition, which describes the proportionality of tangential velocity and shear rate of the Stokes flow. This condition assures the well-posedness of the coupled problem and is a more realistic approach for interface conditions than a vanishing tangential component of the velocity [DQ09]. The Beavers-Joseph condition was formulated in 1967 by Beavers/Joseph [BJ67]. In 1971 Saffman [Saf71] examined this interface condition and discovered that the seepage velocity can be neglected. The Beavers-Joseph-Saffman condition was mathematically justified in [JM00].

For the numerical analysis a least-squares mixed finite element method is used. A comprehensive description of these methods can be found in [BG09]. For the coupled Stokes/Darcy problem all variables of interest are approximated which allows a straightforward treatment of the coupling conditions. Least-squares mixed finite element methods have several advantages compared to standard mixed finite element methods. A compatibility condition as the inf-sup condition for saddle point problems is not necessary and the linear equation systems of the discrete problem is typically positive definite for well-posed problems. Moreover we show in this work that the least-squares functional is an efficient and reliable error estimator. This allows for effective adaptive refinement.

Applications of least-squares finite element methods are widespread and include (Navier-)Stokes flow [CTVW10, BLO12, CW09], linear elasticity [CS03], nonlinear elasto-plasticity [Sta07] and porous media flow [BMMS05].

Mixed finite element methods for the coupled Stokes / Darcy equations by using the Beavers-Joseph-Saffman condition have been analyzed in numerous works. Under the assumption of constant viscosity mixed finite element methods involving Lagrange multipliers have been used in early works [DQM02, LSY02]. The use of discontinuous Galerkin methods can be found in [Riv05, RY05].

The coupling of Navier-Stokes and Darcy equations can be found in [DQ09]. A least-squares finite element method for the coupled Stokes / Darcy problem was analyzed in [MS11] where it was shown that the least-squares functional is an efficient and reliable error estimator. An adaptive refinement strategy that achieved optimal convergence rates was used.

The present work deals with non-Newtonian fluids. We restrict ourselves to the case of generalized Newtonian fluids where the viscosity depends on the shear rate / absolute value of the volumetric flux. Many works deal with these kinds of fluids for Stokes flows as for example [BS08a, BL93, GMS11, BS94]. The models for the coupled Stokes / Darcy problem and a corresponding mixed finite element method can be found in [EJS09]. We draw on the used models in this work and analogously to [MS11] derive a least-squares finite element method to solve the nonlinear problem. The treatment of the nonlinearity is similar to [Sta07]. We take advantage of the least-squares functional being an error estimator to make use of adaptive refinement strategies.

The first part of this work introduces the least-squares finite element method and gives a short overview of the necessary inequalities to prove the main results. A very short introduction to the used finite element spaces is given at the end of the chapter.

In the second part we take a closer look at the separate problems. The main results of the least-squares functional being an efficient and reliable error estimator for the Stokes and Darcy problems is proven under assumptions on the viscosity. Furthermore we use a Gauß-Newton method to solve the nonlinear problem. This method has been used with success in several works dealing with least-squares finite element methods. Examples include the shallow water equations [Sta05], variably saturated subsurface flows [Sta00], shallow water equations coupled with ground water flows [Mün08] and elasto-plasticity [Sta07]. Furthermore we prove that the linear problems are well posed independent of the starting point. We present some numerical examples to illustrate the behavior of an adaptive refinement strategy compared to uniform refinements.

The third part of this work deals with the coupled problem. The main result of the least-squares functional being an efficient and reliable error estimator is proven. We show again that the linear problems arising in the Gauß-Newton method are well posed. At the end of the chapter several numerical examples are presented and the performance of the Gauß-Newton method is examined.

The last part consists of a short outlook considering several open questions that arose in the course of this work and have to be addressed in further research. A short conclusion finishes this thesis.

## Chapter 2

# Basics of LSFEM

### 2.1 Least-Squares Finite Element Methods

A comprehensive introduction to least-squares finite element methods can be found in [BG09]. This section only gives a short introduction of these methods.

Let the following nonlinear partial differential equation be given:

$$\begin{aligned} \mathcal{R}(\mathbf{u}) &= \mathbf{f} && \text{in } \Omega \\ \mathbf{u} &= \mathbf{g}_D && \text{auf } \partial\Omega \end{aligned} \tag{2.1}$$

In this case  $\mathcal{R}$  is an operator from the Hilbert space  $\mathcal{V}$  to a Hilbert space  $\mathcal{W}$ . The space  $\mathcal{W}$  is commonly a tensor product of  $L^2(\Omega)$ -spaces. Considering first order systems typical representatives for  $\mathcal{V}$  are given by products of the spaces  $H^1(\Omega)$  and  $H^{div}(\Omega)$ .

Let  $\mathbf{u}_D \in \mathcal{V}$  satisfy  $\mathbf{u}_D|_{\partial\Omega} = \mathbf{g}_D$  in the sense of traces. For simplicity we introduce  $\hat{\mathbf{u}}$ :

$$\hat{\mathbf{u}} := \mathbf{u} - \mathbf{u}_D$$

with  $\hat{\mathbf{u}}|_{\partial\Omega} = 0$ . Therefore we introduce the space:

$$\mathcal{V}_0 = \{ \mathbf{v} \in \mathcal{V} \mid \mathbf{v}|_{\partial\Omega} = 0 \}$$

**Remark:** The expression  $\cdot|_{\partial\Omega} = 0$  has to be understood in the sense of traces and is not meant to be pointwise satisfied.

The least-squares functional is defined by

$$\mathcal{F}(\mathbf{u}) = \|\mathcal{R}(\mathbf{u}) - \mathbf{f}\|_{\mathcal{W}}^2 \tag{2.2}$$

The least-squares finite element method is based on minimizing the  $\mathcal{W}$  norm of the residual:

Find  $\hat{\mathbf{u}} \in \mathcal{V}_0$  such that

$$\mathcal{F}(\mathbf{u}_D + \hat{\mathbf{u}}) \leq \mathcal{F}(\mathbf{u}_D + \hat{\mathbf{v}}) \quad \forall \hat{\mathbf{v}} \in \mathcal{V}_0 \tag{2.3}$$

holds.

The first variation of the minimization problem is given by:

$$\begin{aligned} \frac{\partial \mathcal{F}(\mathbf{u}_D + \hat{\mathbf{u}} + \theta \hat{\mathbf{v}})}{\partial \theta} \Big|_{\theta=0} &= \frac{\partial}{\partial \theta} \|\mathcal{R}(\mathbf{u}_D + \hat{\mathbf{u}} + \theta \hat{\mathbf{v}}) - \mathbf{f}\|_{\mathcal{W}}^2 \Big|_{\theta=0} \\ &= \frac{\partial}{\partial \theta} (\mathcal{R}(\mathbf{u}_D + \hat{\mathbf{u}} + \theta \hat{\mathbf{v}}) - \mathbf{f}, \mathcal{R}(\mathbf{u}_D + \hat{\mathbf{u}} + \theta \hat{\mathbf{v}}) - \mathbf{f})_{\mathcal{W}} \Big|_{\theta=0} \\ &= 2(\mathcal{R}(\mathbf{u}_D + \hat{\mathbf{u}}), \mathcal{J}(\mathbf{u}_D + \hat{\mathbf{u}})[\hat{\mathbf{v}}])_{\mathcal{W}} - 2(\mathbf{f}, \mathcal{J}(\mathbf{u}_D + \hat{\mathbf{u}})[\hat{\mathbf{v}}])_{\mathcal{W}} \end{aligned} \tag{2.4}$$

with  $\mathcal{J}(\mathbf{u})[\mathbf{v}]$  denoting the Gateaux derivative of  $\mathcal{R}(\mathbf{u})$  in  $\mathbf{u}$  in direction of  $\mathbf{v}$ . For this section we assume  $\mathcal{R}$  to be differentiable. If a minimum  $\mathbf{u}$  of (2.3) exists we therefore have the following necessary condition:

$$(\mathcal{R}(\mathbf{u}_D + \hat{\mathbf{u}}), \mathcal{J}(\mathbf{u}_D + \hat{\mathbf{u}})[\hat{\mathbf{v}}])_{\mathcal{W}} = (\mathbf{f}, \mathcal{J}(\mathbf{u}_D + \hat{\mathbf{u}})[\hat{\mathbf{v}}])_{\mathcal{W}} \quad \forall \hat{\mathbf{v}} \in \mathcal{V}_0 \quad (2.5)$$

Instead of solving the minimization problem (2.3) we can solve the following:

$$\text{Find } \hat{\mathbf{u}} \in \mathcal{V}_0 \text{ such that (2.5) holds.} \quad (2.6)$$

Before we introduce a method for approximately solving the nonlinear PDE we shortly present the finite element method.

Let a triangulation  $\mathcal{T}_h$  of the domain  $\Omega$  be given. Here  $h$  denotes the maximal diameter of the triangles in  $\mathcal{T}_h$ . Using a variational formulation, like in (2.5), the problem is solved in finite dimensional subspaces. Let  $\mathcal{V}_h \subset \mathcal{V}_0$  be such a finite dimensional subspace. An example would be the space of functions that are continuous in  $\Omega$  and linear on every triangle  $T_i \in \mathcal{T}_h$ . The discrete problem is then given by: Find  $\hat{\mathbf{u}}_h \in \mathcal{V}_h$  such that

$$(\mathcal{R}(\mathbf{u}_D + \hat{\mathbf{u}}_h), \mathcal{J}(\mathbf{u}_D + \hat{\mathbf{u}}_h)[\hat{\mathbf{v}}_h])_{\mathcal{W}} = (\mathbf{f}, \mathcal{J}(\mathbf{u}_D + \hat{\mathbf{u}}_h)[\hat{\mathbf{v}}_h])_{\mathcal{W}} \quad \forall \hat{\mathbf{v}}_h \in \mathcal{V}_h \quad (2.7)$$

holds.

This is a nonlinear equation system with  $\dim(\mathcal{V}_h)$  unknowns and equations. One can use standard procedures such as Newton's method to solve this equation system.

**Remark:** It has to be noted that one can solve the minimization problem (2.3) as well. Restricted to finite dimensional subspaces  $\mathcal{V}_h$  one has to solve a minimization problem in  $\mathbb{R}^n$  with a nonlinear objective function, which can be solved with standard procedures:

Find  $\hat{\mathbf{u}}_h \in \mathcal{V}_h$  such that

$$\mathcal{F}(\mathbf{u}_D + \hat{\mathbf{u}}_h) \leq \mathcal{F}(\mathbf{u}_D + \hat{\mathbf{v}}_h) \quad \forall \hat{\mathbf{v}}_h \in \mathcal{V}_h \quad (2.8)$$

holds.

Problem (2.3) is a minimization problem in least-squares form. A standard procedure for solving these kinds of problems is the Gauß-Newton method (see [NW00] for details). For a least-squares FEM it can be found in [Sta00, Sta05] for example.

Let  $\mathbf{u}^{(k)}$  be an approximation of  $\mathbf{u}$  with  $\mathbf{u}^{(k)}|_{\partial\Omega} = \mathbf{g}_D$ . Let the next approximation  $\mathbf{u}^{(k+1)}$  be defined by

$$\mathbf{u}^{(k+1)} = \mathbf{u}^{(k)} + \delta\mathbf{u}$$

We use a linear approximation of  $\mathcal{R}$  around  $\mathbf{u}^{(k)}$

$$\mathcal{R}(\mathbf{u}^{(k+1)}) \approx \mathcal{R}(\mathbf{u}^{(k)}) + \mathcal{J}(\mathbf{u}^{(k)})[\delta\mathbf{u}]$$

The quadratic LSF has the form:

$$\mathcal{F}_{quad}(\delta\mathbf{u}) = \|\mathcal{R}(\mathbf{u}^{(k)}) + \mathcal{J}(\mathbf{u}^{(k)})[\delta\mathbf{u}] - \mathbf{f}\|_{\mathcal{W}}^2 \quad (2.9)$$

This results in the minimization problem: Find  $\delta\mathbf{u} \in \mathcal{V}_0$  such that

$$\mathcal{F}_{quad}(\mathbf{u}^{(k)} + \delta\mathbf{u}) \leq \mathcal{F}_{quad}(\mathbf{u}^{(k)} + \delta\mathbf{v}) \quad \forall \delta\mathbf{v} \in \mathcal{V}_0 \quad (2.10)$$

holds. As before we can set the first variation to 0 and get the necessary condition:

$$(\mathcal{J}(\mathbf{u}^{(k)})[\delta\mathbf{u}], \mathcal{J}(\mathbf{u}^{(k)})[\delta\mathbf{v}])_{\mathcal{W}} = (\mathbf{f} - \mathcal{R}(\mathbf{u}^{(k)}), \mathcal{J}(\mathbf{u}^{(k)})[\delta\mathbf{v}])_{\mathcal{W}} \quad \forall \delta\mathbf{v} \in \mathcal{V}_0 \quad (2.11)$$

Instead of solving the minimization problem (2.3) one can solve the variational problem:

$$\text{Find } \mathbf{u} \in \mathcal{V} \text{ such that (2.11) holds.} \quad (2.12)$$

Setting

$$\begin{aligned} a(\delta \mathbf{u}, \delta \mathbf{v}) &= (\mathcal{J}(\mathbf{u}^{(k)})[\delta \mathbf{u}], \mathcal{J}(\mathbf{u}^{(k)})[\delta \mathbf{v}])_{\mathcal{W}} \\ F(\delta \mathbf{v}) &= (\mathbf{f} - \mathcal{R}(\mathbf{u}^{(k)}), \mathcal{J}(\mathbf{u}^{(k)})[\delta \mathbf{v}])_{\mathcal{W}} \end{aligned}$$

we can write (2.11) in the usual form: Find  $\delta \mathbf{u} \in \mathcal{V}_0$  such that

$$a(\delta \mathbf{u}, \delta \mathbf{v}) = F(\delta \mathbf{v}) \quad \forall \delta \mathbf{v} \in \mathcal{V} \quad (2.13)$$

holds.

Here  $a(\cdot, \cdot)$  is a bilinear form and  $F(\cdot)$  is a linear functional. The reduction to finite dimensional problems is analog to the non-quadratic functional.

A major advantage of the LSFEM is the usage of the LSF as an efficient and reliable a-posteriori error estimator. That means that for a solution  $\mathbf{u} = \mathbf{u}_D + \hat{\mathbf{u}}$  of (2.1) and with  $\mathbf{v} = \mathbf{u}_D + \hat{\mathbf{v}}$  the following holds:

$$C_E \|\mathbf{u} - \mathbf{v}\|_{\mathcal{V}}^2 \leq \mathcal{F}(\mathbf{v}) \leq C_S \|\mathbf{u} - \mathbf{v}\|_{\mathcal{V}}^2 \quad (2.14)$$

for all  $\hat{\mathbf{v}} \in \mathcal{V}_0$ . Inequality (2.14) has to be proven for the specific problem.

The consequences of (2.14) are important for the numerical part. The estimate provides a measure for the error and therefore a local a-posteriori error estimator and allows the usage of effective adaptive algorithms.

Another advantage in the case of FEM is the use of an a-priori error estimator. For the approximate solution of the FEM for (2.8) it holds:

$$\mathcal{F}(\mathbf{u}_h) \leq \mathcal{F}(\mathcal{I}_h(\mathbf{u})) \leq C_S \|\mathbf{u} - \mathcal{I}_h(\mathbf{u})\|_{\mathcal{V}}^2$$

for an arbitrary operator  $\mathcal{I}_h(\mathbf{u}) : \mathcal{V} \rightarrow \mathcal{V}_h$ .

If we assume that under the assumption  $\mathbf{u} \in \mathcal{Y}$  such an operator  $\mathcal{I}_h(\cdot)$  exists with

$$\|\mathbf{u} - \mathcal{I}_h(\mathbf{u})\|_{\mathcal{V}} \leq C_{\mathcal{I}} h^\alpha \|\mathbf{u}\|_{\mathcal{Y}}$$

for  $\alpha > 0$ . Then it follows by (2.14):

$$\|\mathbf{u} - \mathbf{u}_h\|_{\mathcal{V}} \leq \sqrt{\frac{C_S}{C_E}} C_{\mathcal{I}} h^\alpha \|\mathbf{u}\|_{\mathcal{Y}}$$

That means that the FEM converges (with a convergence rate  $\alpha$ ) to the solution  $\mathbf{u}$ . Such interpolation operators are known for standard FE-spaces and are stated in the next section.

For the last part of this section we take a closer look at the special case of linear PDEs. We set

$$\mathcal{R}(\mathbf{u}) = \mathcal{L}\mathbf{u}$$

with a linear operator  $\mathcal{L}$ . The necessary condition 2.5 is then given by:

$$a(\hat{\mathbf{u}}, \hat{\mathbf{v}}) := (\mathcal{L}(\hat{\mathbf{u}}), \mathcal{L}(\hat{\mathbf{v}}))_{\mathcal{W}} = (\mathbf{f} - \mathcal{L}(\mathbf{u}_D), \mathcal{L}(\hat{\mathbf{v}}))_{\mathcal{W}} =: F(\hat{\mathbf{v}}) \quad \forall \hat{\mathbf{v}} \in \mathcal{V}_0$$

Here estimate (2.14) has some additional consequences. It holds:

$$C_E \|\mathbf{w}\|_{\mathcal{V}}^2 = C_E \|\mathbf{u} - \mathbf{v}\|_{\mathcal{V}}^2 \leq \|\mathbf{f} - \mathcal{L}\mathbf{v}\|_{\mathcal{W}}^2 \leq C_S \|\mathbf{u} - \mathbf{v}\|_{\mathcal{V}}^2 = C_S \|\mathbf{w}\|_{\mathcal{V}}^2 \\ = \|\mathcal{L}\mathbf{w}\|_{\mathcal{W}}^2$$

with  $\mathbf{w} := \mathbf{u} - \mathbf{v} \in \mathcal{V}_0$ .

That means

$$C_E \|\mathbf{w}\|_{\mathcal{V}}^2 \leq a(\mathbf{w}, \mathbf{w}) \leq C_S \|\mathbf{w}\|_{\mathcal{V}}^2 \quad \forall \mathbf{w} \in \mathcal{V}_0$$

and (if  $\mathbf{f} \in \mathcal{W}$ )

$$\begin{aligned} F(\mathbf{w}) &= (\mathbf{f} - \mathcal{L}(\mathbf{u}_D), \mathcal{L}(\mathbf{w}))_{\mathcal{W}} \\ &\leq \|\mathbf{f} - \mathcal{L}(\mathbf{u}_D)\|_{\mathcal{W}} \|\mathcal{L}(\mathbf{w})\|_{\mathcal{W}} \\ &\leq C_1 \|\mathcal{L}(\mathbf{w})\|_{\mathcal{W}} \\ &\leq C_1 C_S \|\mathbf{w}\|_{\mathcal{V}} \end{aligned}$$

The consequence of this is that the prerequisites of the lemma of Lax-Milgram are satisfied. Therefore the variational problem (2.6) (and the minimization problem (2.3)) has a unique solution if  $\mathcal{R}(\mathbf{u}) = \mathcal{L}(\mathbf{u})$ .

## 2.2 The Hilbert Spaces $H^{div}(\Omega)$ and $H^1(\Omega)$

In this section we take a closer look at the special case

- $\mathcal{V} = H^{div}(\Omega)$  or  $H^1(\Omega)$
- $\mathcal{W} = L^2(\Omega)$

These are the used solution spaces in chapter 3. The coupled problem is different and is discussed in chapter 4. Nonetheless the results of this section are used there as well.

Before stating important inequalities we need a formal definition for the solution spaces. The following spaces

- $H^{div}(\Omega) = \{\mathbf{v} \in (L^2(\Omega))^d \mid \operatorname{div} \mathbf{v} \in L^2(\Omega)\}$
- $H^1(\Omega) = \{p \in L^2(\Omega) \mid \nabla p \in (L^2(\Omega))^d\}$

are Hilbert spaces with the inner products:

$$\begin{aligned} (\mathbf{v}, \mathbf{u})_{div} &= (\mathbf{v}, \mathbf{u})_{0,\Omega} + (\operatorname{div} \mathbf{v}, \operatorname{div} \mathbf{u})_{0,\Omega} \\ (p, q)_{1,\Omega} &= (p, q)_{0,\Omega} + (\nabla p, \nabla q)_{0,\Omega} \end{aligned}$$

Here  $(\cdot, \cdot)_{0,\Omega}$  denotes the standard  $L^2(\Omega)$  inner product. Here and in the further course we drop the subscript if the  $L^2(\Omega)$  inner product is used. The induced norms are given by

$$\begin{aligned} \|p\|_{1,\Omega}^2 &= \|p\|_{0,\Omega}^2 + \|\nabla p\|_{0,\Omega}^2 \\ \|\mathbf{u}\|_{div,\Omega}^2 &= \|\mathbf{u}\|_{0,\Omega}^2 + \|\operatorname{div} \mathbf{u}\|_{0,\Omega}^2 \end{aligned}$$

Analog to chapter 2.1 we make use of the following spaces:

$$\begin{aligned} H_{\Gamma_N}^{div}(\Omega) &= \operatorname{closure}_{\|\cdot\|_{div}} \{\mathbf{v} \in H^{div}(\Omega) \cap (C^\infty(\Omega))^d \mid \mathbf{v} \cdot \mathbf{n} = 0 \text{ on } \Gamma_N\} \\ H_{\Gamma_D}^{div}(\Omega) &= \operatorname{closure}_{\|\cdot\|_{1}} \{p \in H^1(\Omega) \cap C^\infty(\Omega) \mid p = 0 \text{ on } \Gamma_D\} \end{aligned}$$

**Remark:**  $H^{div}(\Omega)$  and  $H^1(\Omega)$  can be defined in a similar way.

### 2.2.1 Important Inequalities

First we recapitulate the Poincare-Friedrichs inequality (see [EG04]):

**Theorem 2.1** [Poincare-Friedrichs inequality]

Let  $\Omega \subset \mathbb{R}^d$  be a bounded domain with Lipschitz boundary and let  $f$  be a linear form on  $H^1(\Omega)$  whose restriction on constant functions is not zero. Then for all  $p \in H^1(\Omega)$  there exists a constant  $C_D = C_D(\Omega) > 0$  with

$$\|p\|_{1,\Omega}^2 \leq C_D(|f(p)|^2 + \|\nabla p\|_{0,\Omega}^2) \quad (2.15)$$

**proof:** See [EG04, Lemma B.63] combined with [EG04, Theorem B.37].

For our coupled problem of chapter 4 we use  $f(p) = \int_{\Gamma} p ds$  (see [EG04, Example B.64] with  $\Gamma \subset \partial\Omega$  with positive measure and therefore get the following inequality

$$\|p\|_{1,\Omega}^2 \leq C_D \left( \left( \int_{\Gamma} p ds \right)^2 + \|\nabla p\|_{0,\Omega}^2 \right) \quad (2.16)$$

This inequality includes the well known variants as well (as found in [Mat08] for example):

- $\|p\|_{1,\Omega}^2 \leq C_D \|\nabla p\|_{0,\Omega}^2$  for all  $p \in H_{\Gamma_D}^1(\Omega)$  with  $\lambda_{d-1}(\Gamma_D) > 0$
- $\|p\|_{1,\Omega}^2 \leq C_D \|\nabla p\|_{0,\Omega}^2$  for all  $p \in H^1(\Omega)$  with  $\int_{\Omega} p dx = 0$

$\lambda_{d-1}$  denotes the  $d-1$  dimensional Lebesgue measure.

The next theorem is the well known second inequality of Korn:

**Theorem 2.2** [Korn's second inequality]

Let  $\Omega$  be an open and bounded subset of  $\mathbb{R}^d$  with Lipschitz boundary. Furthermore let  $\lambda_d(\Gamma_0) > 0$  with  $\Gamma_0 \subset \partial\Omega$ . Then there exists a  $C_K = C_K(\Omega, \Gamma_0) > 0$  with

$$\int_{\Omega} \varepsilon(\mathbf{v}) : \varepsilon(\mathbf{v}) dx \geq C_K \|\mathbf{v}\|_1^2 \quad \forall \mathbf{v} \in H_{\Gamma_0}^1(\Omega)^d$$

**proof:** See [Bra92] for the case of  $d=3$  or [KO87] for the general case  $d \leq 3$ .

The next lemma is needed for the deviatoric formulation of the Stokes flow. It can be found in [MS11] (for the three dimensional case in [CTVW10]) and in the case of linear elasticity for compressible materials in [CS03]. This lemma goes back to [ADG84].

**Lemma 2.3** Let  $\Omega$  be an open and bounded subset of  $\mathbb{R}^d$  with Lipschitz boundary. There exists a constant  $C_S$  such that

$$\|tr \boldsymbol{\tau}\|_{0,\Omega_S}^2 \leq C_S (\|dev \boldsymbol{\tau}\|_{0,\Omega_S}^2 + \|div \boldsymbol{\tau}\|_{0,\Omega_S}^2)$$

holds for all  $\boldsymbol{\tau} \in (H^{div}(\Omega_S))^d$  with  $\int_{\Omega_S} tr \boldsymbol{\tau} dx = 0$ .

Next we introduce the well known trace theorems that are necessary for the analysis in chapter 3/4.

The following theorem can be found in [Nec12, chapter 2, Theorem 5.5].

**Theorem 2.4** Let  $\Omega$  be a bounded open subset of  $\mathbb{R}^d$  with a Lipschitz-Continuous boundary  $\partial\Omega$ . Let  $u \in H^1(\Omega)$  then the following inequality holds:

$$\|\mathbf{u}\|_{\frac{1}{2},\partial\Omega} \leq C_T \|\mathbf{u}\|_{1,\Omega}$$

**proof:** This is special case of Theorem 5.5 in [Nec12].

The next theorem is a consequence of [GR86, chapter 2: Theorem 2.5].

**Theorem 2.5** *Let  $\Omega$  be a bounded open subset of  $\mathbb{R}^d$  with a Lipschitz-Continuous boundary  $\partial\Omega$ . Let  $u \in H^{div}(\Omega)$  then the following inequality holds:*

$$\|\mathbf{u}\|_{-\frac{1}{2},\partial\Omega} \leq C_T \|\mathbf{u}\|_{div,\Omega}$$

**proof:** see [GR86, chapter 2: Theorem 2.5].

## 2.3 FE-Spaces

In this chapter we shortly introduce the finite element spaces we use in the numerical examples. These are given by

- continuous piecewise polynomials of degree  $k$
- Raviart-Thomas spaces of degree  $k$

For the definition of triangulations / shape-regular triangulations we refer to books as [BF91, BS08b, EG04]. The following parts can be found in [BF91].

### 2.3.1 Approximations of $H^1(\Omega)$

We use piecewise polynomials of degree  $k$  as approximations to the solutions in  $H^1(\Omega)$ . This space is given by

$\mathcal{P}_k(K)$  : the space of polynomials of degree  $\leq k$  on triangle  $K$

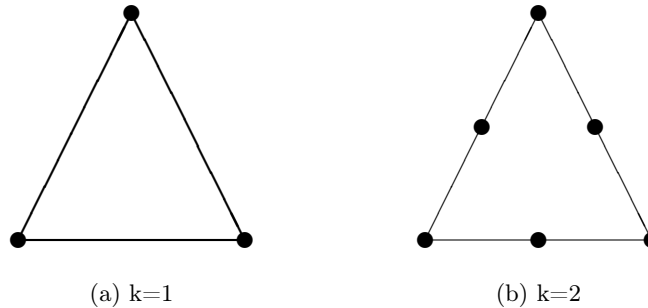


Figure 2.1:  $\mathcal{P}_k(K)$ : Degrees of freedom

The dimension of  $\mathcal{P}_k(K)$  is  $\frac{1}{2}(k+1)(k+2)$  for  $d=2$ . The degrees of freedom are given by the value of the function  $p$  at given interpolation points. For the cases  $k=1, 2$  these are depicted in figure 2.1.

**Remark:** For the general cases  $k \geq 3$  we refer to books as [BF91, Bra92, KA00] for the definition of finite elements and the right choice of the degrees of freedom.



For a given triangulation  $\mathcal{T}_h$  the space of continuous piecewise polynomials can be defined by

$$\mathcal{P}_k(\mathcal{T}_h) = \{p \mid p \in H^1(\Omega), p|_K \in \mathcal{P}_k(K)\}$$

Therefore we define the functions of  $\mathcal{P}_k(\mathcal{T}_h)$  by

- $p$  is a polynomial of degree  $k$  on every triangle  $K$
- $p$  is continuous on  $\Omega$

For a given triangulation  $\mathcal{T}_h$  we ensure the first property by choosing the local basis functions to be of

- Lagrangian type for the given degrees of freedom or
- hierarchical type

One clearly sees that every polynomial of degree  $k = 1, 2$  can be defined by the values at the points depicted in figure 2.1 .

To ensure the continuity of  $p$  we have to assemble the local basis functions for adjacent triangles. Therefore the dimension of  $\mathcal{P}_k(\mathcal{T}_h)$  is given by

- $k = 1$  :  $\#P(\mathcal{T}_h)$
- $k = 2$  :  $\#P(\mathcal{T}_h) + \#E(\mathcal{T}_h)$

where  $\#P(\mathcal{T}_h)/\#E(\mathcal{T}_h)$  denotes the number of nodes / edges of the triangulation  $\mathcal{T}_h$ . Let the diameter  $h_K$  of a triangle be defined as diameter of the smallest circle that includes the triangle. Then the variable  $h$  denotes the maximal diameter of the triangles of the triangulation  $\mathcal{T}_h$ .

An important proposition for our numerical analysis can be found in [BF91, EG04]:

**Proposition 2.6** *Let  $\mathcal{T}_h$  be a shape-regular triangulation. There exists an interpolation operator  $r_h(v) : H^s(\Omega) \rightarrow P_k(\mathcal{T}_h)$  such that there exists a constant  $c$  independent of  $h$  with:*

$$|r_h p - p|_{m,\Omega} \leq c h^{s-m} |p|_{s,\Omega}$$

for  $0 \leq m \leq s$  and  $1 \leq s \leq k + 1$ .

**Remark:** The mentioned interpolation operator is in fact the Clément interpolation operator [Clé75].

### 2.3.2 Approximations of $H^{div}(\Omega)$

For the approximation of  $H^{div}(\Omega)$  we use Raviart-Thomas elements. These are given on every triangle  $K \in \mathcal{T}_h$  by (d=2)

$$RT_k(K) = \left\{ \mathbf{q} \mid \mathbf{q} = \begin{pmatrix} p_k^1(K) \\ p_k^2(K) \end{pmatrix} + p_k^3(K) \cdot \begin{pmatrix} x \\ y \end{pmatrix}, p_k^i \in \mathcal{P}_k(K) \right\}$$

For d=3 see [BF91]. It is easy to see that the following holds along each line  $s$  in the triangle  $K$ :

$$\mathbf{q} \cdot \mathbf{n}|_s \in \mathcal{P}_k(s)$$

This means that the normal component of the function  $\mathbf{q}$  along each line is a polynomial of degree  $k$ . The function  $\mathbf{q}$  by itself is a polynomial of degree  $k + 1$ .

Let the space  $RT_k(\mathcal{T}_h)$  be defined as

$$RT_k(\mathcal{T}_h) = \{\mathbf{v}_h \in H^{div}(\Omega) \mid \mathbf{v} \in RT_k(K) \forall K \in \mathcal{T}_h\}$$

For a function  $\mathbf{v}$  given by piecewise polynomials it is well known (see for example [Bra92]) that

$$\mathbf{v} \in H^{div}(\Omega) \Leftrightarrow \mathbf{v} \cdot \mathbf{n} \text{ is continuous along element edges}$$

This explains the motivation of the choice of degrees of freedom for functions in  $RT_k(K)$  as depicted in figure 2.2. The arrows denote the normal component of the function along the edge at the nodes. The other 2 degrees of freedom are given by the value of  $\mathbf{v}$  at the midpoint of the triangle.

A local basis is typically of *Lagrangian* type considering the degrees of freedom.

As in the case of  $\mathcal{P}_k(\mathcal{T}_h)$  to ensure the property of continuous normal components along all edges of the triangulation the local basis functions have to be assembled to get global basis functions in  $H^{div}(\Omega)$ .

Therefore the dimension of  $\mathcal{RT}_k(\mathcal{T}_h)$  for  $d = 2$  is given by

- $k = 0$  :  $\#E(\mathcal{T}_h)$
- $k = 1$  :  $\#2E(\mathcal{T}_h) + 2\#T(\mathcal{T}_h)$

where  $\#E(\mathcal{T}_h)/\#T(\mathcal{T}_h)$  denotes the number of edges / triangles of the triangulation  $\mathcal{T}_h$ .

An important proposition for our numerical analysis can be found in [BF91]:

**Proposition 2.7** *Let  $\mathcal{T}_h$  be a shape-regular triangulation. There exists an interpolation operator  $r_h(v) : H^{div} \cup (L^r(\Omega))^d \rightarrow RT_k(\mathcal{T}_h)$  with  $r > 2$  fixed. Let  $\mathbf{v} \in H^m(\Omega)$  and  $div \mathbf{v} \in H^s(\Omega)$ . Then there exists a constant  $c$  independent of  $h$  with:*

1.  $\|r_h \mathbf{v} - \mathbf{v}\|_{0,\Omega} \leq ch^m |\mathbf{v}|_{m,\Omega}$
2.  $\|div(r_h \mathbf{v} - \mathbf{v})\|_{0,\Omega} \leq ch^s |div \mathbf{v}|_{s,\Omega}$

for  $1 \leq m \leq k + 1$  and  $s \leq k + 1$ .

**proof:** This can be found in [BF91, Proposition 3.9].

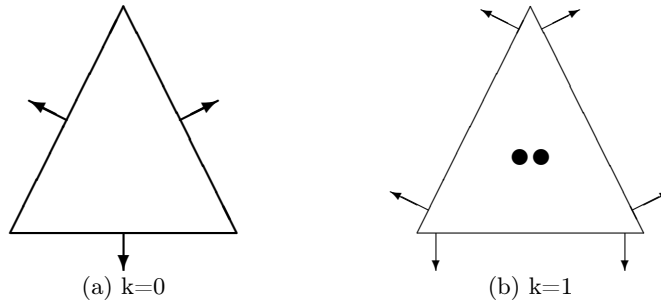


Figure 2.2: Degrees of freedom

## Chapter 3

# Least-Squares Formulation of the Separate Problems

### 3.1 Stokes Flow

The Stokes equations are used for viscous and laminar flows. They can be derived from the Navier-Stokes equations by dropping the advective terms and looking for a stationary solution. Some recent works analyzing the numerical solution of non-Newtonian Stokes flows can be found in [BS08a, EJS09] for example.

The nonlinear Stokes equations are given by:

$$\begin{aligned}
 -\nabla p_S + \operatorname{div} (2\mu_S(|\varepsilon(\mathbf{u}_S)|^2)\varepsilon(\mathbf{u}_S)) &= \mathbf{f} && \text{in } \Omega_S \\
 \operatorname{div} \mathbf{u}_S &= 0 && \text{in } \Omega_S \\
 \mathbf{u}_S &= g_{S_D} && \text{on } \Gamma_{S_D} \\
 \boldsymbol{\sigma}_S \cdot \mathbf{n} &= g_{S_N} && \text{on } \Gamma_{S_N}
 \end{aligned} \tag{3.1}$$

with  $\Omega_S$  being an open subset of  $\mathbb{R}^d$  with Lipschitz boundary. Here  $\mathbf{u}_S$  denotes the velocity and  $p_S$  denotes the pressure. Let furthermore  $\lambda_{d-1}(\Gamma_{S_D}) > 0$  s.t. the inequality of Korn holds. Furthermore we assume  $\partial\Omega_S = \Gamma_{S_D} \cup \Gamma_{S_N}$  with  $\Gamma_{S_D} \cap \Gamma_{S_N} = \emptyset$ . Here and in the following parts of this work the subscript  $S$  indicates the connection to the Stokes flow. For the least-squares FEM we have to reformulate (3.1) as a first order system. Therefore we use the stress tensor:

$$\boldsymbol{\sigma}_S = 2\mu_S(|\varepsilon(\mathbf{u}_S)|^2)\varepsilon(\mathbf{u}_S) - p_S\mathbf{I} \tag{3.2}$$

and use the following which holds for incompressible flows:

$$0 = \operatorname{tr}(\boldsymbol{\sigma}_S - 2\mu_S(|\varepsilon(\mathbf{u}_S)|^2)\varepsilon(\mathbf{u}_S) + p_S\mathbf{I}) = \operatorname{tr} \boldsymbol{\sigma}_S - 2\mu_S(|\varepsilon(\mathbf{u}_S)|^2)\operatorname{div} \mathbf{u}_S + dp_S = \operatorname{tr} \boldsymbol{\sigma}_S + dp_S$$

We use the trace free part of  $\boldsymbol{\sigma}_S$ :

$$\operatorname{dev} \boldsymbol{\sigma}_S = \boldsymbol{\sigma}_S - \frac{1}{d}(\operatorname{tr} \boldsymbol{\sigma}_S)\mathbf{I}$$

An orthogonal decomposition of  $\boldsymbol{\sigma}_S$  is given by:

$$\boldsymbol{\sigma}_S = \operatorname{dev} \boldsymbol{\sigma}_S + \frac{1}{d}(\operatorname{tr} \boldsymbol{\sigma}_S)\mathbf{I}$$

resulting in

$$\|\boldsymbol{\sigma}_S\|_{0,\Omega_S}^2 = \|\operatorname{dev} \boldsymbol{\sigma}_S\|_{0,\Omega_S}^2 + \frac{1}{d} \|\operatorname{tr} \boldsymbol{\sigma}_S\|_{0,\Omega_S}^2$$

We then get the nonlinear first order system:

$$\begin{aligned} \operatorname{div} \boldsymbol{\sigma}_S &= \mathbf{f} && \text{in } \Omega_S \\ \operatorname{dev} \boldsymbol{\sigma}_S - 2\mu_S(|\boldsymbol{\varepsilon}(\mathbf{u}_S)|^2)\boldsymbol{\varepsilon}(\mathbf{u}_S) &= 0 && \text{in } \Omega_S \\ \nabla \cdot \mathbf{u}_S &= 0 && \text{in } \Omega_S \\ \mathbf{u}_S &= g_{S_D} && \text{on } \Gamma_{S_D} \\ \boldsymbol{\sigma}_S \cdot \mathbf{n} &= g_{S_N} && \text{on } \Gamma_{S_N} \\ \int_{\Omega_S} \operatorname{tr} \boldsymbol{\sigma}_S \, dx &= 0 && \text{if } \Gamma_{S_N} = \emptyset \end{aligned} \tag{3.3}$$

This approach to eliminate the pressure  $p_S$  is also used in the recent works (see for example [MS11, GMS11, CWZ10]) where the latter two works used a pseudostress-velocity formulation. In the following parts of this work we use the expression  $\operatorname{div}$  for the case of tensors in  $\mathbb{R}^{d \times d}$  and the standard notation  $\nabla \cdot$  in the case of vectors in  $\mathbb{R}^d$  to describe the divergence.

**Remark:** For the Stokes equations we use  $\int_{\Omega_S} \operatorname{tr} \boldsymbol{\sigma}_S \, dx$  as additional condition if  $\Gamma_{S_N} = \emptyset$ . This follows from

$$\operatorname{tr} \boldsymbol{\sigma} = -dp_S. \tag{3.4}$$

Setting

$$\int_{\Omega_S} \operatorname{tr} \boldsymbol{\sigma}_S \, dx = 0 \quad \text{if } \Gamma_{S_N} = \emptyset \tag{3.5}$$

is equivalent to setting a reference pressure  $p_0$  which is necessary for pure Dirichlet boundary conditions.

The characterization of a non-Newtonian fluid can be found in [OP02]. Though we refer to our case as a non-newtonian fluid flow we only look at a special case of fluids where the viscosity depends on the shear-rate:

$$\mu_S = \mu_S(|\boldsymbol{\varepsilon}(\mathbf{u}_S)|^2)$$

These fluids are known as *generalized Newtonian fluids* in the literature. There are several works analyzing these models (see for example [GMS11, EJS09] for the numerical approach and [BP07, EM09] for analytical works). Other models, as viscoelastic fluids, involve additional stresses. A good example of a LSFEM for these flows can be found in [CW09].

A distinction is drawn between *shear-thinning* and *shear-thickening* flows. The viscosity  $\mu_S$  is monotonous in  $|\boldsymbol{\varepsilon}(\mathbf{u}_S)|^2$  with the following property:

- *shear-thinning*:  $\mu_S(|\boldsymbol{\varepsilon}(\mathbf{u}_S)|^2) \downarrow$  if  $|\boldsymbol{\varepsilon}(\mathbf{u}_S)| \uparrow$
- *shear-thickening*:  $\mu_S(|\boldsymbol{\varepsilon}(\mathbf{u}_S)|^2) \uparrow$  if  $|\boldsymbol{\varepsilon}(\mathbf{u}_S)| \uparrow$

There are several models to be found throughout literature. The following are used in [EJS09] for a coupled generalized Newtonian Stokes-Darcy flow and can be found in [OP02] as well:

- *Carreau model* ([Car72])

$$\mu(|\boldsymbol{\varepsilon}(\mathbf{u}_S)|^2) = \mu_\infty + \frac{(\mu_0 - \mu_\infty)}{(1 + K|\boldsymbol{\varepsilon}(\mathbf{u}_S)|^2)^{\frac{2-r}{2}}}$$

- *Cross model* ([Cro65])

$$\mu(|\varepsilon(\mathbf{u}_S)|^2) = \mu_\infty + \frac{(\mu_0 - \mu_\infty)}{1 + K(|\varepsilon(\mathbf{u}_S)|^2)^{\frac{2-r}{2}}}$$

- *Power law model*

$$\mu(|\varepsilon(\mathbf{u}_S)|^2) = K(|\varepsilon(\mathbf{u}_S)|^2)^{\frac{r-2}{2}}$$

The constants  $r > 1$  and  $K > 0$  determine the characteristics of the *shear-thinning* and *shear-thickening* property. For  $r$  we have in these models:

-  $1 < r < 2$ : *shear-thinning*

-  $r = 2$ : *Newtonian fluid*

-  $2 < r$ : *shear-thickening*

For our numerical analysis we see that the *power law model* does not exhibit the necessary properties to prove the main results of this work. The *Carreau model* can be used for *shear-thinning* fluids and the *Cross model* does not need any further restrictions in the constants  $K$  and  $r$ .

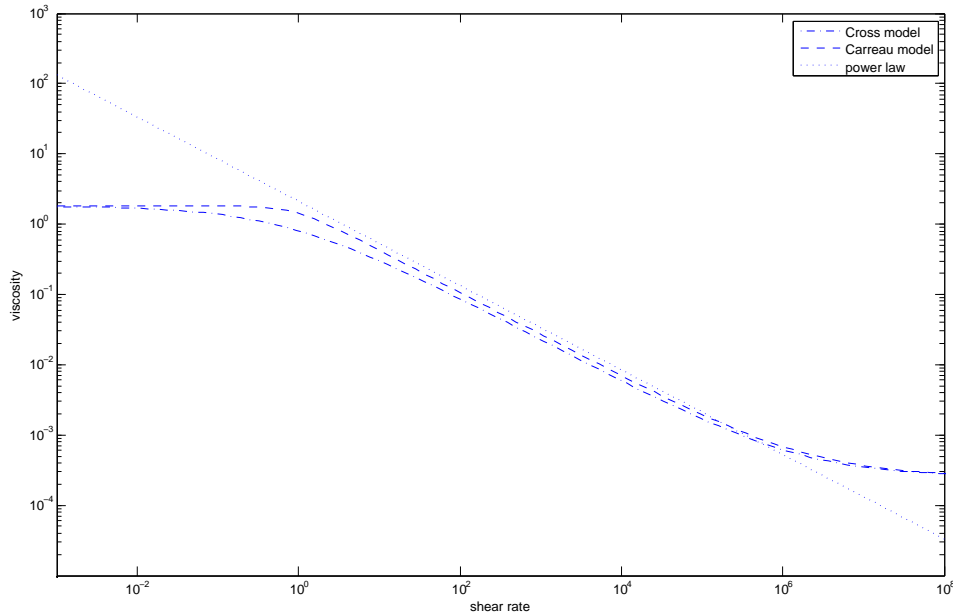
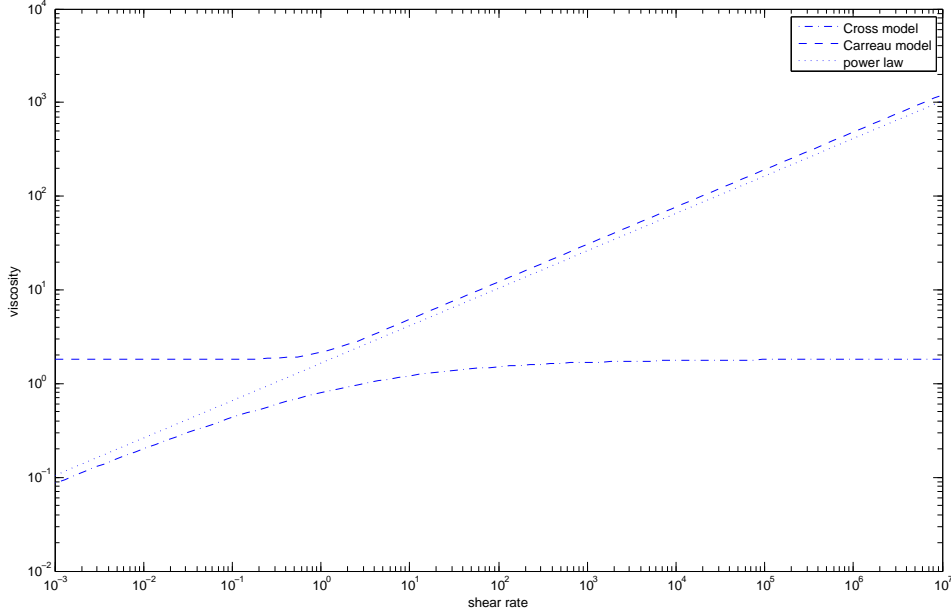


Figure 3.1: Example: polyacrylamide (shear thinning  $r=1.4$ )

An example for the behavior of these models is depicted in figure 3.1. Here we used the example of polyacrylamide (see [OP02]) for the *Cross model*. To compare these models we used the same constants for the power law (adequately scaled) and the *Carreau model*. It has to be noted that these models behave locally (for  $|\varepsilon(\mathbf{u}_S)|^2$  between  $10$  and  $10^6$ ) similar to each other.

In figure 3.2 we used the same constants and set  $r$  to  $2.4$  to depict a shear thickening behavior. One can easily see that the *Carreau model* behaves like the power law for large shear rates. As it

Figure 3.2: Example: shear thickening ( $r=2.4$ )

is unbounded (which holds for all  $r > 2$ ) this model does not satisfy the assumptions of the next section.

### 3.1.1 The Least-Squares Functional as an Error Estimator

As in chapter 2 we define our least-squares functional for the Stokes equations:

$$\mathcal{F}_S(\mathbf{u}_S, \boldsymbol{\sigma}_S; \mathbf{f}) = \|\operatorname{div} \boldsymbol{\sigma}_S - \mathbf{f}\|_{0, \Omega_S}^2 + \|\operatorname{dev} \boldsymbol{\sigma}_S - 2\mu_S(|\boldsymbol{\varepsilon}(\mathbf{u}_S)|^2)\boldsymbol{\varepsilon}(\mathbf{u}_S)\|_{0, \Omega_S}^2 + \|\nabla \cdot \mathbf{u}_S\|_{0, \Omega_S}^2 \quad (3.6)$$

A least-squares FEM for a nonlinear generalized Newtonian flow was considered recently in [CCLT10]. The approach was different in the usage of FEM spaces and weighted least-squares functionals. Approaches for using LSFEM for nonlinear generalized Newtonian flow go back to early works in 1994 ([BS94]).

For our approach we make use of the following spaces

$$\begin{aligned} (H_{\Gamma_{S_N}}^{\operatorname{div}}(\Omega_S))^d &= \{\boldsymbol{\tau} \in (H^{\operatorname{div}}(\Omega_S))^d \mid \boldsymbol{\tau} \cdot \mathbf{n} = 0 \text{ on } \Gamma_{S_N} \mid \int_{\Omega_S} \operatorname{tr} \boldsymbol{\tau} = 0 \text{ if } \Gamma_{S_N} = \emptyset\} \\ (H_{\Gamma_{S_D}}^1(\Omega_S))^d &= \{\mathbf{v} \in (H^1(\Omega_S))^d \mid \mathbf{v} = 0 \text{ on } \Gamma_{S_D}\} \end{aligned}$$

As in chapter 2 we are using the following functions for the boundary conditions:

- $\mathbf{u}_{S_D} \in (H^1(\Omega_S))^d$  with  $\mathbf{u}_{S_D}|_{\Gamma_{S_D}} = g_{S_D}$
- $\boldsymbol{\sigma}_{S_N} \in (H^{\operatorname{div}}(\Omega_S))^d$  with  $\boldsymbol{\sigma}_{S_N}|_{\Gamma_{S_N}} = g_{S_N}$

The restriction on the boundary is again meant to be in the sense of traces. If  $\Gamma_{S_D} = \emptyset / \Gamma_{S_N} = \emptyset$  we set  $\mathbf{u}_{S_D} = 0 / \boldsymbol{\sigma}_{S_N} = 0$ .

Our minimization problem is then given by: Find  $(\hat{\mathbf{u}}_S, \hat{\boldsymbol{\sigma}}_S) \in (H^1_{\Gamma_{S_D}}(\Omega_S))^d \times (H^{div}_{\Gamma_{S_N}}(\Omega_S))^d$  s.t.

$$\mathcal{F}_S(\mathbf{u}_{S_D} + \hat{\mathbf{u}}_S, \boldsymbol{\sigma}_{S_N} + \hat{\boldsymbol{\sigma}}_S; \mathbf{f}) \leq \mathcal{F}_S(\mathbf{u}_{S_D} + \mathbf{v}_S, \boldsymbol{\sigma}_{S_N} + \boldsymbol{\tau}_S; \mathbf{f})$$

holds for all  $(\mathbf{v}_S, \boldsymbol{\tau}_S) \in (H^1_{\Gamma_{S_D}}(\Omega_S))^d \times (H^{div}_{\Gamma_{S_N}}(\Omega_S))^d$ .

For further analysis we need the following assumptions on  $\mu_S(s)$ .

$$\mathbf{(A1}_S) \quad \mu_S(s) \in C^0([0, \infty)) \cap C^1((0, \infty))$$

$$\mathbf{(A2}_S) \quad 0 < K_0 \leq \mu_S(s) \leq K_1$$

$$\mathbf{(A3}_S) \quad 0 < M_0 \leq \mu_S(s) + 2\mu'_S(s)s \leq M_\infty < \infty \text{ for } s > 0$$

These assumptions can be found in [EM09] for example.

**Lemma 3.1** *Assume that  $\mathbf{(A1}_S)$ ,  $\mathbf{(A2}_S)$  and  $\mathbf{(A3}_S)$  hold. Then we have for an arbitrary constant  $\bar{\mu}_S > 0$  :*

$$\begin{aligned} & \|\mu_S(|\varepsilon(\mathbf{u}_S)|^2)\varepsilon(\mathbf{u}_S) - \mu_S(|\varepsilon(\mathbf{v}_S)|^2)\varepsilon(\mathbf{v}_S) - \bar{\mu}_S(\varepsilon(\mathbf{u}_S) - \varepsilon(\mathbf{v}_S))\|_{0,\Omega_S} \\ & \leq C_{\mu,S} \cdot \bar{\mu}_S \|\varepsilon(\mathbf{u}_S) - \varepsilon(\mathbf{v}_S)\|_{0,\Omega_S} \end{aligned} \quad (3.7)$$

which holds for all  $\mathbf{u}_S, \mathbf{v}_S \in (H^1(\Omega_S))^d$  with a constant  $C_{\mu,S}(\bar{\mu}_S)$  given by

$$C_{\mu,S} := \max_{\xi \in \mathbb{R}^{d \times d}} \frac{\max\{|\mu_S(|\xi|^2) - \bar{\mu}_S|, |\mu_S(|\xi|^2) - \bar{\mu}_S + 2\mu'_S(|\xi|^2)|\xi|^2\}}{\bar{\mu}_S} < \infty \quad (3.8)$$

**Proof:** A similar lemma for the case of nonlinear plasticity can be found in [Sta07]. We follow this idea for a proof. We show that

$$|\mu_S(|\varepsilon(\mathbf{u}_S)|^2)\varepsilon(\mathbf{u}_S) - \mu_S(|\varepsilon(\mathbf{v}_S)|^2)\varepsilon(\mathbf{v}_S) - \bar{\mu}_S(\varepsilon(\mathbf{u}_S) - \varepsilon(\mathbf{v}_S))| \leq C_{\mu,S} \cdot \bar{\mu}_S |\varepsilon(\mathbf{u}_S) - \varepsilon(\mathbf{v}_S)| \quad (3.9)$$

holds for almost every  $\mathbf{x} \in \Omega_S$ , whereby 3.7 follows directly.

We define  $S(\xi) : \mathbb{R}^{d \times d} \rightarrow \mathbb{R}^{d \times d}$  by:

$$S(\xi) := (\mu_S(|\xi|^2) - \bar{\mu}_S)\xi \quad (3.10)$$

$S(\xi)$  is differentiable for all  $\xi$  with  $|\xi| > 0$ . If we show that  $S$  is Lipschitz continuous:

$$|S(\xi) - S(\eta)| \leq C_{\mu,S} |\xi - \eta|$$

(3.9) follows immediatly. Therefore by using the mean value theorem in [OR70] we need to show that  $\|S'(\xi)\|$  is bounded for all  $\xi \neq 0$ .  $C_{\mu,S}$  is chosen as an upper bound for  $\|S'(\xi)\|$ .

For the directional derivative  $S'(\xi)[\chi]$  it holds:

$$\begin{aligned} S'(\xi)[\chi] &= \lim_{h \rightarrow 0} \frac{S(\xi + h\chi) - S(\xi)}{h} \\ &= \frac{d}{dh} S(\xi + h\chi)|_{h=0} \\ &= (\mu_S(|\xi|^2) - \bar{\mu}_S)\chi + 2\mu'_S(|\xi|^2) \cdot \xi : \chi \cdot \xi \end{aligned}$$

Obviously we can write  $\chi$  as

$$\chi = \frac{\chi : \xi}{|\xi|^2} \xi + \left( \chi - \frac{\chi : \xi}{|\xi|^2} \xi \right)$$

with

$$\left( \frac{\chi : \xi}{|\xi|^2} \xi \right) : \left( \chi - \frac{\chi : \xi}{|\xi|^2} \xi \right) = 0 \quad (3.11)$$

We then have:

$$\begin{aligned} \|S'(\xi)\| &= \sup_{\chi \neq 0} \frac{|S'(\xi)[\chi]|}{|\chi|} \\ &= \sup_{\chi \neq 0} \left| (\mu_S(|\xi|^2) - \bar{\mu}_S) \frac{\chi}{|\chi|} + 2\mu'_S(|\xi|^2) \cdot \xi : \chi \cdot \frac{\xi}{|\chi|} \right| \\ &= \sup_{\chi \neq 0} \left| (\mu_S(|\xi|^2) - \bar{\mu}_S) \left( \frac{\chi : \xi}{|\xi|^2 |\chi|} \xi + \left( \frac{\chi}{|\chi|} - \frac{\chi : \xi}{|\xi|^2 |\chi|} \xi \right) \right) + 2\mu'_S(|\xi|^2) |\xi|^2 \cdot \frac{\xi : \chi}{|\xi|^2} \cdot \frac{\xi}{|\chi|} \right| \\ &= \sup_{\chi \neq 0} \left| (\mu_S(|\xi|^2) - \bar{\mu}_S) \left( \frac{\chi}{|\chi|} - \frac{\chi : \xi}{|\xi|^2 |\chi|} \xi \right) + (\mu_S(|\xi|) - \bar{\mu}_S + 2\mu'_S(|\xi|^2) |\xi|^2) \cdot \frac{\xi : \chi}{|\xi|^2} \cdot \frac{\xi}{|\chi|} \right| \\ &= \sup_{\chi \neq 0} \left( (\mu_S(|\xi|^2) - \bar{\mu}_S)^2 \left( \frac{\chi}{|\chi|} - \frac{\chi : \xi}{|\xi|^2 |\chi|} \xi \right)^2 + (\mu_S(|\xi|) - \bar{\mu}_S + 2\mu'_S(|\xi|^2) |\xi|^2)^2 \cdot \left( \frac{\xi : \chi}{|\xi|^2} \cdot \frac{\xi}{|\chi|} \right)^2 \right)^{\frac{1}{2}} \end{aligned}$$

where we used the orthogonality (3.11). If we use the following

$$\left( \frac{\chi}{|\chi|} - \frac{\chi : \xi}{|\xi|^2 |\chi|} \xi \right)^2 + \left( \frac{\xi : \chi}{|\xi|^2} \cdot \frac{\xi}{|\chi|} \right)^2 = 1$$

we get

$$\begin{aligned} \|S'(\xi)\| &\leq \sup_{\chi \neq 0} \max\{|\mu_S(|\xi|^2) - \bar{\mu}_S|, |\mu_S(|\xi|^2) - \bar{\mu}_S + 2\mu'_S(|\xi|^2) |\xi|^2|\} \sqrt{\left( \frac{\chi}{|\chi|} - \frac{\chi : \xi}{|\xi|^2 |\chi|} \xi \right)^2 + \left( \frac{\xi : \chi}{|\xi|^2} \cdot \frac{\xi}{|\chi|} \right)^2} \\ &= \max\{|\mu_S(|\xi|^2) - \bar{\mu}_S|, |\mu_S(|\xi|^2) - \bar{\mu}_S + 2\mu'_S(|\xi|^2) |\xi|^2|\} \\ &\leq C_{\mu,S} \bar{\mu}_S \end{aligned}$$

$$\text{with } C_{\mu,S} := \max_{\xi} \frac{\max\{|\mu_S(|\xi|^2) - \bar{\mu}_S|, |\mu_S(|\xi|^2) - \bar{\mu}_S + 2\mu'_S(|\xi|^2) |\xi|^2|\}}{\bar{\mu}_S}.$$

This  $C_{\mu,S}$  exists because of **(A2)**<sub>S</sub> and **(A3)**<sub>S</sub>. ■

**Remark:** To this point only the upper bound on the viscosity was needed. For the next lemma which is crucial for further analysis the lower bound is needed as well.

**Lemma 3.2** *Let the assumptions of lemma 3.1 hold. Then there exists a  $\bar{\mu}_S$  such that for  $C_{\mu,S}$  it holds:*

$$C_{\mu,S} < 1$$

*If the bounds in **(A2)**<sub>S</sub> and **(A3)**<sub>S</sub> are sharp the smallest  $C_{\mu,S}$  that is valid for all  $\zeta \in \mathbb{R}^{d \times d}$  is given by:*

$$C_{\mu,S} = \frac{\bar{\mu}_S - \min\{K_0, M_0\}}{\bar{\mu}_S}$$

*with*

$$\bar{\mu}_S = \max\left\{ \frac{K_1 + K_0}{2}, \frac{M_1 + M_0}{2} \right\}$$



**Proof:** With lemma 3.1 and  $(\mathbf{A2})_S$  we get

$$\frac{|\mu_S(|\xi|^2) - \bar{\mu}_S|}{\bar{\mu}_S} \leq \frac{|\bar{\mu}_S - K_0|}{\bar{\mu}_S} < 1 \quad \text{if } \bar{\mu}_S \geq \frac{K_1 + K_0}{2}$$

With  $(\mathbf{A3})_S$  we get

$$\frac{|\mu_S(|\xi|^2) - \bar{\mu}_S + 2\mu'_S(|\xi|^2)|\xi|^2|}{\bar{\mu}_S} \leq \frac{|\bar{\mu}_S - M_0|}{\bar{\mu}_S} < 1 \quad \text{if } \bar{\mu}_S \geq \frac{M_1 + M_0}{2}$$

The second part follows immediately from (3.8) . ■

It might be necessary to use different/more general assumptions on the viscosity. The former assumptions are not satisfied for a viscosity that is not bounded from above/below. Furthermore one might use a viscosity that is not continuously differentiable and the former assumptions are not satisfied. Therefore we need weaker assumptions that can be found in [BS08a]:

Let  $\mu_S \in C(0, \infty)$  and for a given  $\theta \in (1, \infty)$  there exist constants  $\alpha \in [0, 1]$  and  $\delta, C_4, C_5 > 0$  s.t.

$$\begin{aligned} (\mathbf{A4}_S) \quad & |\mu_S(s)s - \mu_S(t)t| \leq C_4 ((t+s)^\alpha(1+t+s)^{1-\alpha})^{\theta-2} |s-t| \text{ holds for all } s, t > 0 \\ & \text{with } |s/t - 1| \leq \delta \text{ and} \\ & \mu_S(t) \leq C_4 (t^\alpha(1+t)^{1-\alpha})^{\theta-2} \text{ holds for all } t > 0 \end{aligned}$$

$$(\mathbf{A5}_S) \quad \mu_S(t)t - \mu_S(s)s \geq C_5 ((t+s)^\alpha(1+t+s)^{1-\alpha})^{\theta-2} (t-s) \text{ holds for all } t \geq s > 0$$

The following is stated in [BS08a]: The parameter  $\alpha$  measures the singularity/degeneracy in  $\mu_S$  for a given value of  $\theta \in (1, \infty) \setminus 2$  as if  $\alpha$  is closer to 1 the more singular/degenerate the  $\mu_S$  is for  $\theta < 2$  resp.  $\theta > 2$ . For  $\theta = 2$  the viscosity  $\mu_S(s)$  is uniformly monotone and globally Lipschitz continuous. Examples are:

1. the power law model corresponds to  $\alpha = 1$  and  $\theta = r$ . For  $\theta = 2$  the model reduces to Newtonian flow.
2. The *Carreau model* corresponds to  $\alpha = 0$  and  $\theta = r$  if  $\mu_\infty = 0$  and  $\theta = 2$  if  $r \in (1, 2]$  and  $\mu_\infty > 0$

To translate this to our problem we need the following statement from [BS08a, Lemma 3.1]:

**Lemma 3.3** *With  $\Theta_\alpha(t) = t^\alpha(1+t)^{1-\alpha}$  and assumption  $(\mathbf{A5}_S)$  to be satisfied for  $\theta \in (1, \infty)$  and  $\alpha \in [0, 1]$  we have for all symmetric  $\zeta, \eta \in \mathbb{R}^{d \times d}$  and  $\gamma \geq 0$*

$$C_5 (\Theta_\alpha(|\zeta| + |\eta|))^{\theta-2-\gamma} |\zeta - \eta|^{2+\gamma} \leq (\mu_S(|\zeta|)\zeta - \mu_S(|\eta|)\eta) : (\zeta - \eta)$$

*If  $(\mathbf{A4}_S)$  is satisfied for  $\theta \in (1, \infty)$  and  $\alpha \in [0, 1]$  we have for all symmetric  $\zeta, \eta \in \mathbb{R}^{d \times d}$  and  $\gamma \geq 0$ :*

$$|\mu_S(|\zeta|)\zeta - \mu_S(|\eta|)\eta| \leq C_4 (\Theta_\alpha(|\zeta| + |\eta|))^{\theta-2+\gamma} |\zeta - \eta|^{1-\gamma}$$

**Remark:** For our least-squares approach some things have to be noted. As most authors use a mixed FEM approach (for example [BL93, BS08a]) the velocity  $\mathbf{u}_S$  needs to be in  $(W^{1,\theta}(\Omega_S))^d$  as

$$\mu_S(|\cdot|) \cdot : (L^\theta(\Omega_S))^{d \times d} \mapsto (L^\theta(\Omega_S))^{d \times d}$$

with  $1/\theta + 1/\theta' = 1$  (see [BL93]). In contrast to a mixed approach a least-squares method needs  $\mu_S(|\zeta|)\zeta \in (L^2)^{d \times d}$ . Therefore we have to assume  $\mathbf{u}_S \in (W^{1,\beta}(\Omega_S))^d$  with  $\beta(\theta) \geq 2$  chosen s.t.  $\mu_S(|\zeta|)\zeta \in (L^2)^{d \times d}$ .

Using these assumptions we can prove the analog version of lemma 3.1:

**Lemma 3.4** *Assume that (A4<sub>S</sub>) and (A5<sub>S</sub>) hold and let  $\mathbf{u}_S \in (W^{1,\beta}(\Omega_S))^d$ . Then we have for arbitrary constants  $\bar{\mu}_S, \gamma > 0$  :*

$$\begin{aligned} & \|\mu_S(|\varepsilon(\mathbf{u}_S)|)\varepsilon(\mathbf{u}_S) - \mu_S(|\varepsilon(\mathbf{v}_S)|)\varepsilon(\mathbf{v}_S) - \bar{\mu}_S(\varepsilon(\mathbf{u}_S) - \varepsilon(\mathbf{v}_S))\|_{0,\Omega_S} \\ & \leq \frac{C_4^2}{\bar{\mu}_S^2} \|\bar{\mu}_S (\Theta_\alpha(|\varepsilon(\mathbf{u}_S)| + |\varepsilon(\mathbf{v}_S)|))\|^{\theta-2+\gamma} |\varepsilon(\mathbf{u}_S) - \varepsilon(\mathbf{v}_S)|^{1-\gamma}\|_{0,\Omega_S}^2 \\ & \quad - \frac{2C_5}{\bar{\mu}_S} \|(\Theta_\alpha(|\varepsilon(\mathbf{u}_S)| + |\varepsilon(\mathbf{v}_S)|))\|^{\frac{\theta-2-\gamma}{2}} \bar{\mu}_S |\varepsilon(\mathbf{u}_S) - \varepsilon(\mathbf{v}_S)|^{\frac{2+\gamma}{2}}\|_{0,\Omega_S}^2 \\ & \quad + \|\bar{\mu}_S(\varepsilon(\mathbf{u}_S) - \varepsilon(\mathbf{v}_S))\|_{0,\Omega_S}^2 \end{aligned} \quad (3.12)$$

Setting  $\theta = 2$  and  $\gamma = 0$  we get

$$\begin{aligned} & \|\mu_S(|\varepsilon(\mathbf{u}_S)|)\varepsilon(\mathbf{u}_S) - \mu_S(|\varepsilon(\mathbf{v}_S)|)\varepsilon(\mathbf{v}_S) - \bar{\mu}_S(\varepsilon(\mathbf{u}_S) - \varepsilon(\mathbf{v}_S))\|_{0,\Omega_S} \\ & \leq C_{\mu,S} \|\bar{\mu}_S(\varepsilon(\mathbf{u}_S) - \varepsilon(\mathbf{v}_S))\|_{0,\Omega_S}^2 \end{aligned} \quad (3.13)$$

with

$$C_{\mu,S} < 1 \quad (3.14)$$

by choosing  $\bar{\mu}_S$  large enough.

**proof:** We have

$$\begin{aligned} & \|\mu_S(|\varepsilon(\mathbf{u}_S)|)\varepsilon(\mathbf{u}_S) - \mu_S(|\varepsilon(\mathbf{v}_S)|)\varepsilon(\mathbf{v}_S) - \bar{\mu}_S(\varepsilon(\mathbf{u}_S) - \varepsilon(\mathbf{v}_S))\|_{0,\Omega_S}^2 \\ & = \|\mu_S(|\varepsilon(\mathbf{u}_S)|)\varepsilon(\mathbf{u}_S) - \mu_S(|\varepsilon(\mathbf{v}_S)|)\varepsilon(\mathbf{v}_S)\|_{0,\Omega_S}^2 \\ & \quad - 2(\mu_S(|\varepsilon(\mathbf{u}_S)|)\varepsilon(\mathbf{u}_S) - \mu_S(|\varepsilon(\mathbf{v}_S)|)\varepsilon(\mathbf{v}_S), \bar{\mu}_S(\varepsilon(\mathbf{u}_S) - \varepsilon(\mathbf{v}_S))) \\ & \quad + \|\bar{\mu}_S(\varepsilon(\mathbf{u}_S) - \varepsilon(\mathbf{v}_S))\|_{0,\Omega_S}^2 \\ & \leq \frac{C_4^2}{\bar{\mu}_S^2} \|\bar{\mu}_S (\Theta_\alpha(|\varepsilon(\mathbf{u}_S)| + |\varepsilon(\mathbf{v}_S)|))\|^{\theta-2+\gamma} |\varepsilon(\mathbf{u}_S) - \varepsilon(\mathbf{v}_S)|^{1-\gamma}\|_{0,\Omega_S}^2 \\ & \quad - \frac{2C_5}{\bar{\mu}_S} \|(\Theta_\alpha(|\varepsilon(\mathbf{u}_S)| + |\varepsilon(\mathbf{v}_S)|))\|^{\frac{\theta-2-\gamma}{2}} \bar{\mu}_S |\varepsilon(\mathbf{u}_S) - \varepsilon(\mathbf{v}_S)|^{\frac{2+\gamma}{2}}\|_{0,\Omega_S}^2 \\ & \quad + \|\bar{\mu}_S(\varepsilon(\mathbf{u}_S) - \varepsilon(\mathbf{v}_S))\|_{0,\Omega_S}^2 \\ & \stackrel{\theta=2,\gamma=0}{=} \left(1 + \frac{C_4^2}{\bar{\mu}_S^2} - \frac{2C_5}{\bar{\mu}_S}\right) \|\bar{\mu}_S(\varepsilon(\mathbf{u}_S) - \varepsilon(\mathbf{v}_S))\|_{0,\Omega_S}^2 \end{aligned}$$

by choosing  $\bar{\mu}_S > \frac{C_4^2}{2C_5}$  the proof is finished. ■

**Remark:** Behind these assumptions lies a more general approach to nonlinear least-squares problems. The monotonicity (A5<sub>S</sub>) and continuity (A4<sub>S</sub>) with respect to a corresponding linear problem (in our case a Newtonian flow with viscosity  $\bar{\mu}_S$ ) is a sufficient assumption to prove  $C_{\mu,S} < 1$ .

**Remark:** In the following we set  $\theta = 2$  and  $\gamma = 0$  if we refer to assumptions **A4<sub>S</sub>** and **A5<sub>S</sub>** which still implies a bounded viscosity.

The next theorem is the main result for this section and states that the nonlinear least-squares functional is an error estimator. To prove this we need lemma 2.3 which only holds if  $\int_{\Omega_S} \text{tr } \boldsymbol{\tau} dx = 0$ . Therefore we restrict ourselves to the case  $\Gamma_{S_D} = \partial\Omega$  if necessary. In this case we have

$$\begin{aligned} & \boldsymbol{\sigma}_{S_N} = \mathbf{0} \\ & (H_{\Gamma_{S_N}}^{div}(\Omega_S))^d = \{\boldsymbol{\tau} \in (H^{div}(\Omega_S))^d \mid \int_{\Omega_S} \text{tr } \boldsymbol{\tau} = 0\} \end{aligned}$$

For the sake of simplicity we use the following notation in the course of this work

$$a(\xi) \gtrsim b(\xi) \quad \text{if there exists a constant } C \text{ s.t. } a(\xi) \geq Cb(\xi) \quad \forall \text{ admissible } \xi$$

**Theorem 3.5** *Let assumptions (A1)<sub>S</sub>, (A2)<sub>S</sub> and (A3)<sub>S</sub> or assumptions (A4)<sub>S</sub> and (A5)<sub>S</sub> hold. Furthermore  $\Gamma_{S_D} = \partial\Omega_S$  holds. We then have for the solution  $(\mathbf{u}_S, \boldsymbol{\sigma}_S) = (\mathbf{u}_{S_D}, \boldsymbol{\sigma}_{S_N}) + (\hat{\mathbf{u}}_S, \hat{\boldsymbol{\sigma}}_S)$  with  $(\hat{\mathbf{u}}_S, \hat{\boldsymbol{\sigma}}_S) \in (H^1_{\Gamma_{S_D}}(\Omega_S))^d \times (H^{div}_{\Gamma_{S_N}}(\Omega_S))^d$  of (3.3) :*

$$C_{e,S}(\|\mathbf{u}_S - \mathbf{v}_S\|_{1,\Omega_S}^2 + \|\boldsymbol{\sigma}_S - \boldsymbol{\tau}_S\|_{div,\Omega_S}^2) \leq \mathcal{F}_S(\mathbf{v}_S, \boldsymbol{\tau}_S; \mathbf{f}) \leq C_{s,S}(\|\mathbf{u}_S - \mathbf{v}_S\|_{1,\Omega_S}^2 + \|\boldsymbol{\sigma}_S - \boldsymbol{\tau}_S\|_{div,\Omega_S}^2)$$

for all  $(\mathbf{v}_S, \boldsymbol{\tau}_S) = (\mathbf{u}_{S_D}, \boldsymbol{\sigma}_{S_N}) + (\hat{\mathbf{v}}_S, \hat{\boldsymbol{\tau}}_S)$  with  $(\hat{\mathbf{v}}_S, \hat{\boldsymbol{\tau}}_S) \in (H^1_{\Gamma_{S_D}}(\Omega_S))^d \times (H^{div}_{\Gamma_{S_N}}(\Omega_S))^d$  with positive constants  $C_{e,S}$  and  $C_{s,S}$ .

**proof:** The proof is analogous to [MS11]. The nonlinearity has to be considered which is done as in [Sta07]. We have

$$\begin{aligned} \mathcal{F}_S(\mathbf{v}_S, \boldsymbol{\tau}_S; \mathbf{f}) &= \|\operatorname{div} \boldsymbol{\tau}_S - \mathbf{f}\|_{0,\Omega_S}^2 + \|\operatorname{dev} \boldsymbol{\tau}_S - 2(\mu_S(|\varepsilon(\mathbf{v}_S)|^2)\varepsilon(\mathbf{v}_S))\|_{0,\Omega_S}^2 + \|\nabla \cdot \mathbf{v}_S\|_{0,\Omega_S}^2 \\ &= \|\operatorname{div} (\boldsymbol{\sigma}_S - \boldsymbol{\tau}_S)\|_{0,\Omega_S}^2 + \|\nabla \cdot (\mathbf{v}_S - \mathbf{u}_S)\|_{0,\Omega_S}^2 \\ &\quad + \|\operatorname{dev} (\boldsymbol{\sigma}_S - \boldsymbol{\tau}_S) - 2(\mu_S(|\varepsilon(\mathbf{u}_S)|^2)\varepsilon(\mathbf{u}_S) - \mu_S(|\varepsilon(\mathbf{v}_S)|^2)\varepsilon(\mathbf{v}_S))\|_{0,\Omega_S}^2 \end{aligned}$$

The upper bound follows directly from the triangle inequality and lemma 3.1 :

$$\begin{aligned} \mathcal{F}_S(\mathbf{v}_S, \boldsymbol{\tau}_S; \mathbf{f}) &\leq \|\operatorname{div} (\boldsymbol{\sigma}_S - \boldsymbol{\tau}_S)\|_{0,\Omega_S}^2 + 2\|\operatorname{dev} (\boldsymbol{\sigma}_S - \boldsymbol{\tau}_S)\|_{0,\Omega_S}^2 + \|\nabla \cdot (\mathbf{v}_S - \mathbf{u}_S)\|_{0,\Omega_S}^2 \\ &\quad + 8\|(\mu_S(|\varepsilon(\mathbf{u}_S)|^2)\varepsilon(\mathbf{u}_S) - \mu_S(|\varepsilon(\mathbf{v}_S)|^2)\varepsilon(\mathbf{v}_S)) - \bar{\mu}_S(\varepsilon(\mathbf{u}_S) - \varepsilon(\mathbf{v}_S))\|_{0,\Omega_S}^2 \\ &\quad + 8\|\bar{\mu}_S(\varepsilon(\mathbf{u}_S) - \varepsilon(\mathbf{v}_S))\|_{0,\Omega_S}^2 \\ &\leq C_{s,S}(\|\operatorname{div} (\boldsymbol{\sigma}_S - \boldsymbol{\tau}_S)\|_{0,\Omega_S}^2 + \|(\boldsymbol{\sigma}_S - \boldsymbol{\tau}_S)\|_{0,\Omega_S}^2 + \|\varepsilon(\mathbf{u}_S) - \varepsilon(\mathbf{v}_S)\|_{0,\Omega_S}^2) \\ &\leq C_{s,S}(\|\mathbf{u}_S - \mathbf{v}_S\|_{1,\Omega_S}^2 + \|\boldsymbol{\sigma}_S - \boldsymbol{\tau}_S\|_{div,\Omega_S}^2) \end{aligned}$$

where we used

$$\begin{aligned} \|\operatorname{dev} (\boldsymbol{\sigma}_S - \boldsymbol{\tau}_S)\|_{0,\Omega_S}^2 &\leq C\|\boldsymbol{\sigma}_S - \boldsymbol{\tau}_S\|_{0,\Omega_S}^2 \\ \|\nabla \cdot (\mathbf{v}_S - \mathbf{u}_S)\|_{0,\Omega_S}^2 &\leq C\|\varepsilon(\mathbf{u}_S) - \varepsilon(\mathbf{v}_S)\|_{0,\Omega_S}^2 \end{aligned}$$

For the lower bound we need

$$\begin{aligned} \|\operatorname{as} \boldsymbol{\zeta}\| &= \|\operatorname{as} \left( \boldsymbol{\zeta} - \frac{1}{d}(\operatorname{tr} \boldsymbol{\zeta})\mathbf{I} - 2\mu(|\varepsilon(\mathbf{z})|^2)\varepsilon(\mathbf{z}) + 2\mu(|\varepsilon(\mathbf{w})|^2)\varepsilon(\mathbf{w}) \right)\|_{0,\Omega_S} \\ &= \|\operatorname{as} (\operatorname{dev} \boldsymbol{\zeta} - 2\mu_S(|\varepsilon(\mathbf{z})|^2)\varepsilon(\mathbf{z}) + 2\mu_S(|\varepsilon(\mathbf{w})|^2)\varepsilon(\mathbf{w}))\|_{0,\Omega_S} \\ &\leq \|\operatorname{dev} \boldsymbol{\zeta} - 2\mu_S(|\varepsilon(\mathbf{z})|^2)\varepsilon(\mathbf{z}) + 2\mu_S(|\varepsilon(\mathbf{w})|^2)\varepsilon(\mathbf{w})\|_{0,\Omega_S} \end{aligned} \tag{3.15}$$

which holds for all  $\boldsymbol{\zeta} \in (H(\operatorname{div}, \Omega_S))^d$  and  $\mathbf{z}, \mathbf{w} \in (H^1(\Omega_S))^d$ .

For convenience we use the following abbreviations:

$$\begin{aligned} \boldsymbol{\zeta}_S &:= \boldsymbol{\sigma}_S - \boldsymbol{\tau}_S \\ \boldsymbol{\eta}_S &:= \mathbf{v}_S - \mathbf{u}_S \end{aligned}$$

We then have the following:

$$\begin{aligned}\zeta_S &\in (H_{\Gamma_{S_N}}^{div}(\Omega_S))^d \\ \eta_S &\in (H_{\Gamma_{S_D}}^1(\Omega_S))^d\end{aligned}$$

To prove the lower bound we use:

$$\begin{aligned}\mathcal{F}_S(\mathbf{v}_S, \boldsymbol{\tau}_S; \mathbf{f}) &= \|\operatorname{div}(\boldsymbol{\sigma}_S - \boldsymbol{\tau}_S)\|_{0,\Omega_S}^2 + \|\nabla \cdot (\mathbf{v}_S - \mathbf{u}_S)\|_{0,\Omega_S}^2 \\ &\quad + \|\operatorname{dev}(\boldsymbol{\sigma}_S - \boldsymbol{\tau}_S) - 2(\mu_S(|\varepsilon(\mathbf{u}_S)|^2)\varepsilon(\mathbf{u}_S) - \mu_S(|\varepsilon(\mathbf{v}_S)|^2)\varepsilon(\mathbf{v}_S))\|_{0,\Omega_S}^2 \\ &\gtrsim 2C\|\operatorname{div} \zeta_S\|_{0,\Omega_S}^2 + \|\operatorname{dev} \zeta_S - 2(\mu_S(|\varepsilon(\mathbf{u}_S)|^2)\varepsilon(\mathbf{u}_S) - \mu_S(|\varepsilon(\mathbf{v}_S)|^2)\varepsilon(\mathbf{v}_S))\|_{0,\Omega_S}^2 \\ &\quad + C\|\nabla \cdot \boldsymbol{\eta}_S\|_{0,\Omega_S}^2 + C\|\operatorname{as} \zeta_S\|_{0,\Omega_S} \\ &\geq 2C\|\operatorname{div} \zeta_S\|_{0,\Omega_S}^2 + (1-\rho)\|\operatorname{dev} \zeta_S - 2\bar{\mu}_S\varepsilon(\boldsymbol{\eta}_S)\|_{0,\Omega_S}^2 + C\|\nabla \cdot \boldsymbol{\eta}_S\|_{0,\Omega_S}^2 \\ &\quad - \left(\frac{1}{\rho} - 1\right)\|2((\mu_S(|\varepsilon(\mathbf{u}_S)|^2)\varepsilon(\mathbf{u}_S) - \mu_S(|\varepsilon(\mathbf{v}_S)|^2)\varepsilon(\mathbf{v}_S)) - \bar{\mu}_S(\varepsilon(\mathbf{u}_S) - \varepsilon(\mathbf{v}_S)))\|_{0,\Omega_S}^2 \\ &\quad + C\|\operatorname{as} \zeta_S\|_{0,\Omega_S}^2 \\ &\geq 2C\|\operatorname{div} \zeta_S\|_{0,\Omega_S}^2 + (1-\rho)\|\operatorname{dev} \zeta_S - 2\bar{\mu}_S\varepsilon(\boldsymbol{\eta}_S)\|_{0,\Omega_S}^2 + C\|\nabla \cdot \boldsymbol{\eta}_S\|_{0,\Omega_S}^2 \\ &\quad + C\|\operatorname{as} \zeta_S\|_{0,\Omega_S}^2 - C_{\mu,S}^2\left(\frac{1}{\rho} - 1\right)\|2\bar{\mu}_S\varepsilon(\boldsymbol{\eta}_S)\|_{0,\Omega_S}^2 \\ &= (1-\rho)\left(\frac{2C}{1-\rho}\|\operatorname{div} \zeta_S\|_{0,\Omega_S}^2 + \|\operatorname{dev} \zeta_S - 2\bar{\mu}_S\varepsilon(\boldsymbol{\eta}_S)\|_{0,\Omega_S}^2 + \frac{C}{1-\rho}\|\nabla \cdot \boldsymbol{\eta}_S\|_{0,\Omega_S}^2\right) \\ &\quad + \frac{C}{1-\rho}\|\operatorname{as} \zeta_S\|_{0,\Omega_S}^2 - \frac{C_{\mu,S}^2}{\rho}\|2\bar{\mu}_S\varepsilon(\boldsymbol{\eta}_S)\|_{0,\Omega_S}^2 \\ &\gtrsim \frac{2C}{1-\rho}\|\operatorname{div} \zeta_S\|_{0,\Omega_S}^2 + \|\operatorname{dev} \zeta_S - 2\bar{\mu}_S\varepsilon(\boldsymbol{\eta}_S)\|_{0,\Omega_S}^2 + \frac{C}{1-\rho}\|\nabla \cdot \boldsymbol{\eta}_S\|_{0,\Omega_S}^2 \\ &\quad + \frac{C}{1-\rho}\|\operatorname{as} \zeta_S\|_{0,\Omega_S}^2 - \frac{C_{\mu,S}^2}{\rho}\|2\bar{\mu}_S\varepsilon(\boldsymbol{\eta}_S)\|_{0,\Omega_S}^2 \\ &= 2\tilde{C}\|\operatorname{div} \zeta_S\|_{0,\Omega_S}^2 + \|\operatorname{dev} \zeta_S - 2\bar{\mu}_S\varepsilon(\boldsymbol{\eta}_S)\|_{0,\Omega_S}^2 + \tilde{C}\|\nabla \cdot \boldsymbol{\eta}_S\|_{0,\Omega_S}^2 \\ &\quad + \tilde{C}\|\operatorname{as} \zeta_S\|_{0,\Omega_S}^2 - \frac{C_{\mu,S}^2}{\rho}\|2\bar{\mu}_S\varepsilon(\boldsymbol{\eta}_S)\|_{0,\Omega_S}^2\end{aligned}$$

where we used (3.15) and lemma 3.1 and  $\rho \in (0, 1)$  arbitrary. To keep the proof free of unnecessary constants we set

$$\tilde{C} = \frac{C}{1-\rho}$$

which is then still free to be chosen for a given  $\rho \in (0, 1)$ .

partial integration and the use of Korn's inequality (theorem 2.2) and lemma 2.3 leads to:

$$\begin{aligned}
\mathcal{F}_S(\mathbf{v}_S, \boldsymbol{\tau}_S; \mathbf{f}) &\gtrsim 2\tilde{C}\|\operatorname{div} \boldsymbol{\zeta}_S\|_{0,\Omega_S}^2 + \|\operatorname{dev} \boldsymbol{\zeta}_S\|_{0,\Omega_S}^2 + \|2\bar{\mu}_S \boldsymbol{\varepsilon}(\boldsymbol{\eta}_S)\|_{0,\Omega_S}^2 + \tilde{C}\|\nabla \cdot \boldsymbol{\eta}_S\|_{0,\Omega_S}^2 \\
&\quad + \tilde{C}\|\operatorname{as} \boldsymbol{\zeta}_S\|_{0,\Omega_S}^2 - \frac{C_{\mu,S}^2}{\rho}\|2\bar{\mu}_S \boldsymbol{\varepsilon}(\boldsymbol{\eta}_S)\|_{0,\Omega_S}^2 - 4\bar{\mu}_S(\operatorname{dev} \boldsymbol{\zeta}_S, \boldsymbol{\varepsilon}(\boldsymbol{\eta}_S)) \\
&= 2\tilde{C}\|\operatorname{div} \boldsymbol{\zeta}_S\|_{0,\Omega_S}^2 + \|\operatorname{dev} \boldsymbol{\zeta}_S\|_{0,\Omega_S}^2 + \|2\bar{\mu}_S \boldsymbol{\varepsilon}(\boldsymbol{\eta}_S)\|_{0,\Omega_S}^2 + \tilde{C}\|\nabla \cdot \boldsymbol{\eta}_S\|_{0,\Omega_S}^2 \\
&\quad + \tilde{C}\|\operatorname{as} \boldsymbol{\zeta}_S\|_{0,\Omega_S}^2 - \frac{C_{\mu,S}^2}{\rho}\|2\bar{\mu}_S \boldsymbol{\varepsilon}(\boldsymbol{\eta}_S)\|_{0,\Omega_S}^2 - 4\bar{\mu}_S(\boldsymbol{\zeta}_S, \boldsymbol{\varepsilon}(\boldsymbol{\eta}_S)) + 4\bar{\mu}_S(\operatorname{tr} \boldsymbol{\zeta}_S, \nabla \cdot \boldsymbol{\eta}_S) \\
&= 2\tilde{C}\|\operatorname{div} \boldsymbol{\zeta}_S\|_{0,\Omega_S}^2 + \|\operatorname{dev} \boldsymbol{\zeta}_S\|_{0,\Omega_S}^2 + \|2\bar{\mu}_S \boldsymbol{\varepsilon}(\boldsymbol{\eta}_S)\|_{0,\Omega_S}^2 + \tilde{C}\|\nabla \cdot \boldsymbol{\eta}_S\|_{0,\Omega_S}^2 \\
&\quad + \tilde{C}\|\operatorname{as} \boldsymbol{\zeta}_S\|_{0,\Omega_S}^2 - \frac{C_{\mu,S}^2}{\rho}\|2\bar{\mu}_S \boldsymbol{\varepsilon}(\boldsymbol{\eta}_S)\|_{0,\Omega_S}^2 - 4\bar{\mu}_S(\boldsymbol{\zeta}_S, \nabla \boldsymbol{\eta}_S) + 4\bar{\mu}_S(\operatorname{as} \boldsymbol{\zeta}_S, \operatorname{as} \nabla \boldsymbol{\eta}_S) \\
&\quad + 4\bar{\mu}_S(\operatorname{tr} \boldsymbol{\zeta}_S, \nabla \cdot \boldsymbol{\eta}_S) \\
&= 2\tilde{C}\|\operatorname{div} \boldsymbol{\zeta}_S\|_{0,\Omega_S}^2 + \|\operatorname{dev} \boldsymbol{\zeta}_S\|_{0,\Omega_S}^2 + \|2\bar{\mu}_S \boldsymbol{\varepsilon}(\boldsymbol{\eta}_S)\|_{0,\Omega_S}^2 + \tilde{C}\|\nabla \cdot \boldsymbol{\eta}_S\|_{0,\Omega_S}^2 \\
&\quad + \tilde{C}\|\operatorname{as} \boldsymbol{\zeta}_S\|_{0,\Omega_S}^2 - \frac{C_{\mu,S}^2}{\rho}\|2\bar{\mu}_S \boldsymbol{\varepsilon}(\boldsymbol{\eta}_S)\|_{0,\Omega_S}^2 + 4\bar{\mu}_S(\operatorname{div} \boldsymbol{\zeta}_S, \boldsymbol{\eta}_S) + 4\bar{\mu}_S(\operatorname{as} \boldsymbol{\zeta}_S, \operatorname{as} \nabla \boldsymbol{\eta}_S) \\
&\quad + 4\bar{\mu}_S(\operatorname{tr} \boldsymbol{\zeta}_S, \nabla \cdot \boldsymbol{\eta}_S) \\
&\geq 2\tilde{C}\|\operatorname{div} \boldsymbol{\zeta}_S\|_{0,\Omega_S}^2 + \|\operatorname{dev} \boldsymbol{\zeta}_S\|_{0,\Omega_S}^2 + \|2\bar{\mu}_S \boldsymbol{\varepsilon}(\boldsymbol{\eta}_S)\|_{0,\Omega_S}^2 + \tilde{C}\|\nabla \cdot \boldsymbol{\eta}_S\|_{0,\Omega_S}^2 \\
&\quad + \tilde{C}\|\operatorname{as} \boldsymbol{\zeta}_S\|_{0,\Omega_S}^2 - \frac{C_{\mu,S}^2}{\rho}\|2\bar{\mu}_S \boldsymbol{\varepsilon}(\boldsymbol{\eta}_S)\|_{0,\Omega_S}^2 - \tilde{C}\|\operatorname{div} \boldsymbol{\zeta}_S\|_{0,\Omega_S}^2 - \frac{4\bar{\mu}_S^2}{\tilde{C}}\|\boldsymbol{\eta}_S\|_{0,\Omega_S}^2 \\
&\quad - \tilde{C}\|\operatorname{as} \boldsymbol{\zeta}_S\|_{0,\Omega_S}^2 - \frac{4\bar{\mu}_S^2}{\tilde{C}}\|\operatorname{as} \nabla \boldsymbol{\eta}_S\|_{0,\Omega_S}^2 - \frac{4\bar{\mu}_S^2}{\tilde{C}}\|\operatorname{tr} \boldsymbol{\zeta}_S\|_{0,\Omega_S}^2 - \tilde{C}\|\nabla \cdot \boldsymbol{\eta}_S\|_{0,\Omega_S}^2 \\
&\geq \tilde{C}\|\operatorname{div} \boldsymbol{\zeta}_S\|_{0,\Omega_S}^2 + \|\operatorname{dev} \boldsymbol{\zeta}_S\|_{0,\Omega_S}^2 + \|2\bar{\mu}_S \boldsymbol{\varepsilon}(\boldsymbol{\eta}_S)\|_{0,\Omega_S}^2 \\
&\quad - \frac{C_{\mu,S}^2}{\rho}\|2\bar{\mu}_S \boldsymbol{\varepsilon}(\boldsymbol{\eta}_S)\|_{0,\Omega_S}^2 - \frac{4\bar{\mu}_S^2}{\tilde{C}}\|\boldsymbol{\eta}_S\|_{0,\Omega_S}^2 - \frac{4\bar{\mu}_S^2}{\tilde{C}}\|\operatorname{as} \nabla \boldsymbol{\eta}_S\|_{0,\Omega_S}^2 - \frac{4\bar{\mu}_S^2}{\tilde{C}}\|\operatorname{tr} \boldsymbol{\zeta}_S\|_{0,\Omega_S}^2 \\
&\geq \tilde{C}\|\operatorname{div} \boldsymbol{\zeta}_S\|_{0,\Omega_S}^2 + \|\operatorname{dev} \boldsymbol{\zeta}_S\|_{0,\Omega_S}^2 + \|2\bar{\mu}_S \boldsymbol{\varepsilon}(\boldsymbol{\eta}_S)\|_{0,\Omega_S}^2 \\
&\quad - \frac{C_{\mu,S}^2}{\rho}\|2\bar{\mu}_S \boldsymbol{\varepsilon}(\boldsymbol{\eta}_S)\|_{0,\Omega_S}^2 - \frac{4\bar{\mu}_S^2}{\tilde{C}}\|\boldsymbol{\eta}_S\|_{0,\Omega_S}^2 - \frac{4\bar{\mu}_S^2}{\tilde{C}}\|\nabla \boldsymbol{\eta}_S\|_{0,\Omega_S}^2 \\
&\quad - \frac{4C_S \bar{\mu}_S^2}{\tilde{C}}(\|\operatorname{dev} \boldsymbol{\zeta}_S\|_{0,\Omega_S}^2 + \|\operatorname{div} \boldsymbol{\zeta}_S\|_{0,\Omega_S}^2) \\
&\geq (\tilde{C} - \frac{4C_S \bar{\mu}_S^2}{\tilde{C}})\|\operatorname{div} \boldsymbol{\zeta}_S\|_{0,\Omega_S}^2 + (1 - \frac{4C_S \bar{\mu}_S^2}{\tilde{C}})\|\operatorname{dev} \boldsymbol{\zeta}_S\|_{0,\Omega_S}^2 \\
&\quad + \left(4\bar{\mu}_S^2(1 - \frac{C_{\mu,S}^2}{\rho})C_K - \frac{4\bar{\mu}_S^2}{\tilde{C}}\right)\|\boldsymbol{\eta}_S\|_{1,\Omega_S}^2
\end{aligned}$$

With lemma 3.2 we can choose  $\bar{\mu}_S$  such that  $C_{\mu,S} < 1$ . By setting  $\rho \in (C_{\mu,S}^2, 1)$  it follows

$$\frac{C_{\mu,S}^2}{\rho} < 1$$

Finally one can choose  $\tilde{C}$  large enough to show:

$$\mathcal{F}_S(\mathbf{v}_S, \boldsymbol{\tau}_S; \mathbf{f}) \geq C_{e,S}(\|\mathbf{u}_S - \mathbf{v}_S\|_{1,\Omega_S}^2 + \|\boldsymbol{\sigma}_S - \boldsymbol{\tau}_S\|_{div,\Omega_S}^2)$$

by using the fact that lemma 2.3 implies:

$$\begin{aligned} \|\boldsymbol{\sigma}\|_{div,\Omega_S}^2 &\leq \|\text{dev } \boldsymbol{\zeta}_S\|_{0,\Omega_S}^2 + \frac{1}{d}\|\text{tr } \boldsymbol{\zeta}_S\|_{0,\Omega_S}^2 + \|\text{div } \boldsymbol{\zeta}_S\|_{0,\Omega_S}^2 \\ &\leq \left(1 + \frac{C_S}{d}\right)\|\text{dev } \boldsymbol{\zeta}_S\|_{0,\Omega_S}^2 + \left(1 + \frac{C_S}{d}\right)\|\text{div } \boldsymbol{\zeta}_S\|_{0,\Omega_S}^2 \end{aligned}$$

■

Theorem 3.5 gives us an efficient and reliable a-posteriori error estimator for the nonlinear Stokes problem. This allows us to use efficient adaptive algorithms for the numerical treatment of this problem.

Let a triangulation  $\mathcal{T}_h$  and the conforming FEM-spaces  $V_h \subset (\mathbf{u}_{S_D} + (H_{\Gamma_{S_D}}^1(\Omega_S))^d)$  and  $Q_h \in (\boldsymbol{\sigma}_{S_N} + (H_{\Gamma_{S_N}}^{div}(\Omega_S))^d)$  of chapter 2.3 be given. For the sake of simplicity we assume for both spaces (piecewise polynomials / Raviart-Thomas) the same degree of  $k$ . Assume that  $(\mathbf{v}_{S_h}, \boldsymbol{\tau}_{S_h}) \subset V_h \times Q_h$ . In practical applications one uses this error estimator as a local indicator. We define the following local estimator:

$$\eta_{T_i}^2 = \|\text{div } \boldsymbol{\tau}_{S_h} - \mathbf{f}\|_{0,T_i}^2 + \|\text{dev } \boldsymbol{\tau}_{S_h} - 2(\mu_S(|\varepsilon(\mathbf{v}_{S_h})|^2)\varepsilon(\mathbf{v}_{S_h}))\|_{0,T_i}^2 + \|\nabla \cdot \mathbf{v}_{S_h}\|_{0,T_i}^2$$

Then the global version of this error estimator is given by:

$$\eta^2 = \mathcal{F}_S(\mathbf{v}_{S_h}, \boldsymbol{\tau}_{S_h}) = \sum_{T_i \in \mathcal{T}_h} \eta_{T_i}^2$$

Therefore we can look at the local contribution  $\eta_{T_i}$  to the error for our approximated solution and can refine the triangles where the error is large.

Another consequence of theorem 3.5 are the a priori estimates given in chapter 2.1. Let us assume that for the solution holds

$$\begin{aligned} \mathbf{u}_S &\in (H^{1+t}(\Omega_S))^d \\ \boldsymbol{\sigma}_S &\in (H^m(\Omega_S))^{d \times d} \\ \text{div } \boldsymbol{\sigma}_S &\in (H^s(\Omega_S))^d \end{aligned}$$

with  $s > 0$ ,  $m > 1$  and  $t \geq 0$  and  $s_{min} = \min\{t, m, s, k\}$ . With the interpolation operators of chapter 2.3 and the remark about the general case in chapter 2.1 we get:

$$\begin{aligned} \|\mathbf{u}_S - \mathbf{u}_{S_h}\|_{1,\Omega_S}^2 + \|\boldsymbol{\sigma}_S - \boldsymbol{\sigma}_{S_h}\|_{1,\Omega_S}^2 &\leq \frac{1}{C_{e,S}} \mathcal{F}_S(\mathbf{u}_{S_h}, \boldsymbol{\sigma}_{S_h}) \\ &\leq \frac{C_{s,S}}{C_{e,S}} Ch^{2s_{min}} (\|\mathbf{u}_S\|_{1+t,\Omega_S}^2 + \|\boldsymbol{\sigma}_S\|_{m,\Omega_S}^2 + \|\text{div } \boldsymbol{\sigma}_S\|_{s,\Omega_S}^2) \\ &\leq \tilde{C} h^{2s_{min}} \end{aligned}$$

Therefore by refining the triangulation (with  $h \rightarrow 0$ ) we get if  $s_{min} > 0$

$$\|\mathbf{u}_S - \mathbf{u}_{S_h}\|_{1,\Omega_S}^2 + \|\boldsymbol{\sigma}_S - \boldsymbol{\sigma}_{S_h}\|_{1,\Omega_S}^2 \rightarrow 0$$

with convergence rate  $s_{min}$ .

Another consequence of theorem 3.5 is given by the following corollary

**Corollary 3.6** *Let the assumptions of theorem 3.5 hold. If system 3.3 has a solution  $(\mathbf{u}_S, \boldsymbol{\sigma}_S) = (\mathbf{u}_{S_D}, \boldsymbol{\sigma}_{S_N}) + (\hat{\mathbf{u}}_S, \hat{\boldsymbol{\sigma}}_S)$  with  $(\hat{\mathbf{u}}_S, \hat{\boldsymbol{\sigma}}_S) \in (H_{\Gamma_{S_D}}^1(\Omega_S))^d \times (H_{\Gamma_{S_N}}^{div}(\Omega_S))^d$  the solution is unique.*

**proof:** This is a direct consequence of theorem 3.5. Assume  $(\mathbf{v}_S, \boldsymbol{\tau}_S)$  to be another solution. Inserting these two solutions in theorem 3.5 one gets:

$$C_{s,E}(\|\mathbf{u}_S - \mathbf{v}_S\|_{1,\Omega_S}^2 + \|\boldsymbol{\sigma}_S - \boldsymbol{\tau}_S\|_{div,\Omega_S}^2) \leq \mathcal{F}_S(\mathbf{v}_S, \boldsymbol{\tau}_S; \mathbf{f}) = 0$$

which implies the uniqueness of the solution. ■

The following lemma is important if one wants to use the *Cross-* and *Carreau model*. We can, under assumptions on  $r$  in case of the *Carreau model*, show that the assumptions  $(\mathbf{A1})_S$ ,  $(\mathbf{A2})_S$  and  $(\mathbf{A3})_S$  hold. Furthermore some numbers on  $C_{\mu,S}$  are given if  $1 < r \leq 2$  for the *Carreau model* and  $1 < r \leq 3$  for the *Cross model*. If  $3 < r$  for the *Cross model* we give a not necessarily sharp upper bound..

**Lemma 3.7** *Assumptions  $(\mathbf{A1})_S, (\mathbf{A2})_S$  and  $(\mathbf{A3})_S$  hold for*

- the *Carreau model* if  $1 < r \leq 2$
- the *Cross model* for all  $r > 1$

Furthermore for  $\bar{\mu}_S$  and  $C_{\mu,S}$  in lemma 3.2 it holds:

- *Carreau:*  $C_{\mu,S} = \frac{\mu_0 - \mu_\infty}{\mu_0 + \mu_\infty}$  with  $\bar{\mu}_S = \frac{\mu_0 + \mu_\infty}{2}$  and  $1 < r \leq 2$
- *Cross:*  $C_{\mu,S} = \frac{\mu_0 - \mu_\infty}{\mu_0 + \mu_\infty}$ , with  $\bar{\mu}_S = \frac{\mu_0 + \mu_\infty}{2}$  and  $1 < r \leq 3$
- *Cross:*  $C_{\mu,S} \leq \frac{\frac{r-1}{2}(\mu_0 - \mu_\infty)}{\frac{r-1}{2}(\mu_0 - \mu_\infty) + 2\mu_\infty}$ , with  $\bar{\mu}_S = \frac{\frac{r-1}{2}(\mu_0 - \mu_\infty) + 2\mu_\infty}{2}$  and  $3 < r$

**proof:** It is clear that  $(\mathbf{A1})_S$  holds for both models with the choice of  $\bar{\mu}_S$  as above as for both models it holds:

$$\max_{z \geq 0} \frac{|\mu_S(z) - \bar{\mu}_S|}{\bar{\mu}_S} = \frac{\mu_0 - \mu_\infty}{\mu_0 + \mu_\infty}$$

due to  $\mu_0$  and  $\mu_\infty$  being upper and lower bound for the viscosity.

*Carreau model*

Let  $1 < r \leq 2$  which means we have a *shear-thinning flow* / Newtonian flow. It holds:

$$\begin{aligned} \mu_S(z) &= \mu_\infty + \frac{(\mu_0 - \mu_\infty)}{(1 + Kz)^{\frac{2-r}{2}}} \\ \mu'_S(z) &= \frac{(\mu_0 - \mu_\infty)K(r-2)}{2(1 + Kz)^{2-\frac{r}{2}}} \end{aligned}$$

It is clear that

$$K_0 = \mu_\infty \leq \mu_S(z^2) \leq \mu_0 = K_1$$

which indicates  $(\mathbf{A2})_S$ .

If we show that

$$\mu_\infty \leq \mu_S(z^2) + 2\mu'_S(z^2)z^2 \leq \mu_0$$

holds, we get  $(\mathbf{A3})_S$  with

$$M_1 = \mu_0$$

$$M_0 = \mu_\infty$$

as well as the statement for  $C_{\mu,S}$  from lemma 3.2 if we look at the cases  $z \rightarrow 0$  and  $z \rightarrow \infty$ . To proof this we use:

$$\begin{aligned}\mu_S(z^2) + 2\mu'_S(z^2)z^2 &= \mu_\infty + \frac{(\mu_0 - \mu_\infty)}{(1 + Kz^2)^{\frac{2-r}{2}}} + \frac{(\mu_0 - \mu_\infty)K(r-2)z^2}{(1 + Kz^2)^{2-\frac{r}{2}}} \\ &= \mu_\infty + \frac{(\mu_0 - \mu_\infty)(1 + K(r-1)z^2)}{(1 + Kz^2)^{\frac{4-r}{2}}} \\ &\geq \mu_\infty\end{aligned}$$

At the same time it holds:

$$\begin{aligned}\mu_S(z^2) + 2\mu'_S(z^2)z^2 &= \mu_\infty + \frac{(\mu_0 - \mu_\infty)(1 + K(r-1)z^2)}{(1 + Kz^2)^{\frac{4-r}{2}}} \\ &\leq \mu_\infty + \frac{(\mu_0 - \mu_\infty)(1 + Kz^2)}{(1 + Kz^2)^{\frac{4-r}{2}}} \\ &\leq \mu_\infty + \frac{(\mu_0 - \mu_\infty)}{(1 + Kz^2)^{\frac{2-r}{2}}} \\ &\leq \mu_0\end{aligned}$$

*Cross model*

For the *Cross model* we have

$$\begin{aligned}\mu_S(z) &= \mu_\infty + \frac{(\mu_0 - \mu_\infty)}{1 + Kz^{\frac{2-r}{2}}} \\ \mu'_S(z) &= \frac{(\mu_0 - \mu_\infty)K(r-2)z^{-\frac{r}{2}}}{2(1 + Kz^{\frac{2-r}{2}})^2}\end{aligned}$$

and hence

$$K_0 = \mu_\infty \leq \mu(z^2) \leq \mu_0 = K_1$$

which implies **(A2)<sub>S</sub>**. For **(A3)<sub>S</sub>** we get:

$$\begin{aligned}\mu_S(z^2) + 2\mu'_S(z^2)z^2 &= \mu_\infty + \frac{(\mu_0 - \mu_\infty)}{1 + Kz^{2-r}} + \frac{(\mu_0 - \mu_\infty)K(r-2)z^{2-r}}{(1 + Kz^{2-r})^2} \\ &= \mu_\infty + (\mu_0 - \mu_\infty) \frac{1 + K(r-1)z^{2-r}}{(1 + Kz^{2-r})^2} \geq \mu_\infty\end{aligned}$$

Furthermore it holds

$$\begin{aligned}\mu_S(z^2) + 2\mu'_S(z^2)z^2 &= \mu_\infty + \frac{(\mu_0 - \mu_\infty)}{1 + Kz^{2-r}} + \frac{(\mu_0 - \mu_\infty)K(r-2)z^{2-r}}{(1 + Kz^{2-r})^2} \\ &\leq \mu_\infty + (\mu_0 - \mu_\infty) \frac{1 + 2Kz^{2-r}}{(1 + Kz^{2-r})^2} \\ &\leq \mu_\infty + (\mu_0 - \mu_\infty) \frac{1 + 2Kz^{2-r} + K^2z^{4-2r}}{(1 + Kz^{2-r})^2} \\ &= \mu_0\end{aligned}$$

if  $1 < r \leq 3$ . This implies **(A3)<sub>S</sub>** with

$$M_1 = \mu_0$$

$$M_0 = \mu_\infty$$



as well as the statement for  $C_{\mu,S}$  from lemma 3.2 if we take  $z \rightarrow 0$  and  $z \rightarrow \infty$ .

For  $3 < r$  it holds

$$\begin{aligned}
\mu_S(z^2) + 2\mu'_S(z^2)z^2 &= \mu_\infty + \frac{(\mu_0 - \mu_\infty)}{1 + Kz^{2-r}} + \frac{(\mu_0 - \mu_\infty)K(r-2)z^{2-r}}{(1 + Kz^{2-r})^2} \\
&= \mu_\infty + (\mu_0 - \mu_\infty) \frac{1 + (r-1)Kz^{2-r}}{(1 + Kz^{2-r})^2} \\
&\leq \mu_\infty + (\mu_0 - \mu_\infty) \frac{r-1}{2} \frac{\frac{2}{r-1} + 2Kz^{2-r} + K^2z^{4-2r}}{(1 + Kz^{2-r})^2} \\
&\leq \mu_\infty + (\mu_0 - \mu_\infty) \frac{r-1}{2} \frac{1 + 2Kz^{2-r} + K^2z^{4-2r}}{(1 + Kz^{2-r})^2} \\
&= \mu_\infty + (\mu_0 - \mu_\infty) \frac{r-1}{2} \\
&= \frac{r-1}{2} \mu_0 + \mu_\infty \left(1 - \frac{r-1}{2}\right)
\end{aligned}$$

With Lemma 3.2 and

$$\begin{aligned}
M_1 &\leq \frac{r-1}{2} \mu_0 + \mu_\infty \left(1 - \frac{r-1}{2}\right) \\
M_0 &\geq \mu_\infty
\end{aligned}$$

and  $M_1 \geq \mu_0$  ( $z \rightarrow \infty$ ) the proof is finished. ■

**Remark:** For the *Carreau model* it is only possible to show this lemma for  $r \leq 2$ . If  $r > 2$  the assumptions  $(\mathbf{A3})_S$  and  $(\mathbf{A2})_S$  (see figure 3.2) can not be satisfied. Furthermore we see that for the *Cross model* there is no sharp bound. To find this we have to find the maximum of a nonlinear equation. Though an analytical solution is not known to us one can easily find a numerical solution.

### 3.1.2 The Linearized Problem

As our nonlinear functional has the typical least-squares form we use a Gauß-Newton method. Therefore it is necessary to linearize the partial differential equation: Let

$$\begin{pmatrix} \mathbf{u}_{S_D} + \hat{\mathbf{u}}_S^{(k)} \\ \boldsymbol{\sigma}_{S_N} + \hat{\boldsymbol{\sigma}}_S^{(k)} \end{pmatrix} = \begin{pmatrix} \mathbf{u}_S^{(k)} \\ \boldsymbol{\sigma}_S^{(k)} \end{pmatrix}$$

be given. The functions  $(\hat{\mathbf{u}}_S^{(k)}, \hat{\boldsymbol{\sigma}}_S^{(k)})$  lie in  $(H_{\Gamma_{S_D}}^1(\Omega_S))^d \times (H_{\Gamma_{S_N}}^{div}(\Omega_S))^d$ . We look for an approximation given by

$$\begin{pmatrix} \mathbf{u}_S^{(k+1)} \\ \boldsymbol{\sigma}_S^{(k+1)} \end{pmatrix} = \begin{pmatrix} \mathbf{u}_{S_D} + \hat{\mathbf{u}}_S^{(k+1)} \\ \boldsymbol{\sigma}_{S_N} + \hat{\boldsymbol{\sigma}}_S^{(k+1)} \end{pmatrix} = \begin{pmatrix} \mathbf{u}_S^{(k)} \\ \boldsymbol{\sigma}_S^{(k)} \end{pmatrix} + \begin{pmatrix} \delta \mathbf{u}_S \\ \delta \boldsymbol{\sigma}_S \end{pmatrix}.$$

with  $(\delta \mathbf{u}_S^{(k)}, \delta \boldsymbol{\sigma}_S^{(k)}) \in (H_{\Gamma_{S_D}}^1(\Omega_S))^d \times (H_{\Gamma_{S_N}}^{div}(\Omega_S))^d$ .

The idea of the Gauss-Newton method is to minimize the following quadratic functional given by

$$\mathcal{F}_{quad,S}(\delta \mathbf{u}_S, \delta \boldsymbol{\sigma}_S; \mathbf{u}_S^{(k)}, \mathcal{R}(\mathbf{u}_S^{(k)}, \boldsymbol{\sigma}_S^{(k)}, \mathbf{f}))$$

instead of minimizing the nonlinear functional

$$\mathcal{F}_S(\mathbf{u}_S, \boldsymbol{\sigma}_S; \mathbf{f}).$$

The general case for a nonlinear least-squares functional was briefly discussed in chapter 2.1. Our quadratic functional is given by:

$$\mathcal{F}_{quad,S}(\delta\mathbf{u}_S, \delta\boldsymbol{\sigma}_S; \mathbf{u}_S^{(k)}, \mathcal{R}(\mathbf{u}_S^{(k)}, \boldsymbol{\sigma}_S^{(k)}, \mathbf{f})) = \underbrace{\left\| \begin{pmatrix} \mathcal{R}(\mathbf{u}_S^{(k)}, \boldsymbol{\sigma}_S^{(k)}, \mathbf{f}) \\ \operatorname{div} \boldsymbol{\sigma}_S^{(k)} - \mathbf{f} \\ \operatorname{div} \mathbf{u}_S^{(k)} \\ \operatorname{dev} \boldsymbol{\sigma}_S^{(k)} - 2\mu_S(|\varepsilon(\mathbf{u}_S^{(k)})|^2)\varepsilon(\mathbf{u}_S^{(k)}) \end{pmatrix} \right\|}_{\mathcal{L}(\delta\mathbf{u}_S, \delta\boldsymbol{\sigma}_S; \mathbf{u}_S^{(k)})} + \underbrace{\left\| \begin{pmatrix} \operatorname{div} \delta\boldsymbol{\sigma}_S \\ \operatorname{div} \delta\mathbf{u}_S \\ \operatorname{dev} \delta\boldsymbol{\sigma}_S - 2\mu_S(|\varepsilon(\mathbf{u}_S^{(k)})|^2)\varepsilon(\delta\mathbf{u}_S) - 4\mu'_S(|\varepsilon(\mathbf{u}_S^{(k)})|^2)(\varepsilon(\mathbf{u}_S^{(k)}) : \varepsilon(\delta\mathbf{u}_S))\varepsilon(\mathbf{u}_S^{(k)}) \end{pmatrix} \right\|}_{\mathcal{L}(\delta\mathbf{u}_S, \delta\boldsymbol{\sigma}_S; \mathbf{u}_S^{(k)})}^2_{0, \Omega_S}$$

The variational formulation of the minimization problem is given by:

Find  $(\delta\mathbf{u}_S, \delta\boldsymbol{\sigma}_S) \in (H^1_{\Gamma_{SD}}(\Omega_S))^d \times (H^{div}_{\Gamma_{SN}}(\Omega_S))^d$  such that

$$\left( \mathcal{L}(\delta\mathbf{u}_S, \delta\boldsymbol{\sigma}_S; \mathbf{u}_S^{(k)}), \mathcal{L}(\delta\mathbf{v}_S, \delta\boldsymbol{\tau}_S; \mathbf{u}_S^{(k)}) \right) = - \left( \mathcal{R}(\mathbf{u}_S^{(k)}, \boldsymbol{\sigma}_S^{(k)}, \mathbf{f}), \mathcal{L}(\delta\mathbf{v}_S, \delta\boldsymbol{\tau}_S; \mathbf{u}_S^{(k)}) \right) \quad (3.16)$$

for all  $(\delta\mathbf{v}_S, \delta\boldsymbol{\tau}_S) \in (H^1_{\Gamma_{SD}}(\Omega_S))^d \times (H^{div}_{\Gamma_{SN}}(\Omega_S))^d$

For theorem 3.5 we used that the nonlinear Stokes problem has a solution and therefore the least-squares functional constitutes an error estimator. It has to be noted that for the corresponding linearized pde-problem there might not exist a solution  $(\delta\mathbf{u}_S, \delta\boldsymbol{\sigma}_S)$  s.t.

$$\mathcal{F}_{quad,S}(\delta\mathbf{u}_S, \delta\boldsymbol{\sigma}_S; \mathbf{u}_S^{(k)}, \mathcal{R}(\mathbf{u}_S^{(k)}, \boldsymbol{\sigma}_S^{(k)}, \mathbf{f})) = 0$$

This is neither important nor necessary as we are only interested in the nonlinear problem. Nonetheless we are able to prove that there exists a unique minimum of  $\mathcal{F}_{quad,S}$ .

As we want to mimick the proof of theorem 3.5 we need the following lemma which is similar to lemma 3.1:

**Lemma 3.8** *Assume that  $(\mathbf{A1}_S)$ ,  $(\mathbf{A2}_S)$  and  $(\mathbf{A3}_S)$  hold. Then we have for an arbitrary constant  $\bar{\mu}_S > 0$  :*

$$\begin{aligned} & \|\mu_S(|\varepsilon(\mathbf{u}_S^{(k)})|^2)\varepsilon(\delta\mathbf{u}_S) + 2\mu'_S(|\varepsilon(\mathbf{u}_S^{(k)})|^2)(\varepsilon(\mathbf{u}_S^{(k)}) : \varepsilon(\delta\mathbf{u}_S))\varepsilon(\mathbf{u}_S^{(k)}) - \bar{\mu}_S\varepsilon(\delta\mathbf{u}_S)\|_{0, \Omega_S} \\ & \leq C_{\mu,S}^{quad} \cdot \bar{\mu}_S \|\varepsilon(\delta\mathbf{u}_S)\|_{0, \Omega_S} \end{aligned} \quad (3.17)$$

which holds for all  $\delta\mathbf{u}_S \in (H^1(\Omega_S))^d$  with a constant  $C_{\mu,S}(\bar{\mu}_S)$  given by

$$C_{\mu,S}^{quad} := \frac{\max\{|\mu_S(|\varepsilon(\mathbf{u}_S^{(k)})|^2) - \bar{\mu}_S|, |\mu_S(|\varepsilon(\mathbf{u}_S^{(k)})|^2) - \bar{\mu}_S + 2\mu'_S(|\varepsilon(\mathbf{u}_S^{(k)})|^2)|\varepsilon(\mathbf{u}_S^{(k)})|^2|\}}{\bar{\mu}_S} < \infty \quad (3.18)$$

**proof:** This lemma is basically a consequence of lemma 3.1. In the proof we used the following operator

$$S(\xi) := (\mu_S(|\xi|^2) - \bar{\mu}_S)\xi. \quad (3.19)$$

Setting

$$\begin{aligned} \xi & := \varepsilon(\mathbf{u}_S^{(k)}) \\ \chi & := \varepsilon(\delta\mathbf{u}_S) \end{aligned}$$

We got for the directional derivative

$$\begin{aligned}
|S'(\xi)[\chi]| &= \left| \lim_{h \rightarrow 0} \frac{S(\xi + h\chi)}{h} \right| \\
&= \left| \frac{d}{dh} S(\xi + h\chi) \Big|_{h=0} \right| \\
&= |(\mu_S(|\xi|) - \bar{\mu}_S)\chi + 2\mu'_S(|\xi|^2) \cdot (\xi : \chi) \cdot \xi|
\end{aligned}$$

Inserting  $\xi$  and  $\chi$  as above we get the left hand side of 3.17. We then only have to prove that

$$|S'(\xi)[\chi]| \leq C_{\mu,S}^{quad} \bar{\mu}_S |\chi|$$

which was already done in lemma 3.1 for the more general case of arbitrary  $\xi$ . Using the  $C_{\mu,S}$  from lemma 3.1 the proof is completed. ■

As for the nonlinear case we get the following lemma:

**Lemma 3.9** *Let the assumptions of lemma 3.8 hold. Then there exists a  $\bar{\mu}_S$  such that for  $C_{\mu,S}^{quad}$  it holds:*

$$C_{\mu,S}^{quad} < 1$$

**proof:** Analog to lemma 3.2 ■

Now we are able to proof that the linearized minimization problem has a unique solution.

**Theorem 3.10** *Let assumptions  $(A1)_S$ ,  $(A2)_S$  and  $(A3)_S$  hold. Furthermore  $\Gamma_{S_D} = \partial\Omega_S$  holds. For the quadratic approximation of the least-squares functional the following holds:*

$$C_{e,S}^{quad} (\|\mathbf{v}_S\|_{1,\Omega_S}^2 + \|\boldsymbol{\tau}_S\|_{div,\Omega_S}^2) \leq \mathcal{F}_{quad,S}(\mathbf{v}_S, \boldsymbol{\tau}_S; \mathbf{u}_S^{(k)}, \mathbf{0}) \leq C_{s,S}^{quad} (\|\mathbf{v}_S\|_{1,\Omega_S}^2 + \|\boldsymbol{\tau}_S\|_{div,\Omega_S}^2)$$

for all  $(\mathbf{v}_S, \boldsymbol{\tau}_S) \in (H_{\Gamma_{S_D}}^1(\Omega_S))^d \times (H_{\Gamma_{S_N}}^{div}(\Omega_S))^d$  with positive constants  $C_{e,S}^{quad}$  and  $C_{s,S}^{quad}$ . Furthermore the variational problem 3.16 has a unique solution.

**proof:** The proof is more or less identical to the proof of theorem 3.5. Though we shortly sketch the difference:

For the upper bound we use

$$\begin{aligned}
&\mathcal{F}_{quad,S}(\mathbf{v}_S, \boldsymbol{\tau}_S; \mathbf{u}_S^{(k)}, \mathbf{0}) \\
&\leq \|\operatorname{div} \boldsymbol{\tau}_S\|_{0,\Omega_S}^2 + \|\operatorname{dev} \boldsymbol{\tau}_S\|_{0,\Omega_S}^2 + \|\nabla \cdot \mathbf{v}_S\|_{0,\Omega_S}^2 \\
&\quad + 8\|\mu_S(|\varepsilon(\mathbf{u}_S^{(k)})|^2)\varepsilon(\mathbf{v}_S) + 2\mu'_S(|\varepsilon(\mathbf{u}_S^{(k)})|^2)(\varepsilon(\mathbf{u}_S^{(k)}) : \varepsilon(\mathbf{v}_S))\varepsilon(\mathbf{u}_S^{(k)}) - \bar{\mu}_S\varepsilon(\mathbf{v}_S)\|_{0,\Omega_S}^2 \\
&\quad + 2\|2\bar{\mu}_S\varepsilon(\mathbf{v}_S)\|_{0,\Omega_S}^2 \\
&\leq C_{s,S}^{quad} (\|\operatorname{div} \boldsymbol{\tau}_S\|_{0,\Omega_S}^2 + \|\boldsymbol{\tau}_S\|_{0,\Omega_S}^2 + \|\varepsilon(\mathbf{v}_S)\|_{0,\Omega_S}^2) \\
&\leq C_{s,S}^{quad} (\|\mathbf{v}_S\|_{1,\Omega_S}^2 + \|\boldsymbol{\tau}_S\|_{div,\Omega_S}^2)
\end{aligned}$$

using lemma 3.8 and the same arguments as in theorem 3.5. For the lower bound we start with

$$\begin{aligned}
\mathcal{F}_{quad,S}(\mathbf{v}_S, \boldsymbol{\tau}_S; \mathbf{u}_S^{(k)}, \mathbf{0}) &= \|\operatorname{div} \boldsymbol{\tau}_S\|_{0,\Omega_S}^2 + \|\nabla \cdot \mathbf{v}_S\|_{0,\Omega_S}^2 \\
&\quad + \|\operatorname{dev} \boldsymbol{\tau}_S - 2\mu_S(|\varepsilon(\mathbf{u}_S^{(k)})|^2)\varepsilon(\mathbf{v}_S) - 4\mu'_S(|\varepsilon(\mathbf{u}_S^{(k)})|^2)(\varepsilon(\mathbf{u}_S^{(k)}) : \varepsilon(\mathbf{v}_S))\varepsilon(\mathbf{u}_S^{(k)})\|_{0,\Omega_S}^2 \\
&\geq 2\tilde{C}\|\operatorname{div} \boldsymbol{\tau}_S\|_{0,\Omega_S}^2 + \tilde{C}\|\nabla \cdot \mathbf{v}_S\|_{0,\Omega_S}^2 + \|\operatorname{dev} \boldsymbol{\tau}_S - 2\bar{\mu}_S\varepsilon(\mathbf{v}_S)\|_{0,\Omega_S}^2 + \tilde{C}\|\operatorname{as} \boldsymbol{\zeta}_S\|_{0,\Omega_S} \\
&\quad - \frac{1}{\rho}\|2\mu_S(|\varepsilon(\mathbf{u}_S^{(k)})|^2)\varepsilon(\mathbf{v}_S) - 4\mu'_S(|\varepsilon(\mathbf{u}_S^{(k)})|^2)(\varepsilon(\mathbf{u}_S^{(k)}) : \varepsilon(\mathbf{v}_S))\varepsilon(\mathbf{u}_S^{(k)}) - 2\bar{\mu}_S\varepsilon(\mathbf{v}_S)\|_{0,\Omega_S}^2 \\
&\geq 2\tilde{C}\|\operatorname{div} \boldsymbol{\tau}_S\|_{0,\Omega_S}^2 + \tilde{C}\|\nabla \cdot \mathbf{v}_S\|_{0,\Omega_S}^2 + \|\operatorname{dev} \boldsymbol{\tau}_S - 2\bar{\mu}_S\varepsilon(\mathbf{v}_S)\|_{0,\Omega_S}^2 + \tilde{C}\|\operatorname{as} \boldsymbol{\zeta}_S\|_{0,\Omega_S} \\
&\quad - \frac{(C_{\mu,S}^{quad})^2}{\rho}\|2\bar{\mu}_S\varepsilon(\mathbf{v}_S)\|_{0,\Omega_S}^2
\end{aligned}$$

where we used lemma 3.8 and the constants analog to theorem 3.5. The rest of the proof for the lower bound follows by mimicking the proof of theorem 3.5.

The last part of having a unique solution follows by noting

$$\begin{aligned}
\mathcal{F}_{quad,S}(\mathbf{v}_S, \boldsymbol{\tau}_S; \mathbf{u}_S^{(k)}, \mathbf{0}) &= \left( \mathcal{L}(\mathbf{v}_S, \boldsymbol{\tau}_S; \mathbf{u}_S^{(k)}), \mathcal{L}(\mathbf{v}_S, \boldsymbol{\tau}_S; \mathbf{u}_S^{(k)}) \right) \\
&= \|\mathcal{L}(\mathbf{v}_S, \boldsymbol{\tau}_S; \mathbf{u}_S^{(k)})\|_{0,\Omega_S}^2
\end{aligned}$$

Therefore  $\mathcal{F}_{quad,S}(\mathbf{v}_S, \boldsymbol{\tau}_S; \mathbf{u}_S^{(k)}, \mathbf{0})$  is elliptic and continuous. As a result for the associated bilinear form it holds (compare chapter 2.1):

$$\begin{aligned}
\left( \mathcal{L}(\mathbf{v}_S, \boldsymbol{\tau}_S; \mathbf{u}_S^{(k)}), \mathcal{L}(\mathbf{v}_S, \boldsymbol{\tau}_S; \mathbf{u}_S^{(k)}) \right) &\geq C_{e,S}^{quad} (\|\mathbf{v}_S\|_{1,\Omega_S}^2 + \|\boldsymbol{\tau}_S\|_{div,\Omega_S}^2) \\
\left( \mathcal{L}(\mathbf{v}_S, \boldsymbol{\tau}_S; \mathbf{u}_S^{(k)}), \mathcal{L}(\mathbf{z}_S, \boldsymbol{\zeta}_S; \mathbf{u}_S^{(k)}) \right) &\leq C_{s,S}^{quad} (\|\mathbf{v}_S\|_{1,\Omega_S}^2 + \|\boldsymbol{\tau}_S\|_{div,\Omega_S}^2)^{\frac{1}{2}} (\|\mathbf{z}_S\|_{1,\Omega_S}^2 + \|\boldsymbol{\zeta}_S\|_{div,\Omega_S}^2)^{\frac{1}{2}}
\end{aligned}$$

which holds for all  $(\mathbf{v}_S, \boldsymbol{\tau}_S) \in (H_{\Gamma_{SD}}^1(\Omega_S))^d \times (H_{\Gamma_{SN}}^{div}(\Omega_S))^d$ ,  $(\mathbf{z}_S, \boldsymbol{\zeta}_S) \in (H_{\Gamma_{SD}}^1(\Omega_S))^d \times (H_{\Gamma_{SN}}^{div}(\Omega_S))^d$

Furthermore we have

$$\begin{aligned}
\left( \mathcal{R}(\mathbf{u}_S^{(k)}, \boldsymbol{\sigma}_S^{(k)}, \mathbf{f}), \mathcal{L}(\mathbf{v}_S, \boldsymbol{\tau}_S; \mathbf{u}_S^{(k)}) \right) &\leq \|\mathcal{R}(\mathbf{u}_S^{(k)}, \boldsymbol{\sigma}_S^{(k)}, \mathbf{f})\|_{0,\Omega_S} \|\mathcal{L}(\delta\mathbf{v}_S, \delta\boldsymbol{\tau}_S; \mathbf{u}_S^{(k)})\|_{0,\Omega_S} \\
&\leq \|\mathcal{R}(\mathbf{u}_S^{(k)}, \boldsymbol{\sigma}_S^{(k)}, \mathbf{f})\|_{0,\Omega_S} (C_{s,S}^{quad} (\|\mathbf{v}_S\|_{1,\Omega_S}^2 + \|\boldsymbol{\tau}_S\|_{div,\Omega_S}^2))^{\frac{1}{2}} \\
&\leq C (\|\mathbf{v}_S\|_{1,\Omega_S}^2 + \|\boldsymbol{\tau}_S\|_{div,\Omega_S}^2)^{\frac{1}{2}}
\end{aligned}$$

as  $\|\mathcal{R}(\mathbf{u}_S^{(k)}, \boldsymbol{\sigma}_S^{(k)}, \mathbf{f})\|_{0,\Omega_S}$  is bounded due to  $\mathcal{R}(\mathbf{u}_S^{(k)}, \boldsymbol{\sigma}_S^{(k)}, \mathbf{f})$  being in  $L^2(\Omega_S)$ . Therefore the right hand side of the variational problem is continuous. So the requirements of Lax-Milgram are satisfied and (3.16) has a unique solution. ■

For the directional derivative of the nonlinear least-squares functional we have:

$$\mathcal{F}'_S(\mathbf{u}_S^{(k)}, \boldsymbol{\sigma}_S^{(k)}, \mathbf{f}) \begin{bmatrix} \mathbf{v}_S \\ \boldsymbol{\tau}_S \end{bmatrix} = 2 \left( \mathcal{R}(\mathbf{u}_S^{(k)}, \boldsymbol{\sigma}_S^{(k)}, \mathbf{f}), \mathcal{L}(\mathbf{v}_S, \boldsymbol{\tau}_S; \mathbf{u}_S^{(k)}) \right)$$

Inserting the unique solution of the linearized problem (3.16) we get

$$\begin{aligned}
\mathcal{F}'_S(\mathbf{u}_S^{(k)}, \boldsymbol{\sigma}_S^{(k)}, \mathbf{f}) \begin{bmatrix} \delta\mathbf{u}_S \\ \delta\boldsymbol{\sigma}_S \end{bmatrix} &= -2 \left( \mathcal{L}(\delta\mathbf{u}_S, \delta\boldsymbol{\sigma}_S; \mathbf{u}_S^{(k)}), \mathcal{L}(\delta\mathbf{u}_S, \delta\boldsymbol{\sigma}_S; \mathbf{u}_S^{(k)}) \right) \\
&\leq -2C_{e,S}^{quad} (\|\delta\mathbf{u}_S\|_{1,\Omega_S}^2 + \|\delta\boldsymbol{\sigma}_S\|_{div,\Omega_S}^2)
\end{aligned}$$

and therefore we have always a reduction of the nonlinear least-squares functional by using the direction defined by the solution for the linearized problem.

Finally we are able to prove a corollary for our approach for the numerical solution:

**Corollary 3.11** *It holds*

- for the *Cross model*:  $1 < r < \infty$

- for the *Carreau model*:  $1 < r \leq 2$

and  $\Gamma_{S_D} = \partial\Omega_S$ . We then have for the solution  $(\mathbf{u}_S, \boldsymbol{\sigma}_S) = (\mathbf{u}_{S_D}, \boldsymbol{\sigma}_{S_N}) + (\hat{\mathbf{u}}_S, \hat{\boldsymbol{\sigma}}_S)$  with  $(\hat{\mathbf{u}}_S, \hat{\boldsymbol{\sigma}}_S) \in (H^1_{\Gamma_{S_D}}(\Omega_S))^d \times (H^{div}_{\Gamma_{S_N}}(\Omega_S))^d$  of (3.3) :

$C_{e,S}(\|\mathbf{u}_S - \mathbf{v}_S\|_{1,\Omega_S}^2 + \|\boldsymbol{\sigma}_S - \boldsymbol{\tau}_S\|_{div,\Omega_S}^2) \leq \mathcal{F}_S(\mathbf{v}_S, \boldsymbol{\tau}_S; \mathbf{f}) \leq C_{s,S}(\|\mathbf{u}_S - \mathbf{v}_S\|_{1,\Omega_S}^2 + \|\boldsymbol{\sigma}_S - \boldsymbol{\tau}_S\|_{div,\Omega_S}^2)$   
for all  $(\mathbf{v}_S, \boldsymbol{\tau}_S) = (\mathbf{u}_{S_D}, \boldsymbol{\sigma}_{S_N}) + (\hat{\mathbf{v}}_S, \hat{\boldsymbol{\tau}}_S)$  with  $(\hat{\mathbf{v}}_S, \hat{\boldsymbol{\tau}}_S) \in (H^1_{\Gamma_{S_D}}(\Omega_S))^d \times (H^{div}_{\Gamma_{S_N}}(\Omega_S))^d$  with positive constants  $C_{e,S}$  und  $C_{s,S}$ .

Furthermore the sequence

$$\begin{pmatrix} \mathbf{u}_S^{(k+1)} \\ \boldsymbol{\sigma}_S^{(k+1)} \end{pmatrix} = \begin{pmatrix} \mathbf{u}_S^{(k)} \\ \boldsymbol{\sigma}_S^{(k)} \end{pmatrix} + \alpha \begin{pmatrix} \delta \mathbf{u}_S \\ \delta \boldsymbol{\sigma}_S \end{pmatrix}.$$

with  $(\delta \boldsymbol{\sigma}_S, \delta \mathbf{u}_S)$  from solving problem (3.16) is well defined for all  $\alpha > 0$ . By choosing  $\alpha > 0$  small enough it holds:

$$\mathcal{F}_S(\mathbf{u}_S^{(k+1)}, \boldsymbol{\sigma}_S^{(k+1)}; \mathbf{f}) < \mathcal{F}_S(\mathbf{u}_S^{(k)}, \boldsymbol{\sigma}_S^{(k)}; \mathbf{f})$$

if  $(\mathbf{u}_S^{(k)}, \boldsymbol{\sigma}_S^{(k)})$  is not a stationary point of  $\mathcal{F}_S$ .

**proof:** This is a direct consequence of lemma 3.7, theorem 3.5 and 3.10 combined with the remark of the descendent direction  $(\delta \boldsymbol{\sigma}_S, \delta \mathbf{u}_S)$  of  $\mathcal{F}_S(\mathbf{u}_S^{(k)}, \boldsymbol{\sigma}_S^{(k)}; \mathbf{f})$ . ■

The implication of Corollary 3.11 is interesting for our numerical results. We can use the *Cross model* for arbitrary  $r$  and the *Carreau model* for shear-thinning flows. The use of the least-squares functional as an a-posteriori error estimator is then justified by Corollary 3.11. Furthermore we only have to solve symmetric positive equation systems by using a conforming method. Furthermore the consequences of the a priori estimates hold if the solution is regular enough.

### 3.1.3 Numerical Examples

Let a triangulation  $\mathcal{T}_h$  of  $\Omega_S$  be given. In this section we always use the space of piecewise quadratic and continuous functions (see chapter 2.3)  $(\mathcal{P}_2(\mathcal{T}_h))^2 \subset (H^1(\Omega_S))^2$  for the velocity:

$$\mathbf{u}_{S_h} \in (\mathcal{P}_2(\mathcal{T}_h))^2 \subset (H^1(\Omega_S))^2$$

For the stress  $\boldsymbol{\sigma}_S$  we use the space of Raviart-Thomas functions  $(RT_1(\mathcal{T}_h))^2$  consisting of piecewise quadratic polynomials on each triangle (see chapter 2.3):

$$\boldsymbol{\sigma}_{S_h} \in (RT_1(\mathcal{T}_h))^2 \subset (H^{div}(\Omega_S))^2$$

In this part we discuss several numerical examples for a shear thinning and shear thickening case.

For the plots in chapter 3 and 4 we made use of the pde toolbox of matlab. Additionally we used the following tools

- *distmesh2d* as mesh generator [PS04]: Initial triangulations
- The LS-MFE toolbox [KS]: local/global representation of basis functions, basic tools for triangulations

for the above mentioned functionality.

### 3.1.3.1 Example I

We start with a regular example. For this example we use a slightly altered example given in [DQ09] for the case of linear Stokes flow. We have to adapt this problem for our non Newtonian flows which results in a more complicated forcing term  $\mathbf{f}$  to ensure that the unique solution is known. Let

$$\begin{aligned}\Omega_S &= (0 \times 1) \times (1 \times 2) \\ \Gamma_{D_S} &= \partial\Omega\end{aligned}$$

The unique solution shall be given by:

$$\begin{aligned}\mathbf{u}_S &= \begin{pmatrix} -\sin(\frac{\pi}{2}x_1) \cdot \cos(\frac{\pi}{2}x_2) \\ \cos(\frac{\pi}{2}x_1) \cdot \sin(\frac{\pi}{2}x_2) - 1 + x_1 \end{pmatrix} \quad \text{in } \Omega_S \\ \text{tr}\boldsymbol{\sigma} &= -2p_S = 1 - 2x_1 \\ \boldsymbol{\sigma}_S &= \mu_S(|\varepsilon(\mathbf{u}_S)|^2) \begin{pmatrix} -\pi \cos(\frac{\pi}{2}x_1) \cos(\frac{\pi}{2}x_2) & 1 \\ 1 & \pi \cos(\frac{\pi}{2}x_1) \cos(\frac{\pi}{2}x_2) \end{pmatrix} + \frac{1}{2} \begin{pmatrix} 1 - 2x_1 & 0 \\ 0 & 1 - 2x_1 \end{pmatrix}\end{aligned}$$

We therefore have to construct an appropriate forcing term  $\mathbf{f}$  dependant on  $\mathbf{u}_S$ , the viscosity  $\mu_S(|\varepsilon(\mathbf{u}_S)|^2)$  and the derivative of the viscosity  $\frac{\partial\mu_S}{\partial r}(|\varepsilon(\mathbf{u}_S)|^2)$ . With

$$\begin{aligned}|\varepsilon(\mathbf{u}_S)|^2 &= \frac{\pi^2}{2} \cos^2(\frac{\pi}{2}x_1) \cos^2(\frac{\pi}{2}x_2) + \frac{1}{2} \\ \frac{\partial\mu_S(|\varepsilon(\mathbf{u}_S)|^2)}{\partial x_1} &= - \left( \frac{\partial\mu_S}{\partial r}(|\varepsilon(\mathbf{u}_S)|^2) \right) \left( \frac{\pi^3}{2} \cos(\frac{\pi}{2}x_1) \sin(\frac{\pi}{2}x_1) \cos^2(\frac{\pi}{2}x_2) \right) \\ \frac{\partial\mu_S(|\varepsilon(\mathbf{u}_S)|^2)}{\partial x_2} &= - \left( \frac{\partial\mu_S}{\partial r}(|\varepsilon(\mathbf{u}_S)|^2) \right) \left( \frac{\pi^3}{2} \cos(\frac{\pi}{2}x_2) \sin(\frac{\pi}{2}x_2) \cos^2(\frac{\pi}{2}x_1) \right)\end{aligned}$$

we get

$$\mathbf{f} = \begin{pmatrix} -\pi \frac{\partial\mu_S(|\varepsilon(\mathbf{u}_S)|^2)}{\partial x_1} \cos(\frac{\pi}{2}x_1) \cos(\frac{\pi}{2}x_2) + \mu_S(|\varepsilon(\mathbf{u}_S)|^2) \frac{\pi^2}{2} \sin(\frac{\pi}{2}x_1) \cos(\frac{\pi}{2}x_2) - 1 + \frac{\partial\mu_S(|\varepsilon(\mathbf{u}_S)|^2)}{\partial x_2} \\ \frac{\partial\mu_S(|\varepsilon(\mathbf{u}_S)|^2)}{\partial x_1} + \frac{\partial\mu_S(|\varepsilon(\mathbf{u}_S)|^2)}{\partial x_2} \pi \cos(\frac{\pi}{2}x_1) \cos(\frac{\pi}{2}x_2) - \mu_S(|\varepsilon(\mathbf{u}_S)|^2) \frac{\pi^2}{2} \cos(\frac{\pi}{2}x_1) \sin(\frac{\pi}{2}x_2) \end{pmatrix}$$

using this  $\mathbf{f}$  as forcing term results in solutions  $\mathbf{u}_S \in (C^\infty(\Omega_S))^2$  and  $\boldsymbol{\sigma}_S \in (C^\infty(\Omega_S))^{2 \times 2}$  as given above. For our problem we set the boundary conditions to

$$\mathbf{u}_S = \begin{pmatrix} -\sin(\frac{\pi}{2}x_1) \cdot \cos(\frac{\pi}{2}x_2) \\ \cos(\frac{\pi}{2}x_1) \cdot \sin(\frac{\pi}{2}x_2) - 1 + x_1 \end{pmatrix} \quad \text{on } \Gamma_{S_D}$$

and the forcing term  $\mathbf{f}$  as stated before. Our necessary normalization of the reference pressure given by

$$\int_{\Omega_S} \text{tr } \boldsymbol{\sigma}_S dx = 0$$

is satisfied by the solution as well.

The behavior of the Newtonian case is easily predictable to be optimal in the sense of convergence rates. For this first example we want to compare it to the non-Newtonian case though we expect optimal convergence rates due to corollary 3.11. This corresponds to  $s_{min} = 2$  in the remark after theorem 3.5. The plot of the velocity  $\mathbf{u}_S$  and  $|\varepsilon(\mathbf{u}_S)|^2$  can be found in 3.3. It has to be noted that we can easily get the pressure by post-processing (see (3.4)):

$$p_{S_h} = -\frac{1}{2}\text{tr}\sigma_{S_h}$$

By approximating  $\sigma_{S_h}$  in  $(H^{div}(\Omega_S))^d$  we approximate  $p_S$  by  $p_{S_h} \in L^2(\Omega_S)$ . We will see that we achieve optimal convergence rates of 2 for the error  $\|p_S - p_{S_h}\|_{0,\Omega_S}^2$  as well.

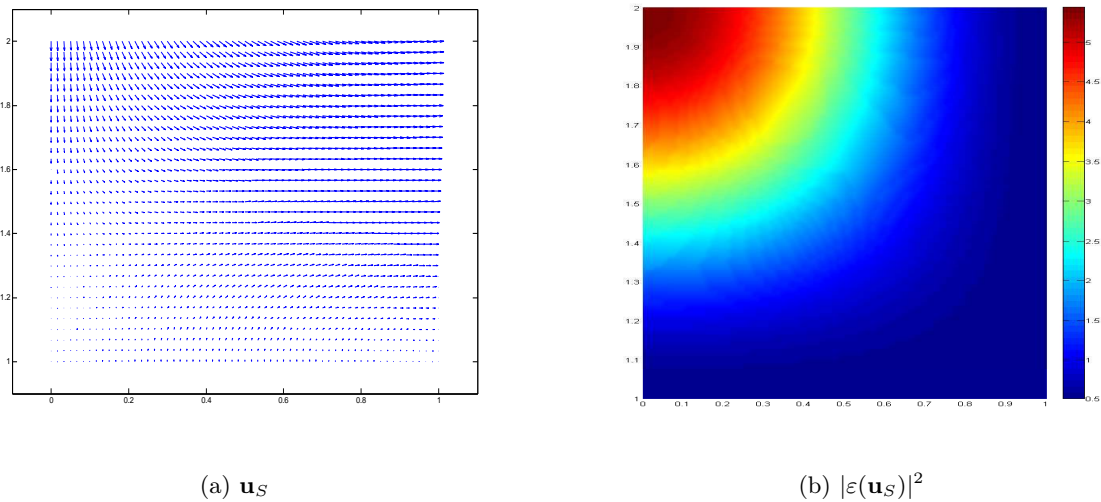


Figure 3.3: Plots of  $\mathbf{u}_S$  /  $|\varepsilon(\mathbf{u}_S)|^2$

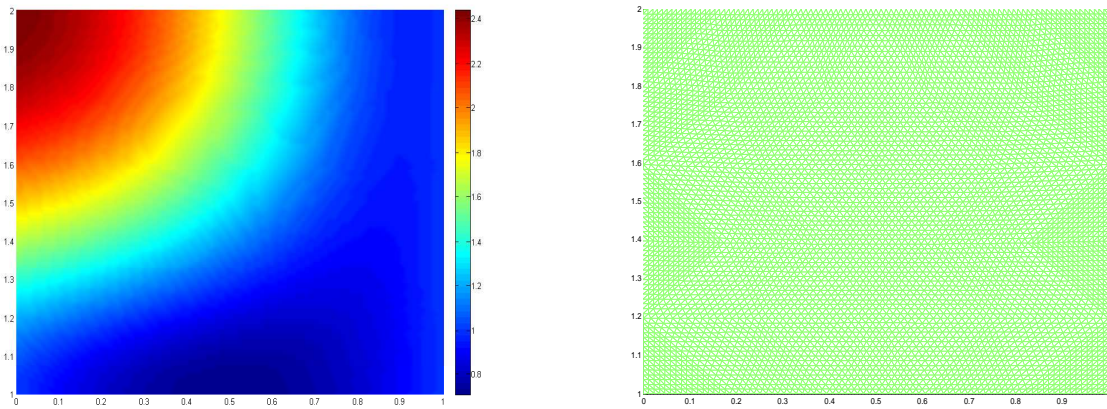
### The linear case

For this case we set the viscosity to  $\mu_S = 0.5005$  which is the mean value of  $\mu_\infty$  and  $\mu_0$  for the following nonlinear cases. As stated before we expect the solution of the discrete problem to converge with a convergence rate of 2. For the LSF in theorem 3.5 this means that the reduction of  $\mathcal{F}_S(\mathbf{u}_{S_h}, \sigma_{S_h})$  by halving  $h$  which means a quadruplication of  $\#T(\mathcal{T}_h)$  happens by a factor of  $\frac{1}{16}$ . This behavior of the convergence rates is visible in figure 3.5 and the values of the LSF and the actual error are given in table 3.1. We see optimal convergence rates for the least-squares functional as well as for the errors as expected. Very small variations might be due to boundary conditions / quadrature errors. The norm of the stress can be observed in 3.4. This constructed problem is mainly of theoretical interest to observe the convergence rates for regular solutions. We take a closer look at more interesting/difficult problems later in this section.

We won't use an adaptive algorithm as it is not expected to deliver better results.

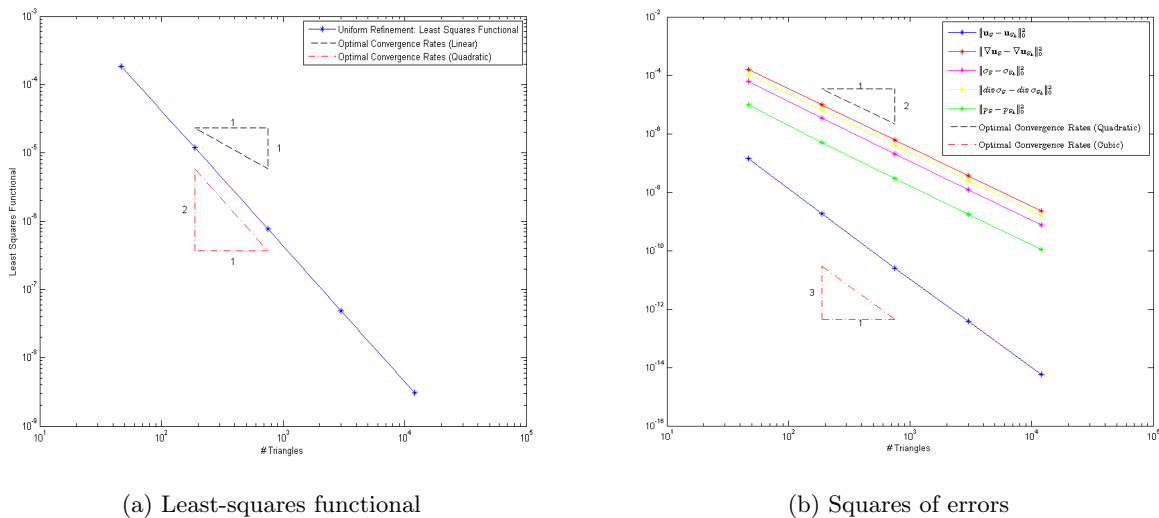
level	# triangles	# dofs	$\mathcal{F}_S$	$\ \sigma_S - \sigma_{S_h}\ _{div}^2$	$\ \mathbf{u}_S - \mathbf{u}_{S_h}\ _1^2$
0	47	744	1.8633e-04	1.6353e-04	1.5939e-04
1	188	2802	1.2058e-05	9.8556e-06	9.8165e-06
2	752	10866	7.6980e-07	6.0240e-07	5.9640e-07
3	3008	42786	4.8662e-08	3.7174e-08	3.6513e-08
4	12032	169794	3.0589e-09	2.3080e-09	2.2562e-09

Table 3.1: LSF and errors (example 1): Newtonian flow



(a) Stress

(b) Triangulation

Figure 3.4: Plots of  $|\sigma_{S_h}|$  and the triangulation: Newtonian flow

(a) Least-squares functional

(b) Squares of errors

Figure 3.5: Convergence Rates : Newtonian flow



### The shear thinning case

For this example we take a closer look at the *Cross model* and the *Carreau model* and observe how these models behave in this highly regular case. The forcing term  $\mathbf{f}$  is set as before with respect to the different viscosities. As for the constants we set

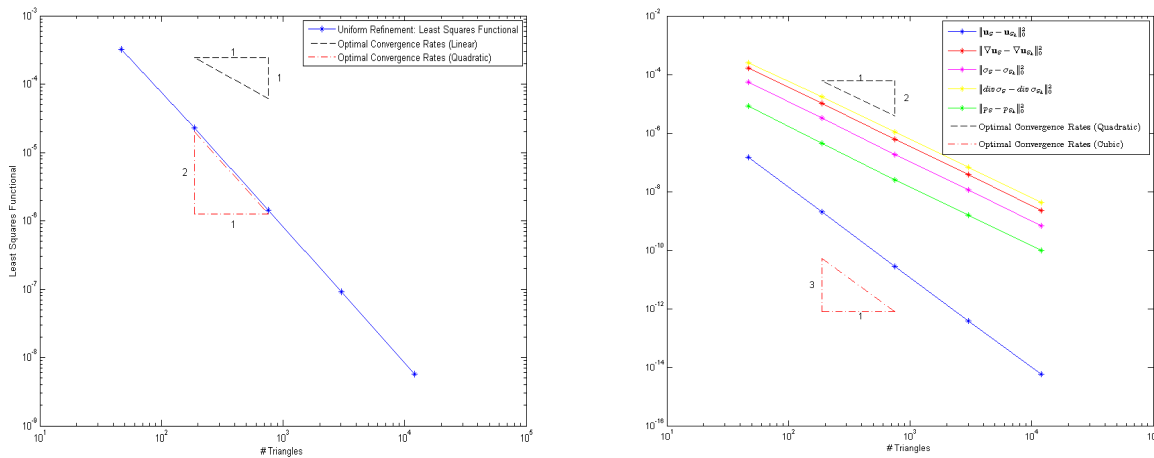
$$\begin{aligned} K &= 1 \\ \mu_\infty &= 10^{-3} \\ \mu_0 &= 1 \\ r &= 1.5 \end{aligned}$$

It has to be noted that the constants of the *Cross model* and *Carreau model* are not the same despite the same usage. Therefore these constants do not describe the same flow problems. There are major differences in the magnitude of stress and viscosity.

Corollary 3.11 states that the least-squares functional is an efficient and reliable error estimator for this case. As stated before we can expect in this case optimal convergence rates as in the linear case. These can be observed in figure 3.6 with the LSF and errors given in table 3.2.

level	# triangles	# dofs	$\mathcal{F}_S$	$\ \sigma_S - \sigma_{S_h}\ _{div}^2$	$\ \mathbf{u}_S - \mathbf{u}_{S_h}\ _1^2$
0	47	744	3.2549e-04	3.0270e-04	1.6573e-04
1	188	2802	2.2645e-05	2.0508e-05	1.0228e-05
2	752	10866	1.4432e-06	1.2802e-06	6.1327e-07
3	3008	42786	9.0979e-08	7.9744e-08	3.7087e-08
4	12032	169794	5.7083e-09	4.9724e-09	2.2748e-09

Table 3.2: LSF and errors (example 1): *Cross* / shear thinning



(a) Least-squares functional

(b) Squares of errors

Figure 3.6: Convergence Rates : *Cross* / shear thinning

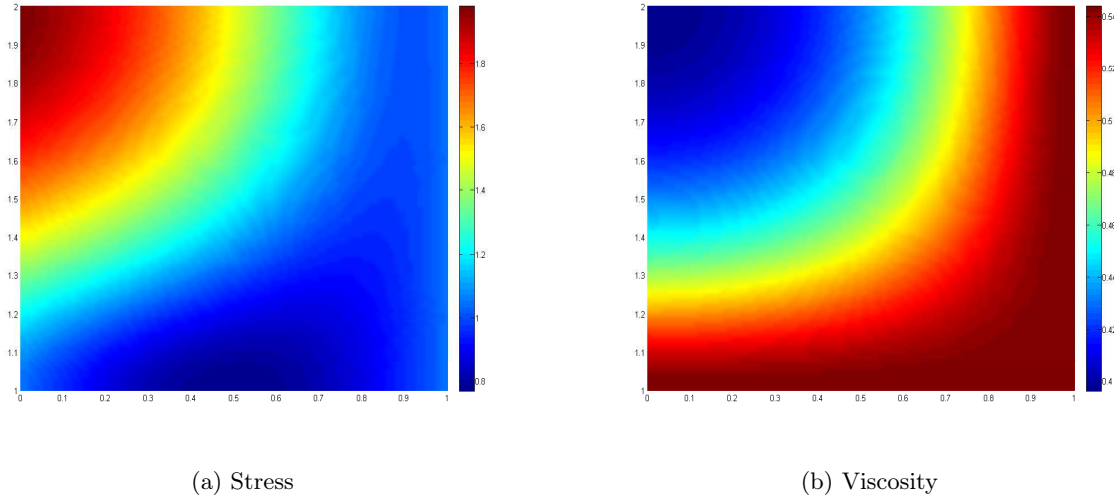


Figure 3.7: Plots of  $|\boldsymbol{\sigma}_{S_h}|$  and the viscosity  $\mu_S(\boldsymbol{\varepsilon}(\mathbf{u}_{S_h}))$ : *Cross* / shear thinning

Though as we have a shear thinning case we expect the stress and the viscosity to be different. The approximated values  $|\boldsymbol{\sigma}_{S_h}|$  and  $\mu_S(|\boldsymbol{\varepsilon}(\mathbf{u}_{S_h})|^2)$  can be observed in figure 3.7. Obviously the stress looks just slightly different to the linear case in its distribution. The main difference lies in the maximal value: The stress tends to be big where the shear rate is large. This is close to  $(x_1, x_2) = (0, 2)$ . As we have a thinning behaviour the decreasing viscosity is apparent and therefore the stress is smaller as for the linear case in regions of large shear rates.

For the *Carreau model* the convergence rates can be observed in figure 3.8 whereas the LSF and the error is given in table 3.3. Again the least-squares approximation delivers optimal convergence rates as predicted by Corollary 3.11. The stress and the viscosity can be observed in figure 3.9. Again the same argument as for the *Cross model* applies for the stress. As the minimal viscosity for this model is  $\approx 0.65$  the stress tends to be higher due to the high viscosity.

level	# triangles	# dofs	$\mathcal{F}_S$	$\ \boldsymbol{\sigma}_S - \boldsymbol{\sigma}_{S_h}\ _{div}^2$	$\ \mathbf{u}_S - \mathbf{u}_{S_h}\ _1^2$
0	47	744	8.2555e-04	8.1923e-04	1.5208e-04
1	188	2802	5.3443e-05	5.1357e-05	9.5098e-06
2	752	10866	3.3769e-06	3.1903e-06	5.8530e-07
3	3008	42786	2.1208e-07	1.9861e-07	3.6161e-08
4	12032	169794	1.3285e-08	1.2386e-08	2.2453e-09

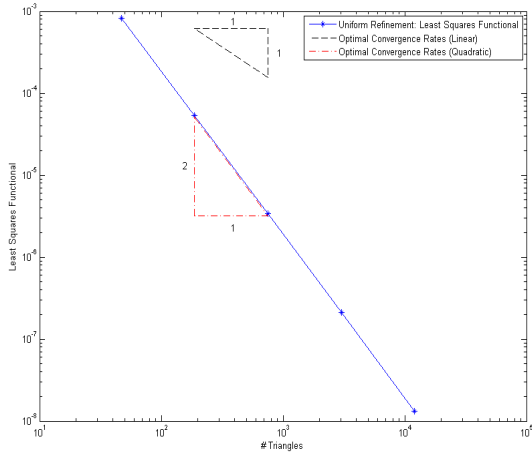
Table 3.3: LSF and errors (example 1): *Carreau* / shear thinning

### The shear thickening case

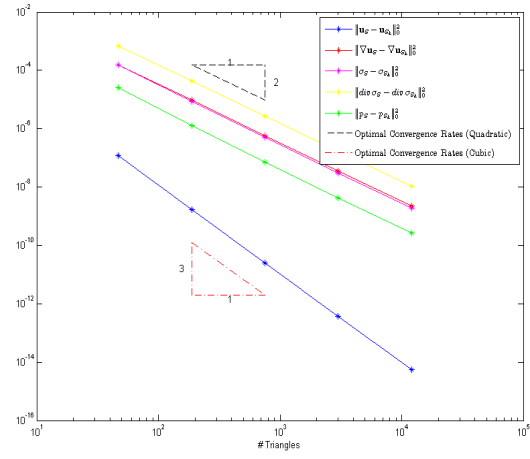
For this case we set

$$r = 2.5$$

and the other constants as in the shear thinning case.

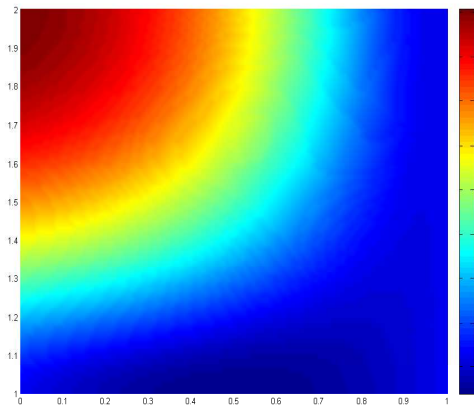


(a) Least-squares functional

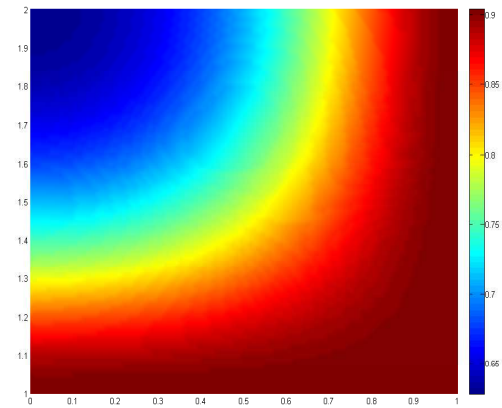


(b) Squares of errors

Figure 3.8: Convergence Rates : *Carreau* / shear thinning



(a) Stress



(b) Viscosity

Figure 3.9: Plots of  $|\sigma_{S_h}|$  and the viscosity  $\mu_S(\varepsilon(\mathbf{u}_{S_h}))$ : *Carreau* / shear thinning

For the case of *shear thickening* flow we are taking again a closer look at the *Cross-* and *Carreau-model*. The shear thickening case for the *Carreau model* is not covered by the theory as the assumptions  $(\mathbf{A2})_S$  and  $(\mathbf{A3})_S$  do not hold. We still see that the convergence behavior depicted in figure 3.11 with actual values of the lsf and error given in table 3.5 is exactly the same as for the other models. Though we do not know that the least-squares functional is an error estimator it behaves like one. It has to be noted that problematic behavior of solutions occurs if the shear rate tends to  $\infty$  leading to unbounded viscosities which is not the case for this solution. Using the *Carreau model* for problems with bounded shear rates seems to work fine.

The convergence rates for the *Cross model* are optimal as well and depicted in figure 3.10 with the LSF and errors given in table 3.4.

level	# triangles	# dofs	$\mathcal{F}_S$	$\ \sigma_S - \sigma_{S_h}\ _{div}^2$	$\ \mathbf{u}_S - \mathbf{u}_{S_h}\ _1^2$
0	47	744	3.8781e-04	3.7248e-04	1.5666e-04
1	188	2802	2.6569e-05	2.4693e-05	9.6463e-06
2	752	10866	1.6942e-06	1.5436e-06	5.8994e-07
3	3008	42786	1.0672e-08	9.6189e-08	3.6301e-08
4	12032	169794	6.6921e-09	5.9986e-09	2.2495e-09

Table 3.4: LSF and errors (example 1): *Cross* / shear thickening

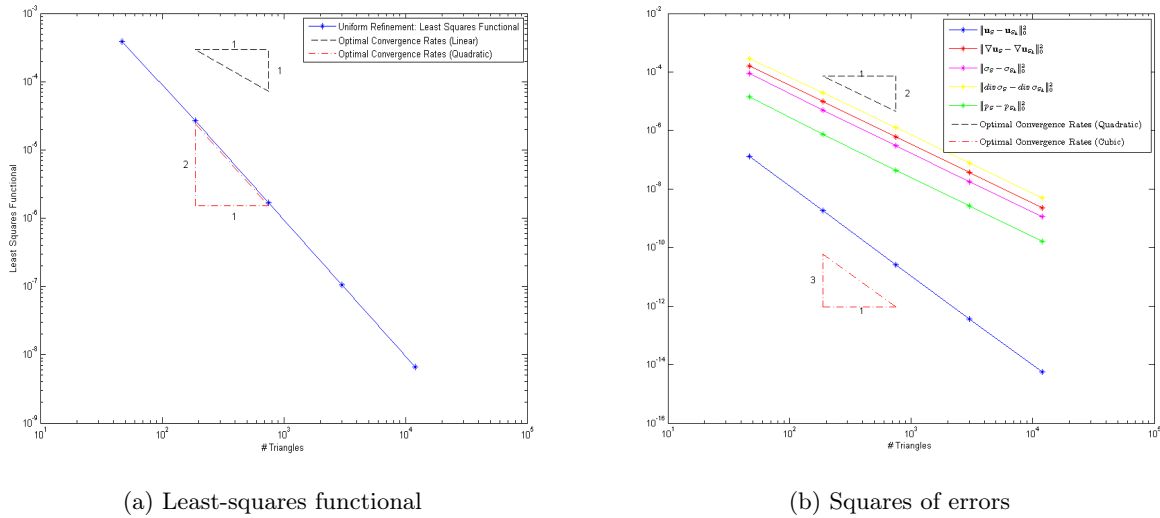


Figure 3.10: Convergence Rates : *Cross* / shear thickening

The approximated stress/viscosity for the *Cross model* can be found in figure 3.12 and for the *Carreau model* in figure 3.13 . For the *Cross model* we get a higher viscosity near  $(0, 2)$  where we have high shear rates. The high viscosity results in a higher stress than for the shear thinning / Newtonian case. One can observe a very high stress/viscosity near  $(0, 2)$  in the *Carreau model*. This is due to the fact that the Carreau model for this constants is bounded by 1 from below and not bounded from above.

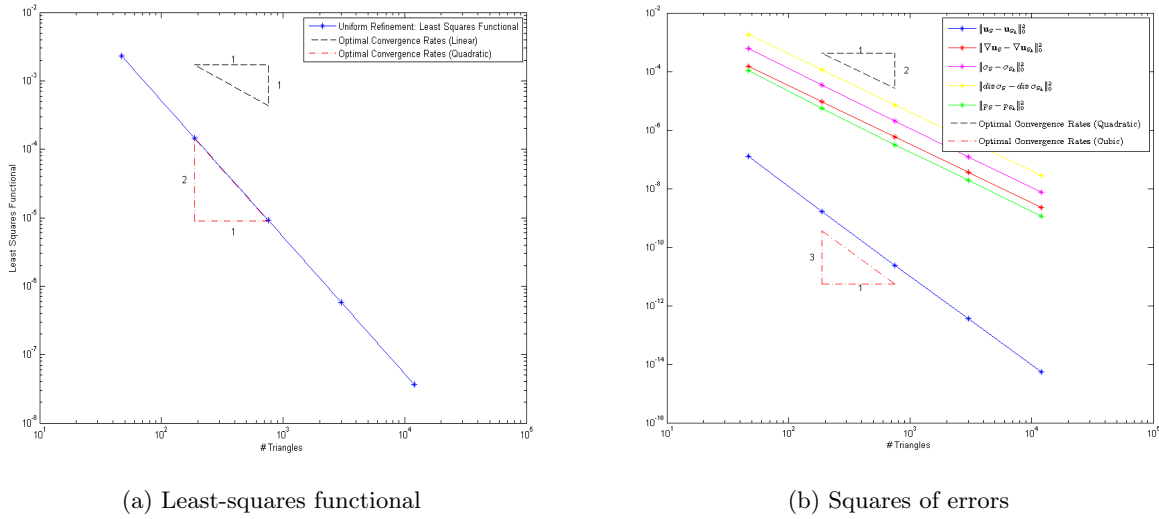


Figure 3.11: Convergence Rates : *Carreau* / shear thickening

level	# triangles	# dofs	$\mathcal{F}_S$	$\ \sigma_S - \sigma_{S_h}\ _{div}^2$	$\ \mathbf{u}_S - \mathbf{u}_{S_h}\ _1^2$
0	47	744	2.2839e-03	2.3926e-03	1.4815e-04
1	188	2802	1.4697e-04	1.4806e-04	9.2150e-06
2	752	10866	9.2736e-06	9.1955e-06	5.7358e-07
3	3008	42786	5.8174e-07	5.7266e-07	3.5761e-08
4	12032	169794	3.6416e-08	3.5721e-08	2.2323e-09

Table 3.5: LSF and errors (example 1): *Carreau* / shear thickening

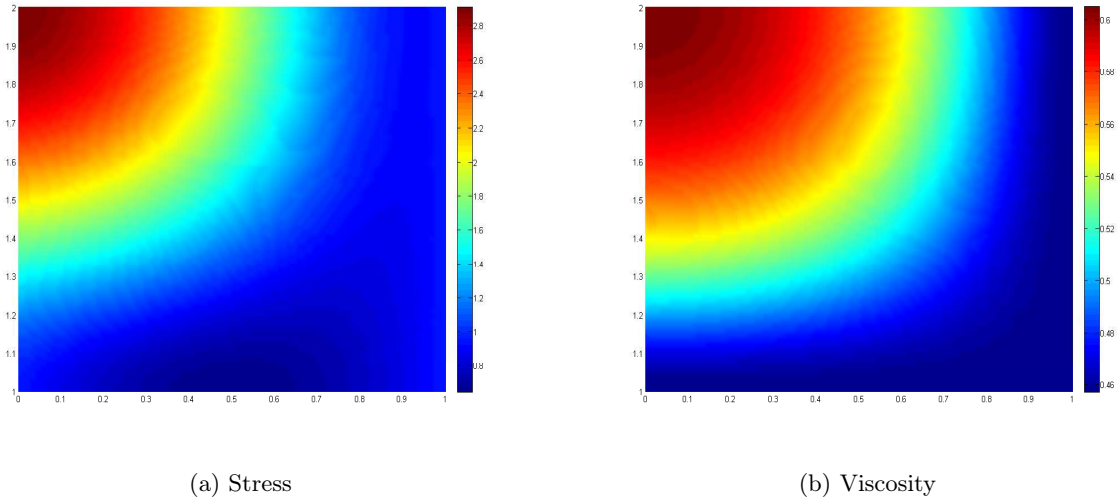
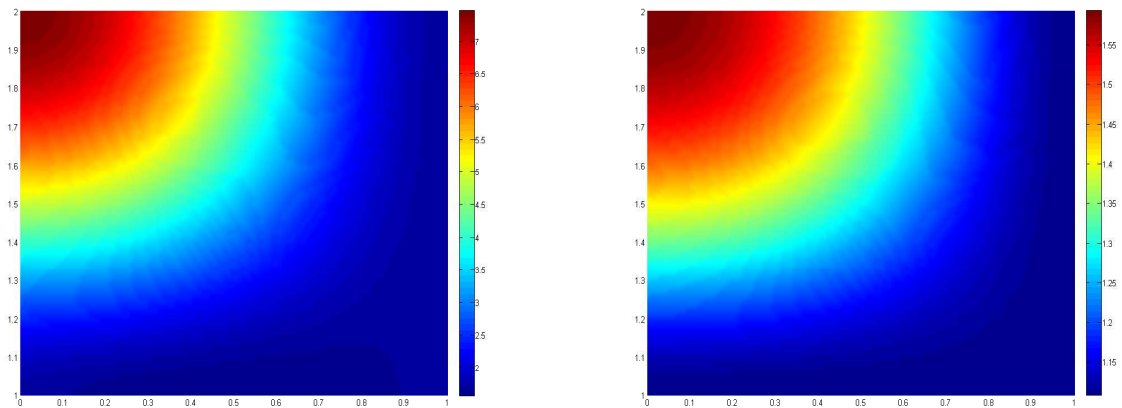


Figure 3.12: Plots of  $|\sigma_{S_h}|$  and the viscosity  $\mu_S(\epsilon(\mathbf{u}_{S_h}))$ : *Cross* / shear thickening



(a) Stress

(b) Viscosity

Figure 3.13: Plots of  $|\sigma_{S_h}|$  and the viscosity  $\mu_S(\varepsilon(\mathbf{u}_{S_h}))$ : *Carreau* / shear thickening

### 3.1.3.2 Example II

In this second example we take a closer look at an example where we expect the solution to have a singularity. To treat singularities an adaptive refinement for the triangulation is necessary to keep convergence rates reasonable. For the adaptive method we use two basic refinement strategies:

1. Mark 4% of the triangles for refinement and collect hanging nodes afterwards
2. Mark 10% of the triangles for refinement and collect hanging nodes afterwards

Afterwards adjacent triangles are refined to keep the triangulation conforming. To keep the quality of the triangulation we try to prevent the angles of the triangle to get too small. Therefore a triangle which was bisected before by the refinement strategy is not bisected again but refined regularly. This results in more triangles to be refined but keep angles larger than without this strategy.

Additionally to the two refinement strategies from above we used a uniform refinement as well to compare the results.

**Remark:** It has to be noted that this strategy is very basic. One might use more sophisticated approaches for the refinement. Numerical examples using the refinement strategy of [Doe95] did not show a significant difference in the behavior.

It has to be noted that the a priori estimates as a consequence of corollary 3.11 might depend on a very large constant. Therefore optimal convergence rates might only be visible in the asymptotic case. This is indicated in figures 3.1 and 3.2. These models behave locally like the power law which tends to weaken / strengthen singularities where the shear rate tends to go to  $\infty$ . Therefore optimal convergence rates or the same convergence rates as in the Newtonian case might only be visible for cases where the viscosity almost approached its minimum / maximum.

We also give the following approximated convergence rates:

$$\theta_{lsf}(k+1) = \frac{\log\left(\frac{\mathcal{F}_S(k+1)}{\mathcal{F}_S(k)}\right)}{-\log\left(\frac{\#T(k+1)}{\#T(k)}\right)}$$

$$\theta_{imp}(k+1) = \frac{\log\left(\frac{\|\operatorname{div}(\boldsymbol{\sigma}_S - \boldsymbol{\sigma}_{S,k+1})\|_{0,\Omega_D}^2}{\|\operatorname{div}(\boldsymbol{\sigma}_S - \boldsymbol{\sigma}_{S,k})\|_{0,\Omega_S}^2}\right)}{-\log\left(\frac{\#T(k+1)}{\#T(k)}\right)}$$

where  $k$  denotes the level of refinement and  $\#T(k)$  is the number of triangles. The approximated convergence rates for the different levels are given in the respective tables. We expect the error  $\|\operatorname{div}(\boldsymbol{\sigma}_S - \boldsymbol{\sigma}_{S_h})\|_{0,\Omega_D}^2$  to converge faster than  $\mathcal{F}_S$  as typically visible in numerical examples for  $\mathbf{f}$  being a piecewise polynomial of degree  $k$ .

The computational domain is depicted in 3.14. This domain will be met again in chapter 4 and was also used in [MS11].

The boundary conditions for a shear flow are given by:

$$\begin{aligned} \mathbf{u}_S &= \begin{pmatrix} 1 \\ 0 \end{pmatrix} && \text{on } \Gamma_{S_{D_1}} \\ \mathbf{u}_S &= \begin{pmatrix} -1 + \frac{1}{50}x_2 \\ 0 \end{pmatrix} && \text{on } \Gamma_{S_{D_{in}}} \\ \mathbf{u}_S &= \begin{pmatrix} -1 + \frac{1}{50}x_2 \\ 0 \end{pmatrix} && \text{on } \Gamma_{S_{D_{out}}} \\ \mathbf{u}_S &= \begin{pmatrix} 0 \\ 0 \end{pmatrix} && \text{on } \Gamma_{S_{D_0}} \end{aligned}$$

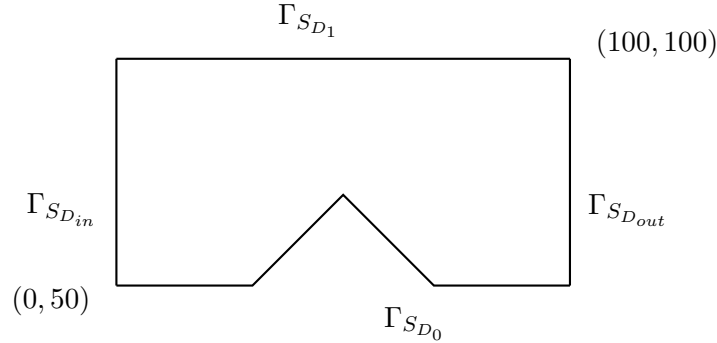


Figure 3.14: Domain for Example II

Furthermore we set  $\mathbf{f} = 0$ . Especially the upper boundary part together with the re-entrant corner leads to very low convergence rates. Therefore this example is chosen to show the advantage of adaptive refinement in difficult problems.

### The linear case

For the linear case we set the viscosity to

$$\mu_S = 0.5005$$

as being the mean of the maximal/minimal viscosity for the following cases where we used the *Cross model*. First off we start by comparing the results of the three mentioned refinement strategies. The results are shown in table 3.6. It is clear that uniform refinement results in the smallest  $\mathcal{F}_S$  for a set level. This is bought by a high number of triangles/degrees of freedom (dofs). By comparing the dofs of the different refinement strategies the most efficient is clearly the strong local refinement (4%). This is observable in the plot of the convergence rates in figure 3.17.

The comparison of the triangulations of the 2 adaptive refinement strategies is shown in figure 3.18. Refinement strategy 2 tends to refine outer parts of the domain as well. This is mainly done at step 6 and 7. Though the focus is still close to the re-entrant corner. The very high convergence rates of strategy 1 might drop down at later steps where outer parts might need some minor refinement as well. Nonetheless a very strong local refinement is advised for these kinds of problems where a singularity is present. Both strategies refine triangles close to the upper boundary as well indicating higher errors due to the boundary condition.

For all strategies we see the proposed improved convergence rate of  $\|\operatorname{div}(\boldsymbol{\sigma}_S - \boldsymbol{\sigma}_{S_h})\|_{0,\Omega_D}^2$  being double the convergence rate for uniform refinement / strategy 2. Strategy 1 tends to perform similar for early steps but drops down to be only better by a factor of  $h$ . This is the asymptotic behavior one would expect for this combination of FE-spaces and a LSFEM.

The approximated velocity  $\mathbf{u}_{S_h}$  and the absolute value of  $\mathbf{u}_{S_h}$  is plotted in figure 3.15. The solution for this problem looks as one would expect for this kind of shear flow with a contraction. The absolute value of  $\mathbf{u}_{S_h}$  being larger than 1 is due to the imposed boundary condition at  $x_2 = 100$ .

For the absolute value of the stress that is depicted in figure 3.16 the singularity is clearly visible. The more refinements we apply the higher the absolute value of the stress gets. Same can be said about the shear rate which is not depicted here but is of interest in the *shear-thinning / shear-thickening* case. We used a logarithmic scale for this plot as the large differences make it hard to



depict it on a linear scale. For the pressure we see a large gradient close to the re-entrant corner indicating a major effect of the pressure on the flow there.

level	# triangles	# dofs	$\mathcal{F}_S$	$\theta_{lsf}$	$\ \text{div } \boldsymbol{\sigma}_S - \text{div } \boldsymbol{\sigma}_{S_h}\ _0^2$	$\theta_{imp}$
0	389	5708	9.2645e-003		5.4277e-003	
1	453	6612	6.6225e-003	2.2041	3.0594e-003	3.7638
2	517	7516	4.3459e-003	3.1876	1.3128e-003	6.4026
3	633	9148	2.5320e-003	2.6688	4.3605e-004	5.4445
4	807	11600	1.3953e-003	2.4537	1.3410e-004	4.8556
5	1031	14768	7.4285e-004	2.5733	3.9582e-005	4.9811
6	1477	21052	3.8523e-004	1.8266	1.3685e-005	2.9544
7	1870	26622	2.0630e-004	2.6471	5.4925e-006	3.8696
0 – 7				2.4231		4.392

(a) refinement strategy: 4% marked

level	# triangles	# dofs	$\mathcal{F}_S$	$\theta_{lsf}$	$\ \text{div } \boldsymbol{\sigma}_S - \text{div } \boldsymbol{\sigma}_{S_h}\ _0^2$	$\theta_{imp}$
0	389	5708	9.2645e-003		5.4277e-003	
1	537	7788	6.5766e-003	1.0628	3.0517e-003	1.7859
2	815	11688	4.2586e-003	1.0417	1.2892e-003	2.0654
3	1355	19272	2.4422e-003	1.0938	4.1890e-004	2.2113
4	2362	33422	1.2736e-003	1.1715	1.1383e-004	2.3447
5	3756	53042	6.2484e-004	1.5353	2.8243e-005	3.0049
6	6422	90526	2.9908e-004	1.3736	6.5061e-006	2.7371
7	10846	152646	1.5060e-004	1.3091	1.6542e-006	2.6131
0 – 7				1.2378		2.4327

(b) refinement strategy: 10% marked

level	# triangles	# dofs	$\mathcal{F}_S$	$\theta_{lsf}$	$\ \text{div } \boldsymbol{\sigma}_S - \text{div } \boldsymbol{\sigma}_{S_h}\ _0^2$	$\theta_{imp}$
0	389	5708	9.2645e-003		5.4277e-003	
1	1556	22306	6.4735e-003	0.2586	3.0666e-003	0.4118
2	6224	88178	4.1644e-003	0.3182	1.2811e-003	0.6296
3	24896	350626	2.3670e-003	0.4075	4.0984e-004	0.8221
0 – 3				0.3281		0.6212

(c) uniform refinement

Table 3.6: LSF (example 2): Newtonian flow

### the shear thinning case

for the constants we set

$$\begin{aligned}
 K &= 1 \\
 \mu_\infty &= 10^{-3} \\
 \mu_0 &= 1 \\
 r &= 1.5
 \end{aligned}$$

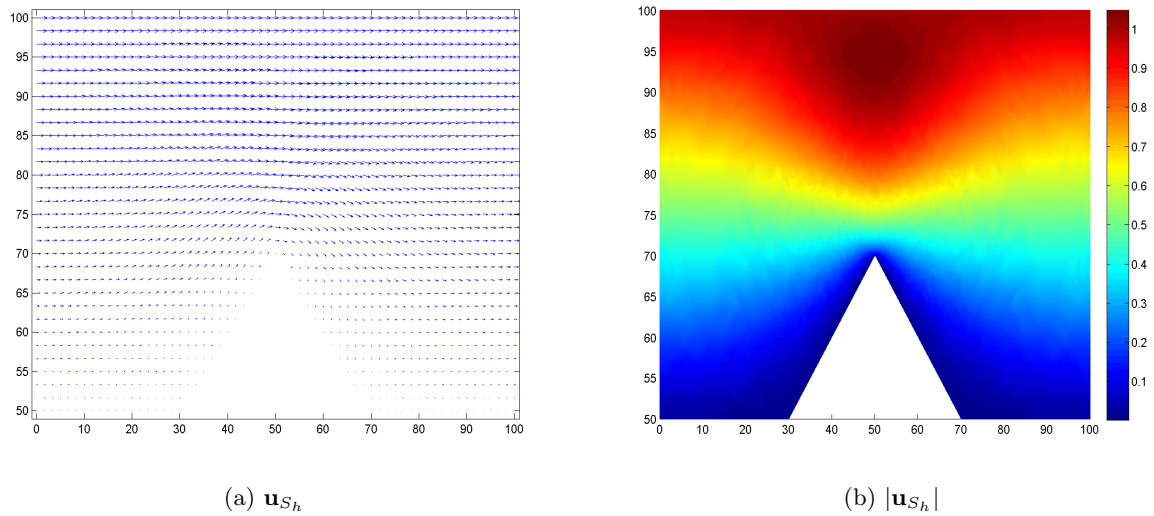


Figure 3.15: Plots of  $\mathbf{u}_{S_h}$  and  $|\mathbf{u}_{S_h}|$ : Newtonian flow

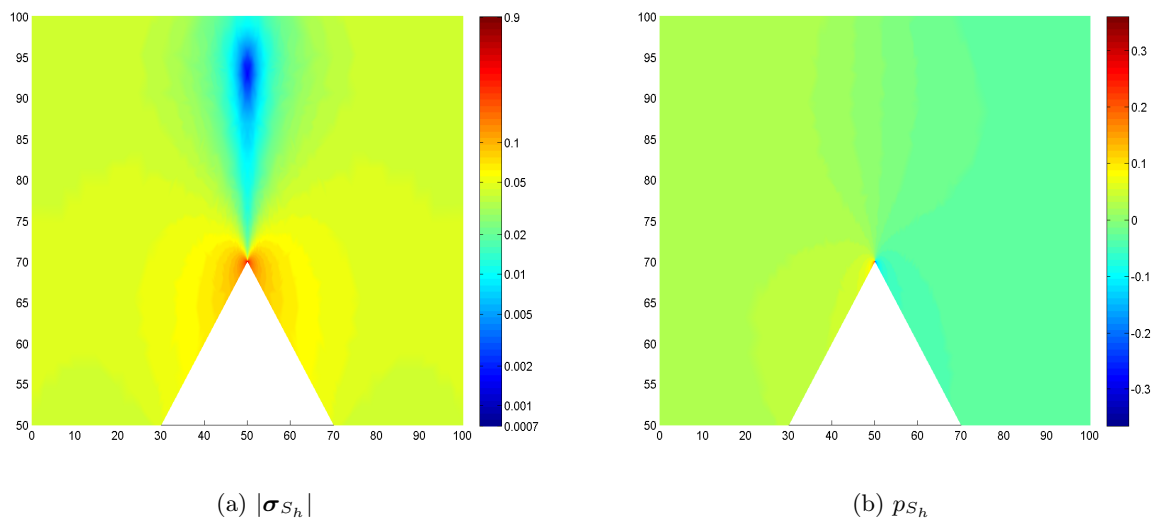
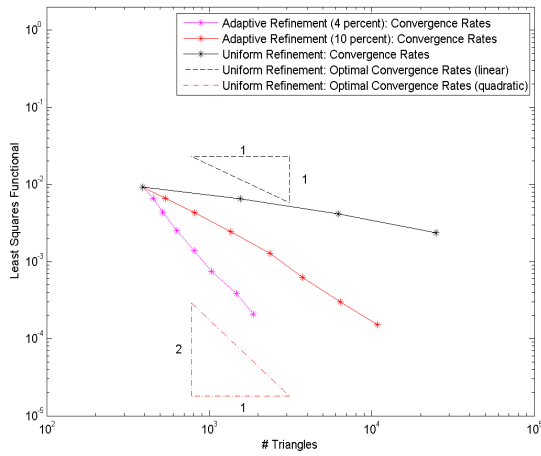
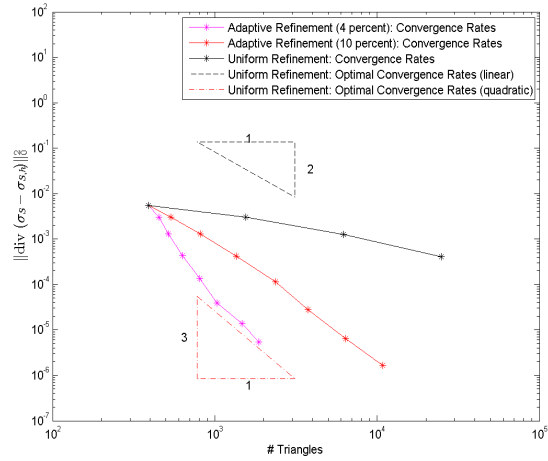


Figure 3.16: Plot of  $|\boldsymbol{\sigma}_{S_h}|$  and  $p_{S_h}$ : Newtonian flow

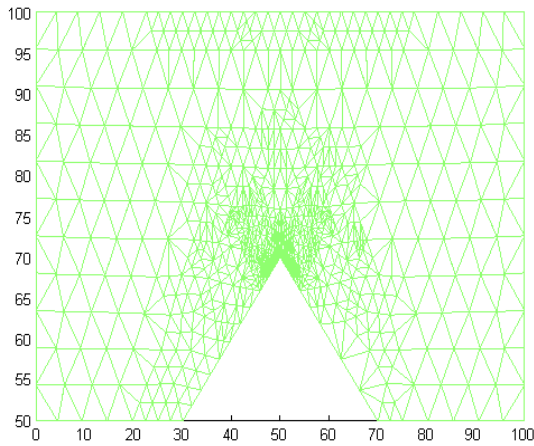


(a) convergence rates:  $\mathcal{F}_S$

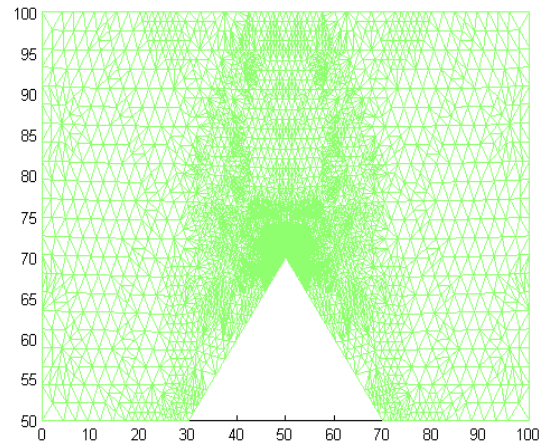


(b) convergence rates:  $\|\text{div} \sigma_{S_h}\|_0^2$

Figure 3.17: Convergence rates: Newtonian flow



(a) strategy: 4% marked



(b) strategy: 10% marked

Figure 3.18: Plots of triangulation after 7 refinements: Newtonian flow

We only take a closer look at the *Cross model*. The *Carreau model* behaves, considering convergence rates and refinement strategies, very similar. We used the same refinement strategies as for the constant case and table 3.7 shows the actual values of the LSF and the number of triangles/dofs. The convergence rates can be observed in figure 3.19. We see that the convergence rates are slightly better which is an effect of the singularity as stated before. They will at some point show the same asymptotic behavior as indicated by corollary 3.11. We again see the better convergence rates for  $\|\operatorname{div} \boldsymbol{\sigma}_S - \operatorname{div} \boldsymbol{\sigma}_{S_h}\|_0^2$  which indicates that this feature carries over to the nonlinear case.

We won't depict the velocity here as it looks similar to the constant case and therefore refer to the case before. Slight differences can be seen close to the upper boundary due to the different model for viscosity. The stress, pressure and viscosity is depicted in figure 3.20. The absolute value of the stress tends to be slightly higher than for the constant case but the characteristic looks very similar. The distribution of viscosity shows a strong decrease of viscosity close to the re-entrant corner where the absolute value of the stress is very high. Higher viscosities can be seen where the stress is low. This is visible right above the re-entrant corner. The different characteristic of the stress and viscosity can especially close to the lower boundary is due to the higher/lower pressures left/right from the singularity that are contributing a major part to  $|\boldsymbol{\sigma}_{S_h}|$ . Due to the very high variations in viscosity a problem with that kind of viscosity won't be well approximated by a linear model.

The refined triangles are depicted figure 3.21. These look only slightly different from the constant case, so it can be said that more or less the same triangles are refined.

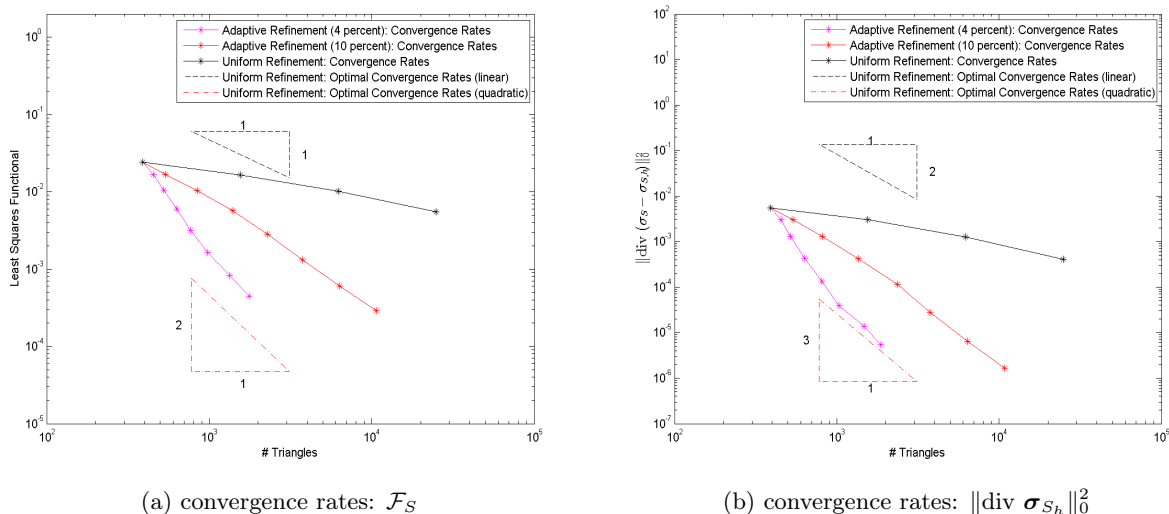


Figure 3.19: Convergence rates: *Cross* / shear thinning

### shear thickening case

For the shear thickening case we again take a closer look only at the *Cross model*. The *Carreau model* behaves again quite similar with respect to convergence rates though the property of being an error estimator is not established. We set  $r = 2.5$  and the rest of the constants as in the shear thinning case. The errors are depicted in table 3.8 and the convergence rates can be found in figure 3.22. The convergence rates are considerably lower than for the constant/shear thinning case. This is the opposite behavior to the shear thinning case as the viscosity strongly increases close to the

level	# triangles	# dofs	$\mathcal{F}_S$	$\theta_{lsf}$	$\ \text{div } \boldsymbol{\sigma}_S - \text{div } \boldsymbol{\sigma}_{S_h}\ _0^2$	$\theta_{imp}$
0	389	5708	2.4163e-002		1.3213e-002	
1	451	6584	1.6859e-002	2.4337	6.9626e-003	4.3319
2	525	7628	1.0566e-002	3.0756	2.6790e-003	6.2864
3	633	9148	5.9614e-003	3.0593	8.3574e-004	6.227
4	765	11012	3.1556e-003	3.3586	2.4319e-004	6.5175
5	979	14040	1.6246e-003	2.6916	7.3744e-005	4.8378
6	1336	19066	8.2628e-004	2.1746	2.8087e-005	3.1048
7	1754	24990	4.4337e-004	2.2869	1.2237e-005	3.0522
0 – 7				2.6547		4.6375

(a) refinement strategy: 4% marked

level	# triangles	# dofs	$\mathcal{F}_S$	$\theta_{lsf}$	$\ \text{div } \boldsymbol{\sigma}_S - \text{div } \boldsymbol{\sigma}_{S_h}\ _0^2$	$\theta_{imp}$
0	389	5708	2.4163e-002		1.3213e-002	
1	537	7788	1.6785e-002	1.13	6.9489e-003	1.9931
2	847	12136	1.0383e-002	1.0539	2.6307e-003	2.1315
3	1397	19868	5.6498e-003	1.2163	7.4982e-004	2.5084
4	2274	32214	2.8085e-003	1.4346	1.8334e-004	2.8909
5	3744	52890	1.3212e-003	1.5124	4.1029e-005	3.0025
6	6354	89638	6.0437e-004	1.4787	8.3877e-006	3.0014
7	10682	150422	2.9072e-004	1.4087	1.9585e-006	2.8001
0 – 7				1.3343		2.6615

(b) refinement strategy: 10% marked

level	# triangles	# dofs	$\mathcal{F}_S$	$\theta_{lsf}$	$\ \text{div } \boldsymbol{\sigma}_S - \text{div } \boldsymbol{\sigma}_{S_h}\ _0^2$	$\theta_{imp}$
0	389	5708	2.4163e-002		1.3213e-002	
1	1556	22306	1.6579e-002	0.2717	6.9656e-003	0.4618
2	6224	88178	1.0189e-002	0.3512	2.6002e-003	0.7108
3	24896	350626	5.4964e-003	0.4452	7.3302e-004	0.9134
0 – 3				0.356		0.6953

(c) uniform refinement

Table 3.7: LSF (example 2): *Cross* / shear thinning

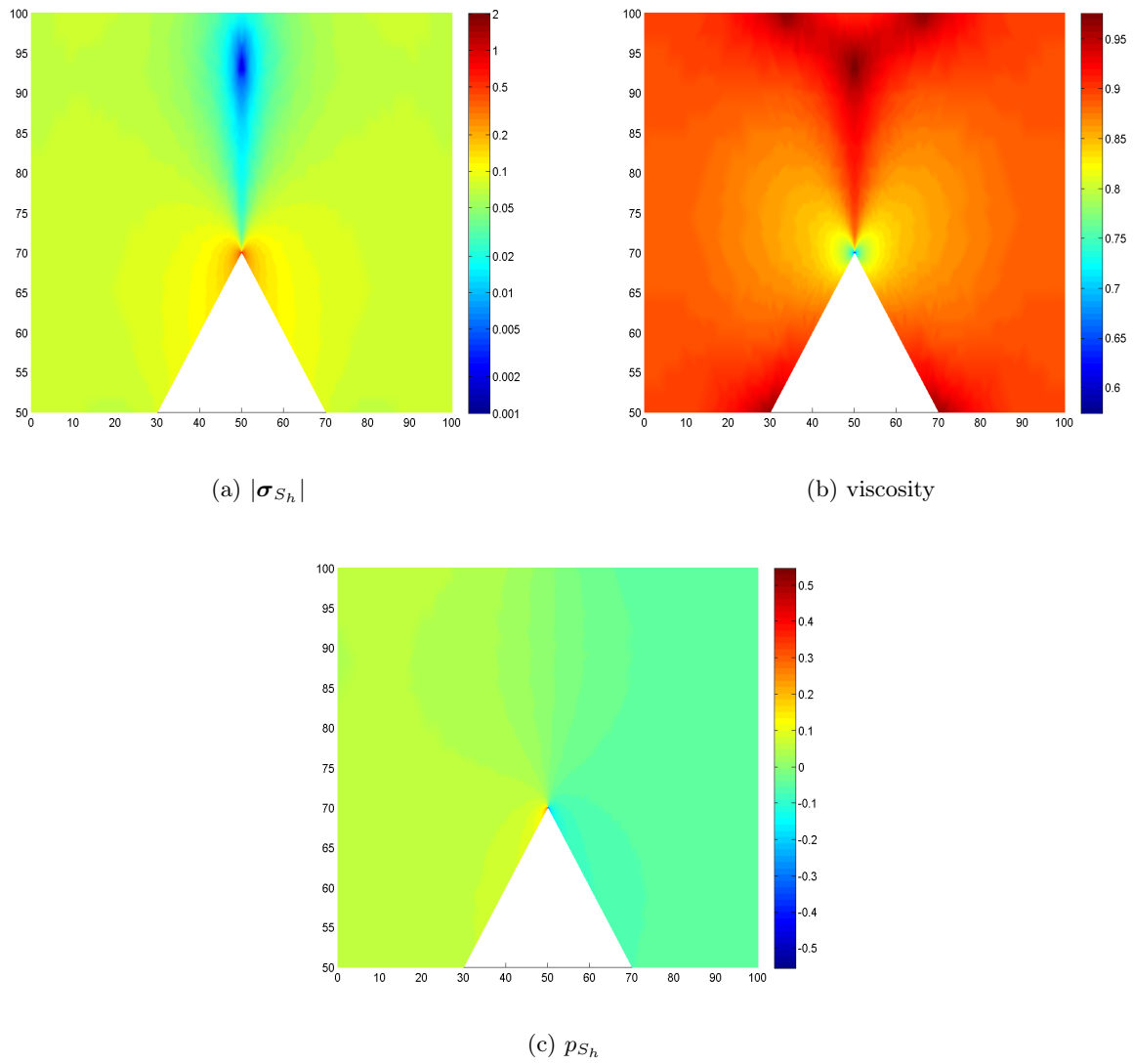


Figure 3.20: Plots of  $|\sigma_{S_h}|$ ,  $p_{S_h}$  and viscosity: *Cross* / shear thinning

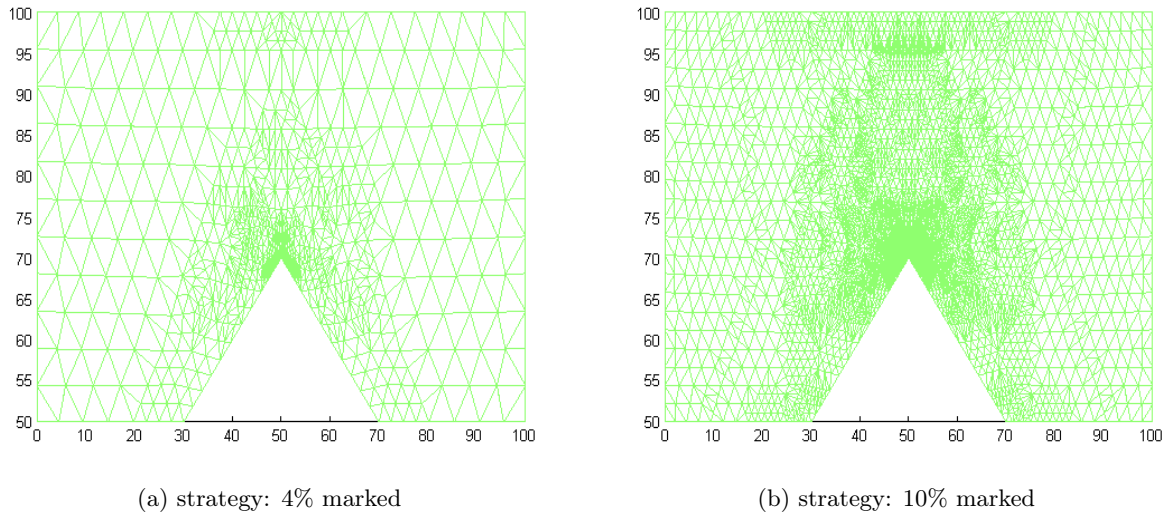


Figure 3.21: Plots of triangulation after 7 refinements: *Cross* / shear thinning

singularity. The effect is again visible in all refinement strategies. This holds true for the least-squares functional and the error  $\|\operatorname{div} \boldsymbol{\sigma}_S - \operatorname{div} \boldsymbol{\sigma}_{S_h}\|_0^2$ . Nonetheless the improved convergence rate is still visible in all 3 strategies.

The behavior of the pressure, absolute value of stress and the viscosity is depicted in figure 3.24: Again the absolute value of the stress looks considerably different close to the singularity. For the viscosity we see the expected increase close to the re-entrant corner. The parts where the viscosity (and the shear-rate) tends to be very low are the same where the shear-thinning flow tends to have high viscosities. The pressure gradient is again very high close to the re-entrant corner.

The triangulations after 7 refinement steps are depicted in figure 3.23. Though again the areas close to the re-entrant corner are refined the refinement close to the upper boundary is considerably different to the other 2 cases. It can be stated that the error distribution, aside from close to the re-entrant corner, seems to be different from the other two cases. Therefore having an a-posteriori error estimator at hand is important for an efficient refinement strategy.

level	# triangles	# dofs	$\mathcal{F}_S$	$\theta_{lsf}$	$\ \text{div } \boldsymbol{\sigma}_S - \text{div } \boldsymbol{\sigma}_{S_h}\ _0^2$	$\theta_{imp}$
0	389	5708	1.1635e-003		7.2465e-004	
1	457	6668	8.3273e-004	2.0761	4.4909e-004	2.9699
2	521	7572	6.0684e-004	2.4143	2.4409e-004	4.6516
3	667	9624	4.1220e-004	1.5656	1.1210e-004	3.1501
4	881	12628	2.5526e-004	1.7222	4.2319e-005	3.5007
5	1054	15078	1.4939e-004	2.9882	1.6673e-005	5.1953
6	1422	20294	8.3561e-005	1.9399	5.8282e-006	3.5097
7	2118	30070	4.6356e-005	1.4789	2.1328e-006	2.5232
0 – 7				1.9018		3.4392

(a) refinement strategy: 4% marked

level	# triangles	# dofs	$\mathcal{F}_S$	$\theta_{lsf}$	$\ \text{div } \boldsymbol{\sigma}_S - \text{div } \boldsymbol{\sigma}_{S_h}\ _0^2$	$\theta_{imp}$
0	389	5708	1.1635e-003		7.2465e-004	
1	533	7732	8.1361e-004	1.1357	4.5131e-004	1.5036
2	795	11408	5.8109e-004	0.8418	2.4464e-004	1.5316
3	1191	16968	3.7688e-004	1.0712	1.0981e-004	1.9817
4	2197	31116	2.2088e-004	0.8726	3.9761e-005	1.6591
5	3742	52798	1.1909e-004	1.16	1.2152e-005	2.2259
6	6708	94442	6.1798e-005	1.124	3.3820e-006	2.1913
7	11405	160364	3.2861e-005	1.19	9.5911e-007	2.3744
0 – 7				1.0558		1.9618

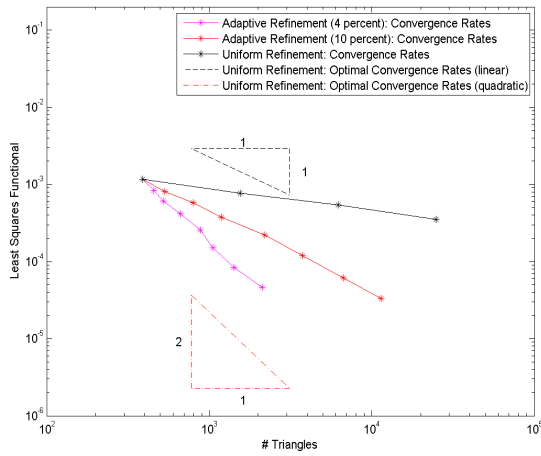
(b) refinement strategy: 10% marked

level	# triangles	# dofs	$\mathcal{F}_S$	$\theta_{lsf}$	$\ \text{div } \boldsymbol{\sigma}_S - \text{div } \boldsymbol{\sigma}_{S_h}\ _0^2$	$\theta_{imp}$
0	389	5708	1.1635e-003		7.2465e-004	
1	1556	22306	7.6355e-004	0.3038	4.5427e-004	0.3369
2	6224	88178	5.3855e-004	0.2518	2.4713e-004	0.4391
3	24896	350626	3.5147e-004	0.3078	1.0833e-004	0.5949
0 – 3				0.2878		0.457

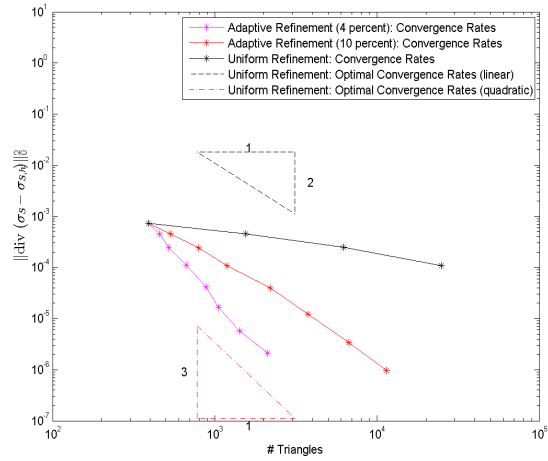
(c) uniform refinement

Table 3.8: LSF(example 2): *Cross* / shear thickening



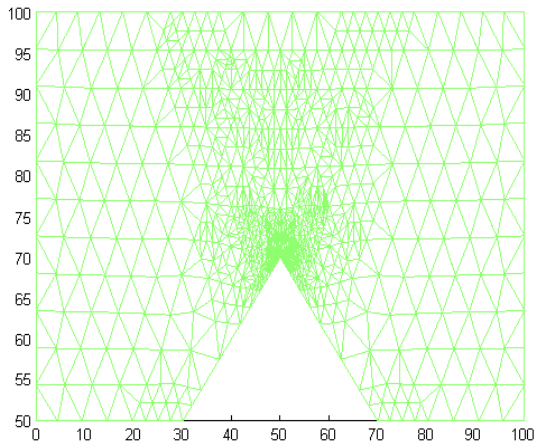


(a) convergence rates:  $\mathcal{F}_S$

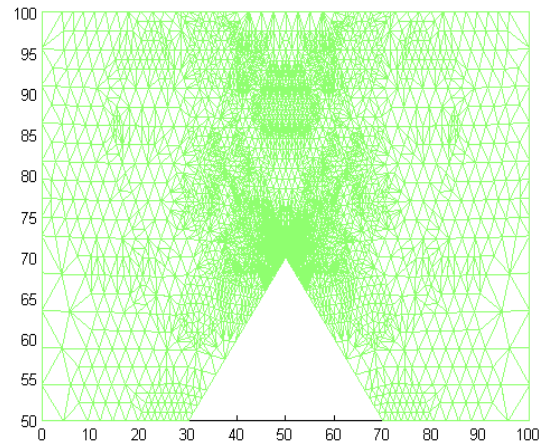


(b) convergence rates:  $\|\text{div} \sigma_{s,h}\|_0^2$

Figure 3.22: Convergence rates: *Cross* / shear thickening



(a) strategy: 4% marked



(b) strategy: 10% marked

Figure 3.23: Plots of triangulation after 7 refinements: *Cross* / shear thickening

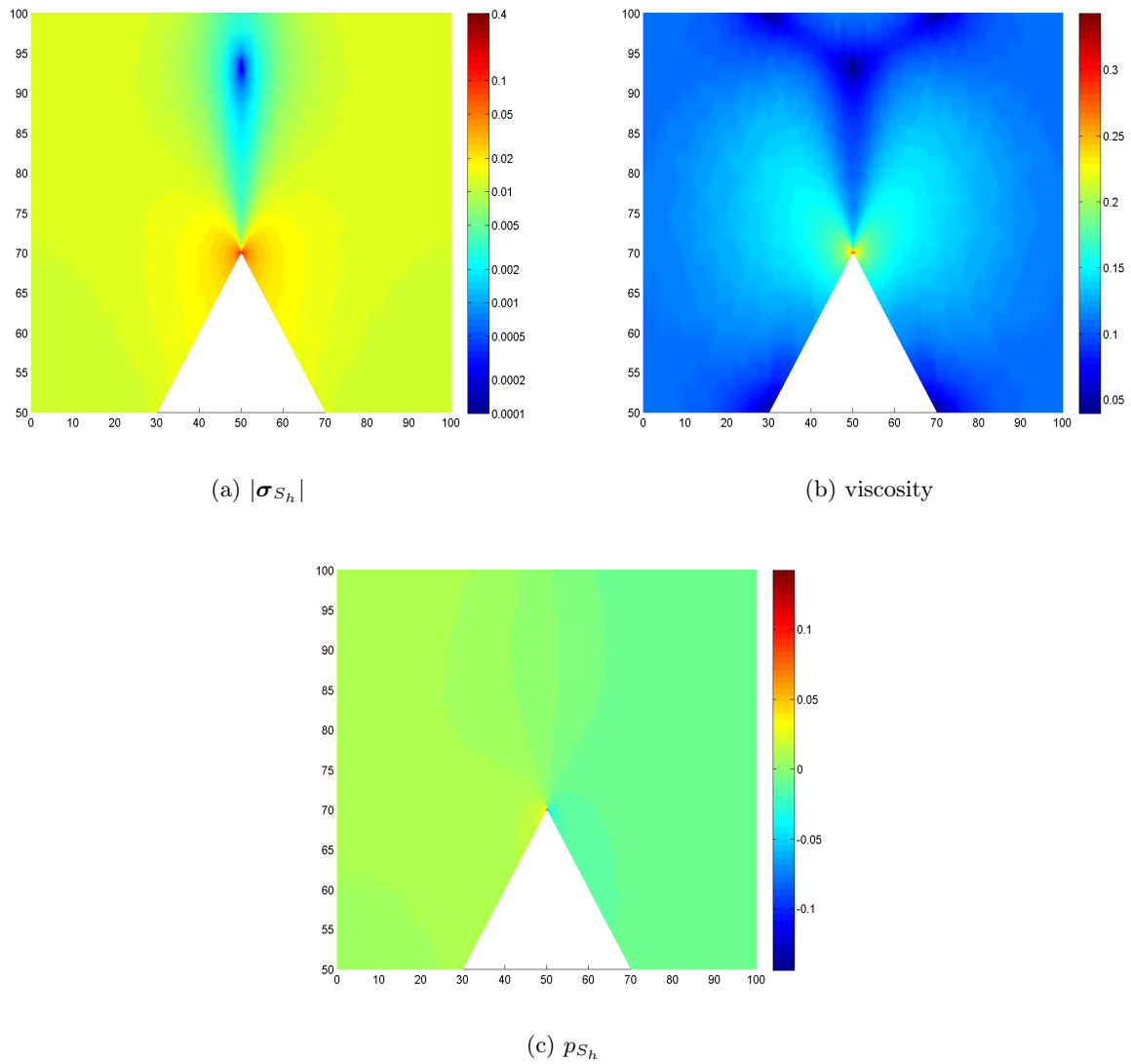


Figure 3.24: Plots of  $|\sigma_{S_h}|$ ,  $p_{S_h}$  and viscosity: *Cross* / shear thickening

### 3.2 Darcy Flow

The nonlinear Darcy-flow is given by

$$\begin{aligned}
\mathbf{u}_D + \frac{\kappa}{\mu_D(|\mathbf{u}_D|^2)} \nabla p_D &= 0 & \text{in } \Omega_D \\
\nabla \cdot \mathbf{u}_D &= f & \text{in } \Omega_D \\
p_D &= g_{D_D} & \text{on } \Gamma_{D_D} \\
\mathbf{u}_D \cdot \mathbf{n} &= g_{D_N} & \text{on } \Gamma_{D_N}
\end{aligned} \tag{3.20}$$

with

- $\mathbf{u}_D$ : volumetric flux
- $p_D$ : hydraulic potential
- $\kappa(\mathbf{x})$ : Permeability

This formulation was used in [EJS09]. For this section we again assume the domain  $\Omega_D$  to have a Lipschitz boundary with  $\partial\Omega_D = \Gamma_{D_D} \cup \Gamma_{D_N}$  and  $\Gamma_{D_D} \cap \Gamma_{D_N} = \emptyset$ . Therefore we are able to use the inequalities of section 2.

The permeability  $\kappa(\mathbf{x}) \in L^\infty(\Omega_D)$  is assumed to be a function from  $\Omega_D$  to  $\mathbb{R}_{>0}$  bounded from below by  $\kappa_{min}$  and bounded from above by  $\kappa_{max}$ .

For the viscosity in the Darcy domain we have analog to the Stokes case:

$$\mu_D = \mu_D(|\mathbf{u}_D|^2)$$

Models for the viscosity include the following [EJS09]:

- *Cross model*

$$\mu(|\mathbf{u}_D|^2) = \mu_\infty + \frac{(\mu_0 - \mu_\infty)}{1 + K(|\mathbf{u}_D|^2)^{\frac{2-r}{2}}}$$

- *Power law model*

$$\mu(|\mathbf{u}_D|^2) = K \left( \frac{|\mathbf{u}_D|^2}{\kappa m_c^2} \right)^{\frac{r-2}{2}}$$

with  $m_c$  being a constant dependent on the internal structure of the porous medium. For the *Cross model* we have

$$- \mu_\infty \leq \mu(|\mathbf{u}_D|^2) \leq \mu_0$$

The upper/lower bound for the viscosity is a crucial part of the proof for the LSF being an error estimator. Therefore the following numerical analysis is only valid for the *Cross model*.

As in the Stokes case we need an additional condition if  $\lambda_d(\Gamma_{D_D}) = 0$  which is the following

$$\int_{\Omega_D} p_D dx = 0.$$

### 3.2.1 The Least-Squares Functional as an Error Estimator

In this section we show that the LSF is an efficient and reliable error estimator for the nonlinear Darcy-problem.

the first equation of the Darcy-problem is scaled differently compared to (3.20).

$$\kappa^{-1/2} \mu_D (|\mathbf{u}_D|^2) \mathbf{u}_D + \kappa^{1/2} \nabla p_D = 0 \quad \in \Omega_D \quad (3.21)$$

which leads to the following least-squares functional

$$\mathcal{F}_D(\mathbf{u}_D, p_D; f) = \|\kappa^{-1/2} \mu_D (|\mathbf{u}_D|^2) \mathbf{u}_D + \kappa^{1/2} \nabla p_D\|_{0, \Omega_D}^2 + \|\nabla \cdot \mathbf{u}_D - f\|_{0, \Omega_D}^2. \quad (3.22)$$

For our approach we make use of the following spaces

$$\begin{aligned} H_{\Gamma_{D_N}}^{div}(\Omega_D) &= \{\mathbf{v} \in H^{div}(\Omega_D) \mid \mathbf{v} \cdot \mathbf{n} = 0 \text{ on } \Gamma_{D_N}\} \\ H_{\Gamma_{D_D}}^1(\Omega_D) &= \{q \in H^1(\Omega_D) \mid q = 0 \text{ on } \Gamma_{D_D} \mid \int_{\Omega_D} q = 0 \text{ if } \Gamma_{D_D} = \emptyset\} \end{aligned}$$

As for the Stokes case we need to define the functions that satisfy the boundary conditions:

- $\mathbf{u}_{D_N} \in (H^{div}(\Omega_D))^d$  with  $\mathbf{u}_{D_N}|_{\Gamma_{D_N}} = g_{D_N}$
- $p_{D_D} \in (H^1(\Omega_D))^d$  with  $p_{D_D}|_{\Gamma_{D_D}} = g_{D_D}$

If  $\Gamma_{D_D} = \emptyset$  we use the natural choice of  $p_{D_D} = 0$  which lies in  $H_{\Gamma_{D_D}}^1(\Omega_D)$ .

Our minimization problem is then given by: Find  $(\hat{\mathbf{u}}_D, \hat{p}_D) \in H_{\Gamma_{D_N}}^{div}(\Omega_D) \times H_{\Gamma_{D_D}}^1(\Omega_D)$  s.t.

$$\mathcal{F}_D(\mathbf{u}_{D_N} + \hat{\mathbf{u}}_D, p_{D_D} + \hat{p}_D; f) \leq \mathcal{F}_D(\mathbf{u}_{D_N} + \hat{\mathbf{v}}_D, p_{D_D} + \hat{q}_D; f)$$

holds for all  $(\hat{\mathbf{v}}_D, \hat{q}_D) \in H_{\Gamma_{D_N}}^{div}(\Omega_D) \times H_{\Gamma_{D_D}}^1(\Omega_D)$ .

Again we need the following assumptions on the viscosity  $\mu_D(s)$ :

- (A1<sub>D</sub>)  $\mu_D(s) \in C^0([0, \infty)) \cap C^1((0, \infty))$
- (A2<sub>D</sub>)  $0 < K_0 \leq \mu_D(s) \leq K_1$
- (A3<sub>D</sub>)  $0 < M_0 \leq \mu_D(s) + 2\mu'_D(s)s \leq M_\infty < \infty$  for  $s > 0$

As in the section before we need the following lemma:

**Lemma 3.12** *Let assumptions (A1<sub>D</sub>), (A2<sub>D</sub>) and (A3<sub>D</sub>) hold. Then for arbitrary  $\bar{\mu}_D > 0$  it holds:*

$$\begin{aligned} \|\kappa^{-1/2} (\mu_D (|\mathbf{u}_D|^2) \mathbf{u}_D - \mu_D (|\mathbf{v}_D|^2) \mathbf{v}_D) - \kappa^{-1/2} \bar{\mu}_D (\mathbf{u}_D - \mathbf{v}_D)\|_{0, \Omega_D} \\ \leq C_{\mu, D} \cdot \bar{\mu}_D \|\kappa^{-1/2} (\mathbf{u}_D - \mathbf{v}_D)\|_{0, \Omega_D} \end{aligned} \quad (3.23)$$

with a constant dependant on  $\bar{\mu}_D$ :

$$C_{\mu, D} := \max_{\mathbf{w} \in \mathbb{R}^d} \frac{\max \{|\mu_D (|\mathbf{w}|^2) - \bar{\mu}_D|, |\mu_D (|\mathbf{w}|^2) - \bar{\mu}_D + 2\mu'_D (|\mathbf{w}|^2) |\mathbf{w}|^2|\}}{\bar{\mu}_D} < \infty$$

**proof:** Analog to the proof of lemma 3.1. The main difference is that we only have to consider first-order tensors and the permeability has to be taken into account. Therefore we sketch the beginning of the proof: We show that

$$|\kappa^{-1/2}(\mu_D(|\mathbf{u}_D|^2)\mathbf{u}_D - \mu_D(|\mathbf{v}_D|^2)\mathbf{v}_D) - \kappa^{-1/2}\bar{\mu}_D(\mathbf{u}_D - \mathbf{v}_D)| \leq C_{\mu,D} \cdot \bar{\mu}_D |\kappa^{-1/2}(\mathbf{u}_D - \mathbf{v}_D)| \quad (3.24)$$

holds for almost every  $\mathbf{x} \in \Omega_D$ , whereby (3.23) follows directly. As  $\kappa^{-1/2}$  is bounded and only dependent on  $\mathbf{x}$  we can as well show

$$|(\mu_D(|\mathbf{u}_D|^2)\mathbf{u}_D - \mu_D(|\mathbf{v}_D|^2)\mathbf{v}_D) - \bar{\mu}_D(\mathbf{u}_D - \mathbf{v}_D)| \leq C_{\mu,D} \cdot \bar{\mu}_D |(\mathbf{u}_D - \mathbf{v}_D)| \quad (3.25)$$

which we get by following the proof of lemma 3.1. ■

**Remark:** Assumptions **(A2<sub>D</sub>)** and **(A3<sub>D</sub>)** do not hold for the power law. Therefore the following theorems are not proven for the power law.

An analog version of lemma 3.2 holds as well:

**Lemma 3.13** *Let the assumptions of lemma 3.12 hold. Then there exists a  $\bar{\mu}_D$  s.t. for  $C_{\mu,D}$  we have:*

$$C_{\mu,D} < 1$$

If the bounds in **(A2<sub>D</sub>)** and **(A3<sub>D</sub>)** are sharp the smallest  $C_{\mu,D}$  is given by:

$$C_{\mu,D} = \frac{\bar{\mu}_D - \min\{K_0, M_0\}}{\bar{\mu}_D}$$

with

$$\bar{\mu}_D = \max\left\{\frac{K_1 + K_0}{2}, \frac{M_1 + M_0}{2}\right\}$$

**proof:** Analog to lemma 3.2. ■

**Remark:** One might as well assume  $\kappa$  to be a positive definite matrix. Lemma 3.12 and lemma 3.13 can be proven if we assume  $\kappa$  to be orthogonal. If  $\kappa$  is not orthogonal the  $C_{\mu,D}$  of lemma 3.12 looks different and one might not be able to prove lemma 3.13 without altering the assumption **(A3<sub>D</sub>)** and taking  $\kappa$  into account.

**Remark:** Analog to the Stokes flow we are able to formulate alternative assumptions on the viscosity. We use the version of lemma 3.3 and restrict ourselves to the cases that can be used for our least-squares approach. For general viscosity functions we refer to the Stokes case.

$$\mathbf{(A4}_D) \quad C_5 |\mathbf{z}_D - \mathbf{v}_D|^2 \leq (\mu_D(|\mathbf{z}_D|^2)\mathbf{z}_D - \mu_D(|\mathbf{v}_D|^2)\mathbf{v}_D) : (\mathbf{z}_D - \mathbf{v}_D)$$

$$\mathbf{(A5}_D) \quad |\mu_D(|\mathbf{z}_D|^2)\mathbf{z}_D - \mu_D(|\mathbf{v}_D|^2)\mathbf{v}_D| \leq C_4 |\mathbf{z}_D - \mathbf{v}_D|$$

An analog version of lemma 3.4 holds with the remark about the permeability in the proof of lemma 3.12.

Now we can prove that the nonlinear least-squares functional is an efficient and reliable error estimator:

**Theorem 3.14** *Let assumptions  $(\mathbf{A}1_D)$ ,  $(\mathbf{A}2_D)$  and  $(\mathbf{A}3_D)$  or  $(\mathbf{A}4_D)$  and  $(\mathbf{A}5_D)$  hold. Then we have for the solution  $(\mathbf{u}_D, p_D) = (\mathbf{u}_{D_D}, p_{D_D}) + (\hat{\mathbf{u}}_D, \hat{p}_D)$  with  $(\hat{\mathbf{u}}_D, \hat{p}_D) \in H_{\Gamma_{D_N}}^{div}(\Omega_D) \times H_{\Gamma_{D_D}}^1(\Omega_D)$  of (3.20):*

$$\begin{aligned} C_{e,D}(\|\mathbf{u}_D - \mathbf{v}_D\|_{div,\Omega_D}^2 + \|p_D - q_D\|_{1,\Omega_D}^2) \\ \leq \mathcal{F}_D(\mathbf{v}_D, q_D) \\ \leq C_{s,D}(\|\mathbf{u}_D - \mathbf{v}_D\|_{div,\Omega_D}^2 + \|p_D - q_D\|_{1,\Omega_D}^2) \end{aligned}$$

for all  $(\mathbf{v}_D, q_D) = (\mathbf{u}_{D_D}, p_{D_D}) + (\hat{\mathbf{v}}_D, \hat{q}_D)$  with  $(\hat{\mathbf{v}}_D, \hat{q}_D) \in H_{\Gamma_{D_N}}^{div}(\Omega_D) \times H_{\Gamma_{D_D}}^1(\Omega_D)$  with positive constants  $C_{e,D}$  and  $C_{s,D}$ .

**proof:** the proof can be found in [MS11] for the linear case. The nonlinearity is treated as in the proof of theorem 3.5 in the Stokes case.

For the least-squares functional we have:

$$\begin{aligned} \mathcal{F}_D(\mathbf{v}_D, q_D) &= \|\kappa^{-1/2} \mu_D (|\mathbf{v}_D|^2) \mathbf{v}_D + \kappa^{1/2} \nabla q_D\|_{0,\Omega_D}^2 + \|\nabla \cdot \mathbf{v}_D - f\|_{0,\Omega_D}^2 \\ &= \|\kappa^{-1/2} \mu_D (|\mathbf{u}_D|^2) \mathbf{u}_D + \kappa^{1/2} \nabla p_D - \kappa^{-1/2} \mu_D (|\mathbf{v}_D|^2) \mathbf{v}_D - \kappa^{1/2} \nabla q_D\|_{0,\Omega_D}^2 \\ &\quad + \|\nabla \cdot \mathbf{u}_D - \nabla \cdot \mathbf{v}_D\|_{0,\Omega_D}^2 \\ &\leq 2\|\kappa^{-1/2} (\mu_D (|\mathbf{u}_D|^2) \mathbf{u}_D - \mu_D (|\mathbf{v}_D|^2) \mathbf{v}_D - \bar{\mu}_D (\mathbf{u}_D - \mathbf{v}_D))\|_{0,\Omega_D}^2 \\ &\quad + 2\|\kappa^{-1/2} \bar{\mu}_D (\mathbf{u}_D - \mathbf{v}_D) + \kappa^{1/2} (\nabla p_D - \nabla q_D)\|_{0,\Omega_D}^2 + \|\nabla \cdot \mathbf{u}_D - \nabla \cdot \mathbf{v}_D\|_{0,\Omega_D}^2 \\ &\leq 2C_{\mu,D} \|\kappa^{-1/2} (\bar{\mu}_D (\mathbf{u}_D - \mathbf{v}_D))\|_{0,\Omega_D}^2 + 2\|\kappa^{-1/2} \bar{\mu}_D (\mathbf{u}_D - \mathbf{v}_D) + \kappa^{1/2} (\nabla p_D - \nabla q_D)\|_{0,\Omega_D}^2 \\ &\quad + \|\nabla \cdot \mathbf{u}_D - \nabla \cdot \mathbf{v}_D\|_{0,\Omega_D}^2 \\ &\leq 2(1 + C_{\mu,D}) \bar{\mu}_D \kappa_{max} \|\mathbf{u}_D - \mathbf{v}_D\|_{0,\Omega_D}^2 + \|\nabla \cdot \mathbf{u}_D - \nabla \cdot \mathbf{v}_D\|_{0,\Omega_D}^2 \\ &\quad + 2\kappa_{max} \|\nabla p_D - \nabla q_D\|_{0,\Omega_D}^2 \\ &\leq \max\{1, 2(1 + C_{\mu,D}) \bar{\mu}_D \kappa_{max}\} \|\mathbf{u} - \mathbf{v}\|_{div,\Omega_D} + 2\kappa_{max} \|p_D - q_D\|_{1,\Omega_D} \end{aligned}$$

Using  $C_{s,D} := \max\{1, (1 + C_{\mu,D}) \bar{\mu}_D \kappa_{max}, 2\kappa_{max}\}$  the upper bound is proven.

For the lower bound we need the Poincare-Friedrichs inequality (theorem 2.1). As in the case of

the Stokes flow we use an arbitrary  $\rho \in (0, 1)$ .

$$\begin{aligned}
\mathcal{F}_D(\mathbf{v}_D, q_D) &= \|\kappa^{-1/2} \mu_D (|\mathbf{v}_D|^2) \mathbf{v}_D + \kappa^{1/2} \nabla q_D\|_{0, \Omega_D}^2 + \|\nabla \cdot \mathbf{v}_D\|_{0, \Omega_D}^2 \\
&\gtrsim \|\kappa^{-1/2} \mu_D (|\mathbf{u}_D|^2) \mathbf{u}_D + \kappa^{1/2} \nabla p_D - \kappa^{-1/2} \mu_D (|\mathbf{v}_D|^2) \mathbf{v}_D + \kappa^{1/2} \nabla q_D\|_{0, \Omega_D}^2 \\
&\quad + 2C \|\nabla \cdot \mathbf{u}_D - \nabla \cdot \mathbf{v}_D\|_{0, \Omega_D}^2 \\
&\geq -\frac{1-\rho}{\rho} \|\kappa^{-1/2} (\mu_D (|\mathbf{u}_D|^2) \mathbf{u}_D - \mu_D (|\mathbf{v}_D|^2) \mathbf{v}_D - \bar{\mu}_D (\mathbf{u}_D - \mathbf{v}_D))\|_{0, \Omega_D}^2 \\
&\quad + (1-\rho) \|\kappa^{1/2} (\nabla p_D - \nabla q_D) + \kappa^{-1/2} \bar{\mu}_D (\mathbf{u}_D - \mathbf{v}_D)\|_{0, \Omega_D}^2 + 2C \|\nabla \cdot \mathbf{u}_D - \nabla \cdot \mathbf{v}_D\|_{0, \Omega_D}^2 \\
&\gtrsim -\frac{C_{\mu, D}^2}{\rho} \|\kappa^{-1/2} \bar{\mu}_D (\mathbf{u}_D - \mathbf{v}_D)\|_{0, \Omega_D}^2 + \|\kappa^{1/2} (\nabla p_D - \nabla q_D) + \kappa^{-1/2} \bar{\mu}_D (\mathbf{u}_D - \mathbf{v}_D)\|_{0, \Omega_D}^2 \\
&\quad + \frac{2C}{1-\rho} \|\nabla \cdot \mathbf{u}_D - \nabla \cdot \mathbf{v}_D\|_{0, \Omega_D}^2 \\
&= \|\kappa^{1/2} \nabla (p_D - q_D)\|_{0, \Omega_D}^2 + (1 - \frac{C_{\mu, D}^2}{\rho}) \|\kappa^{-1/2} \bar{\mu}_D (\mathbf{u}_D - \mathbf{v}_D)\|_{0, \Omega_D}^2 \\
&\quad + \frac{2C}{1-\rho} \|\nabla \cdot (\mathbf{u}_D - \mathbf{v}_D)\|_{0, \Omega_D}^2 + 2(\nabla (p_D - q_D), \bar{\mu}_D (\mathbf{u}_D - \mathbf{v}_D))_{0, \Omega_D} \\
&= \|\kappa^{1/2} \nabla (p_D - q_D)\|_{0, \Omega_D}^2 + (1 - \frac{C_{\mu, D}^2}{\rho}) \|\kappa^{-1/2} \bar{\mu}_D (\mathbf{u}_D - \mathbf{v}_D)\|_{0, \Omega_D}^2 \\
&\quad + \frac{2C}{1-\rho} \|\nabla \cdot (\mathbf{u}_D - \mathbf{v}_D)\|_{0, \Omega_D}^2 - 2(p_D - q_D, \bar{\mu}_D \nabla \cdot (\mathbf{u}_D - \mathbf{v}_D))_{0, \Omega_D} \\
&\geq (\frac{\kappa_{min}}{C_D} - \frac{\bar{\mu}_D^2 (1-\rho)}{C}) \|p_D - q_D\|_{1, \Omega_D}^2 + (1 - \frac{C_{\mu, D}^2}{\rho}) \kappa_{max}^{-1} \|\bar{\mu}_D (\mathbf{u}_D - \mathbf{v}_D)\|_{0, \Omega_D}^2 \\
&\quad + \frac{C}{1-\rho} \|\nabla \cdot (\mathbf{u}_D - \mathbf{v}_D)\|_{0, \Omega_D}^2 \\
&\geq C_{e, D} (\|\mathbf{u}_D - \mathbf{v}_D\|_{div, \Omega_D}^2 + \|p_D - q_D\|_{1, \Omega_D}^2)
\end{aligned}$$

with

$$C_{e, D} = \min\left\{\frac{\kappa_{min}}{C_D} - \frac{\bar{\mu}_D^2 (1-\rho)}{C}, (1 - \frac{C_{\mu, D}^2}{\rho}) \kappa_{max}^{-1} \bar{\mu}_D^2, \frac{C}{1-\rho}\right\}$$

Again setting  $\rho \in (C_{\mu, D}^2, 1)$  the constant  $C_{e, D}$  is positive if one chooses  $C$  large enough. ■

**Remark:** As for the Stokes flow it is easy to see that we have again uniqueness of the solution and a-priori / a-posteriori error estimates.

As for the Stokes problem we can show that the *Cross model* satisfies assumptions  $(\mathbf{A1})_D, (\mathbf{A2})_D$  and  $(\mathbf{A3})_D$ :

**Lemma 3.15** *Assumptions  $(\mathbf{A1})_D, (\mathbf{A2})_D$  and  $(\mathbf{A3})_D$  hold for the Cross-model. Furthermore we have for the constants from lemma 3.13:*

- $C_{\mu, D} = \frac{\mu_0 - \mu_\infty}{\mu_0 + \mu_\infty}$ , with  $\bar{\mu}_D = \frac{\mu_0 + \mu_\infty}{2}$  and  $1 < r \leq 3$
- $C_{\mu, D} \leq \frac{\frac{r-1}{2}(\mu_0 - \mu_\infty)}{\frac{r-1}{2}(\mu_0 - \mu_\infty) + 2\mu_\infty}$ , with  $\bar{\mu}_S = \frac{\frac{r-1}{2}(\mu_0 - \mu_\infty) + 2\mu_\infty}{2}$  and  $3 < r$

**proof:** See lemma 3.7. ■

### 3.2.2 The Linearized Problem

As in the case of Stokes flow our nonlinear functional has the typical least-squares form and we use a Gauß-Newton method for the linearization. All propositions of the Stokes case are valid for the Darcy flow as well. Therefore there won't be any proofs given for the theorems in this section and the reader might refer to section 3.1.2.

As usual for Gauß-Newton methods the partial differential equation needs to be linearized: Let

$$\begin{pmatrix} \mathbf{u}_{D_N} + \hat{\mathbf{u}}_D^{(k)} \\ p_{D_D} + \hat{p}_D^{(k)} \end{pmatrix} = \begin{pmatrix} \mathbf{u}_D^{(k)} \\ p_D^{(k)} \end{pmatrix}$$

be given. Here  $(\mathbf{u}_{D_N}, p_{D_D}) \in H^{div}(\Omega_D) \times H^1(\Omega_D)$  satisfy the boundary conditions and  $(\hat{\mathbf{u}}_D^{(k)}, \hat{p}_D^{(k)})$  lies in  $H_{\Gamma_{D_N}}^{div}(\Omega_D) \times H_{\Gamma_D}^1(\Omega_D)$ . We look for an approximation

$$\begin{pmatrix} \mathbf{u}_D^{(k+1)} \\ p_D^{(k+1)} \end{pmatrix} = \begin{pmatrix} \mathbf{u}_{D_N} + \hat{\mathbf{u}}_D^{(k+1)} \\ p_{D_D} + \hat{p}_D^{(k+1)} \end{pmatrix} = \begin{pmatrix} \mathbf{u}_D^{(k)} \\ p_D^{(k)} \end{pmatrix} + \begin{pmatrix} \delta \mathbf{u}_D \\ \delta p_D \end{pmatrix}.$$

of the solution. The quadratic functional which is minimized is given by:

$$\begin{aligned} \mathcal{F}_{quad,D}(\delta \mathbf{u}_D, \delta p_D; \mathbf{u}_D^{(k)}, \mathcal{R}(\mathbf{u}_D^{(k)}, p_D^{(k)}, \mathbf{f})) &= \overbrace{\left\| \begin{pmatrix} \mathcal{R}(\mathbf{u}_D^{(k)}, p_D^{(k)}, \mathbf{f}) \\ \text{div } \mathbf{u}_D^{(k)} - \mathbf{f} \\ \kappa^{-1/2} \mu_D (|\mathbf{u}_D^{(k)}|^2) \mathbf{u}_D^{(k)} + \kappa^{1/2} \nabla p_D^{(k)} \end{pmatrix} \right\|}_{\mathcal{L}(\delta \mathbf{u}_D, \delta p_D; \mathbf{u}_D^{(k)})} + \\ &\quad \left\| \begin{pmatrix} \text{div } \delta \mathbf{u}_D \\ \kappa^{-1/2} (\mu_D (|\mathbf{u}_D^{(k)}|^2) \delta \mathbf{u}_D + 2\mu'_D (|\mathbf{u}_D^{(k)}|^2) (\mathbf{u}_D^{(k)} \cdot \delta \mathbf{u}_D) \mathbf{u}_D^{(k)} + \kappa^{1/2} \nabla \delta p_D) \end{pmatrix} \right\|_{0, \Omega_D}^2 \end{aligned}$$

The variational formulation of the minimization problem is given by:

Find  $(\delta \mathbf{u}_D, \delta p_D) \in H_{\Gamma_{S_N}}^{div}(\Omega_D) \times H_{\Gamma_S}^1(\Omega_D)$  such that

$$\left( \mathcal{L}(\delta \mathbf{u}_D, \delta p_D; \mathbf{u}_D^{(k)}), \mathcal{L}(\delta \mathbf{v}_D, \delta q_D; \mathbf{u}_D^{(k)}) \right) = - \left( \mathcal{R}(\mathbf{u}_D^{(k)}, p_D^{(k)}, \mathbf{f}), \mathcal{L}(\delta \mathbf{v}_D, \delta q_D; \mathbf{u}_D^{(k)}) \right) \quad (3.26)$$

holds for all  $(\delta \mathbf{v}_D, \delta q_D) \in H_{\Gamma_{D_N}}^{div}(\Omega_D) \times H_{\Gamma_D}^1(\Omega_D)$ .

With the same argument as in the section before we show that the quadratic Approximation has a unique solution. An analog version of lemma 3.8 holds:

**Lemma 3.16** *Assume that (A1<sub>D</sub>), (A2<sub>D</sub>) and (A3<sub>D</sub>) holds. Then we have for an arbitrary constant  $\bar{\mu}_D > 0$  :*

$$\begin{aligned} \left\| \kappa^{-1/2} (\mu_D (|\mathbf{u}_D^{(k)}|^2) \delta \mathbf{u}_D + 2\mu'_D (|\mathbf{u}_D^{(k)}|^2) (\mathbf{u}_D^{(k)} \cdot \delta \mathbf{u}_D) \mathbf{u}_D^{(k)} - \bar{\mu}_D \delta \mathbf{u}_D) \right\|_{0, \Omega_D} \\ \leq C_{\mu,D}^{quad} \cdot \bar{\mu}_D \left\| \kappa^{-1/2} \delta \mathbf{u}_D \right\|_{0, \Omega_S} \end{aligned} \quad (3.27)$$

which holds for all  $\delta \mathbf{u}_D \in H^1(\Omega_D)$  with a constant  $C_{\mu,D}(\bar{\mu}_D)$  given by

$$C_{\mu,D}^{quad} := \frac{\max\{|\mu_D (|\mathbf{u}_D^{(k)}|^2) - \bar{\mu}_D|, |\mu_D (|\mathbf{u}_D^{(k)}|^2) - \bar{\mu}_D + 2\mu'_D (|\mathbf{u}_D^{(k)}|^2) |\mathbf{u}_D^{(k)}|^2\}}{\bar{\mu}_D} < \infty \quad (3.28)$$

Furthermore by choosing  $\bar{\mu}_D$  large enough it holds  $C_{\mu,D}^{quad} < 1$ .



**Proof:** The proof is analog to lemma 3.8 and lemma 3.9 with the remark about the permeability of lemma 3.12. ■

Analog to the case of Stokes flow one gets the following theorem:

**Theorem 3.17** *Let assumptions  $(A1)_D$ ,  $(A2)_D$  and  $(A3)_D$  hold. For the quadratic approximation of the least-squares functional the following holds:*

$$C_{e,D}^{quad} (\|\mathbf{v}_D\|_{div,\Omega_D}^2 + \|q_D\|_{1,\Omega_S}^2) \leq \mathcal{F}_{quad,D}(\mathbf{v}_D, q_D; \mathbf{u}_D^{(k)}, \mathbf{0}) \leq C_{s,D}^{quad} (\|\mathbf{v}_D\|_{div,\Omega_D}^2 + \|q_D\|_{1,\Omega_S}^2)$$

for all  $(\mathbf{v}_D, q_D) \in H_{\Gamma_{D,N}}^{div}(\Omega_D) \times H_{\Gamma_{D,D}}^1(\Omega_D)$  with positive constants  $C_{e,D}^{quad}$  and  $C_{s,D}^{quad}$ . Furthermore the variational problem 3.26 has a unique solution.

**proof:** As in theorem 3.10 we have to follow the proof of theorem 3.14. ■

As before by inserting the unique solution of the linearized problem (3.26) we get

$$\mathcal{F}_D(\mathbf{u}_D^{(k)}, p_D^{(k)}, \mathbf{f}) \begin{bmatrix} \delta \mathbf{u}_D \\ \delta p_D \end{bmatrix} \leq -2C_{D,E}^{quad} (\|\delta \mathbf{u}_D\|_{div,\Omega_D}^2 + \|\delta p_D\|_{1,\Omega_1}^2)$$

and therefore we have always a reduction in the nonlinear least-squares problem by using the direction defined by the solution of the linearized problem.

**Remark:** An analog version to corollary 3.11 can be proven as well.

### 3.2.3 Numerical Examples

As for the Stokes flow we choose

$$\begin{aligned} p_{D_h} &\in \mathcal{P}_2(\mathcal{T}_h) \\ \mathbf{u}_{D_h} &\in RT_1(\mathcal{T}_h) \end{aligned}$$

In this section we take a closer look at a numerical example for a Darcy flow. The problem is chosen to benefit from adaptive refinement. We have already seen in the Stokes case that we achieve optimal convergence rates for smooth solutions by using uniform refinement. For the Darcy case we expect the same as the theory is basically identical. Therefore we focus on a more complicated problem/example.

In this subsection we take a closer look at the local mass conservation of the least-squares finite element method. Brandts et al. showed in [BCY06] that under some assumptions on the permeability / regularity of the solution the error in local mass conservation converges faster to 0 by a factor of  $h$ . For our case this means:  $\|\operatorname{div}(\mathbf{u}_D - \mathbf{u}_{D_h})\|_{0,\Omega_D} \approx Ch^3$ . Standard analysis involving interpolation operators would only provide  $\|\operatorname{div}(\mathbf{u}_D - \mathbf{u}_{D_h})\|_{0,\Omega_D} \approx Ch^2$ .

**Remark:** It has to be noted that the assumptions on the permeability in [BCY06] are very strict and the faster convergence is still visible in cases where these assumptions are not met.

The question is if this faster convergence can be observed in generalized Newtonian flows as well. To confirm this we are using the following approximated convergence rate given by:

$$\begin{aligned} \theta_{lsf}(k+1) &= \frac{\log\left(\frac{\mathcal{F}_D(k+1)}{\mathcal{F}_D(k)}\right)}{-\log\left(\frac{\#T(k+1)}{\#T(k)}\right)} \\ \theta_{mass}(k+1) &= \frac{\log\left(\frac{\|\operatorname{div}(\mathbf{u}_D - \mathbf{u}_{D,k+1})\|_{0,\Omega_D}^2}{\|\operatorname{div}(\mathbf{u}_D - \mathbf{u}_{D,k})\|_{0,\Omega_D}^2}\right)}{-\log\left(\frac{\#T(k+1)}{\#T(k)}\right)} \end{aligned}$$

where  $k$  denotes the level of refinement and  $\#T(k)$  is the number of triangles. The approximated convergence rates for the different levels are given in the respective tables. We are giving the overall convergence rate which is computed by comparing the error/ $\#\text{Triangles}$  of the first and last level of the uniform/adaptive algorithm as well.

### 3.2.3.1 Example

For this example we take a closer look at a problem with several singularities where an adaptive refinement strategy should refine several regions of the domain. The computational domain is depicted in 3.25. The problematic regions are around the re-entrant corners.

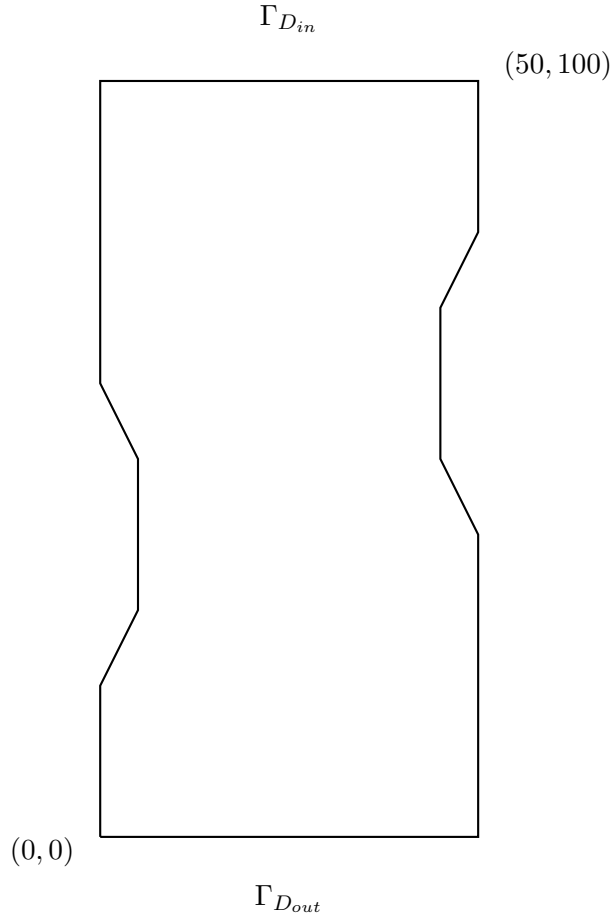


Figure 3.25: Domain for Example

The boundary conditions for this problem are given by

$$\begin{aligned} \mathbf{u}_D \cdot \mathbf{n} &= -1 && \text{on } \Gamma_{D_{in}} \\ \mathbf{u}_D \cdot \mathbf{n} &= 0 && \text{on } \Gamma_{D_0} = \Gamma_D \setminus (\Gamma_{D_{out}} \cup \Gamma_{D_{in}}) \\ \mathbf{u}_D \cdot \mathbf{n} &= 1 && \text{on } \Gamma_{D_{out}} \end{aligned}$$

Therefore we have a forced inflow/outflow with non-permeable walls. We use the same marking strategy as in the Stokes case for adaptive refinement with the exception of refining 5% instead of 4%.

### Newtonian flow

For the Newtonian flow we choose

$$\begin{aligned}\mu_D &= 0.5005 \\ \kappa &= 1\end{aligned}$$

The viscosity is chosen to the mean of minimal/maximal viscosity for the following cases. The actual errors for the uniform/adaptive refinement strategy is given in table 3.9. The solution lacks regularity due to the re-entrant corners and therefore we can not expect optimal convergence rates for the least-squares functional. As mentioned before optimal convergence rates would be 2 for the least-squares functional and 3 for the error in local mass conservation. For the uniform refinement the suboptimal convergence rates are clearly visible. As expected they are below 1 for the least-squares functional which is an error estimator for the overall error. The error in the local mass conservation goes faster to zero (where the convergence rate is twice as the one mentioned before) but not by a whole factor of  $h$ . This is again due to the lack of regularity of the solution and is visible in many examples.

For the adaptive algorithm the convergence rate varies. Starting with high convergence rates that are lower for later refinement steps. This is because our strategy starts with refining very few triangles with high errors in the beginning. Later on the error decreases slower and there are more triangles refined to keep the quality of the triangulation. Therefore the convergence rate drops though still being just slightly below optimal convergence rates for refinement strategy 2. The overall convergence rates are optimal for refinement strategy 2 and above optimal for strategy 1. The adaptive refinement strategies seems to keep the factor of  $h$  for the local mass conservation.

It has to be noted that our refinement strategy refines triangles where the least-squares functional tends to be large. If the regions where the error in local mass conservation differs it might happen that the convergence rate for  $\|\operatorname{div}(\mathbf{u}_D - \mathbf{u}_{D_h})\|_{0,\Omega_D}^2$  decreases as it might not be the dominant part of the least-squares functional. This will be observed in the next section. The plot of the convergence rate is depicted in figure 3.26.

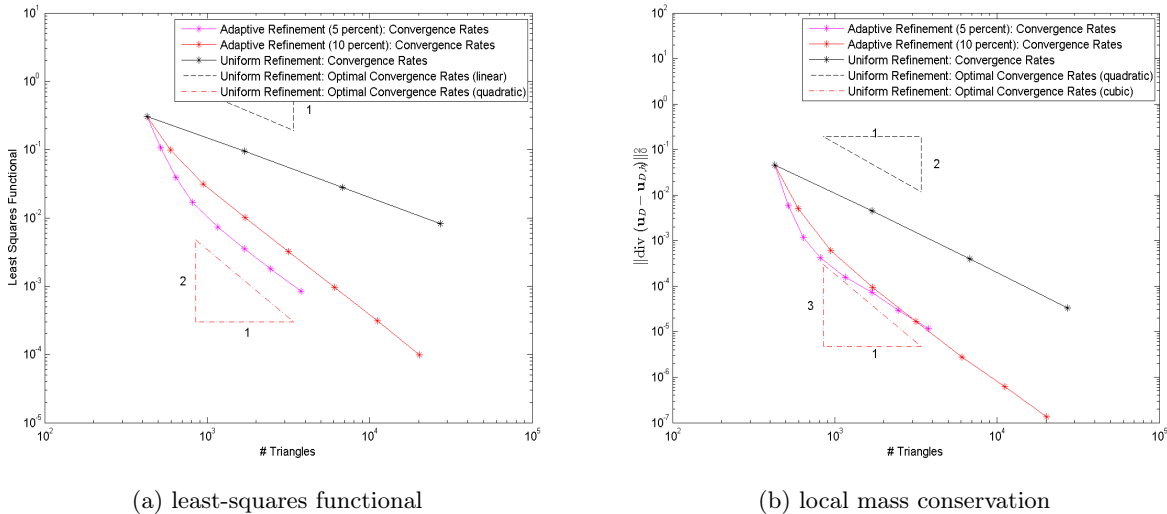


Figure 3.26: Plots of the convergence rates: Newtonian flow

The approximate solution for the volumetric flux and the hydraulic potential can be found in figure 3.27. The approximate solution looks as expected.

level	# triangles	# dofs	$\mathcal{F}_D$	$\theta_{lsf}$	$\ \text{div}(\mathbf{u}_D - \mathbf{u}_{D_h})\ _{0,\Omega_D}^2$	$\theta_{mass}$
0	425	3106	3.0499e-01		4.5236e-02	
1	516	3773	1.0605e-01	5.4448	5.8689e-03	10.5260
2	641	4682	3.9293e-02	4.5770	1.1553e-03	7.4926
3	815	5936	1.6915e-02	3.5095	4.1736e-04	4.2396
4	1163	8408	7.3929e-03	2.3278	1.5776e-04	2.7362
5	1691	12152	3.4917e-03	2.0040	7.3769e-05	2.0307
6	2452	17541	1.7710e-03	1.8269	2.9162e-05	2.4976
7	3770	26839	8.4548e-04	1.7189	1.1481e-05	2.1671
0-7				2.6976		3.7929

(a) refinement strategy: 5 % marked

level	# triangles	# dofs	$\mathcal{F}_D$	$\theta_{lsf}$	$\ \text{div}(\mathbf{u}_D - \mathbf{u}_{D_h})\ _{0,\Omega_D}^2$	$\theta_{mass}$
0	425	3106	3.0499e-01		4.5236e-02	
1	596	4341	9.9191e-02	3.3217	5.0400e-03	6.4897
2	943	6812	3.1476e-02	2.5016	6.0334e-04	4.6263
3	1705	12202	1.0050e-02	1.9277	9.5040e-05	3.1206
4	3169	22526	3.1792e-03	1.8568	1.6668e-05	2.8084
5	6087	43084	9.6577e-04	1.8253	2.7881e-06	2.7395
6	11155	78700	3.0890e-04	1.8819	6.2054e-07	2.4805
7	20161	141938	9.9371e-05	1.9162	1.3497e-07	2.5775
0-7				2.0804		3.2964

(b) refinement strategy: 10 % marked

level	# triangles	# dofs	$\mathcal{F}_D$	$\theta_{lsf}$	$\ \text{div}(\mathbf{u}_D - \mathbf{u}_{D_h})\ _{0,\Omega_D}^2$	$\theta_{mass}$
0	425	3106	3.0499e-01		4.5236e-02	
1	1700	12161	9.5028e-02	0.8412	4.5267e-03	1.6605
2	6800	48121	2.8017e-02	0.8810	3.9431e-04	1.7605
3	27200	191441	8.1867e-03	0.8875	3.3393e-05	1.7809
0-3				0.8699		1.7340

(c) uniform refinement

Table 3.9: LSF and error in mass conservation: Newtonian flow

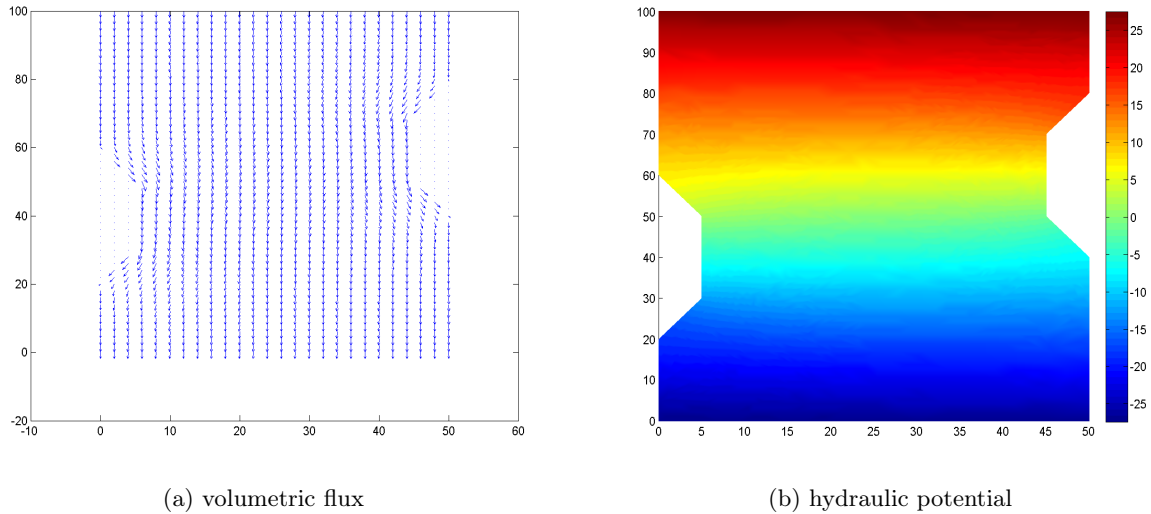


Figure 3.27: Volumetric flux and hydraulic potential: Newtonian flow

**Cross model:  $r=1.5$** 

For this example we set

$$\begin{aligned}\mu_\infty &= 10^{-3} \\ \mu_0 &= 1 \\ r &= 1.5 \\ \kappa &= 1\end{aligned}$$

As  $r = 1.5$  the viscosity decreases as  $|\mathbf{u}_D|$  increases. The actual errors and convergence rates can be found in 3.10. The behavior is similar to the Newtonian case as the error in local mass conservation decreases faster in the same way as before. The faster convergence by a factor  $h$  for the adaptive refinement strategies are observable as well. The actual convergence rates are slightly higher for this case for the uniform and adaptive refinement which indicates that the varying viscosity has a small effect on the least-squares functional. As our assumptions on the viscosity are satisfied both problems tend to the same convergence rate if  $h \rightarrow 0$ . As in the Newtonian case an adaptive refinement is highly advisable to keep computational costs reasonable. The convergence rates are depicted in figure 3.28.

The approximate solution for the volumetric flux and the hydraulic potential can be found in figure 3.29 and looks similar to the Newtonian case.

Another important plot for the non-Newtonian case is the viscosity and the absolute value of  $\mathbf{u}_{D_h}$ . These can be found in figure 3.30. For the viscosity we see that we have a strong thinning property close to the re-entrant corners. This is due to the very high absolute value of the volumetric flux which tends to  $\infty$  for the solution  $\mathbf{u}_D$ . Vice versa the viscosity tends to be high close to the corners where the absolute value of the volumetric flux is small due to the boundary conditions.

level	# triangles	# dofs	$\mathcal{F}_D$	$\theta_{lsf}$	$\ \operatorname{div}(\mathbf{u}_D - \mathbf{u}_{D_h})\ _{0,\Omega_D}^2$	$\theta_{mass}$
0	425	3106	2.6757e-01		2.3506e-02	
1	516	3773	8.6253e-02	5.8350	2.5373e-03	11.4739
2	647	4724	3.0293e-02	4.6250	5.1668e-04	7.0343
3	833	6062	1.2720e-02	3.4341	1.9597e-04	3.8365
4	1153	8350	5.7190e-03	2.4589	9.4728e-05	2.2362
5	1759	12636	2.7458e-03	1.7371	4.4210e-05	1.8042
6	2600	18593	1.3176e-03	1.8791	1.9687e-05	2.0703
7	3961	28190	6.1451e-04	1.8118	5.9561e-06	2.8399
0-7				2.7222		3.7097

(a) refinement strategy: 5 % marked

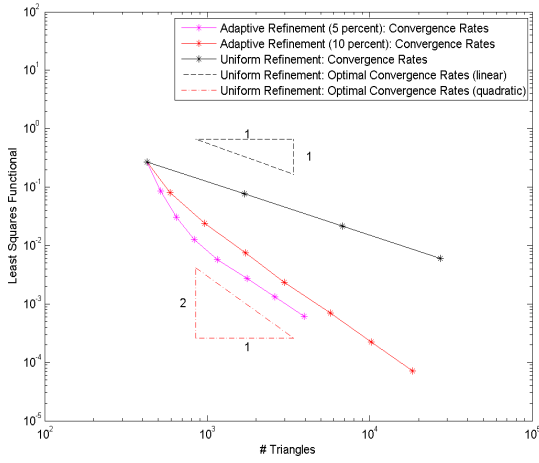
level	# triangles	# dofs	$\mathcal{F}_D$	$\theta_{lsf}$	$\ \operatorname{div}(\mathbf{u}_D - \mathbf{u}_{D_h})\ _{0,\Omega_D}^2$	$\theta_{mass}$
0	425	3106	2.6757e-01		2.3506e-02	
1	590	4299	7.9796e-02	3.6883	2.0821e-03	7.3891
2	964	6961	2.4104e-02	2.4382	2.4695e-04	4.3424
3	1725	12354	7.5280e-03	2.0000	5.1564e-05	2.6919
4	2973	21162	2.3279e-03	2.1561	8.8184e-06	3.2442
5	5732	40613	7.0203e-04	1.8260	1.8634e-06	2.3678
6	10228	72221	2.2280e-04	1.9820	4.3532e-07	2.5111
7	18362	129371	7.1897e-05	1.9329	9.6832e-08	2.5687
0-7				2.1832		3.2926

(b) refinement strategy: 10 % marked

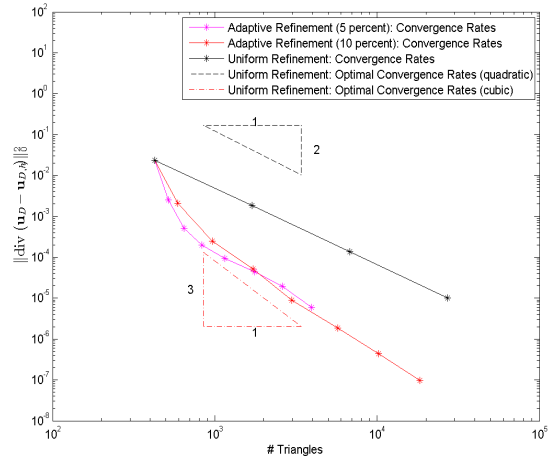
level	# triangles	# dofs	$\mathcal{F}_D$	$\theta_{lsf}$	$\ \operatorname{div}(\mathbf{u}_D - \mathbf{u}_{D_h})\ _{0,\Omega_D}^2$	$\theta_{mass}$
0	425	3106	2.6757e-01		2.3506e-02	
1	1700	12161	7.6488e-02	0.9033	1.8343e-03	1.8399
2	6800	48121	2.1340e-02	0.9208	1.3648e-04	1.8743
3	27200	191441	5.9660e-03	0.9194	1.0204e-05	1.8707
0-3				0.9145		1.8616

(c) uniform refinement

Table 3.10: LSF and error in mass conservation: *Cross model* with  $r=1.5$

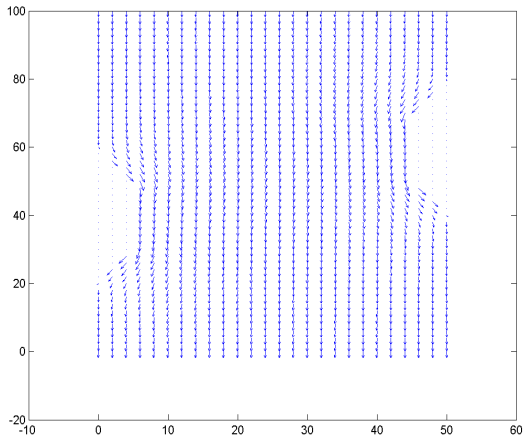


(a) least-squares functional

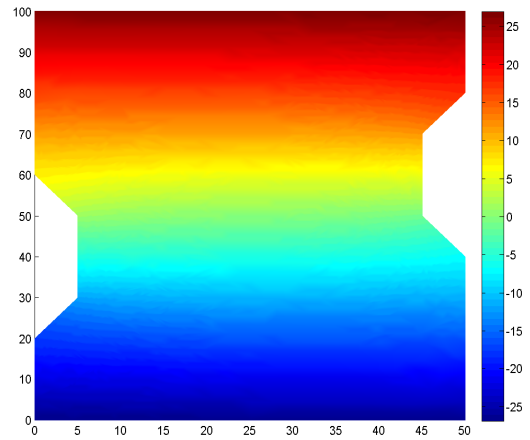


(b) local mass conservation

Figure 3.28: Plots of the convergence rates: *Cross model* with  $r=1.5$



(a) volumetric flux



(b) hydraulic potential

Figure 3.29: Volumetric flux and hydraulic potential: *Cross model* with  $r=1.5$

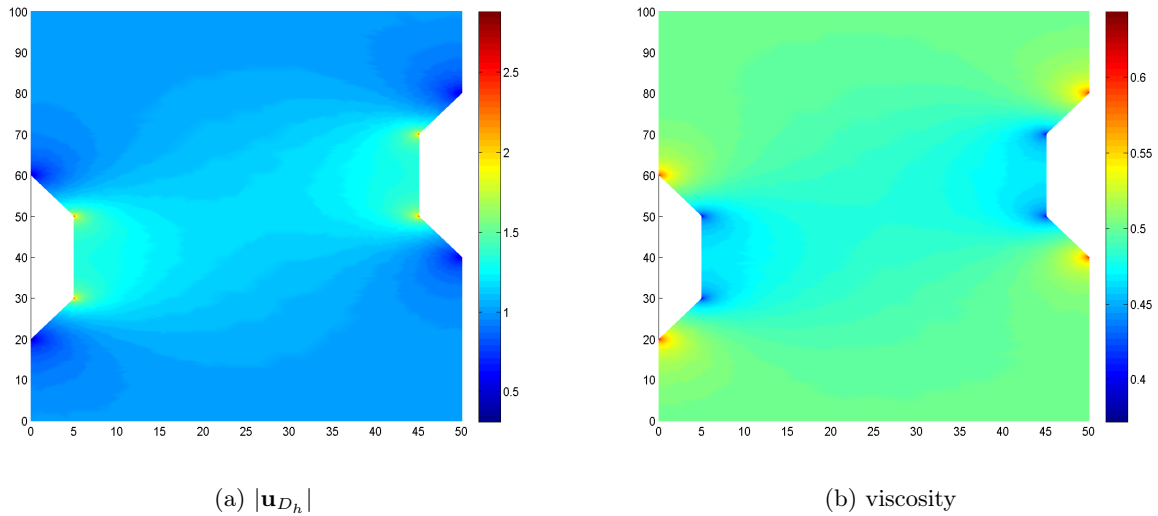


Figure 3.30:  $|\mathbf{u}_{D_h}|$  and viscosity: *Cross model* with  $r=1.5$

### Cross model: $r=2.5$

For this example we set

$$\begin{aligned}\mu_\infty &= 10^{-3} \\ \mu_0 &= 1 \\ r &= 2.5 \\ \kappa &= 1\end{aligned}$$

As  $r = 2.5$  the viscosity increases as  $|\mathbf{u}_D|$  increases. The errors and convergence rates can be found in table 3.11. Again the behavior is similar to the Newtonian case as the error in local mass conservation decreases faster in the same way as for the two examples before. We have a slight decrease in convergence rates due to the effect of the increasing viscosity close to the singularities.

The convergence rates are depicted in 3.31.

The approximate solution for the volumetric flux and the hydraulic potential can be found in figure 3.32. They look similar to the plots for the other two flows with a small difference in the maximal/minimal values of  $p_h$

The plot of the viscosity and the absolute value of  $\mathbf{u}_{D_h}$  can be found in figure 3.33. For the viscosity we see that we have the opposite behavior to the case before. The high absolute value of the volumetric flux results in higher viscosity close to the re-entrant corners. Vice versa the viscosity tends to be small close to the corners where the absolute value of the volumetric flux is small due to the boundary conditions. The maximal value of  $|\mathbf{u}_{D_h}|$  tends to be lower than for the case of  $r = 1.5$ , which is because of the higher viscosity in the relevant regions. Therefore we see again the necessity to use appropriate models for different types of flows as in contrast to the similarity of the overall flow the solution might differ in local regions considerably.

As in the two examples before an adaptive refinement is advisable.



level	# triangles	# dofs	$\mathcal{F}_D$	$\theta_{lsf}$	$\ \operatorname{div}(\mathbf{u}_D - \mathbf{u}_{D_h})\ _{0,\Omega_D}^2$	$\theta_{mass}$
0	425	3106	3.3684e-01		7.1534e-02	
1	511	3736	1.2798e-01	5.2514	1.1349e-02	9.9905
2	639	4664	4.9643e-02	4.2365	2.2973e-03	7.1461
3	856	6217	2.0784e-02	2.9781	7.2246e-04	3.9567
4	1212	8749	9.0846e-03	2.3798	2.6735e-04	2.8587
5	1843	13216	4.1059e-03	1.8948	9.9896e-05	2.3488
6	2869	20466	1.8640e-03	1.7844	3.8145e-05	2.1753
7	4299	30548	8.7576e-04	1.8679	1.4263e-05	2.4324
0-7				2.5722		3.6820

(a) refinement strategy: 5 % marked

level	# triangles	# dofs	$\mathcal{F}_D$	$\theta_{lsf}$	$\ \operatorname{div}(\mathbf{u}_D - \mathbf{u}_{D_h})\ _{0,\Omega_D}^2$	$\theta_{mass}$
0	425	3106	3.3684e-01		7.1534e-02	
1	603	4388	1.1787e-01	3.0016	9.6053e-03	5.7396
2	994	7179	3.8827e-02	2.2217	1.2005e-03	4.1606
3	1671	11964	1.2607e-02	2.1655	1.7230e-04	3.7373
4	3054	21723	4.0574e-03	1.8800	2.7315e-05	3.0542
5	5713	40458	1.2747e-03	1.8488	4.9290e-06	2.7341
6	10624	74969	4.0129e-04	1.8630	8.9206e-07	2.7554
7	19355	136284	1.3008e-04	1.8781	2.2405e-07	2.3034
0-7				2.0581		3.3190

(b) refinement strategy: 10 % marked

level	# triangles	# dofs	$\mathcal{F}_D$	$\theta_{lsf}$	$\ \operatorname{div}(\mathbf{u}_D - \mathbf{u}_{D_h})\ _{0,\Omega_D}^2$	$\theta_{mass}$
0	425	3106	3.3684e-01		7.1534e-02	
1	1700	12161	1.1352e-01	0.7846	8.8160e-03	1.5102
2	6800	48121	3.4998e-02	0.8488	8.5831e-04	1.6803
3	27200	191441	1.0525e-02	0.8667	7.7618e-05	1.7335
0-3				0.8334		1.6413

(c) uniform refinement

Table 3.11: LSF and error in mass conservation: *Cross model* with  $r=2.5$

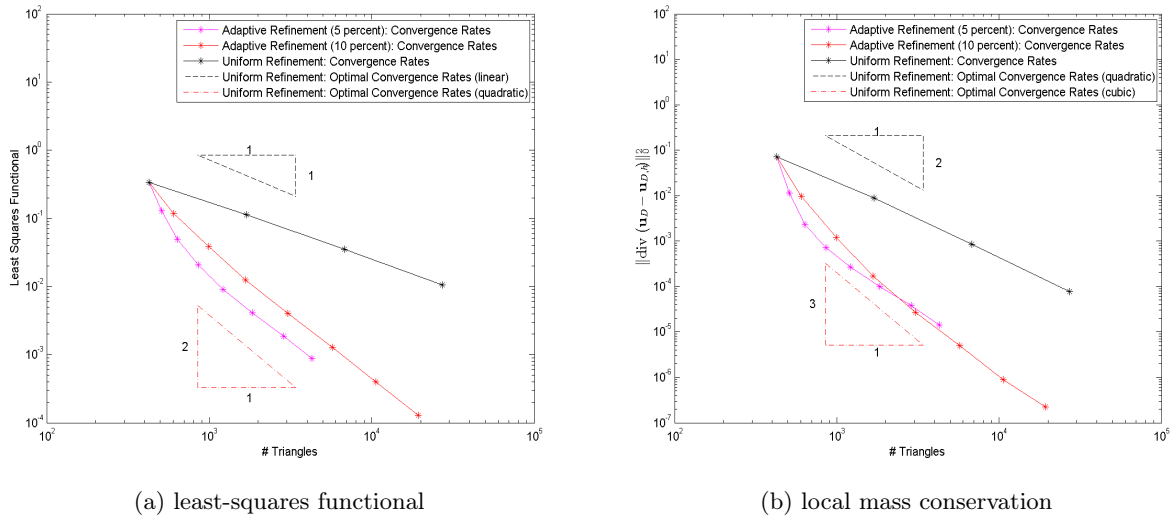


Figure 3.31: Plots of the convergence rates: *Cross model* with  $r=2.5$

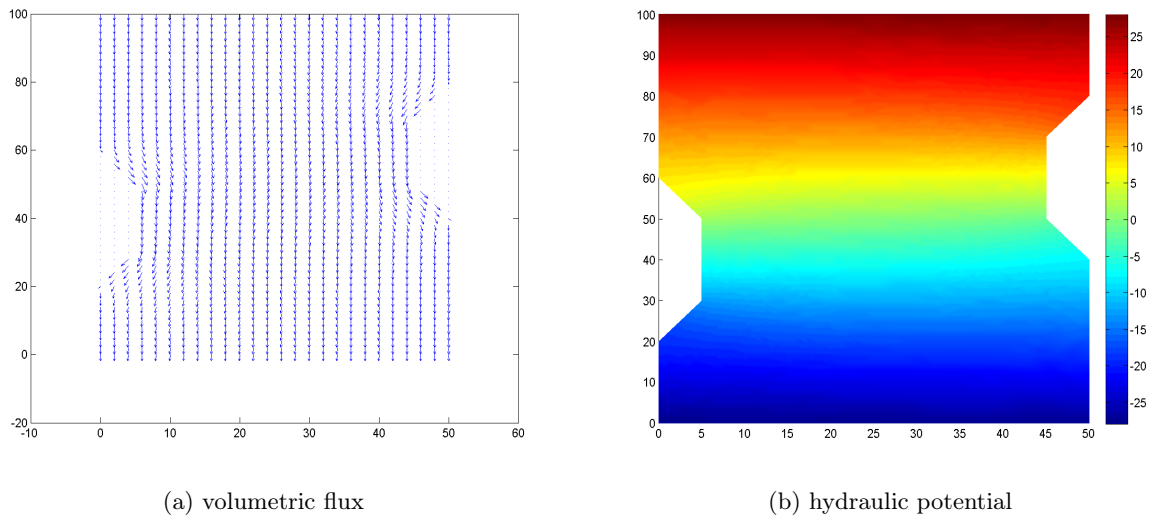


Figure 3.32: Volumetric flux and hydraulic potential: *Cross model* with  $r=2.5$

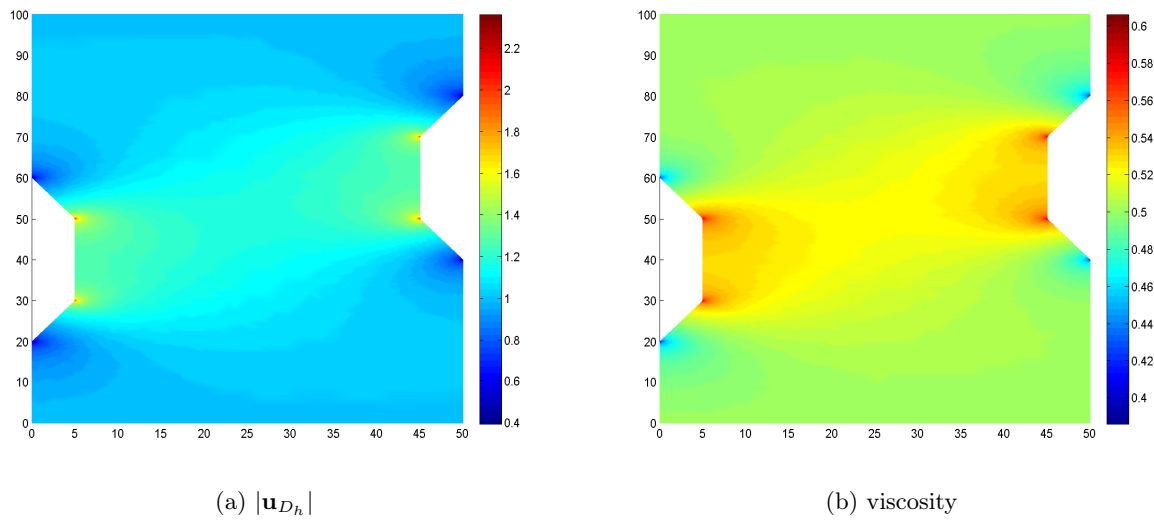


Figure 3.33:  $|\mathbf{u}_{D_h}|$  and viscosity: *Cross model* with  $r=2.5$



# Chapter 4

## The Coupled Problem

For the following section we assume  $\Omega \subset \mathbb{R}^d$  bounded and to be composed of two domains  $\Omega_S, \Omega_D \subset \mathbb{R}^d$  with Lipschitz-continuous boundary. For the boundary/interface we assume  $\partial(\Omega_S \cap \Omega) = \Gamma_S$ ,  $\partial(\Omega_D \cap \Omega) = \Gamma_D$ . Furthermore the interface is given by  $\Gamma_I = \partial\Omega_S \cap \partial\Omega_D \neq \emptyset$ .

Two examples are depicted in figure 4.1 for the case  $d = 2$ . This is a typical example of two fluid domains. The first domain has a regular interface whereas the second domain has some re-entrant corners that might result in singularities/decrease of convergence rates as shown in the section before.

We note that a regular interface might still be problematic as we have two different types of flow coupled along an interface. Therefore boundary conditions that at a first glance seem to fit might cause problems as we see in an example later in this chapter.

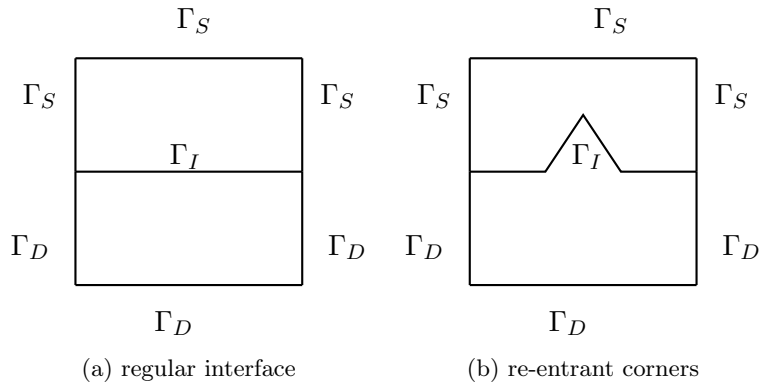


Figure 4.1: examples

We solve the Stokes equations in the fluid domain and the Darcy equations in the porous medium. Again we use a first order system least-squares finite element method to find a numerical solution.

The following interface/coupling conditions are commonly used along the interface:

$$\begin{aligned} \mathbf{u}_D \cdot \mathbf{n} - \mathbf{u}_S \cdot \mathbf{n} &= 0, \\ \mathbf{n} \cdot (\boldsymbol{\sigma} \cdot \mathbf{n}) + p &= 0, \\ \beta(\boldsymbol{\sigma} \cdot \mathbf{n}) \times \mathbf{n} + \mathbf{u}_S \times \mathbf{n} &= 0 \end{aligned} \tag{4.1}$$

with  $\mathbf{n}$  being the unit normal pointing from  $\Omega_S$  to  $\Omega_D$  along the interface.

These interface conditions are known as Beavers-Joseph-Saffman conditions [Saf71]. The positive constant  $\beta$  depending on the shape of  $\Omega_S$  and  $\Omega_D$  has to be evaluated by experiment.

The coupled problem is given by:

$$\begin{aligned} \operatorname{div} \boldsymbol{\sigma}_S &= \mathbf{f}_S && \text{in } \Omega_S \\ \operatorname{dev} \boldsymbol{\sigma}_S - 2(\mu_S(|\varepsilon(\mathbf{u}_S)|^2)\varepsilon(\mathbf{u}_S)) &= 0 && \text{in } \Omega_S \\ \nabla \cdot \mathbf{u}_S &= 0 && \text{in } \Omega_S \\ \mathbf{u}_S &= g_{SD} && \text{on } \Gamma_{SD} \\ \boldsymbol{\sigma}_S \cdot \mathbf{n} &= g_{SN} && \text{on } \Gamma_{SN} \\ \kappa^{-1/2} \mu_D(|\mathbf{u}_D|^2) \mathbf{u}_D + \kappa^{1/2} \nabla p_D &= 0 && \text{in } \Omega_D \\ \nabla \cdot \mathbf{u}_D &= f_D && \text{in } \Omega_D \\ p &= g_{DD} && \text{on } \Gamma_{DD} \\ \mathbf{u}_D \cdot \mathbf{n} &= g_{DN} && \text{on } \Gamma_{DN} \\ \mathbf{u}_D \cdot \mathbf{n} - \mathbf{u}_S \cdot \mathbf{n} &= 0 && \text{on } \Gamma_I \\ \mathbf{n} \cdot (\boldsymbol{\sigma} \cdot \mathbf{n}) + p &= 0 && \text{on } \Gamma_I \\ \beta(\boldsymbol{\sigma} \cdot \mathbf{n}) \times \mathbf{n} + \mathbf{u}_S \times \mathbf{n} &= 0 && \text{on } \Gamma_I \\ \int_{\Omega_S} \operatorname{tr} \boldsymbol{\sigma}_S \, dx &= 0 && \text{if } \Gamma_{SN} = \emptyset \text{ and } \Gamma_{DD} = \emptyset \end{aligned} \tag{4.2}$$

A similar system can be found in [EJS09].

## 4.1 The Least-Squares Functional

In the following section we introduce the least-squares functional. The notation is the same as in chapter 3. First we need the two functionals introduced in the the sections before:

$$\begin{aligned} \mathcal{F}_S(\mathbf{u}_S, \boldsymbol{\sigma}_S; \mathbf{f}_S) &= \|\operatorname{div} \boldsymbol{\sigma}_S - \mathbf{f}_S\|_{0, \Omega_S}^2 + \|\operatorname{dev} \boldsymbol{\sigma}_S - 2(\mu_S(|\varepsilon(\mathbf{u}_S)|^2)\varepsilon(\mathbf{u}_S))\|_{0, \Omega_S}^2 + \|\nabla \cdot \mathbf{u}_S\|_{0, \Omega_S}^2 \\ \mathcal{F}_D(\mathbf{u}_D, p_D; f_D) &= \|\kappa^{-1/2} \mu_D(|\mathbf{u}_D|^2) \mathbf{u}_D + \kappa^{1/2} \nabla p_D\|_{0, \Omega_D}^2 + \|\nabla \cdot \mathbf{u}_D - f_D\|_{0, \Omega_D}^2 \end{aligned}$$

we define the following norm:

$$\|\mathbf{v}\|_{div, \Omega} := \|\mathbf{v}\|_{div, \Omega} + \|\mathbf{v} \cdot \mathbf{n}\|_{0, \Gamma_I}$$

Let the following space be given

$$\bar{H}^{\Gamma_I, div}(\Omega_*) := \{\mathbf{v} \in H^{div}(\Omega_*) \mid \mathbf{v} \cdot \mathbf{n} \in L^2(\Gamma_I)\}$$

For our approach we make use of the following spaces:

$$\begin{aligned} \bar{H}_{\Gamma_{SN}}^{\Gamma_I, div}(\Omega_S) &:= \text{Closure of } (C_{\Gamma_{SN}}^\infty(\Omega_S))^d \cap \bar{H}^{\Gamma_I, div}(\Omega_S) \text{ with respect to } \|\cdot\|_{div, \Omega} \\ \bar{H}_{\Gamma_{DN}}^{\Gamma_I, div}(\Omega_D) &:= \text{Closure of } (C_{\Gamma_{DN}}^\infty(\Omega_D))^d \cap \bar{H}^{\Gamma_I, div}(\Omega_D) \text{ with respect to } \|\cdot\|_{div, \Omega} \end{aligned}$$

Again we need to address the case of  $\Gamma_{S_N} = \emptyset$  and  $\Gamma_{D_D} = \emptyset$ . Therefore we define the space  $(\bar{H}_{\Gamma_{S_N}}^{\Gamma_I, div}(\Omega_S))^d$  in this case as:

$$(\bar{H}_{\Gamma_{S_N}}^{\Gamma_I, div}(\Omega_S))^d = \{\mathbf{v} \in (\bar{H}^{\Gamma_I, div}(\Omega_S))^d \mid \int_{\Omega_S} \text{tr } \boldsymbol{\sigma}_S \, dx = 0\}$$

**Remark:** As we approximate the velocity and the volumetric flux in different spaces we need to make sure that expressions like  $\mathbf{u}_D \cdot \mathbf{n} / \boldsymbol{\sigma}_S \cdot \mathbf{n}$  are in  $L^2(\Gamma_I) / (L^2(\Gamma_I))^d$ . Therefore we need the spaces mentioned before. For the solution of (4.2) this holds as  $\mathbf{u}_S \cdot \mathbf{n}$  is especially in  $L^2(\Gamma_I)$  due to  $\mathbf{u}_S \in (H^{\frac{1}{2}}(\partial\Omega_S))^d$ . The same argument holds for  $\boldsymbol{\sigma}_S \cdot \mathbf{n}$  as  $\mathbf{u}_S \in (H^{\frac{1}{2}}(\partial\Omega_S))^d$  and  $p \in H^{\frac{1}{2}}(\partial\Omega_D)$ .

Therefore we can write the least-squares functional for the interface terms as

$$\mathcal{F}_I(\mathbf{u}_S, \boldsymbol{\sigma}_S, \mathbf{u}_D, p_D) := \|\mathbf{u}_D \cdot \mathbf{n} - \mathbf{u}_S \cdot \mathbf{n}\|_{0, \Gamma_I}^2 + \|\mathbf{n} \cdot (\boldsymbol{\sigma}_S \cdot \mathbf{n}) + p_D\|_{0, \Gamma_I}^2 + \|\beta(\boldsymbol{\sigma}_S \cdot \mathbf{n}) \times \mathbf{n} + \mathbf{u}_S \times \mathbf{n}\|_{0, \Gamma_I}^2$$

The least-squares functional of the coupled problem is given by

$$\mathcal{F}_C(\mathbf{u}_S, \boldsymbol{\sigma}_S, \mathbf{u}_D, p_D; \mathbf{f}_S, f_D) := \mathcal{F}_S(\mathbf{u}_S, \boldsymbol{\sigma}_S; \mathbf{f}_S) + \mathcal{F}_D(\mathbf{u}_D, p_D; f_D) + \mathcal{F}_I(\mathbf{u}_S, \boldsymbol{\sigma}_S, \mathbf{u}_D, p_D) \quad (4.3)$$

For convenience we define the following solution spaces

$$\begin{aligned} \mathcal{X} &= (H^1(\Omega_S))^d \times (\bar{H}^{\Gamma_I, div}(\Omega_S))^d \times \bar{H}^{\Gamma_I, div}(\Omega_D) \times H^1(\Omega_D) \\ \mathcal{X}_0 &= (H_{\Gamma_{S_D}}^1(\Omega_S))^d \times (\bar{H}_{\Gamma_{S_N}}^{\Gamma_I, div}(\Omega_S))^d \times \bar{H}_{\Gamma_{D_N}}^{\Gamma_I, div}(\Omega_D) \times H_{\Gamma_{D_D}}^1(\Omega_D) \end{aligned}$$

#### 4.1.1 The Least-Squares Functional as an Error Estimator

In this section we show that the least-squares functional  $\mathcal{F}_C(\mathbf{u}_S, \boldsymbol{\sigma}_S, \mathbf{u}_D, p_D; \mathbf{f}_S, f_D)$  can be used as an error estimator. For the linear case of Newtonian flows this was already shown in [MS11].

First we note that this chapter only consists of the proof of the two main theorems similar to chapter 3. Therefore we restrict our boundary conditions to be able to prove the desired results. First we set

$$\Gamma_{S_D} = \Gamma_S$$

with the same argument and natural choice of  $\boldsymbol{\sigma}_{S_N} = \mathbf{0}$  as in chapter 3 for the whole of chapter 4. We have not imposed any compatibility conditions so far as the assumed existence of a solution of the partial differential equation implies these. For the coupled problem though it has to be noted that aside from typical conditions as *inflow=outflow* if  $f_D = 0$  one has to be careful as the choice of  $\Gamma_{D_D} \neq \emptyset$  is already adequate to set a reference pressure and therefore our additional condition  $\int_{\Omega_S} \text{tr } \boldsymbol{\sigma}_S \, dx = 0$  can not be used. Therefore we set

$$\Gamma_{D_N} = \Gamma_D$$

with the natural choice of  $p_{D_D} = 0$  for the whole of chapter 4.

Now we define the following norm on  $\mathcal{X}$ :

$$\|(\mathbf{u}_S, \boldsymbol{\sigma}_S, \mathbf{u}_D, p_D)\|_{c, \Omega}^2 := \|\mathbf{u}_S\|_{1, \Omega_S}^2 + \|\boldsymbol{\sigma}_S\|_{div0, \Omega_S}^2 + \|\mathbf{u}_D\|_{div0, \Omega_D}^2 + \|p_D\|_{1, \Omega_D}^2$$

To show that the least-squares functional is an error estimator we need the following lemma from [MS11]:

**Lemma 4.1** *There exists an arbitrary constant  $\rho \in (0, 1)$  such that for all sufficiently small  $\alpha > 0$ ,*

$$\begin{aligned} & \frac{2}{\alpha} \mathcal{F}_I(\mathbf{z}, \boldsymbol{\tau}, \mathbf{v}, q) + \alpha (\|\mathbf{z} \cdot \mathbf{n}\|_{0, \Gamma_I}^2 + \|q\|_{0, \Gamma_I}^2) \\ & \geq 2(\mathbf{v} \cdot \mathbf{n}, q)_{0, \Gamma_I} + 2(\boldsymbol{\tau} \cdot \mathbf{n}, \mathbf{z})_{0, \Gamma_I} \\ & \quad + \frac{1}{\alpha |\Gamma_I|} \left( (1 - \rho) \left( \int_{\Gamma_I} q ds \right)^2 - \frac{1 - \rho}{\rho} \left( \int_{\Gamma_I} \mathbf{n} \cdot (\boldsymbol{\tau} \cdot \mathbf{n}) ds \right)^2 \right) \end{aligned}$$

holds for all  $(\mathbf{z}, \boldsymbol{\tau}, \mathbf{v}, q) \in \mathcal{X}$

**proof:** see [MS11] for details with the slight alteration in the proof:

$$((\boldsymbol{\tau} \cdot \mathbf{n}) \times \mathbf{n}, \mathbf{v} \times \mathbf{n})_{0, \Gamma_I} = (\boldsymbol{\tau} \cdot \mathbf{n}, \mathbf{z})_{0, \Gamma_I} - (\mathbf{n} \cdot \boldsymbol{\tau} \cdot \mathbf{n}, \mathbf{z} \cdot \mathbf{n})_{0, \Gamma_I}$$

■

Analog to the Stokes/Darcy case we have the following continuity estimate (see [MS11]):

**Lemma 4.2** *For the boundary functional  $\mathcal{F}_I$  the following continuity estimate*

$$\begin{aligned} \mathcal{F}_I(\mathbf{z}, \boldsymbol{\tau}, \mathbf{v}, q) & \leq 2C_T \|\mathbf{z}\|_{1, \Omega_S}^2 + 2 \max\{1, \beta^2\} \|\boldsymbol{\tau} \cdot \mathbf{n}\|_{0, \Gamma_I}^2 \\ & \quad + 2C_T \|q\|_{1, \Omega_D} + 2 \|\mathbf{v} \cdot \mathbf{n}\|_{0, \Gamma_I}^2 \end{aligned}$$

holds for all  $(\mathbf{z}, \boldsymbol{\tau}, \mathbf{v}, q) \in \mathcal{X}$ .

**proof:** For the boundary functional we have by using  $|\mathbf{r} \times \mathbf{n}|^2 = |\mathbf{r}|^2 - \mathbf{r} \cdot \mathbf{n}$  for all  $\mathbf{r} \in \mathbb{R}^d$ :

$$\begin{aligned} \mathcal{F}_I(\mathbf{z}, \boldsymbol{\tau}, \mathbf{v}, q) & = \|\mathbf{v} \cdot \mathbf{n} - \mathbf{z} \cdot \mathbf{n}\|_{0, \Gamma_I}^2 + \|\mathbf{n} \cdot (\boldsymbol{\tau} \cdot \mathbf{n}) + q\|_{0, \Gamma_I}^2 + \|\beta(\boldsymbol{\tau} \cdot \mathbf{n}) \times \mathbf{n} + \mathbf{z} \times \mathbf{n}\|_{0, \Gamma_I}^2 \\ & \leq 2\|\mathbf{v} \cdot \mathbf{n}\|_{0, \Gamma_I}^2 + 2\|\mathbf{z} \cdot \mathbf{n}\|_{0, \Gamma_I}^2 + 2\|\mathbf{n} \cdot (\boldsymbol{\tau} \cdot \mathbf{n})\|_{0, \Gamma_I}^2 + 2\|q\|_{0, \Gamma_I}^2 \\ & \quad + 2\beta^2 \|(\boldsymbol{\tau} \cdot \mathbf{n}) \times \mathbf{n}\|_{0, \Gamma_I}^2 + 2\|\mathbf{z} \times \mathbf{n}\|_{0, \Gamma_I}^2 \\ & \leq 2\|\mathbf{v} \cdot \mathbf{n}\|_{0, \Gamma_I}^2 + 2\|\mathbf{z}\|_{0, \Gamma_I}^2 + 2 \max\{1, \beta^2\} \|\boldsymbol{\tau} \cdot \mathbf{n}\|_{0, \Gamma_I}^2 + 2\|q\|_{0, \Gamma_I}^2 \\ & \leq 2\|\mathbf{v} \cdot \mathbf{n}\|_{0, \Gamma_I}^2 + 2\|\mathbf{z}\|_{\frac{1}{2}, \partial \Omega_S}^2 + 2 \max\{1, \beta^2\} \|\boldsymbol{\tau} \cdot \mathbf{n}\|_{0, \Gamma_I}^2 + 2\|q\|_{\frac{1}{2}, \partial \Omega_D}^2 \\ & \leq 2\|\mathbf{v} \cdot \mathbf{n}\|_{0, \Gamma_I}^2 + 2C_T \|\mathbf{z}\|_{1, \Omega_S}^2 + 2 \max\{1, \beta^2\} \|\boldsymbol{\tau} \cdot \mathbf{n}\|_{0, \Gamma_I}^2 + 2C_T \|q\|_{1, \Omega_D}^2 \end{aligned}$$

where for the last inequality theorem 2.4 was used.

■

Now we prove the important theorem that the least-squares functional is an error estimator. This theorem is based on the corresponding theorems of chapter 3.

**Remark:** For the following proof it is necessary to scale the least-squares functionals appropriately to keep the proof simple. This can be done in 2 ways:

1. Scaling the second term of 4.2 by  $\sqrt{\frac{1}{2\mu_S}}$  and the sixth term of 4.2 by  $\sqrt{\frac{1}{\mu_D}}$  beforehand.
2. Using the following easy inequality:  $\|a\| + \|b\| \gtrsim \|a\| + s\|b\|$  with an arbitrary  $s$  as it was used before in Theorems 3.5 and 3.14 for example .

For our case we use the second approach for scaling the corresponding terms in the least-squares functional. The second approach takes into account that the property of being an error estimator is independent of scaling (by constants) individual parts of the least-squares functional.



**Theorem 4.3** *Let assumptions*

- $(\mathbf{A1})_S, (\mathbf{A2})_S$  and  $(\mathbf{A3})_S$     *or*     $(\mathbf{A4})_S$  and  $(\mathbf{A5})_S$
- $(\mathbf{A1})_D, (\mathbf{A2})_D$  and  $(\mathbf{A3})_D$     *or*     $(\mathbf{A4})_D$  and  $(\mathbf{A5})_D$

hold.

Let  $\mathcal{F}_C(\mathbf{u}_S, \boldsymbol{\sigma}_S, \mathbf{u}_D, p_D)$  be the least-squares functional given by (4.3). Let  $(\mathbf{u}_S, \boldsymbol{\sigma}_S, \mathbf{u}_D, p_D) = (\mathbf{u}_{S_D}, \boldsymbol{\sigma}_{S_N}, \mathbf{u}_{D_N}, p_{D_D}) + (\hat{\mathbf{u}}_S, \hat{\boldsymbol{\sigma}}_S, \hat{\mathbf{u}}_D, \hat{p}_D)$  with  $(\hat{\mathbf{u}}_S, \hat{\boldsymbol{\sigma}}_S, \hat{\mathbf{u}}_D, \hat{p}_D) \in \mathcal{X}_0$  be the solution of 4.2. Then there exist positive constants  $C_{e,C}$  and  $C_{s,C}$  s.t.

$$\begin{aligned} C_{e,C} \|(\mathbf{u}_S - \mathbf{v}_S, \boldsymbol{\sigma}_S - \boldsymbol{\tau}_S, \mathbf{u}_D - \mathbf{v}_D, p_D - q_D)\|_{c,\Omega} \\ \leq \mathcal{F}_C(\mathbf{v}_S, \boldsymbol{\tau}_S, \mathbf{v}_D, q_D; \mathbf{f}_S, f_D) \\ \leq C_{s,C} \|(\mathbf{u}_S - \mathbf{v}_S, \boldsymbol{\sigma}_S - \boldsymbol{\tau}_S, \mathbf{u}_D - \mathbf{v}_D, p_D - q_D)\|_{c,\Omega} \end{aligned} \quad (4.4)$$

holds for all  $(\mathbf{v}_S, \boldsymbol{\tau}_S, \mathbf{v}_D, q_D) = (\mathbf{u}_{S_D}, \boldsymbol{\sigma}_{S_N}, \mathbf{u}_{D_N}, p_{D_D}) + (\hat{\mathbf{v}}_S, \hat{\boldsymbol{\tau}}_S, \hat{\mathbf{v}}_D, \hat{q}_D)$  with  $(\hat{\mathbf{v}}_S, \hat{\boldsymbol{\tau}}_S, \hat{\mathbf{v}}_D, \hat{q}_D) \in \mathcal{X}_0$ .

**proof:** This proof is based on the corresponding theorems in chapter 3 and the proof for the linear case in [MS11].

The upper bound follows directly from theorems 3.5 and 3.14 combined with lemma 4.2.

For the lower bound we use the following abbreviations:

$$\begin{aligned} \boldsymbol{\eta}_S &= \mathbf{u}_S - \mathbf{v}_S \\ \boldsymbol{\zeta}_S &= \boldsymbol{\sigma}_S - \boldsymbol{\tau}_S \\ \boldsymbol{\eta}_D &= \mathbf{u}_D - \mathbf{v}_D \\ \zeta_D &= p_D - q_D \end{aligned}$$

With the preceding remark in mind we get:

$$\begin{aligned} \mathcal{F}_S(\mathbf{u}_S, \boldsymbol{\sigma}_S; \mathbf{f}) &\gtrsim \|\operatorname{div} \boldsymbol{\sigma}_S - \mathbf{f}_S\|_{0,\Omega_S}^2 + \|\nabla \cdot \mathbf{u}_S\|_{0,\Omega_S}^2 \\ &\quad + \sqrt{\frac{1}{2\bar{\mu}_S}} \|\operatorname{dev} \boldsymbol{\sigma}_S - 2(\mu_S(|\varepsilon(\mathbf{u}_S)|)\varepsilon(\mathbf{u}_S))\|_{0,\Omega_S}^2 \end{aligned} \quad (4.5)$$

where  $\bar{\mu}_S$  can be chosen as in Lemma 3.7

Following the proof of theorem 3.5 with the appropriately scaled least-squares functional of 4.5 the following result is straightforward:

$$\begin{aligned} \mathcal{F}_S(\mathbf{u}_S, \boldsymbol{\sigma}_S; \mathbf{f}) &\gtrsim (C - \frac{C_S}{C}) \|\operatorname{div} \boldsymbol{\zeta}_S\|_{0,\Omega_S}^2 + (\frac{1}{2\bar{\mu}_S} - \frac{C_S}{C}) \|\operatorname{dev} \boldsymbol{\zeta}_S\|_{0,\Omega_S}^2 \\ &\quad + \left( \frac{2\bar{\mu}_S(1 - \tilde{C}_{\mu,S}^2)}{C_K} - \frac{1}{C} \right) \|\boldsymbol{\eta}_S\|_{1,\Omega_S}^2 - 2(\boldsymbol{\zeta}_S \cdot \mathbf{n}, \boldsymbol{\eta}_S)_{0,\Gamma_I} \end{aligned} \quad (4.6)$$

Here we used

$$-(\boldsymbol{\zeta}_S, \nabla \boldsymbol{\eta}_S) = (\operatorname{div} \boldsymbol{\zeta}_S, \boldsymbol{\eta}_S) - (\boldsymbol{\zeta}_S \cdot \mathbf{n}, \boldsymbol{\eta}_S)_{0,\Gamma_I}$$

which is due to integration by parts. We got rid of the  $\rho$  which was apparent in the proof of theorem 3.5. This is hidden in the constants  $C$  and  $\tilde{C}_{\mu,S}^2 = \frac{C_{\mu,S}^2}{\rho}$  and was chosen accordingly with  $\rho \in (C_{\mu,S}^2, 1)$ .

Again, we scale an individual part of  $\mathcal{F}_D(\mathbf{u}_D, p_D)$ :

$$\mathcal{F}_D(\mathbf{u}_D, p_D) \gtrsim \frac{1}{\bar{\mu}_D} \|\kappa^{-\frac{1}{2}} \mu_D (|\mathbf{u}_D|) \mathbf{u}_D + \kappa^{\frac{1}{2}} \nabla p_D\|_{0,\Omega_D}^2 + \|\nabla \cdot \mathbf{u}_D - f_D\|_{0,\Omega_D}^2 \quad (4.7)$$

where  $\bar{\mu}_D$  can be chosen as in Lemma 3.13.

Following the proof of theorem 3.14 with 4.7 (without using the Poincare-Friedrichs inequality) we get the following:

$$\begin{aligned} \mathcal{F}_D(\mathbf{u}_D, p_D) &\gtrsim \frac{\kappa_{min}}{\bar{\mu}_D} \|\nabla \zeta_D\|_{0,\Omega_D}^2 - \frac{1}{C} \|\zeta_D\|_{0,\Omega_D}^2 + \left(\frac{1 - \tilde{C}_{\mu,D}^2}{\kappa_{max}}\right) \bar{\mu}_D \|\boldsymbol{\eta}_D\|_{0,\Omega_D}^2 \\ &\quad + C \|\nabla \cdot \boldsymbol{\eta}_D\|_{0,\Omega_D}^2 - 2(\zeta_D, \boldsymbol{\eta}_D \cdot \mathbf{n})_{0,\Gamma_I} \end{aligned} \quad (4.8)$$

Here we used

$$(\nabla \zeta_D, \boldsymbol{\eta}_D)_{0,\Omega_D} + (\zeta_D, \nabla \cdot \boldsymbol{\eta}_D)_{0,\Omega_D} = -(\zeta_D, \boldsymbol{\eta}_D \cdot \mathbf{n})_{0,\Gamma_I}$$

which follows from the direction of  $\mathbf{n}$  (outward normal of  $\Omega_S$ ) and integration by parts. Again  $\rho$  is hidden in the constants  $C$  and  $\tilde{C}_{\mu,D}^2 = \frac{C_{\mu,D}^2}{\rho}$  and was chosen accordingly with  $\rho \in (C_{\mu,D}^2, 1)$ .

For the interface functional the following holds:

$$\mathcal{F}_I(\mathbf{v}_S, \boldsymbol{\tau}_S, \mathbf{v}_D, q_D) \gtrsim \mathcal{F}_I(\mathbf{v}_S, \boldsymbol{\tau}_S, \mathbf{v}_D, q_D) + \frac{2}{\alpha} \mathcal{F}_I(\mathbf{v}_S, \boldsymbol{\tau}_S, \mathbf{v}_D, q_D) \quad (4.9)$$

For the interface functional we can prove the following estimate (with  $C_b > 0$ ):

$$\begin{aligned} \mathcal{F}_I(\mathbf{v}_S, \boldsymbol{\tau}_S, \mathbf{v}_D, q_D) &= \|\boldsymbol{\eta}_D \cdot \mathbf{n} - \boldsymbol{\eta}_S \cdot \mathbf{n}\|_{0,\Gamma_I}^2 + \|\mathbf{n} \cdot (\boldsymbol{\zeta}_S \cdot \mathbf{n}) + \zeta_D\|_{0,\Gamma_I}^2 \\ &\quad + \|\beta(\boldsymbol{\zeta}_S \cdot \mathbf{n}) \times \mathbf{n} + \boldsymbol{\eta}_S \times \mathbf{n}\|_{0,\Gamma_I}^2 \\ &\geq (1 - \frac{1}{C_b})(\|\boldsymbol{\eta}_D \cdot \mathbf{n}\|_{0,\Gamma_I}^2 + \|\mathbf{n} \cdot (\boldsymbol{\zeta}_S \cdot \mathbf{n})\|_{0,\Gamma_I}^2 + \|\beta(\boldsymbol{\zeta}_S \cdot \mathbf{n}) \times \mathbf{n}\|_{0,\Gamma_I}^2) \\ &\quad + (1 - C_b)(\|\boldsymbol{\eta}_S \cdot \mathbf{n}\|_{0,\Gamma_I}^2 + \|\zeta_D\|_{0,\Gamma_I}^2 + \|\boldsymbol{\eta}_S \times \mathbf{n}\|_{0,\Gamma_I}^2) \\ &\geq (1 - \frac{1}{C_b})(\|\boldsymbol{\eta}_D \cdot \mathbf{n}\|_{0,\Gamma_I}^2 + \max\{1, \beta^2\} \|(\boldsymbol{\zeta}_S \cdot \mathbf{n})\|_{0,\Gamma_I}^2) \\ &\quad + (1 - C_b)(\|\boldsymbol{\eta}_S \cdot \mathbf{n}\|_{0,\Gamma_I}^2 + \|\zeta_D\|_{0,\Gamma_I}^2) \end{aligned} \quad (4.10)$$

If we set  $\delta = (1 - \frac{1}{C_b})$  and restrict  $C_b$  to  $1 < C_b \leq 2$  (which is equivalent to  $0 < \delta \leq \frac{1}{2}$ ) we get:

$$\begin{aligned} \mathcal{F}_I(\mathbf{v}_S, \boldsymbol{\tau}_S, \mathbf{v}_D, q_D) &\geq \delta(\|\boldsymbol{\eta}_D \cdot \mathbf{n}\|_{0,\Gamma_I}^2 + \max\{1, \beta\} \|(\boldsymbol{\zeta}_S \cdot \mathbf{n})\|_{0,\Gamma_I}^2) \\ &\quad - 2\delta(\|\boldsymbol{\eta}_S \cdot \mathbf{n}\|_{0,\Gamma_I}^2 + \|\zeta_D\|_{0,\Gamma_I}^2) \\ &\geq \delta(\|\boldsymbol{\eta}_D \cdot \mathbf{n}\|_{0,\Gamma_I}^2 + \max\{1, \beta\} \|(\boldsymbol{\zeta}_S \cdot \mathbf{n})\|_{0,\Gamma_I}^2) \\ &\quad - 2\delta C_T(\|\boldsymbol{\eta}_S\|_{1,\Omega_S}^2 + \|\zeta_D\|_{1,\Omega_D}^2) \end{aligned} \quad (4.11)$$

where we used theorem 2.4.

If we combine (4.6), (4.8), (4.11) and Lemma 4.1 we get the following for  $\alpha$  sufficiently small:

$$\begin{aligned}
\mathcal{F}_C(\mathbf{v}_S, \boldsymbol{\tau}_S, \mathbf{v}_D, q_D) &\gtrsim (C - \frac{C_S}{C}) \|\operatorname{div} \boldsymbol{\zeta}_S\|_{0,\Omega_S}^2 + (\frac{1}{2\bar{\mu}_S} - \frac{C_S}{C}) \|\operatorname{dev} \boldsymbol{\zeta}_S\|_{0,\Omega_S}^2 \\
&+ \left( \frac{2\bar{\mu}_S(1 - \tilde{C}_{\mu,S}^2)}{C_K} - \frac{1}{C} - 2\delta C_T \right) \|\boldsymbol{\eta}_S\|_{1,\Omega_S}^2 - 2(\boldsymbol{\zeta}_S \cdot \mathbf{n}, \boldsymbol{\eta}_S)_{0,\Gamma_I} \\
&+ \frac{\kappa_{min}}{\bar{\mu}_D} \|\nabla \zeta_D\|_{0,\Omega_D}^2 - \frac{1}{C} \|\zeta_D\|_{0,\Omega_D}^2 - 2\delta C_T \|\zeta_D\|_{1,\Omega_D}^2 \\
&+ C \|\nabla \cdot \boldsymbol{\eta}_D\|_{0,\Omega_D}^2 - 2(\zeta_D, \boldsymbol{\eta}_D \cdot \mathbf{n})_{0,\Gamma_I} + (\frac{1 - \tilde{C}_{\mu,D}^2}{\kappa_{max}}) \bar{\mu}_D \|\boldsymbol{\eta}_D\|_{0,\Omega_D}^2 \\
&- \alpha (\|\boldsymbol{\eta}_S \cdot \mathbf{n}\|_{0,\Gamma_I}^2 + \|\zeta_D\|_{0,\Gamma_I}^2) + 2(\boldsymbol{\eta}_D \cdot \mathbf{n}, \zeta_D)_{0,\Gamma_I} + 2(\boldsymbol{\zeta}_S \cdot \mathbf{n}, \boldsymbol{\eta}_S)_{0,\Gamma_I} \\
&+ \frac{1}{\alpha |\Gamma_I|} \left( (1 - \rho) \left( \int_{\Gamma_I} \zeta_D ds \right)^2 - \frac{1 - \rho}{\rho} \left( \int_{\Gamma_I} \mathbf{n} \cdot (\boldsymbol{\zeta}_S \cdot \mathbf{n}) ds \right)^2 \right) \\
&+ \delta (\|\boldsymbol{\eta}_D \cdot \mathbf{n}\|_{0,\Gamma_I}^2 + \max\{1, \beta^2\} \|(\boldsymbol{\zeta}_S \cdot \mathbf{n})\|_{0,\Gamma_I}^2)
\end{aligned} \tag{4.12}$$

with arbitrary  $\delta \in (0, \frac{1}{2}]$ ,  $C > 0$  and sufficiently small  $\alpha$ .

We can now use the following:

$$\begin{aligned}
\frac{1}{|\Gamma_I|} \left( \int_{\Gamma_I} \mathbf{n} \cdot (\boldsymbol{\zeta}_S \cdot \mathbf{n}) ds \right)^2 &\leq \|\mathbf{n} \cdot (\boldsymbol{\zeta}_S \cdot \mathbf{n})\|_{-\frac{1}{2},\Gamma_I}^2 \\
&\leq C_T (\|\boldsymbol{\zeta}_S\|_{0,\Omega_S}^2 + \|\operatorname{div} \boldsymbol{\zeta}_S\|_{0,\Omega_S}^2) \\
&\leq C_T \left( \frac{1}{d} \|\operatorname{tr} \boldsymbol{\zeta}_S\|_{0,\Omega_S}^2 + \|\operatorname{dev} \boldsymbol{\zeta}_S\|_{0,\Omega_S}^2 + \|\operatorname{div} \boldsymbol{\zeta}_S\|_{0,\Omega_S}^2 \right) \\
&\leq C_T \left( 1 + \frac{C_S}{d} \right) (\|\operatorname{dev} \boldsymbol{\zeta}_S\|_{0,\Omega_S}^2 + \|\operatorname{div} \boldsymbol{\zeta}_S\|_{0,\Omega_S}^2)
\end{aligned} \tag{4.13}$$

where we used theorem 2.5 and lemma 2.3.

With theorem 2.4 in mind we get:

$$\begin{aligned}
\|\boldsymbol{\eta}_S \cdot \mathbf{n}\|_{0,\Gamma_I}^2 + \|\zeta_D\|_{0,\Gamma_I}^2 &\leq \|\boldsymbol{\eta}_S\|_{\frac{1}{2},\Gamma_I}^2 + \|\zeta_D\|_{\frac{1}{2},\Gamma_I}^2 \\
&\leq C_T (\|\boldsymbol{\eta}_S\|_{1,\Omega_S}^2 + \|\zeta_D\|_{1,\Omega_D}^2)
\end{aligned} \tag{4.14}$$

Merging terms in (4.12) and using (4.13) and (4.14) leads to:

$$\begin{aligned}
\mathcal{F}_C(\mathbf{v}_S, \boldsymbol{\tau}_S, \mathbf{v}_D, q_D) &\gtrsim \left( C - \frac{C_S}{C} - \frac{1 - \rho}{\rho \alpha} C_T \left( 1 + \frac{C_S}{d} \right) \right) \|\operatorname{div} \boldsymbol{\zeta}_S\|_{0,\Omega_S}^2 \\
&+ \left( \frac{1}{2\bar{\mu}_S} - \frac{C_S}{C} - \frac{1 - \rho}{\rho \alpha} C_T \left( 1 + \frac{C_S}{d} \right) \right) \|\operatorname{dev} \boldsymbol{\zeta}_S\|_{0,\Omega_S}^2 \\
&+ \left( \frac{2\bar{\mu}_S(1 - \tilde{C}_{\mu,S}^2)}{C_K} - \frac{1}{C} - 2\delta C_T - \alpha C_T \right) \|\boldsymbol{\eta}_S\|_{1,\Omega_S}^2 \\
&+ \left( \frac{\kappa_{min}}{\bar{\mu}_D} - 2\delta C_T - \alpha C_T \right) \|\nabla \zeta_D\|_{0,\Omega_D}^2 \\
&+ \left( \frac{1 - \tilde{C}_{\mu,D}^2}{\kappa_{max}} \right) \bar{\mu}_D \|\boldsymbol{\eta}_D\|_{0,\Omega_D}^2 + C \|\nabla \cdot \boldsymbol{\eta}_D\|_{0,\Omega_D}^2 \\
&+ \left( \frac{1}{\alpha |\Gamma|} (1 - \rho) \right) \left( \int_{\Gamma_I} \zeta_D ds \right)^2 - \left( \frac{1}{C} + 2\delta C_T + \alpha C_T \right) \|\zeta_D\|_{0,\Omega_D}^2 \\
&+ \delta (\|\boldsymbol{\eta}_D \cdot \mathbf{n}\|_{0,\Gamma_I}^2 + \max\{1, \beta^2\} \|(\boldsymbol{\zeta}_S \cdot \mathbf{n})\|_{0,\Gamma_I}^2)
\end{aligned} \tag{4.15}$$

Using theorem 2.1 we get:

$$\begin{aligned}
\mathcal{F}_C(\mathbf{v}_S, \boldsymbol{\tau}_S, \mathbf{v}_D, q_D) &\gtrsim \left( C - \frac{C_S}{C} - \frac{1-\rho}{\rho\alpha} C_T \left( 1 + \frac{C_S}{d} \right) \right) \|\operatorname{div} \boldsymbol{\zeta}_S\|_{0,\Omega_S}^2 \\
&+ \left( \frac{1}{2\bar{\mu}_S} - \frac{C_S}{C} - \frac{1-\rho}{\rho\alpha} C_T \left( 1 + \frac{C_S}{d} \right) \right) \|\operatorname{dev} \boldsymbol{\zeta}_S\|_{0,\Omega_S}^2 \\
&+ \left( \frac{2\bar{\mu}_S(1 - \tilde{C}_{\mu,S}^2)}{C_K} - \frac{1}{C} - 2\delta C_T - \alpha C_T \right) \|\boldsymbol{\eta}_S\|_{1,\Omega_S}^2 \\
&+ \left( \frac{\kappa_{min}}{\bar{\mu}_D} - C_D C_T \alpha - \frac{C_D - 1}{C} - 2\delta C_D C_T \right) \|\nabla \zeta_D\|_{0,\Omega_D}^2 \\
&+ \left( \frac{1 - \tilde{C}_{\mu,D}^2}{\kappa_{max}} \right) \bar{\mu}_D \|\boldsymbol{\eta}_D\|_{0,\Omega_D}^2 + C \|\nabla \cdot \boldsymbol{\eta}_D\|_{0,\Omega_D}^2 \\
&+ \left( \frac{1}{\alpha|\Gamma|} (1 - \rho) - C_D \left( \frac{1}{C} + 2\delta C_T + \alpha C_T \right) \right) \left( \int_{\Gamma_I} \zeta_D ds \right)^2 \\
&+ \delta (\|\boldsymbol{\eta}_D \cdot \mathbf{n}\|_{0,\Gamma_I}^2 + \max\{1, \beta^2\} \|(\boldsymbol{\zeta}_S \cdot \mathbf{n})\|_{0,\Gamma_I}^2)
\end{aligned} \tag{4.16}$$

To ensure that all of these terms are positive we have to choose  $\rho \in (0, 1)$  and  $\alpha$  accordingly:

$$\alpha = \frac{1}{C} \tag{4.17}$$

$$\delta = \frac{1}{C} \tag{4.18}$$

$$\rho = \left( 1 + \frac{1}{4\bar{\mu}_S C C_T \left( 1 + \frac{C_S}{d} \right)} \right)^{-1} \left( \Leftrightarrow \frac{C(1-\rho)}{\rho} = \frac{1}{4\bar{\mu}_S C_T \left( 1 + \frac{C_S}{d} \right)} \right) \tag{4.19}$$

We then get:

$$\begin{aligned}
\mathcal{F}_C(\mathbf{v}_S, \boldsymbol{\tau}_S, \mathbf{v}_D, q_D) &\gtrsim \left( C - \frac{C_S}{C} - \frac{1}{4\bar{\mu}_S} \right) \|\operatorname{div} \boldsymbol{\zeta}_S\|_{0,\Omega_S}^2 \\
&+ \left( \frac{1}{4\bar{\mu}_S} - \frac{C_S}{C} \right) \|\operatorname{dev} \boldsymbol{\zeta}_S\|_{0,\Omega_S}^2 \\
&+ \left( \frac{2\bar{\mu}_S(1 - \tilde{C}_{\mu,S}^2)}{C_K} - \frac{1 + 3C_T}{C} \right) \|\boldsymbol{\eta}_S\|_{1,\Omega_S}^2 \\
&+ \left( \frac{\kappa_{min}}{\bar{\mu}_D} - \frac{C_D(3C_T + 1)}{C} \right) \|\nabla \zeta_D\|_{0,\Omega_D}^2 \\
&+ \left( \frac{1 - \tilde{C}_{\mu,D}^2}{\kappa_{max}} \right) \bar{\mu}_D \|\boldsymbol{\eta}_D\|_{0,\Omega_D}^2 + C \|\nabla \cdot \boldsymbol{\eta}_D\|_{0,\Omega_D}^2 \\
&+ \frac{1}{|\Gamma|} \left( \frac{1}{C^{-1} + 4\bar{\mu}_S C_T \left( 1 + \frac{C_S}{d} \right)} - \left( \frac{|\Gamma| C_D (1 + 3C_T)}{C} \right) \right) \left( \int_{\Gamma_I} \zeta_D ds \right)^2 \\
&+ \frac{1}{C} (\|\boldsymbol{\eta}_D \cdot \mathbf{n}\|_{0,\Gamma_I}^2 + \max\{1, \beta^2\} \|(\boldsymbol{\zeta}_S \cdot \mathbf{n})\|_{0,\Gamma_I}^2)
\end{aligned} \tag{4.20}$$

Using

$$\|\operatorname{dev} \boldsymbol{\zeta}_S\|_{0,\Omega_S}^2 + \|\operatorname{div} \boldsymbol{\zeta}_S\|_{0,\Omega_S}^2 \gtrsim \|\boldsymbol{\zeta}_S\|_{0,\Omega_S}^2 \tag{4.21}$$

as a direct consequence of lemma 2.3 and theorem 2.1 we get :

$$\mathcal{F}_C(\mathbf{v}_S, \boldsymbol{\tau}_S, \mathbf{v}_D, q_D) \gtrsim C_{C,E} \|(\mathbf{u}_S - \mathbf{v}_S, \boldsymbol{\sigma}_S - \boldsymbol{\tau}_S, \mathbf{u}_D - \mathbf{v}_D, p_D - q_D)\|_{c,\Omega} \quad (4.22)$$

by choosing  $C$  large enough. ■

**Remark:** As for the Stokes/Darcy problem a consequence of theorem 4.3 is the uniqueness of the solution. The a-priori estimates and the choice of a local error estimator is analog to chapter 3. Furthermore it has to be noted that we are not restricted to use the same models for the nonlinear viscosity. They might be completely independent as long as each model satisfies the assumptions.

### 4.1.2 The Linearized Problem

As in chapter 3 we use a Gauß-Newton method to solve the nonlinear problem. Analog to chapter 3 the following approximation shall be given:

$$\begin{pmatrix} \mathbf{u}_S^{(k)} \\ \boldsymbol{\sigma}_S^{(k)} \\ \mathbf{u}_D^{(k)} \\ p_D^{(k)} \end{pmatrix}$$

This approximation satisfies the boundary conditions. The next approximation shall be given by:

$$\begin{pmatrix} \mathbf{u}_S^{(k+1)} \\ \boldsymbol{\sigma}_S^{(k+1)} \\ \mathbf{u}_D^{(k+1)} \\ p_D^{(k+1)} \end{pmatrix} = \begin{pmatrix} \mathbf{u}_S^{(k)} \\ \boldsymbol{\sigma}_S^{(k)} \\ \mathbf{u}_D^{(k)} \\ p_D^{(k)} \end{pmatrix} + \begin{pmatrix} \delta \mathbf{u}_S \\ \delta \boldsymbol{\sigma}_S \\ \delta \mathbf{u}_D \\ \delta p_D \end{pmatrix}.$$

with  $(\delta \mathbf{u}_S, \delta \boldsymbol{\sigma}_S, \delta \mathbf{u}_D, \delta p_D) \in \mathcal{X}_0$ .

For convenience we define the inner product  $(\cdot, \cdot)_{0,\Omega}$  on

$$(L^2(\Omega_S))^d \times L^2(\Omega_S) \times (L^2(\Omega_S))^{d \times d} \times L^2(\Omega_D) \times (L^2(\Omega_D))^d \times L^2(\Gamma_I) \times L^2(\Gamma_I) \times (L^2(\Gamma_I))^d$$

by the sum of the  $L^2$  inner products on the individual spaces. The induced norm is denoted by  $\|\cdot\|_{0,\Omega}$ .

Again we want to minimize a quadratic functional

$$\mathcal{F}_{quad,C}(\delta \mathbf{u}_S, \delta \boldsymbol{\sigma}_S, \delta \mathbf{u}_D, \delta p_D; \mathbf{u}_S^{(k)}, \mathbf{u}_D^{(k)}, \mathcal{R}(\mathbf{u}_S^{(k)}, \boldsymbol{\sigma}_S^{(k)}, \mathbf{u}_D^{(k)}, p_D^{(k)}, \mathbf{f}_S, f_D))$$

which is given by:

$$\begin{aligned}
& \mathcal{F}_{quad,C}(\delta \mathbf{u}_S, \delta \boldsymbol{\sigma}_S, \delta \mathbf{u}_D, \delta p_D; \mathbf{u}_S^{(k)}, \mathbf{u}_D^{(k)}, \mathcal{R}(\mathbf{u}_S^{(k)}, \boldsymbol{\sigma}_S^{(k)}, \mathbf{u}_D^{(k)}, p_D^{(k)}, \mathbf{f}_S, f_D)) = \\
& \underbrace{\mathcal{R}(\mathbf{u}_S^{(k)}, \boldsymbol{\sigma}_S^{(k)}, \mathbf{u}_D^{(k)}, p_D^{(k)}, \mathbf{f}_S, f_D)}_{\left( \begin{array}{c} \operatorname{div} \boldsymbol{\sigma}_S^{(k)} - \mathbf{f}_S \\ \operatorname{div} \mathbf{u}_S^{(k)} \\ \operatorname{dev} \boldsymbol{\sigma}_S^{(k)} - 2\mu_S(|\boldsymbol{\varepsilon}(\mathbf{u}_S^{(k)})|^2)\boldsymbol{\varepsilon}(\mathbf{u}_S^{(k)}) \\ \operatorname{div} \mathbf{u}_D^{(k)} - f_D \\ \kappa^{-1/2}\mu_D(|\mathbf{u}_D^{(k)}|^2)\mathbf{u}_D^{(k)} + \kappa^{1/2}\nabla p_D^{(k)} \\ \mathbf{u}_D^{(k)} \cdot \mathbf{n} - \mathbf{u}_S^{(k)} \cdot \mathbf{n} \\ \mathbf{n} \cdot (\boldsymbol{\sigma}_S^{(k)} \mathbf{n}) + p_D^{(k)} \\ \beta(\boldsymbol{\sigma}_S^{(k)} \cdot \mathbf{n}) \times \mathbf{n} + \mathbf{u}_S^{(k)} \times \mathbf{n} \end{array} \right)} + \\
& \underbrace{\left( \begin{array}{c} \operatorname{div} \delta \boldsymbol{\sigma}_S \\ \operatorname{div} \delta \mathbf{u}_S \\ \operatorname{dev} \delta \boldsymbol{\sigma}_S - 2\mu_S(|\boldsymbol{\varepsilon}(\mathbf{u}_S^{(k)})|^2)\boldsymbol{\varepsilon}(\delta \mathbf{u}_S) - 4\mu'_S(|\boldsymbol{\varepsilon}(\mathbf{u}_S^{(k)})|^2)(\boldsymbol{\varepsilon}(\mathbf{u}_S^{(k)}) : \boldsymbol{\varepsilon}(\delta \mathbf{u}_S))\boldsymbol{\varepsilon}(\mathbf{u}_S^{(k)}) \\ \operatorname{div} \delta \mathbf{u}_D \\ \kappa^{-1/2}(\mu_D(|\mathbf{u}_D^{(k)}|^2)\delta \mathbf{u}_D + 2\mu'_D(|\mathbf{u}_D^{(k)}|^2)(\mathbf{u}_D^{(k)} \cdot \delta \mathbf{u}_D)\mathbf{u}_D^{(k)}) + \kappa^{1/2}\nabla \delta p_D \\ \delta \mathbf{u}_D \cdot \mathbf{n} - \delta \mathbf{u}_S \cdot \mathbf{n} \\ \mathbf{n} \cdot (\delta \boldsymbol{\sigma}_S \mathbf{n}) + \delta p_D \\ \beta(\delta \boldsymbol{\sigma}_S \cdot \mathbf{n}) \times \mathbf{n} + \delta \mathbf{u}_S \times \mathbf{n} \end{array} \right)}_{\mathcal{L}(\delta \mathbf{u}_S, \delta \boldsymbol{\sigma}_S, \delta \mathbf{u}_D, \delta p_D; \mathbf{u}_S^{(k)}, \mathbf{u}_D^{(k)})} \quad \|\cdot\|_{0,\Omega}^2
\end{aligned}$$

The variational formulation of the minimization problem is given by:

Find  $(\delta \mathbf{u}_S, \delta \boldsymbol{\sigma}_S, \delta \mathbf{u}_D, \delta p_D) \in \mathcal{X}_0$  such that

$$\begin{aligned}
& \left( \mathcal{L}(\delta \mathbf{u}_S, \delta \boldsymbol{\sigma}_S, \delta \mathbf{u}_D, \delta p_D; \mathbf{u}_S^{(k)}, \mathbf{u}_D^{(k)}), \mathcal{L}(\delta \mathbf{v}_S, \delta \boldsymbol{\tau}_S, \delta \mathbf{v}_D, \delta q_D; \mathbf{u}_S^{(k)}, \mathbf{u}_D^{(k)}) \right)_{0,\Omega} \\
& = - \left( \mathcal{R}(\mathbf{u}_S^{(k)}, \boldsymbol{\sigma}_S^{(k)}, \mathbf{u}_D^{(k)}, p_D^{(k)}, \mathbf{f}_S, f_D), \mathcal{L}(\delta \mathbf{v}_S, \delta \boldsymbol{\tau}_S, \delta \mathbf{v}_D, \delta q_D; \mathbf{u}_S^{(k)}, \mathbf{u}_D^{(k)}) \right)_{0,\Omega}
\end{aligned} \tag{4.23}$$

for all  $(\delta \mathbf{v}_S, \delta \boldsymbol{\tau}_S, \delta \mathbf{v}_D, \delta q_D) \in \mathcal{X}_0$ .

Again we are able to prove that there exists a unique minimum of  $\mathcal{F}_{quad,C}$ :

**Theorem 4.4** *Let assumptions*

- (A1)<sub>S</sub>, (A2)<sub>S</sub> and (A3)<sub>S</sub>
- (A1)<sub>D</sub>, (A2)<sub>D</sub> and (A3)<sub>D</sub>

hold.

For the quadratic approximation of the least-squares functional the following holds:

$$\begin{aligned}
& C_{e,C}^{quad} \|\|(\mathbf{v}_S, \boldsymbol{\tau}_S, \mathbf{v}_D, q_D)\|\|_{e,\Omega}^2 \\
& \leq \mathcal{F}_{quad,C}(\mathbf{v}_S, \boldsymbol{\tau}_S, \mathbf{v}_D, q_D; \mathbf{u}_S^{(k)}, \mathbf{u}_D^{(k)}, \mathbf{0}) \\
& \leq C_{s,C}^{quad} \|\|(\mathbf{v}_S, \boldsymbol{\tau}_S, \mathbf{v}_D, q_D)\|\|_{e,\Omega}^2
\end{aligned}$$

for all  $(\mathbf{v}_S, \boldsymbol{\tau}_S, \mathbf{v}_D, q_D) \in \mathcal{X}_0$  with positive constants  $C_{e,C}^{quad}$  and  $C_{s,C}^{quad}$ . Furthermore the variational problem 4.23 has a unique solution.

**proof:** Keeping the proof of theorem 3.10 in mind and using lemmas 3.9 and 3.16 the proof is analog to theorem 4.3. ■

Again we can easily deduce that the directional derivative is always negative. The following corollary is important for the numerical examples:

**Corollary 4.5** *It holds*

- for the Cross model:  $1 < r < \infty$
- for the Carreau model:  $1 < r \leq 2$

By using either the Cross model or the the Carreau model for  $\mu_S$  and the Cross model for  $\mu_D$  we then have for the solution  $(\mathbf{u}_S, \boldsymbol{\sigma}_S, \mathbf{u}_D, p_D) = (\mathbf{u}_{S_D}, \boldsymbol{\sigma}_{S_N}, \mathbf{u}_{D_N}, p_{D_D}) + (\hat{\mathbf{u}}_S, \hat{\boldsymbol{\sigma}}_S, \hat{\mathbf{u}}_D, \hat{p}_D)$  with  $(\hat{\mathbf{u}}_S, \hat{\boldsymbol{\sigma}}_S, \hat{\mathbf{u}}_D, \hat{p}_D) \in \mathcal{X}_0$  of (4.2):

$$\begin{aligned} C_{e,C} \|(\mathbf{u}_S - \mathbf{v}_S, \boldsymbol{\sigma}_S - \boldsymbol{\tau}_S, \mathbf{u}_D - \mathbf{v}_D, p_D - q_D)\|_{c,\Omega} \\ \leq \mathcal{F}_C(\mathbf{v}_S, \boldsymbol{\tau}_S, \mathbf{v}_D, q_D; \mathbf{f}_S, f_D) \\ \leq C_{s,C} \|(\mathbf{u}_S - \mathbf{v}_S, \boldsymbol{\sigma}_S - \boldsymbol{\tau}_S, \mathbf{u}_D - \mathbf{v}_D, p_D - q_D)\|_{c,\Omega} \end{aligned}$$

for all  $(\mathbf{v}_S, \boldsymbol{\tau}_S, \mathbf{v}_D, q_D) = (\mathbf{u}_{S_D}, \boldsymbol{\sigma}_{S_N}, \mathbf{u}_{D_N}, p_{D_D}) + (\hat{\mathbf{v}}_S, \hat{\boldsymbol{\tau}}_S, \hat{\mathbf{v}}_D, \hat{q}_D)$  with  $(\hat{\mathbf{v}}_S, \hat{\boldsymbol{\tau}}_S, \hat{\mathbf{v}}_D, \hat{q}_D) \in \mathcal{X}_0$ .  
Furthermore the sequence

$$\begin{pmatrix} \mathbf{u}_S^{(k+1)} \\ \boldsymbol{\sigma}_S^{(k+1)} \\ \mathbf{u}_D^{(k+1)} \\ p_D^{(k+1)} \end{pmatrix} = \begin{pmatrix} \mathbf{u}_S^{(k)} \\ \boldsymbol{\sigma}_S^{(k)} \\ \mathbf{u}_D^{(k)} \\ p_D^{(k)} \end{pmatrix} + \alpha \begin{pmatrix} \delta \mathbf{u}_S \\ \delta \boldsymbol{\sigma}_S \\ \delta \mathbf{u}_D \\ \delta p_D \end{pmatrix}.$$

with  $(\delta \mathbf{u}_S, \delta \boldsymbol{\sigma}_S, \delta \mathbf{u}_D, \delta p_D)$  from solving problem (4.23) is well defined for all  $\alpha > 0$ . By choosing  $\alpha > 0$  small enough it holds:

$$\mathcal{F}_C(\mathbf{u}_S^{(k+1)}, \boldsymbol{\sigma}_S^{(k+1)}, \mathbf{u}_D^{(k+1)}, p_D^{(k+1)}; \mathbf{f}_S, f_D) < \mathcal{F}_C(\mathbf{u}_S^{(k)}, \boldsymbol{\sigma}_S^{(k)}, \mathbf{u}_D^{(k)}, p_D^{(k)}; \mathbf{f}_S, f_D)$$

if  $(\mathbf{u}_S^{(k)}, \boldsymbol{\sigma}_S^{(k)}, \mathbf{u}_D^{(k)}, p_D^{(k)})$  is not a stationary point of  $\mathcal{F}_C$ .

**proof:** This is a direct consequence of lemma 3.7, lemma 3.15, theorem 4.3 and 4.4 combined with the remark of the descendent direction. ■

## 4.2 Numerical Examples

For this subsection we take a closer look at 2 numerical examples. The first one is characterized by a regular interface. It is depicted in figure 4.1 (a). In the second example there is a re-entrant corner (see figure 4.1 (b)). In the application of filtration processes these examples can be considered as dead-end filters [HWNW06]. As in section 3 we make use of corollary 4.5 where we have proven the least-squares functional to be an error estimator. Therefore we have again an efficient way to

treat boundary singularities by adaptive refinement. The finite element spaces we use are given by the ones of chapter 3 in their respective domains:

$$\begin{aligned}\mathbf{u}_{S_h} &\in (\mathcal{P}_2(\mathcal{T}_h(\Omega_S)))^2 \\ \boldsymbol{\sigma}_{S_h} &\in (RT_1(\mathcal{T}_h(\Omega_S)))^2 \\ \mathbf{u}_{D_h} &\in RT_1(\mathcal{T}_h(\Omega_D)) \\ p_{D_h} &\in \mathcal{P}_2(\mathcal{T}_h(\Omega_D))\end{aligned}$$

For a priori estimates we refer to chapter 2.3 and 3. For the additional term we expect optimal convergence rates of 2 as we have (see [MS11]) for the interpolation operator of chapter 2.3 and the spaces  $RT_k(\mathcal{T}_h(\Omega_D))/RT_k(\mathcal{T}_h(\Omega_S))$ :

$$\begin{aligned}\|\mathbf{u}_D \cdot \mathbf{n} - r_h(\mathbf{u}_D) \cdot \mathbf{n}\|_{0,\Gamma_I} &\leq h^{k+1} \|\mathbf{u} \cdot \mathbf{n}\|_{k+1,\Gamma_I} \\ \|\boldsymbol{\sigma}_S \cdot \mathbf{n} - r_h(\boldsymbol{\sigma}_S) \cdot \mathbf{n}\|_{0,\Gamma_I} &\leq h^{k+1} \|\boldsymbol{\sigma}_S \cdot \mathbf{n}\|_{k+1,\Gamma_I}\end{aligned}$$

if  $\mathbf{v} \cdot \mathbf{n} \in H^{k+1}(\Gamma_I)$  and  $\boldsymbol{\sigma}_S \cdot \mathbf{n} \in H^{k+1}(\Gamma_I)$ .

It has to be noted that we do not need any fitting of the triangles at the interface as the interface condition is imposed in a weak sense. Therefore the refinement can be done independently in both domains (see example I). For these problems we use 2 different strategies to refine the triangles. The first one is given by:

1. the local error-estimators are computed.
2. A given percentage  $p_S$  of triangles in the Stokes domain are marked for refinement (dependent on  $\mathcal{F}_S$ ).
3. A given percentage  $p_D$  of triangles in the Darcy domain are marked for refinement (dependent on  $\mathcal{F}_D$ ).
4. A given percentage  $p_I$  of triangles at the interface are marked for refinement (dependent on  $\mathcal{F}_I$ ).
5. The hanging nodes are computed for the union of the marked triangles (red-green refinement).
6. If a triangle was bisected before and will be bisected again it is instead marked for refinement  $\rightarrow$  return to step 5.
7. Refinement.

Especially step 5 might lead to refining more triangles than necessary. This was already observed in the previous chapters and might be visible in a major decrease of the convergence rate. Therefore we use a slightly relaxed version of step 5 here where the property *bisected before* is reset after 3 refinement steps. This leads to a more local refinement strategy.

The second refinement strategy is considerably different:

1. the local error-estimators are computed. The local value of the interface functional  $\mathcal{F}_I$  is added to adjacent triangles in both domains.
2. A given percentage  $p_C$  of all triangles in the domain  $\Omega_S \cup \Omega_D$  are marked for refinement.
3. The hanging nodes are computed for the the marked triangles (red-green refinement).



4. If a triangle was bisected before and will be bisected again it is instead be marked for refinement  
→ return to step 3.
5. Refinement.

This refinement strategy takes into account that the error might be dominant in one domain and negligible in the other. Therefore the algorithm does only refine triangles in the problematic domain and close to the interface if necessary. For the second algorithm we used a level-dependent  $p_C$  with  $p_C(0) = 20\%$ ,  $p_C(1) = 17.5\%$ , ...,  $p_C(6) = 5\%$ . We use the same approach for step as in refinement strategy I.

It has to be noted that the second algorithm is more prone to badly scaled problems. Though if scaling is done properly it addresses the problematic regions better than refinement strategy I.

### 4.2.1 Example I

The domain for this example is depicted in figure 4.2 with  $\Omega = (0, 100) \times (0, 100)$  similar to the examples in [MS11]. For the boundary conditions we impose a forced inflow at the upper boundary of the Stokes domain and a forced outflow at the lower boundary of the Darcy domain. For the rest of the boundaries we impose no normal force in the Stokes domain and impermeable walls for the volumetric flux:

$$\begin{aligned} \mathbf{u}_S &= \begin{pmatrix} 0 \\ -1 \end{pmatrix} && \text{on } \Gamma_{S_{in}} \\ \boldsymbol{\sigma}_S \cdot \mathbf{n} &= \begin{pmatrix} 0 \\ 0 \end{pmatrix} && \text{on } \Gamma_{S_0} \\ \mathbf{u}_D \cdot \mathbf{n} &= 0 && \text{on } \Gamma_{D_0} \\ \mathbf{u}_D \cdot \mathbf{n} &= \pi/2 \cdot \sin(\pi x/100) && \text{on } \Gamma_{D_{out}} \end{aligned}$$

For the right hand side we have

$$\mathbf{f}_S = \mathbf{0} \text{ and } f_D = 0$$

For the constants  $\kappa$  and  $\beta$  we use

$$\begin{aligned} \kappa &= 1 \\ \beta &= 1 \end{aligned}$$

We expect the error to be dominant in the Darcy domain and maybe close to the boundary of the interface as the flow might not fit well together due to the jump of boundary conditions (no normal force/impermeable wall).

It has to be noted that the boundary conditions do not fit the theory of chapter 4.1 as it is not proven that the least-squares functional is an error estimator. The lower bound needs lemma 2.3 to hold. The upper bound still holds and we can therefore analyze the behavior of the least-squares functional with respect to convergence rates. The examples used in [MS11] have very similar boundary conditions and the behavior of the least-squares functional was similar to problems with  $\Gamma_{S_D} = \Gamma_S$ .

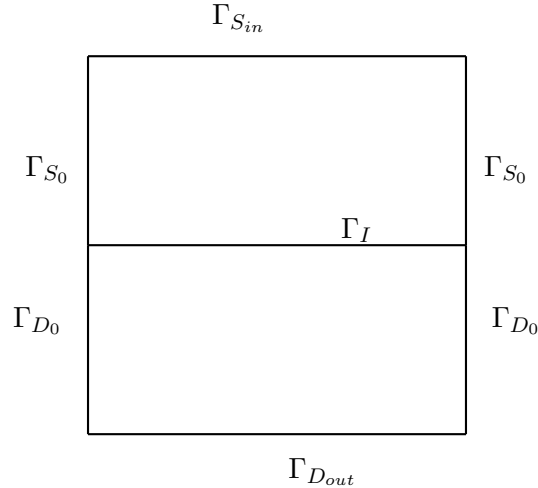


Figure 4.2: Domain for example 1

### Newtonian flow

For the Newtonian flow we get the results shown in table 4.1. We clearly see that uniform refinement achieves almost optimal convergence rates which is due to the dominant error in the Darcy domain. For  $\mathcal{F}_S$  we clearly see a reduction in error but not as fast as for  $\mathcal{F}_D$  or  $\mathcal{F}_I$ . The convergence rate for  $\mathcal{F}_S$  is close to 1.

As expected refinement strategy I achieves almost optimal convergence rates and refinement strategy II even better than optimal overall convergence rates. This is due to large reductions in the error in early refinements and was already visible in chapter 3. The convergence rates for later refinement steps are again close to 2.

For both refinement strategies a very small reduction of  $\mathcal{F}_S$  is visible in early refinement steps. This is not surprising for strategy II. For strategy I this lies in the nature of the coupled problem: Starting with a very coarse triangulation the computed flow considerably changes by refining the problematic regions in the Darcy domain. Therefore the regions with large errors might change in the Stokes domain due to a significant change in boundary conditions. Regions with large errors for early refinements might be different from regions with large errors in later refinements and therefore unnecessarily refined. When the characteristics of the flow do not change drastically (as in later refinements)  $\mathcal{F}_S$  is reduced in the usual way. The behavior for the uniform refinement strategy underscores this argument.

This is another advantage of refinement strategy II as the triangles are only refined if necessary. The refinements done in strategy II always result in a reduction of  $\mathcal{F}_S$  as seen in table 4.1.

The approximated solution for the velocity  $\mathbf{u}_{S_h}$ , the volumetric flux  $\mathbf{u}_{D_h}$ , the stress  $\boldsymbol{\sigma}_{S_h}$ , the hydraulic potential  $p_{D_h}$  and the pressure  $p_{S_h}$  can be found in figure 4.3. These plots include the streamlines as well. We clearly see the effect of the volumetric flux  $\mathbf{u}_{D_h}$  on the solution  $\mathbf{u}_{S_h}$  due to the coupling across the interface. This results in a slightly higher absolute value  $\mathbf{u}_{S_h}$  in the center of the domain. This change of behavior is driven by the pressure gradient. The solution seems to fit well together across the interface.

For the absolute value of the stress we see that the maximum/minimum are presumed close to the interface. Taking a closer look at figure 4.4 (a) we see that refinement is almost exclusively done close to the interface in regions of high absolute value of the stress. Regions with low stress, around

level	$\#T_D$	$\#T_S$	$\mathcal{F}_D$	$\mathcal{F}_S$	$\mathcal{F}_I$	$\theta_{lsf}$
0	114	97	1.5526e-001	3.7647e-005	9.9815e-006	
1	155	139	4.1141e-002	2.5634e-005	5.4106e-006	4.0023
2	224	223	2.0781e-002	1.6815e-005	3.6396e-006	1.6295
3	422	389	8.2428e-003	1.5096e-005	3.3758e-006	1.5502
4	623	648	3.5972e-003	1.4968e-005	3.4552e-006	1.8391
5	1040	1101	1.6021e-003	9.2102e-006	1.6077e-006	1.548
6	1497	1730	7.7890e-004	5.1190e-006	1.5693e-006	1.7534
7	2617	2983	3.2981e-004	2.6610e-006	7.2102e-007	1.556
0 – 7						1.8741

(a) refinement strategy I: 10 % marked

level	$\#T_D$	$\#T_S$	$\mathcal{F}_D$	$\mathcal{F}_S$	$\mathcal{F}_I$	$\theta_{lsf}$
0	114	97	1.5526e-001	3.7647e-005	9.9815e-006	
1	268	97	1.6847e-002	2.9926e-005	9.7230e-006	4.0487
2	526	97	4.2223e-003	2.9885e-005	1.0949e-005	2.5747
3	886	97	1.4909e-003	2.6351e-005	4.2215e-006	2.2592
4	1407	105	6.5018e-004	1.8990e-005	3.0798e-006	1.897
5	2052	113	3.3163e-004	1.5797e-005	2.0480e-006	1.8223
6	2728	165	1.9595e-004	9.2924e-006	6.4969e-007	1.8253
7	3394	165	1.2719e-004	9.2198e-006	6.1914e-007	1.965
0 – 7						2.4892

(b) refinement strategy II: 20-5 % marked

level	$\#T_D$	$\#T_S$	$\mathcal{F}_D$	$\mathcal{F}_S$	$\mathcal{F}_I$	$\theta_{lsf}$
0	114	97	1.5526e-001	3.7647e-005	9.9815e-006	
1	456	388	1.2966e-002	1.0367e-005	1.3230e-006	1.7905
2	1824	1552	9.8635e-004	3.1743e-006	2.9760e-007	1.8563
3	7296	6208	7.1780e-005	9.2297e-007	5.6087e-008	1.883
4	29184	24832	5.1022e-006	2.7021e-007	8.3841e-009	1.8786
0 – 4						1.8521

(c) uniform refinement

Table 4.1: Example I (Newtonian flow): LSF and convergence rates

(25,50) and (75,50), are barely refined. This is a commonly seen behavior of adaptive refinement strategies for Stokes flow.

Taking a closer look at figure 4.4 we see that Strategy II refines more triangles in  $\Omega_D$  as table 4.1 already showed which seems to be a good strategy for this problem. The refinement in  $\Omega_D$  is well distributed with a slight preference for the two lower corners. This explains why uniform refinement works very well for this problem. For the Stokes domain we see that the refinement done by both adaptive strategies is almost exclusively close to the 4 corners and the interface. What has been stated before concerning the absolute value of stress/ refinement can be stated for strategy II as well. Though the regions of high error in  $\Omega_S$  being almost identical for both strategies we see in table 4.1 that the overly refinement of strategy I does only reduce  $\mathcal{F}_S$  slightly.

Figure 4.5 shows the convergence rates of  $\|\text{div } \boldsymbol{\sigma}_{D_h}\|_0^2$ ,  $\|\text{div } \mathbf{u}_{D_h}\|_0^2$  and  $\mathcal{F}_C$ . As stated for the two separate problems we assume  $\|\text{div } \boldsymbol{\sigma}_{D_h}\|_0^2$  and  $\|\text{div } \mathbf{u}_{D_h}\|_0^2$  to converge faster to 0 by an order of  $h$  compared to  $\mathcal{F}_C$ . This is visible for the term  $\|\text{div } \mathbf{u}_{D_h}\|_0^2$  for uniform refinement. Strategy II behaves even better than uniform refinement and achieves optimal overall convergence rates. Strategy I fails to achieve better convergence rates for  $\|\text{div } \mathbf{u}_{D_h}\|_0^2$ . This is due to refining not enough triangles in  $\Omega_D$  and missing triangles where the error  $\|\text{div } \mathbf{u}_{D_h}\|_0^2$  would be considerably reduced. The term  $\|\text{div } \boldsymbol{\sigma}_{D_h}\|_0^2$  does not show the improved convergence rate. The convergence rate is not better than for  $\mathcal{F}_C$ . Even if we assume the asymptotic convergence rate for this problem to be closer to 1 as the reduction of  $\mathcal{F}_S$  indicates we do not see the predicted rate of 2 for  $\|\text{div } \boldsymbol{\sigma}_{D_h}\|_0^2$ . More refinement steps might be necessary to examine this behavior but computational capacities limit us here. Both adaptive refinement methods perform equally bad in regard of the error  $\|\text{div } \boldsymbol{\sigma}_{D_h}\|_0^2$ . Uniform refinement performs better here. This is understandable for strategy II but underscores again that the refinement in  $\Omega_S$  of strategy I is unnecessary and not efficient.

It has to be noted that a differently scaled problem in [MS11] exhibits the same behavior. The question of scaling arises by considering the quantities of interest in applications. For this example we consider the Stokes flow of being of lesser importance for the overall flow. Different scaling might be needed if the application changes.

### Cross model: $r=1.5$

For the *Cross model* with  $r = 1.5$  we use the same constants as in chapter 3:

$$\begin{aligned}\mu_{\infty_S} &= \mu_{\infty_D} = 10^{-3} \\ \mu_{0_S} &= \mu_{0_D} = 1 \\ K_S &= K_D = 1 \\ r &= 1.5\end{aligned}$$

The results are shown in table 4.2. The overall convergence rates are similar to the Newtonian case for the adaptive refinement strategies.

A difference can be seen for strategy II: More triangles in the domain  $\Omega_S$  are refined as in the case of Newtonian flow. The nonlinearity seems to result in a larger error-estimator  $\mathcal{F}_S$  for some triangles in  $\Omega_S$ . Due to the shear thinning property of the flow in  $\Omega_S$  the problem seems more demanding there. We observe this in a later example as well. Therefore the mentioned problem of unnecessary refinements with refinement strategy I is still visible but less prevalent.

For the uniform refinement we see a slightly smaller convergence rate. Obviously the nonlinearity has an effect on the reduction of the error as stated in chapter 3. We see again the same behavior in  $\mathcal{F}_S$ : The convergence rate is close to 1 for  $\mathcal{F}_S$  indicating that the asymptotic convergence rate for the coupled problem is different from the convergence rate for  $\mathcal{F}_D$ .

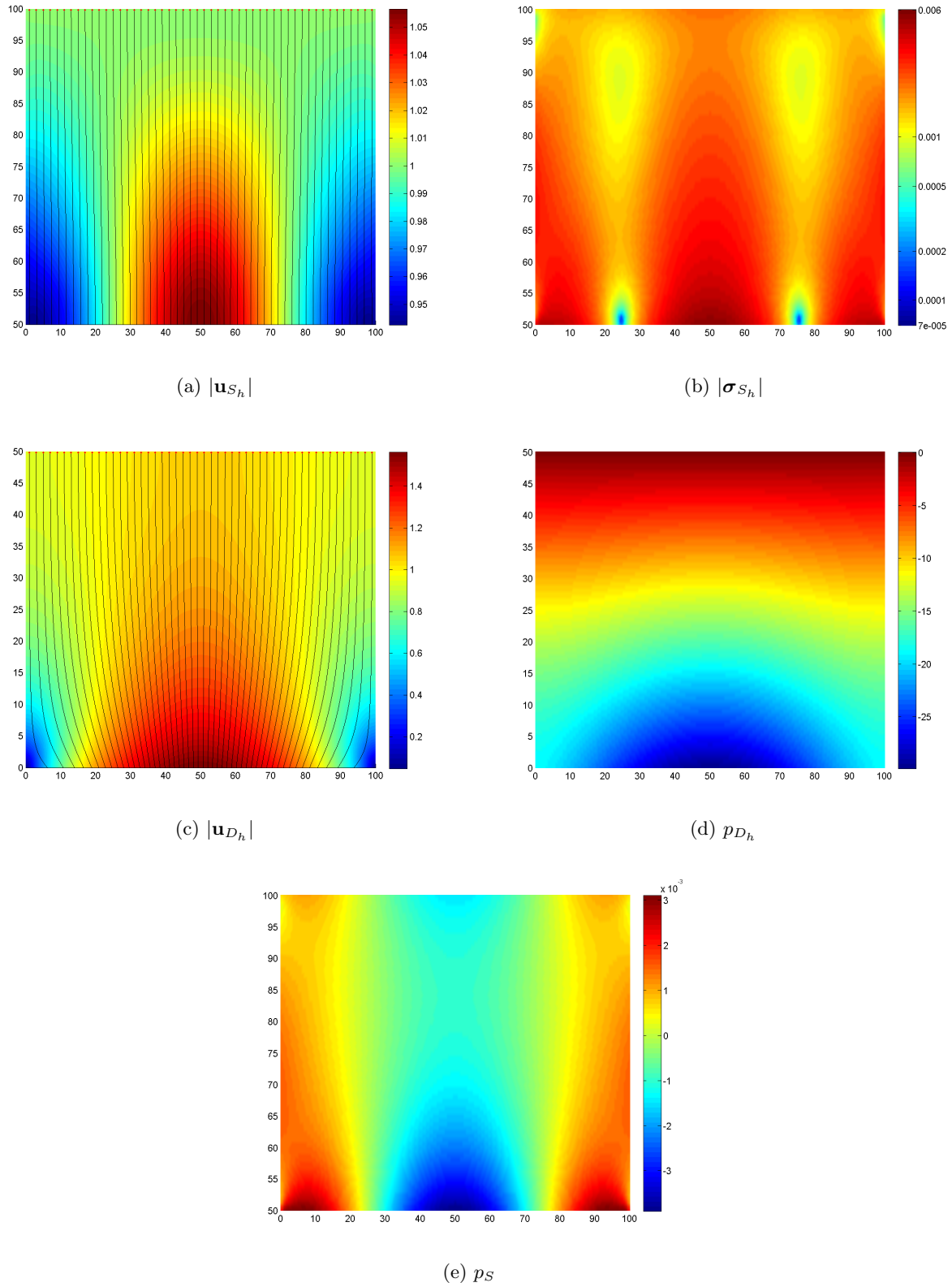
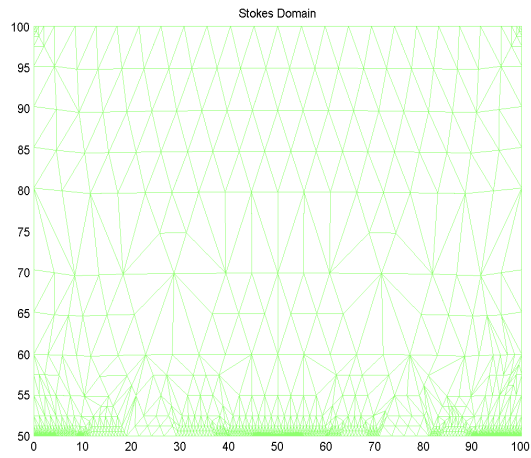
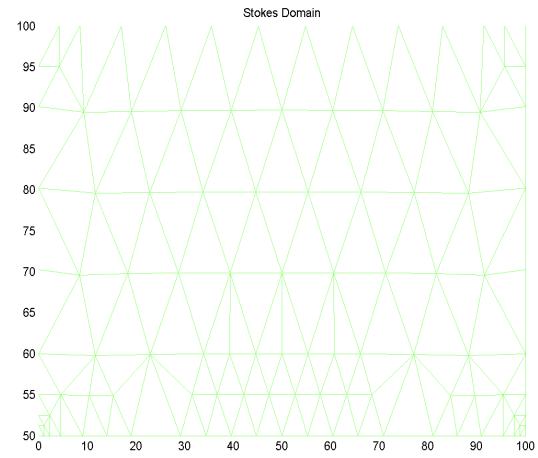


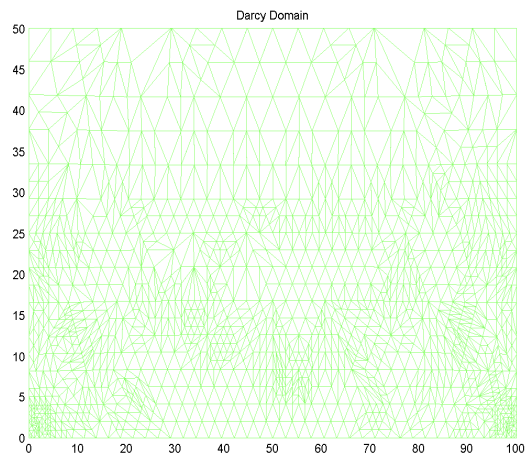
Figure 4.3: Example I (Newtonian flow): Plots of the approximate solutions



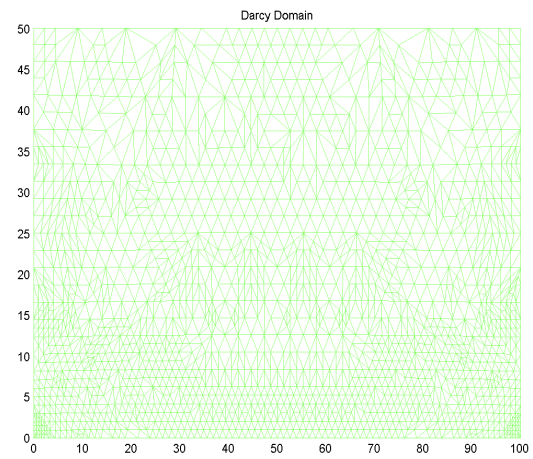
(a) Strategy I: Triangulation (Stokes)



(b) Strategy II: Triangulation (Stokes)

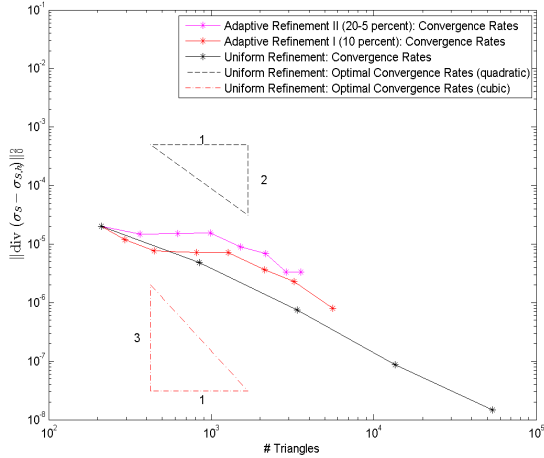


(c) Strategy I: Triangulation (Darcy)

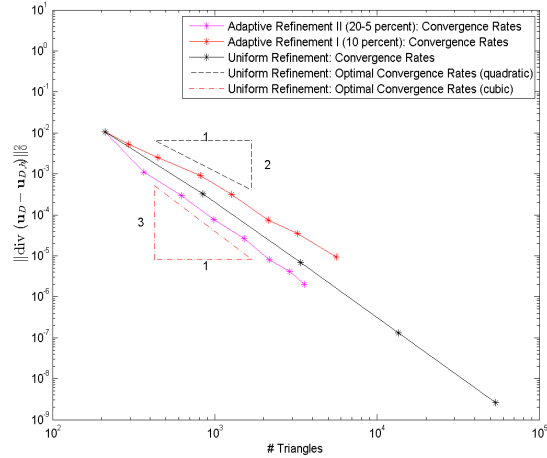


(d) Strategy II: Triangulation (Darcy)

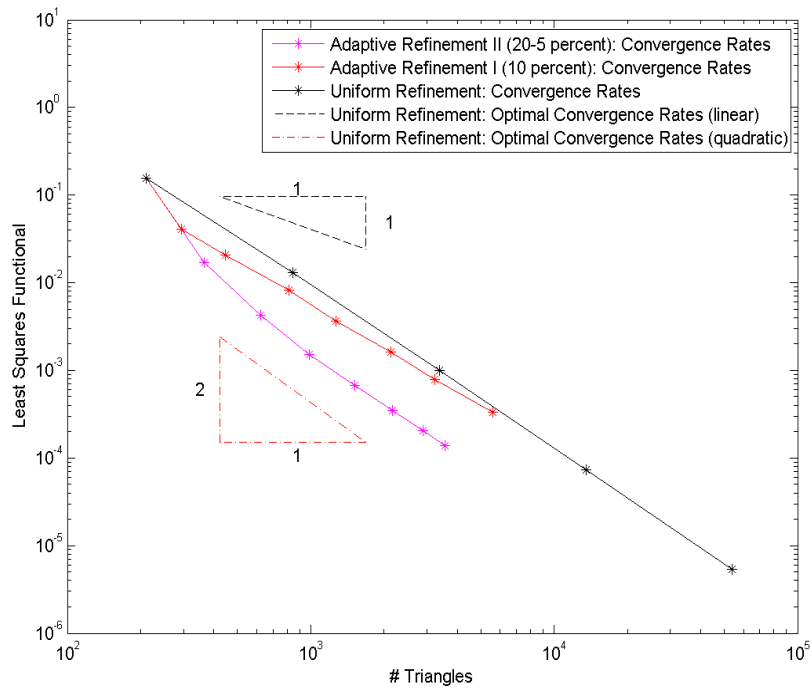
Figure 4.4: Example I (Newtonian flow): Plots of both triangulation strategies



(a) Convergence rates:  $\|\text{div} \sigma_{D_h}\|_0^2$



(b) Convergence rates:  $\|\text{div} \mathbf{u}_{D_h}\|_0^2$



(c) Convergence rates:  $\mathcal{F}_C$

Figure 4.5: Example I (Newtonian flow): Plots of convergence rates

level	$\#T_D$	$\#T_S$	$\mathcal{F}_D$	$\mathcal{F}_S$	$\mathcal{F}_I$	$\theta_{lsf}$
0	114	97	1.3119e-001	1.8057e-004	4.0201e-005	
1	155	139	3.2032e-002	1.1623e-004	2.7315e-005	4.2418
2	228	223	1.5516e-002	7.6181e-005	1.9489e-005	1.6901
3	435	389	6.9795e-003	6.5611e-005	1.7604e-005	1.3161
4	623	650	2.7931e-003	6.0334e-005	1.6513e-005	2.0704
5	1084	1103	1.1673e-003	4.2293e-005	6.7524e-006	1.5862
6	1572	1767	5.5391e-004	1.1723e-005	3.8180e-006	1.7936
7	2676	3007	2.3549e-004	8.8394e-006	2.2886e-006	1.5735
0 – 7						1.9063

(a) refinement strategy I: 10 % marked

level	$\#T_D$	$\#T_S$	$\mathcal{F}_D$	$\mathcal{F}_S$	$\mathcal{F}_I$	$\theta_{lsf}$
0	114	97	1.3119e-001	1.8057e-004	4.0201e-005	
1	256	97	1.5975e-002	1.6754e-004	3.9011e-005	4.0699
2	494	97	3.6928e-003	1.6953e-004	4.1079e-005	2.7594
3	886	105	1.2418e-003	1.1598e-004	7.3217e-006	2.0325
4	1334	133	5.6934e-004	8.1849e-005	5.7276e-006	1.8647
5	1920	209	2.8343e-004	4.0760e-005	3.3003e-006	1.869
6	2532	296	1.6452e-004	2.6618e-005	2.1905e-006	1.8564
7	3050	440	1.2042e-004	1.7685e-005	1.0008e-006	1.5651
0 – 7						2.4417

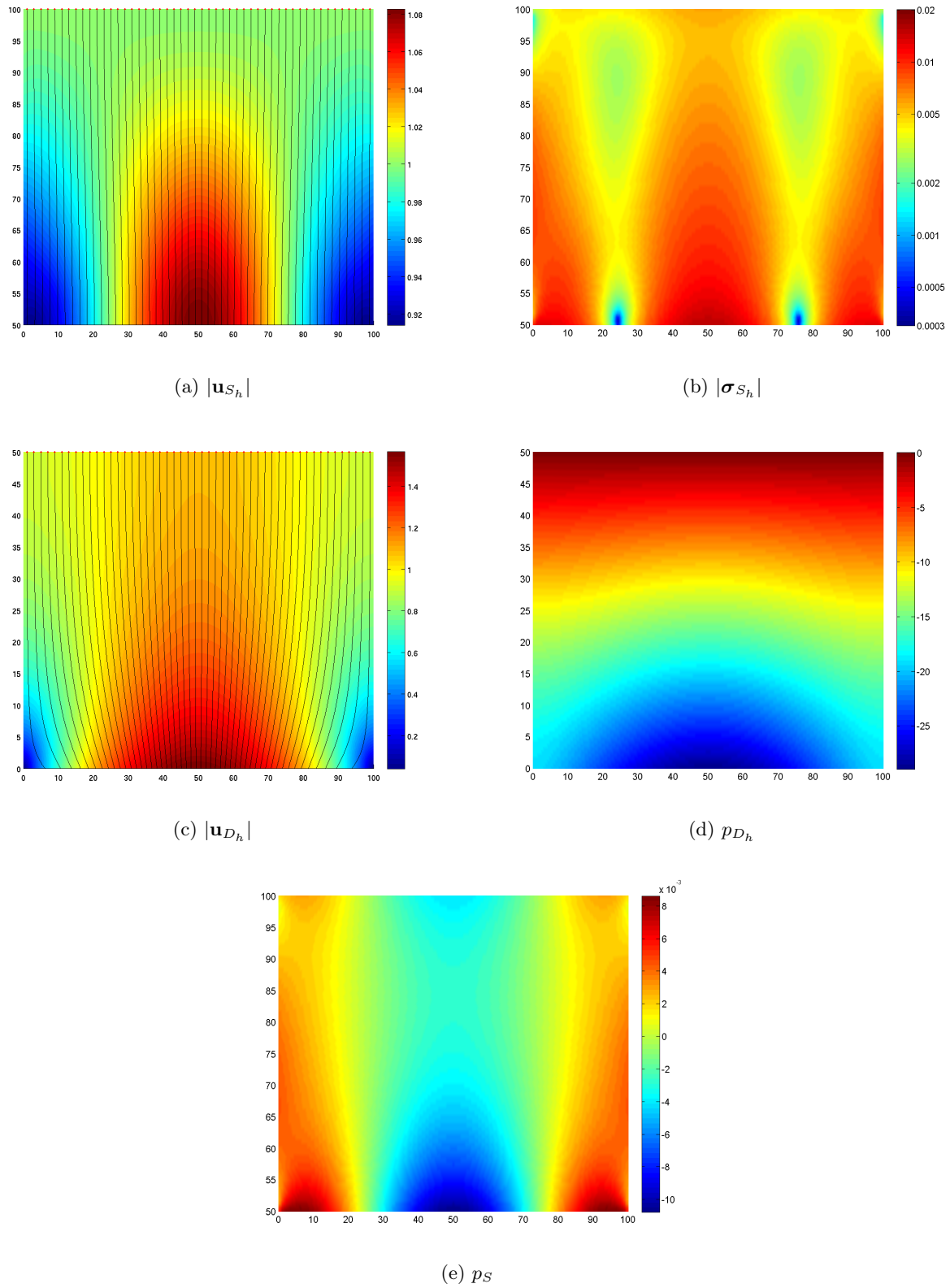
(b) refinement strategy II: 20-5 % marked

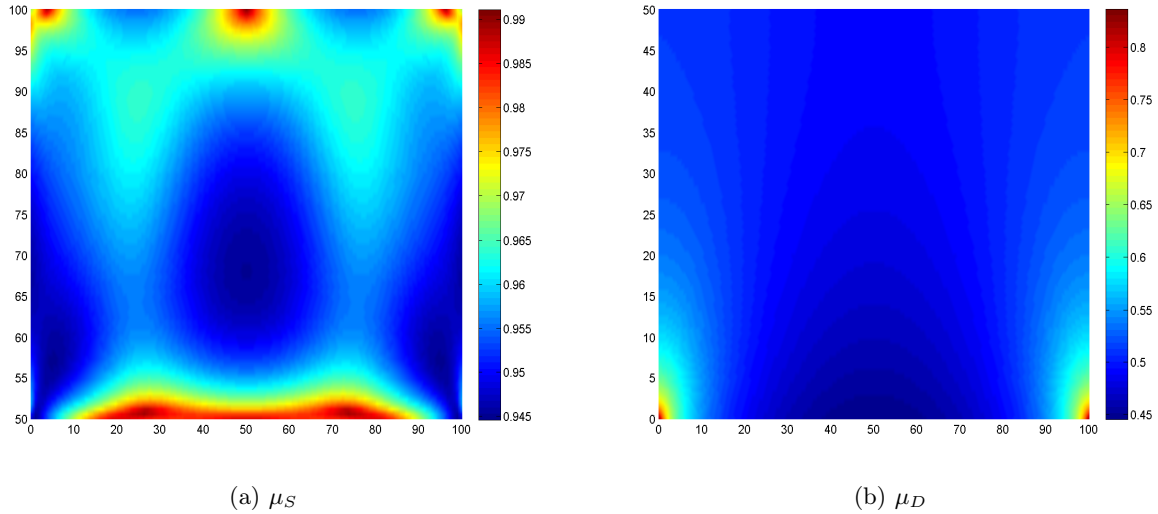
level	$\#T_D$	$\#T_S$	$\mathcal{F}_D$	$\mathcal{F}_S$	$\mathcal{F}_I$	$\theta_{lsf}$
0	114	97	1.3119e-001	1.8057e-004	4.0201e-005	
1	456	388	1.1900e-002	5.6349e-005	6.7941e-006	1.7287
2	1824	1552	1.0038e-003	1.6464e-005	1.5052e-006	1.7747
3	7296	6208	8.1390e-005	4.7338e-006	2.7160e-007	1.782
4	29184	24832	6.4270e-006	1.4344e-006	4.0549e-008	1.7253
0 – 4						1.7527

(c) uniform refinement

Table 4.2: Example 1 (Cross model  $r=1.5$ ): LSF and convergence rates



Figure 4.6: Example I (Cross:  $r=1.5$ ): Plots of the approximate solutions

Figure 4.7: Example I (Cross:  $r=1.5$ ): Viscosities

The solutions for this problem are plotted in figure 4.6. In addition to the interesting physical quantities the viscosity for both domains is plotted in figure 4.7. The solutions for velocity/volumetric flux look very similar to the Newtonian case. The maximal / minimal value  $|\mathbf{u}_S|$  differs due to the viscosity being generally larger.

Larger differences can be seen for the stress  $|\boldsymbol{\sigma}_{S_h}|$  and the the pressure  $p_S$  which differ especially in its minimal/maximal value. This is again due to the viscosity being larger compared to the Newtonian case. The distribution looks slightly different as well.

More interesting is the difference in  $p_{D_h}$  close to the corners where the viscosity is small. Here we see the main difference of the different solutions.

An interesting plot is the viscosity. Close to the interface the shear rate  $|\varepsilon(\mathbf{u}_{S_h})|$  is small which results in a higher viscosity  $\mu_S$ . This is not true around the corners  $(0, 50)$  and  $(100, 50)$ . The shear rate increases and results in a lower viscosity. For  $\mu_D$  we see the highest values close to the corners where  $|\mathbf{u}_{D_h}|$  tends to 0 due to boundary conditions.

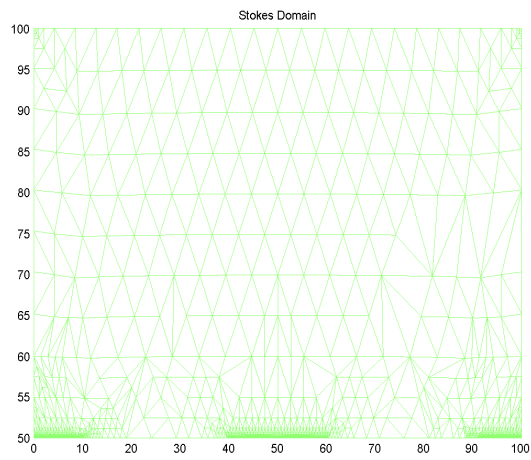
The refined triangulations can be found in 4.8. The regions where more triangles are refined are similar to the Newtonian case with the differences already stated before. The main difference can be seen in figure 4.8 (a). This should not be overestimated as many of these refinements are unnecessary as in the Newtonian case. For strategy II we see the main refinement in the 4 corners.

The convergence rates can be found in figure 4.9. The results look again similar to the Newtonian case. A slight difference can be seen as for the error  $\|\text{div } \boldsymbol{\sigma}_{D_h}\|_0^2$  as adaptive strategy I is almost as effective (see level 6) as uniform refinement. This is a slight improvement compared to the Newtonian case.

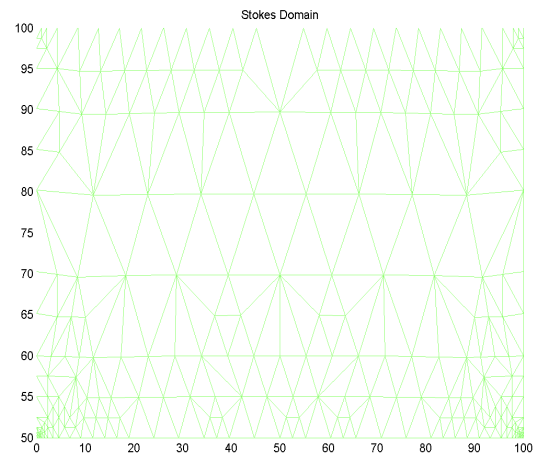
### Cross model: $r=2.5$

For the Cross model with  $r = 2.5$  we use the same values for the remaining constants as before. The results are shown in table 4.3.

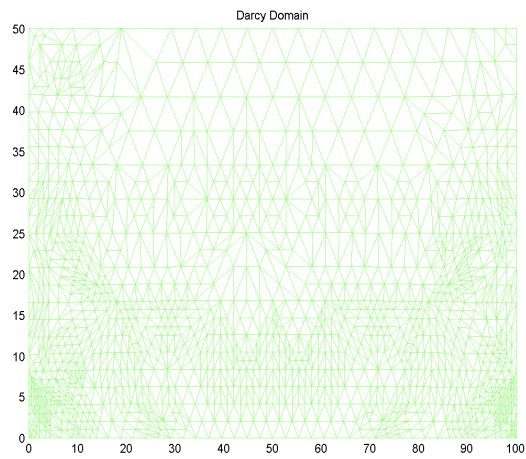
Again the results are similar to the other 2 cases. The main difference for this case is that for this example refinement strategy II does not refine any triangle in  $\Omega_S$ . The reduction of  $\mathcal{F}_S$  is solely due to the change in boundary conditions along the interface.



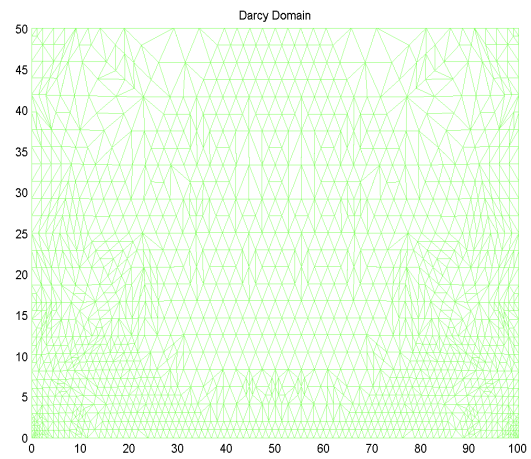
(a) Strategy I: Triangulation (Stokes)



(b) Strategy II: Triangulation (Stokes)

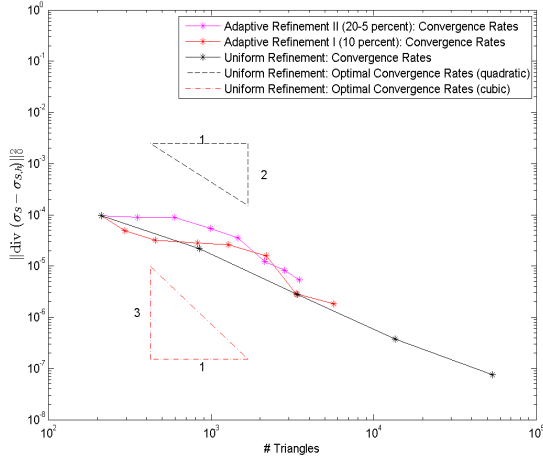


(c) Strategy I: Triangulation (Darcy)

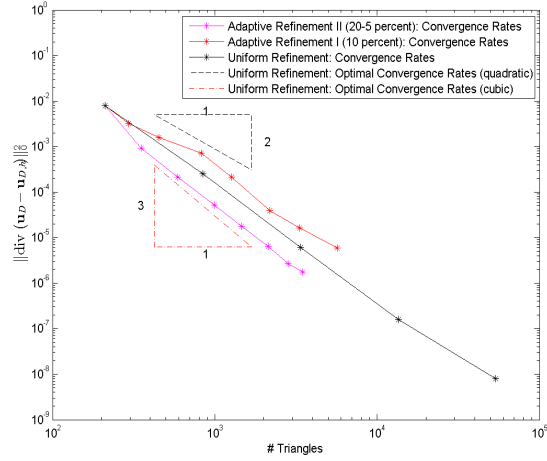


(d) Strategy II: Triangulation (Darcy)

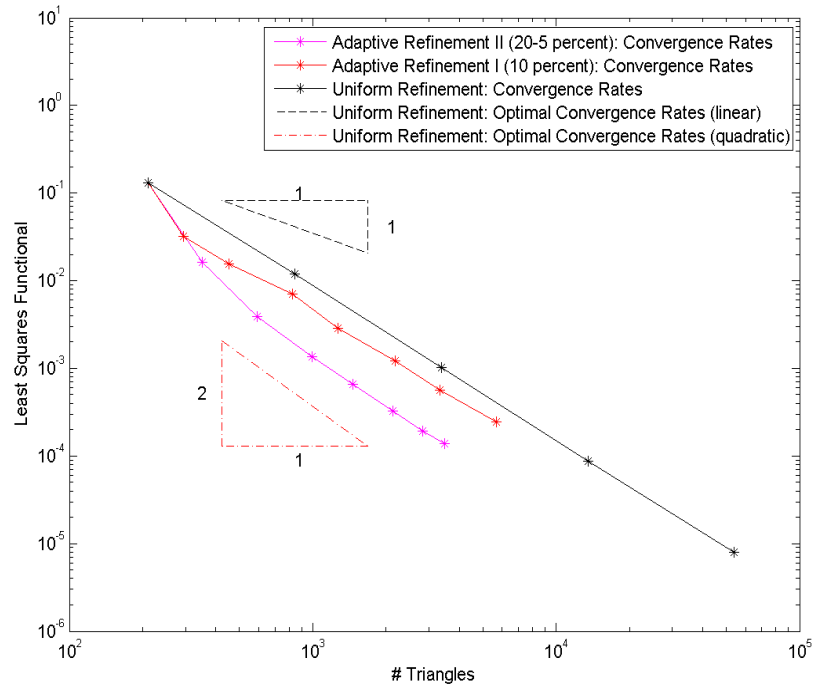
Figure 4.8: Example I (Cross:  $r=1.5$ ): Plots of both triangulation strategies



(a) Convergence rates:  $\|\text{div} \sigma_{D_h}\|_0^2$



(b) Convergence rates:  $\|\text{div} \mathbf{u}_{D_h}\|_0^2$



(c) Convergence rates:  $\mathcal{F}_C$

Figure 4.9: Example I (Cross:  $r=1.5$ ): Plots of convergence rates

level	$\#T_D$	$\#T_S$	$\mathcal{F}_D$	$\mathcal{F}_S$	$\mathcal{F}_I$	$\theta_{lsf}$
0	114	97	2.0004e-001	1.0922e-006	2.6284e-006	
1	155	163	5.4354e-002	1.6551e-006	1.0971e-006	3.1765
2	224	267	2.5186e-002	1.6376e-006	6.3736e-007	1.7707
3	418	461	1.0286e-002	1.6956e-006	5.2076e-007	1.5376
4	604	771	4.8664e-003	1.5130e-006	3.9289e-007	1.6723
5	1040	1368	2.0740e-003	1.0938e-006	2.8985e-007	1.5216
6	1492	2241	9.7312e-004	1.1016e-006	2.6974e-007	1.7244
7	2420	3853	4.3244e-004	8.4425e-007	2.1310e-007	1.5606
0 – 7						1.8084

(a) refinement strategy I: 10 % marked

level	$\#T_D$	$\#T_S$	$\mathcal{F}_D$	$\mathcal{F}_S$	$\mathcal{F}_I$	$\theta_{lsf}$
0	114	97	2.0004e-001	1.0922e-006	2.6284e-006	
1	263	97	2.1751e-002	5.0440e-007	3.3150e-006	4.153
2	505	97	5.9357e-003	4.5966e-007	3.0761e-006	2.5251
3	841	97	2.1618e-003	4.8809e-007	1.6206e-006	2.2766
4	1348	97	9.1655e-004	4.4353e-007	1.7807e-006	1.9824
5	1947	97	4.9668e-004	2.6371e-007	1.1179e-006	1.7656
6	2647	97	2.9261e-004	2.0932e-007	8.2114e-007	1.7941
7	3241	97	1.9805e-004	2.1793e-007	4.8268e-007	1.9918
0 – 7						2.504

(b) refinement strategy II: 20-5 % marked

level	$\#T_D$	$\#T_S$	$\mathcal{F}_D$	$\mathcal{F}_S$	$\mathcal{F}_I$	$\theta_{lsf}$
0	114	97	2.0004e-001	1.0922e-006	2.6284e-006	
1	456	388	1.6614e-002	7.8464e-008	1.2528e-007	1.7949
2	1824	1552	1.2442e-003	2.6329e-008	3.6350e-009	1.8696
3	7296	6208	8.9022e-005	1.1188e-008	5.7650e-010	1.9023
4	29184	24832	6.2327e-006	3.9372e-009	3.4893e-010	1.9177
0 – 4						1.8711

(c) uniform refinement

Table 4.3: Example 1 (Cross model r=2.5): LSF and convergence rates

For the uniform refinement it has to be noted that the overall convergence rate is comparable to the Newtonian case. For the functional  $\mathcal{F}_S$  the overall convergence rate is slightly better compared to the other 2 cases but this is mainly due to the very large decrease in the first step and might even out with later refinements as the convergence rate decreased significantly after the first step.

The solutions for this problem are plotted in figure 4.10 with viscosities in figure 4.11. Again the solutions for velocity/volumetric flux look very similar to the other two cases. The slight differences absolute value can be seen again.

Again  $|\sigma_{S_h}|$  differs especially in its minimal/maximal value which might be because the viscosity is considerably smaller compared to the other cases.

Again  $p_{D_h}$  is different to the two cases before. Here the nonlinearity of the viscosity has an effect on the solution. This is visible if we compare the solution to the Newtonian flow as both have a similar viscosity in most parts of the domain: The hydraulic potential is slightly lower for the *Cross model* with  $r = 2.5$  in the two corners but higher in the center.

The viscosity shows a similar behavior to the case before (with regard to the change of roles) implying a similarly distributed shear rate for both problems.

The refined triangulations can be found in 4.12. Again the main difference can be seen in figure 4.8 (a) but should not be overvalued.

The convergence rates can be found in figure 4.9. The results look again similar to the other two cases with the exception of the error  $\|\operatorname{div} \sigma_{D_h}\|_0^2$ . Refinement strategy I does not even significantly reduce the error. Obviously the error  $\|\operatorname{div} \sigma_{D_h}\|_0^2$  is even less significant than in the cases before close to the interface. It is noteworthy that strategy II (despite refining a single triangle) behaves even better. This indicates that a better solution  $(\mathbf{u}_{D_h}, p_{D_h})$  is of more influence on the error  $\|\operatorname{div} \sigma_{D_h}\|_0^2$  than the refinement of the triangles close to  $\Gamma_I$ .

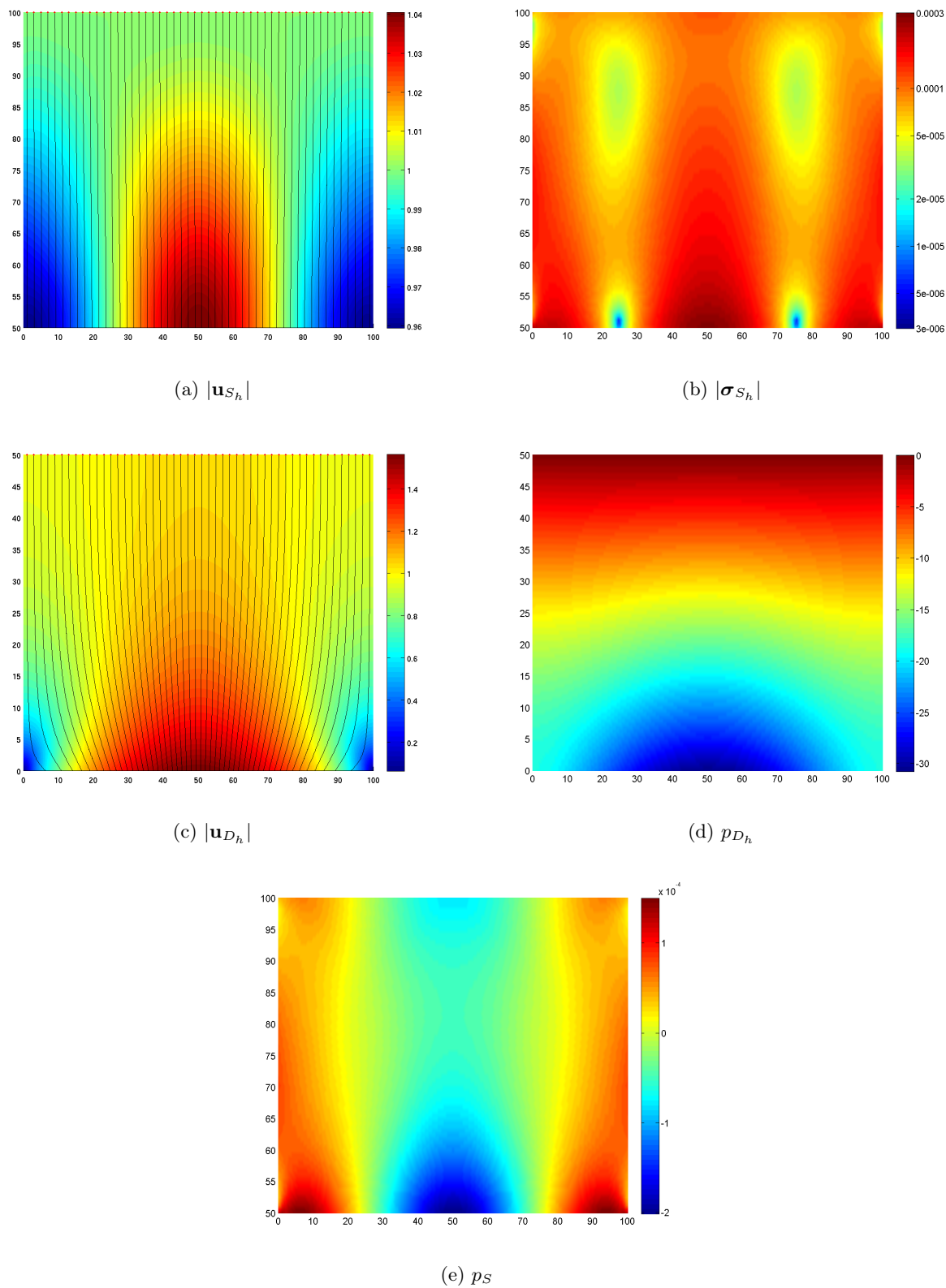


Figure 4.10: Example I (Cross:  $r=2.5$ ): Plots of the approximate solutions

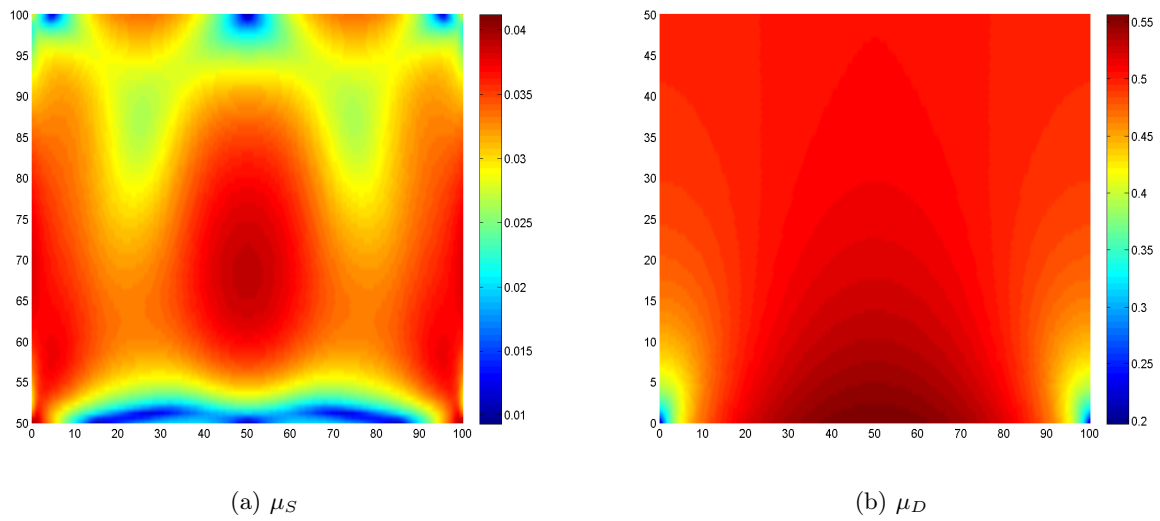
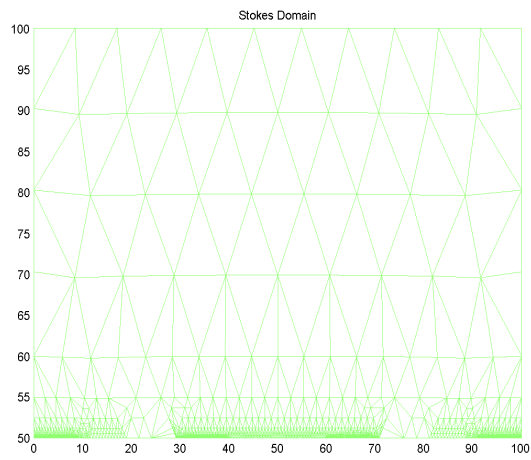
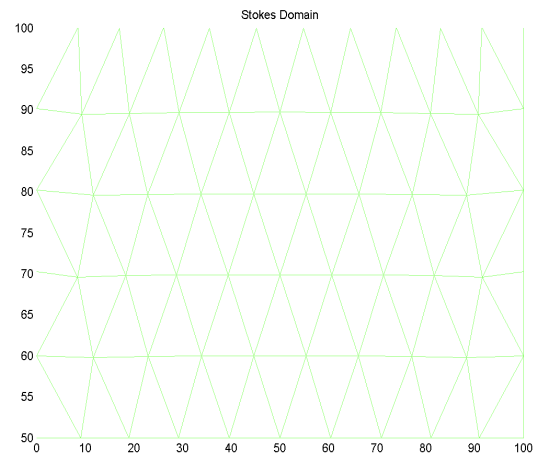


Figure 4.11: Example I (Cross:  $r=2.5$ ): Viscosities

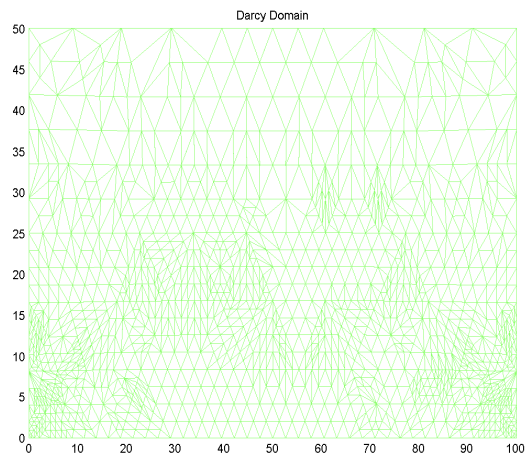




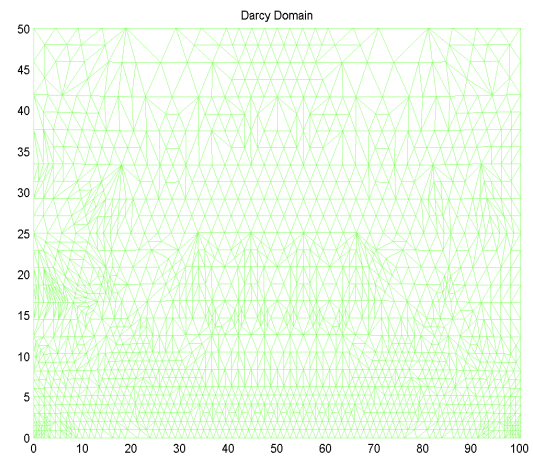
(a) Strategy I: Triangulation (Stokes)



(b) Strategy II: Triangulation (Stokes)

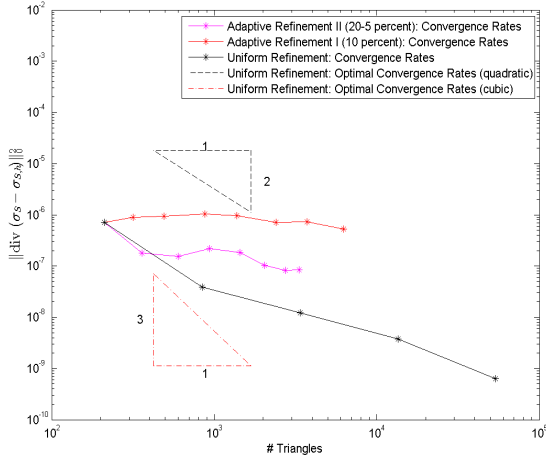


(c) Strategy I: Triangulation (Darcy)

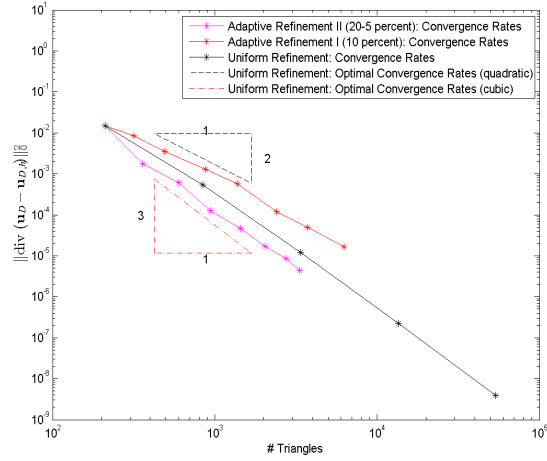


(d) Strategy II: Triangulation (Darcy)

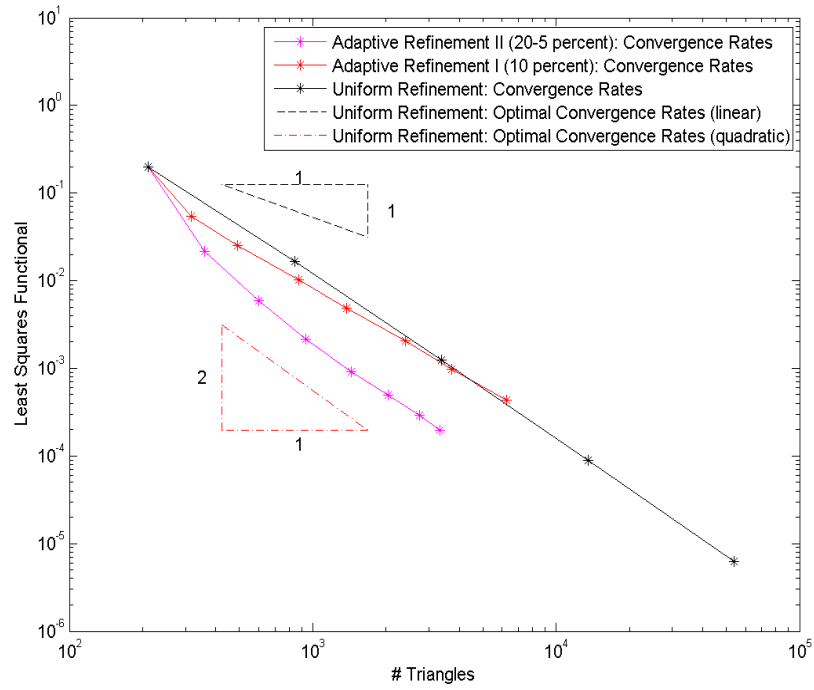
Figure 4.12: Example I (Cross:  $r=2.5$ ): Plots of both triangulation strategies



(a) Convergence rates:  $\|\text{div } \sigma_{D_h}\|_0^2$



(b) Convergence rates:  $\|\text{div } \mathbf{u}_{D_h}\|_0^2$



(c) Convergence rates:  $\mathcal{F}_C$

Figure 4.13: Example I (Cross:  $r=2.5$ ): Plots of convergence rates

### 4.2.2 Example II

For the boundary conditions we impose a forced inflow at the upper boundary of the Stokes domain and a forced inflow at the lower boundary of the Darcy domain. The domain is depicted in figure 4.14 with  $\Omega = (0, 100 \times (0, 100))$ . For the rest of the boundaries we impose no-slip conditions at the impermeable walls for the velocity and impermeable walls for the volumetric flux:

$$\begin{aligned} \mathbf{u}_S &= \begin{pmatrix} 0 \\ -\sin(\pi x/100) \end{pmatrix} && \text{on } \Gamma_{S_{in}} \\ \mathbf{u}_S &= \begin{pmatrix} 0 \\ 0 \end{pmatrix} && \text{on } \Gamma_{S_0} \\ \mathbf{u}_D \cdot \mathbf{n} &= 0 && \text{on } \Gamma_{D_0} \\ \mathbf{u}_D \cdot \mathbf{n} &= \sin(\pi x/100) && \text{on } \Gamma_{D_{out}} \end{aligned}$$

For the right hand side we have

$$\mathbf{f}_S = \mathbf{0} \text{ and } f_D = 0$$

For the constants  $\kappa$  and  $\beta$  we use

$$\begin{aligned} \kappa &= 1 \\ \beta &= 1 \end{aligned}$$

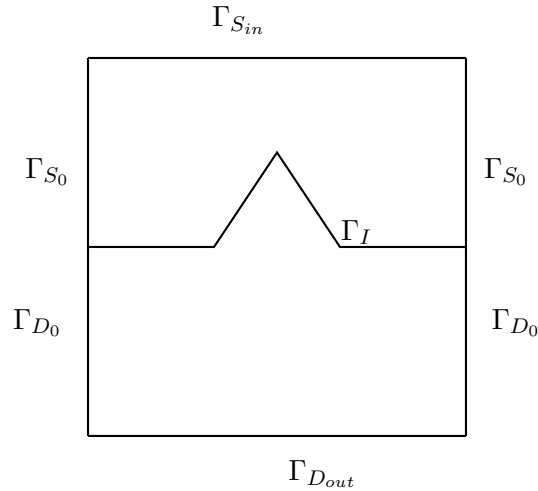


Figure 4.14: Domain for example II

We expect the error to be dominant around the re-entrant corners and close to the boundary of the interface as the flow does not fit well together due to the jump of boundary conditions (no-slip/impermeable wall).

#### Newtonian flow

For the Newtonian flow we get the results shown in table 4.4. There are several differences to example I visible.

The first difference is the reduced rate of convergence for all parts of the least-squares functional for uniform refinement. This is due to the re-entrant corners that results in solutions not being in  $H^2(\Omega_S) / H^2(\Omega_D)$  (see proposition 2.6 and 2.7). Therefore we can only expect convergence rates  $\alpha < 1$ . This is confirmed by table 4.4.

The second difference is that the different parts of  $\mathcal{F}_C$  are in the same scale. Therefore there is no domain with dominant error.

We see that adaptive refinement leads to almost optimal overall convergence rates. The behavior of both strategies is slightly different but lead to approximately the same magnitude of error.

For strategy I we see a decrease of the convergence rate in steps 5/6. This is not visible in strategy II and might happen because too many triangles are refined as it was stated at the beginning of this section. Strategy II refines a smaller effective percentage of triangles and does not exhibit this behavior. The smaller rate of convergence for early refinements in strategy II indicates that we refine too many triangles for the coarse grids to achieve optimal convergence rates. This is confirmed by the better behavior of strategy I for the first two steps. Another interesting occurrence is the shift of the predominantly refined domain. The first three steps refine mainly the the triangles in  $\Omega_D$  whereas in the last three steps the algorithm refines more triangles in  $\Omega_S$ . This might as well be a cause why strategy II performs better for late refinement steps.

Noteworthy is the fast decrease of  $\mathcal{F}_I$  for both adaptive refinement strategies. For the coarsest grid it lies in the same order of magnitude as the other two parts of the error estimator. After 7 refinement steps it is significantly smaller. The uniform refinement does exhibit this behavior to a lesser extent if we compare it to the overall error. It seems that the refinement close to the singularities has a positive effect to the interface part of the error  $\mathcal{F}_I$ .

The solutions are plotted in figure 4.15. The solution for the velocity/volumetric flux look as expected. One clearly sees the effect of the Beavers-Joseph-Saffman condition as the flow tends to be almost orthogonal for parts of the interface where the absolute value of stress is small. Furthermore we can see the highest values of  $|\mathbf{u}_{S_h}|$  and  $|\mathbf{u}_{D_h}|$  close to the corners (30,50) and (70,30). Here the tangential component of the velocity is higher (which can as well be seen by comparing it to the volumetric flux and keeping the conservation of mass in mind) which is a result of the high stresses. This is visible for other parts of the interface as well. For the volumetric flux we see a flowing together in the center  $x = 50$  which results in an increasing absolute value to keep local mass balance.

The absolute value of the stress can be observed in figure 4.15 (b). We see high absolute values in the corners. These are mainly due to the coupling with the Darcy flow and for the outer corners due to the jump in boundary conditions. For the pressure  $p_S$  in figure 4.15 (e) we see the expected high gradients close to the corners where the pressure-gradient has a significant effect on the flow by accelerating the flow-particles as seen in figure 4.15 (a).

The refined triangulations are depicted in 4.16. Both strategies refine triangles close to the corners which is expected for this problem.

The convergence rates are depicted in figure 4.17. Still we are not able to achieve better convergence rates for  $\|\text{div } \boldsymbol{\sigma}_{D_h}\|_0^2$ . It has to be noted that uniform refinement achieves better convergence rates than for  $\mathcal{F}_C$ . This indicates that this property is still present in the coupled case but can not be resolved to its full extent by our adaptive refinement strategies. A different refinement strategy might work better. Our strategy works better for the error  $\|\text{div } \mathbf{u}_{D_h}\|_0^2$ . This can be seen in figure 4.17 (b). Here we are able to achieve almost optimal convergence rates of 3 by adaptive refinement.

level	$\#T_D$	$\#T_S$	$\mathcal{F}_D$	$\mathcal{F}_S$	$\mathcal{F}_I$	$\theta_{lsf}$
0	118	97	3.4070e-001	2.3234e-001	1.8712e-001	
1	166	152	1.4707e-001	1.3735e-001	9.0244e-002	1.8076
2	264	239	5.5427e-002	7.6959e-002	2.6520e-002	1.8705
3	402	393	2.3244e-002	3.7822e-002	6.3066e-003	1.8746
4	581	557	1.0708e-002	2.0394e-002	1.7855e-003	1.9994
5	1011	934	4.7567e-003	9.8537e-003	5.3571e-004	1.4465
6	1820	1720	1.7257e-003	4.4552e-003	1.5862e-004	1.4543
7	2650	2536	7.2278e-004	2.0634e-003	5.6492e-005	2.1005
0 – 7						1.7558

(a) refinement strategy I: 10 % marked

level	$\#T_D$	$\#T_S$	$\mathcal{F}_D$	$\mathcal{F}_S$	$\mathcal{F}_I$	$\theta_{lsf}$
0	118	97	3.4070e-001	2.3234e-001	1.8712e-001	
1	232	173	1.2632e-001	1.3151e-001	9.0990e-002	1.2301
2	458	279	3.7253e-002	6.9174e-002	2.6517e-002	1.6112
3	680	576	1.0869e-002	2.9456e-002	5.8469e-003	1.9838
4	1048	888	3.8181e-003	1.3489e-002	1.3634e-003	2.0926
5	1383	1452	2.2342e-003	6.4475e-003	3.5303e-004	1.9031
6	1953	1939	1.2422e-003	3.4917e-003	1.1399e-004	1.9646
7	2272	2533	9.2254e-004	1.9185e-003	4.7566e-005	2.457
0 – 7						1.7937

(b) refinement strategy II: 20-5 % marked

level	$\#T_D$	$\#T_S$	$\mathcal{F}_D$	$\mathcal{F}_S$	$\mathcal{F}_I$	$\theta_{lsf}$
0	118	97	3.4070e-001	2.3234e-001	1.8712e-001	
1	472	388	1.1025e-001	1.2599e-001	9.2037e-002	0.6057
2	1888	1552	2.4452e-002	6.1327e-002	2.6678e-002	0.7728
3	7552	6208	3.8071e-003	2.4382e-002	5.7758e-003	0.8636
4	30208	24832	5.5059e-004	9.9492e-003	1.2728e-003	0.7643
0 – 4						0.7516

(c) uniform refinement

Table 4.4: Example II (Newtonian flow): LSF and convergence rates

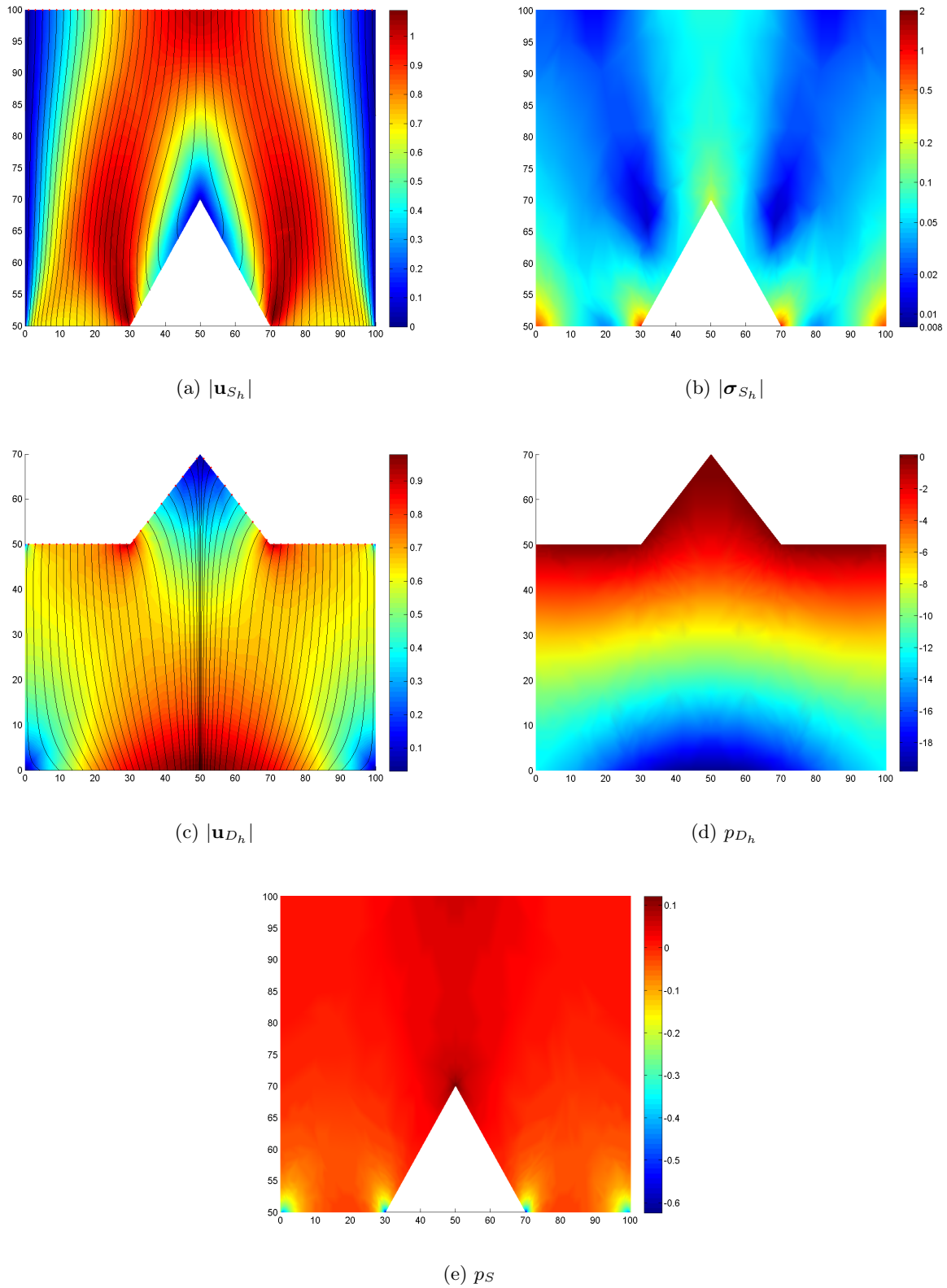
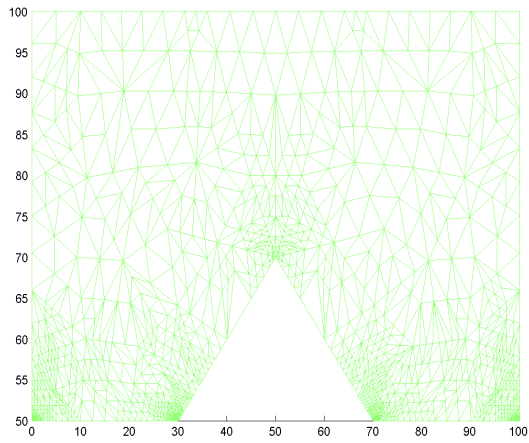
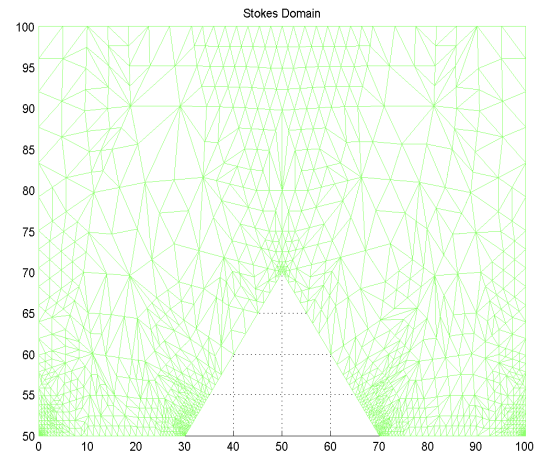


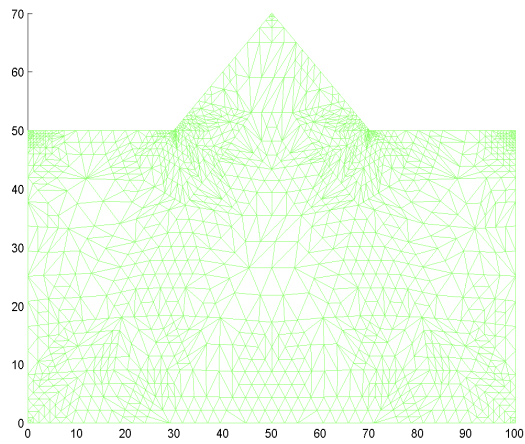
Figure 4.15: Example II (Newtonian flow): Plots of the approximate solutions



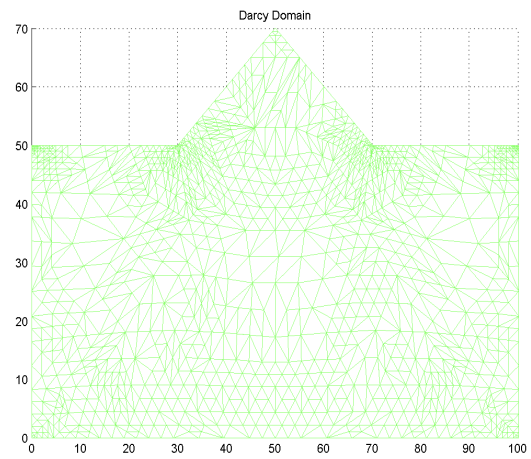
(a) Strategy I: Triangulation (Stokes)



(b) Strategy II: Triangulation (Stokes)

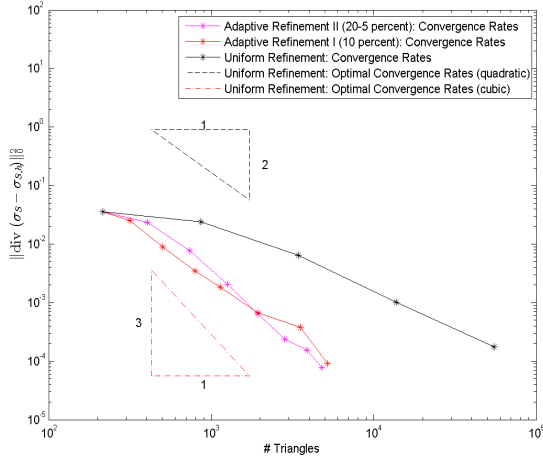


(c) Strategy I: Triangulation (Darcy)

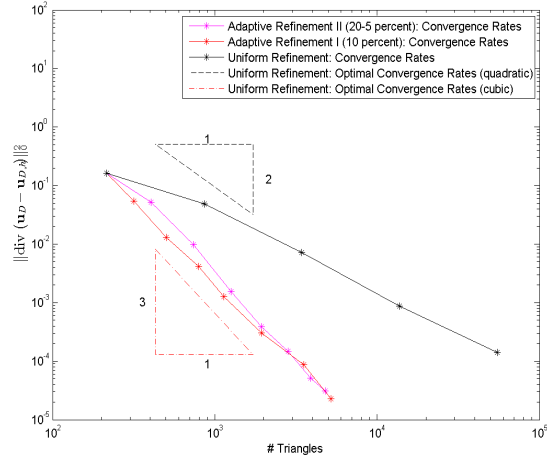


(d) Strategy II: Triangulation (Darcy)

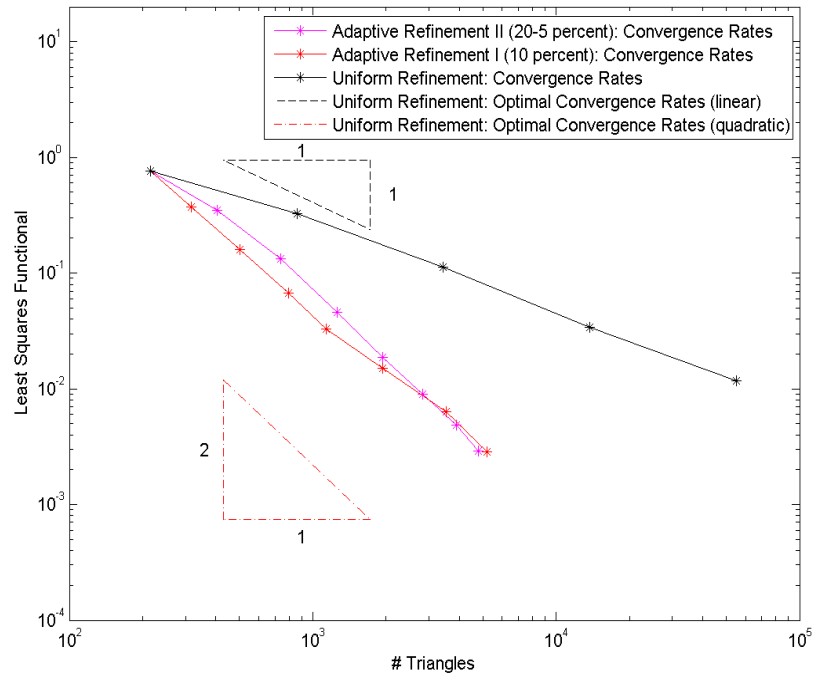
Figure 4.16: Example II (Newtonian flow): Plots of both triangulation strategies



(a) Convergence rates:  $\|\text{div} \sigma_{D_h}\|_0^2$



(b) Convergence rates:  $\|\text{div} \mathbf{u}_{D_h}\|_0^2$



(c) Convergence rates:  $\mathcal{F}_C$

Figure 4.17: Example II (Newtonian flow): Plots of convergence rates



**Cross model:  $r=1.5$** 

For the cross model with  $r = 1.5$  we choose the same constants as for example I. The results are shown in table 4.5.

level	$\#T_D$	$\#T_S$	$\mathcal{F}_D$	$\mathcal{F}_S$	$\mathcal{F}_I$	$\theta_{lsf}$
0	118	97	3.8794e-001	2.8714e-001	2.2783e-001	
1	166	153	1.5251e-001	1.8190e-001	1.0091e-001	1.849
2	276	225	5.9467e-002	1.0703e-001	2.9714e-002	1.7653
3	431	359	2.4784e-002	5.7760e-002	7.7573e-003	1.704
4	629	535	1.0321e-002	3.1486e-002	2.1012e-003	1.8604
5	1096	818	4.1551e-003	1.5982e-002	6.9637e-004	1.4991
6	2151	1555	1.5510e-003	7.5498e-003	2.3491e-004	1.2148
7	3161	2266	6.0771e-004	3.4891e-003	5.8734e-005	2.122
0 – 7						1.6668

(a) refinement strategy I: 10 % marked

level	$\#T_D$	$\#T_S$	$\mathcal{F}_D$	$\mathcal{F}_S$	$\mathcal{F}_I$	$\theta_{lsf}$
0	118	97	3.8794e-001	2.8714e-001	2.2783e-001	
1	238	173	1.3461e-001	1.7206e-001	1.0001e-001	1.2309
2	402	315	4.1086e-002	9.0716e-002	2.9263e-002	1.6644
3	628	538	1.2565e-002	4.3382e-002	7.0806e-003	1.9295
4	814	968	5.9723e-003	1.9700e-002	1.7909e-003	1.9585
5	1181	1454	2.7429e-003	9.8094e-003	5.0327e-004	1.9011
6	1453	2165	1.8812e-003	4.8526e-003	1.7136e-004	2.009
7	1902	2674	1.2520e-003	2.8932e-003	6.5306e-005	2.106
0 – 7						1.7554

(b) refinement strategy II: 20-5 % marked

level	$\#T_D$	$\#T_S$	$\mathcal{F}_D$	$\mathcal{F}_S$	$\mathcal{F}_I$	$\theta_{lsf}$
0	118	97	3.8794e-001	2.8714e-001	2.2783e-001	
1	472	388	1.1374e-001	1.6145e-001	1.0099e-001	0.6316
2	1888	1552	2.3117e-002	7.7938e-002	2.9454e-002	0.7637
3	7552	6208	3.7531e-003	3.1551e-002	6.9729e-003	0.8131
4	30208	24832	6.0653e-004	1.3371e-002	1.6562e-003	0.7176
0 – 4						0.7315

(c) uniform refinement

Table 4.5: Example II (Cross model  $r=1.5$ ): LSF and convergence rates

The behavior is again similar to the Newtonian case. The overall convergence rates for all refinement strategies are slightly worse to the Newtonian case, though strategy II still delivers the very good convergence rates for late refinement steps.

The solutions are plotted in figure 4.18. The solution for the velocity/volumetric flux looks similar to the case before. We see a slight difference by taking a closer look at the streamlines close to (50, 70) in figure 4.18 (a).

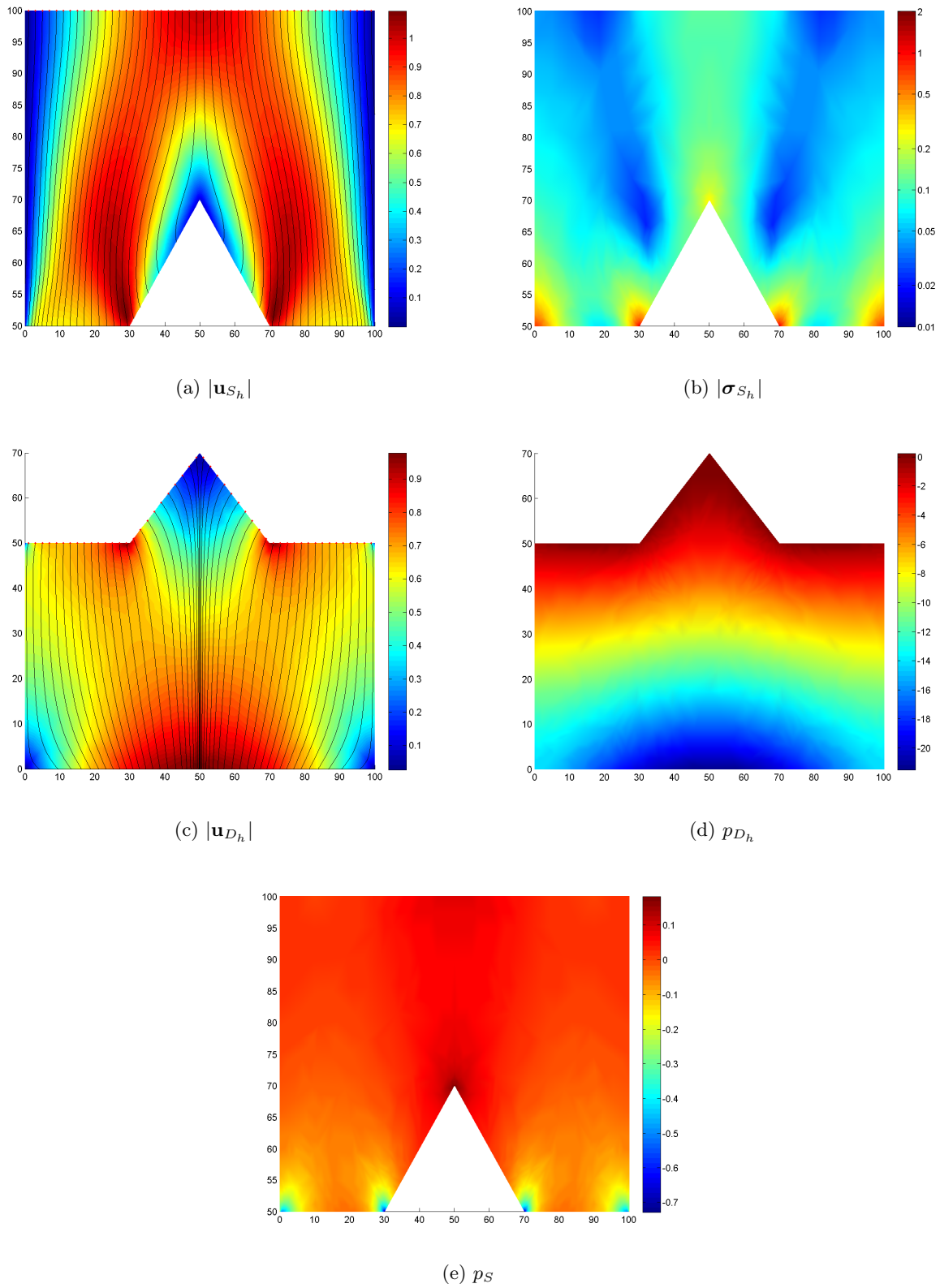
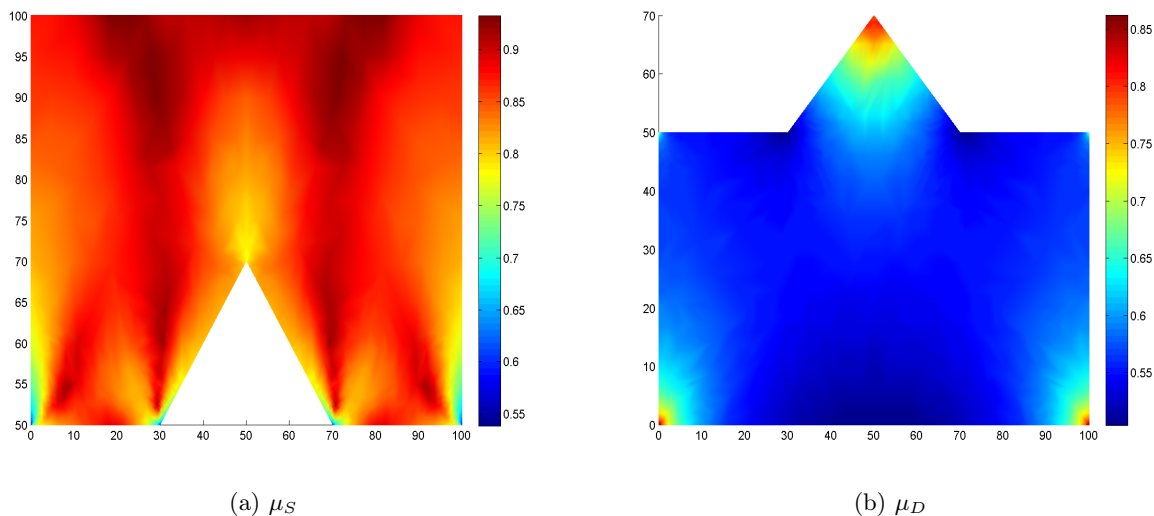


Figure 4.18: Example II (Cross:  $r=1.5$ ): Plots of the approximate solutions

Figure 4.19: Example II (Cross:  $r=1.5$ ): Viscosities

The main difference to the Newtonian case can be seen in the plots of  $|\sigma_{S_h}|$ ,  $p_{S_h}$  and  $p_{D_h}$ . Though  $|\sigma_{S_h}|$  is not differing in its maximum/minimum we clearly see a different characteristic. The regions where  $|\sigma_{S_h}|$  is close to its minimum are smaller. For  $p_{D_h}$  we see that the solution is slightly different in its minimal value. For  $p_{S_h}$  we observe a larger range due to a generally higher viscosity. The smaller gradient close to the singularities is due to the decreasing viscosity close to the relevant corners.

For the plotted viscosity in figure 4.19 (a) we see the shear-thinning property close to the corners of high stress. These are the regions where the minimal viscosity is observed. Though both plots look similar we see regions where the viscosity seems to be of different characteristic (see right above (30,52) and (70,52) for example). These are the regions where the higher absolute values of  $|\sigma_{S_h}|$  are due to higher absolute values of  $p_{S_h}$  as can be seen in 4.18 (e) .

For the viscosity  $\mu_D$  we see high viscosity value close to the three corners where  $\mathbf{u}_{D_h}$  is small / almost zero. A slight increase in viscosity is also seen close to (0, 50) and (100, 50) as the no-slip boundary conditions of the Stokes flow comes into effect.

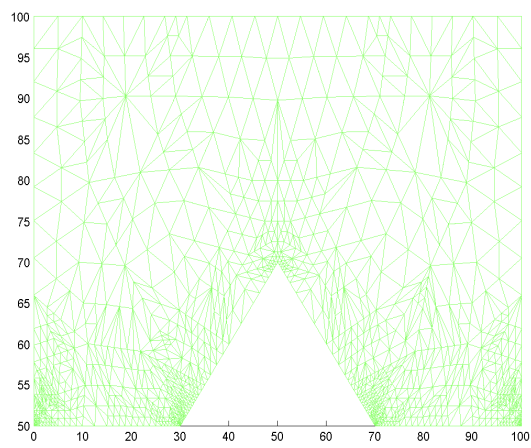
The triangulations are depicted in figure 4.20. They look similar to the Newtonian case and both strategies behave very similar.

### Cross model: $r=2.5$

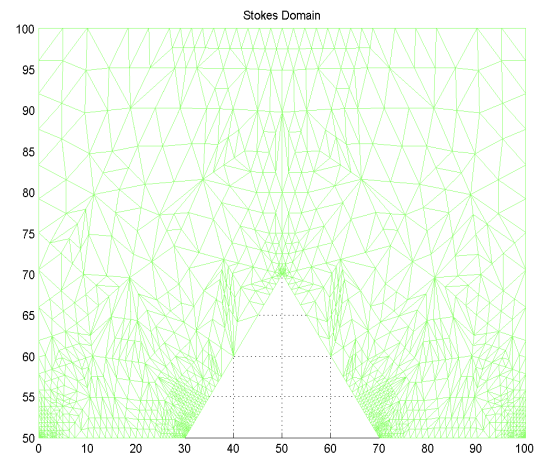
For the cross model with  $r = 2.5$  we choose again the same constants as for example I. The results are shown in table 4.6.

This case behaves different from the two cases before. First we state that the convergence rates are slightly better than for the other two cases. The algorithms still show the same characteristics in convergence rates but it has to be noted that the shift of predominantly refined domains as seen before is not as clearly visible in strategy II. We still have the primarily refinement in  $\Omega_D$  for the first steps but then it only evens out in later steps and does not result in  $\#T_S > \#T_D$  as for the two cases before. Again the convergence rates of adaptive refinement strategy II are clearly superior to the other two strategies.

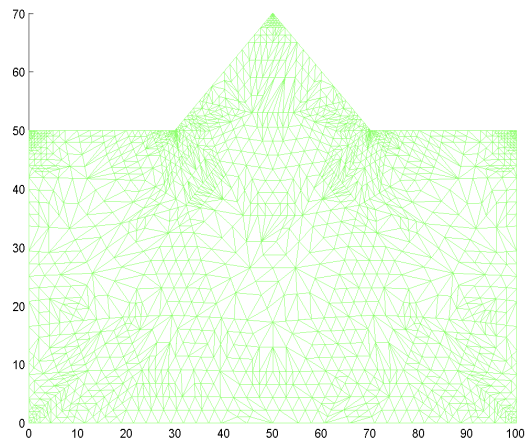
The solutions are plotted in figure 4.22. We see again only a slight difference in  $\mathbf{u}_{S_h}$  by taking a



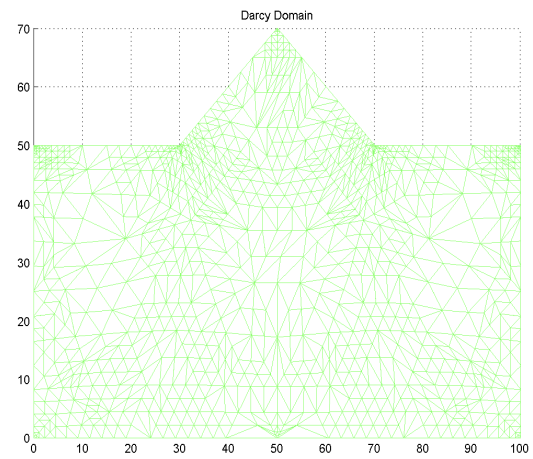
(a) Strategy I: Triangulation (Stokes)



(b) Strategy II: Triangulation (Stokes)

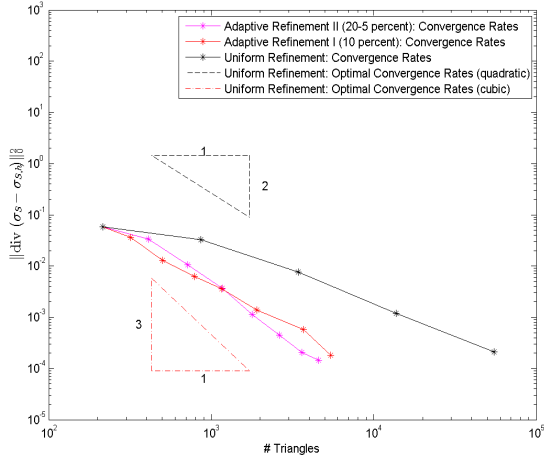


(c) Strategy I: Triangulation (Darcy)

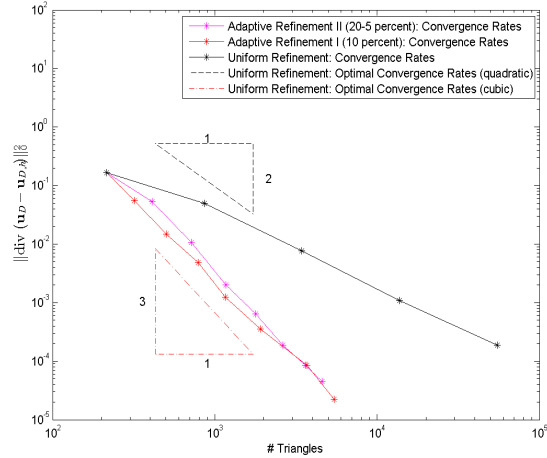


(d) Strategy II: Triangulation (Darcy)

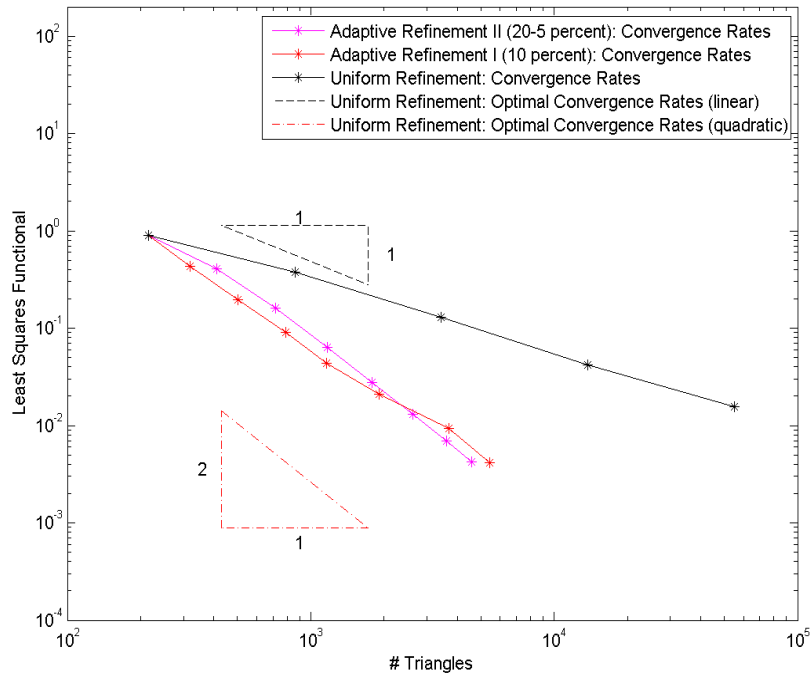
Figure 4.20: Example II (Cross:  $r=1.5$ ): Plots of both triangulation strategies



(a) Convergence rates:  $\|\text{div} \sigma_{D_h}\|_0^2$



(b) Convergence rates:  $\|\text{div} \mathbf{u}_{D_h}\|_0^2$



(c) Convergence rates:  $\mathcal{F}_C$

Figure 4.21: Example II (Cross:  $r=1.5$ ): Plots of convergence rates

level	$\#T_D$	$\#T_S$	$\mathcal{F}_D$	$\mathcal{F}_S$	$\mathcal{F}_I$	$\theta_{lsf}$
0	118	97	3.1631e-001	1.8721e-001	1.5929e-001	
1	166	139	1.4839e-001	1.0490e-001	8.4254e-002	1.9298
2	255	221	5.7905e-002	5.4816e-002	2.4435e-002	2.0233
3	456	384	2.0626e-002	2.3883e-002	4.9974e-003	1.7941
4	663	531	8.6152e-003	1.1765e-002	1.1609e-003	2.3663
5	1161	861	3.4784e-003	5.7737e-003	3.4959e-004	1.5339
6	2236	1574	1.3144e-003	2.7028e-003	1.0214e-004	1.3357
7	3217	2374	5.2458e-004	1.2638e-003	2.9166e-005	2.1334
0 – 7						1.8105

(a) refinement strategy I: 10 % marked

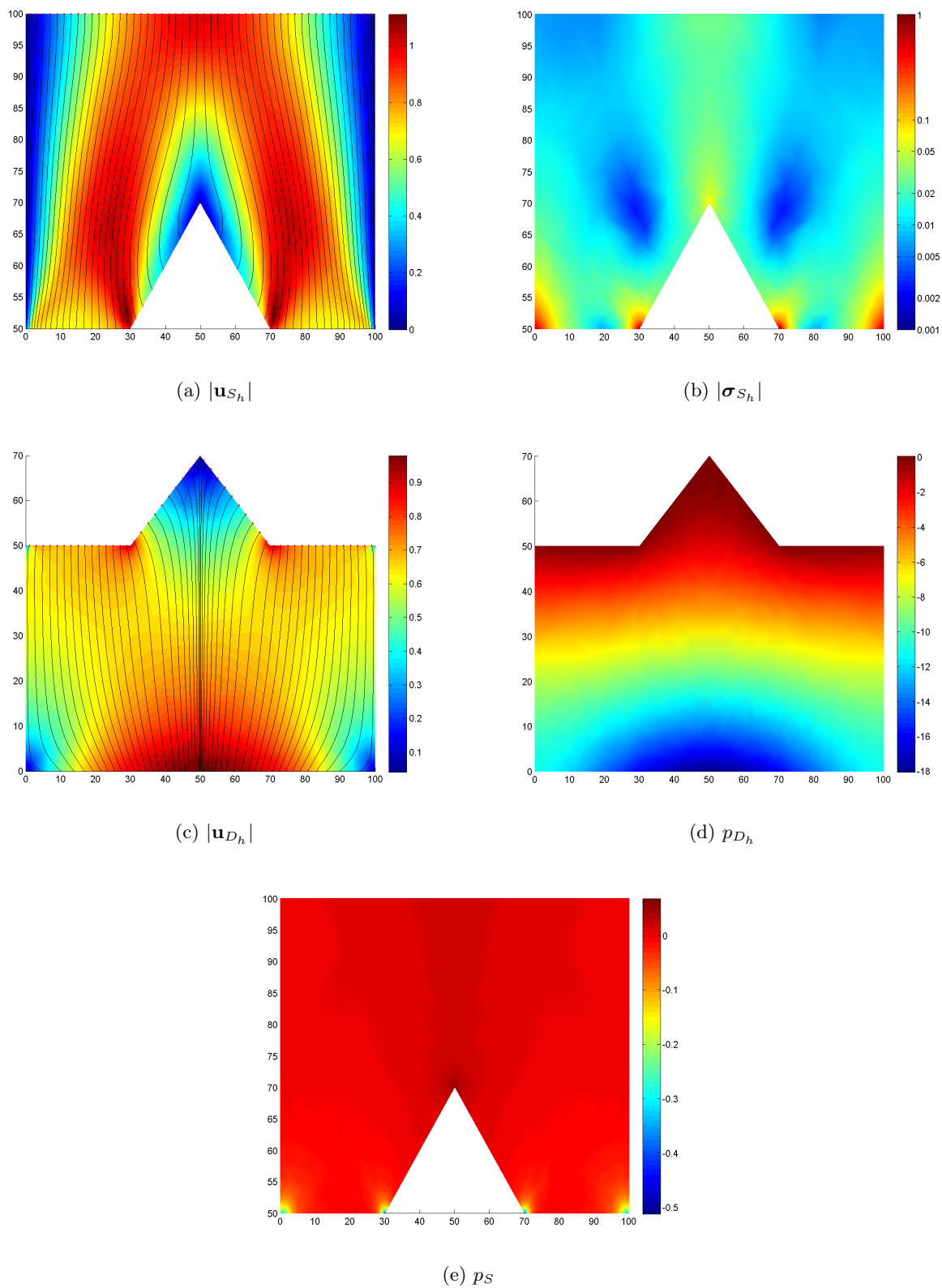
level	#	$\#T_D$	$\#T_S$	$\mathcal{F}_D$	$\mathcal{F}_S$	$\mathcal{F}_I$	$\theta_{lsf}$
0		118	97	3.1631e-001	1.8722e-001	1.5929e-001	
1	266		139	1.2406e-001	1.0456e-001	8.4798e-002	1.1828
2	482		265	3.9763e-002	5.2295e-002	2.4559e-002	1.6149
3	757		433	9.7155e-003	2.1919e-002	4.9535e-003	2.4894
4	1107		734	3.7207e-003	9.4502e-003	1.0227e-003	2.1701
5	1537		1130	1.8858e-003	4.5536e-003	2.6286e-004	2.0244
6	2014		1664	1.1567e-003	2.3196e-003	9.0091e-005	1.9629
7	2553		2047	7.5153e-004	1.3530e-003	3.5653e-005	2.2829
0 – 7							1.8724

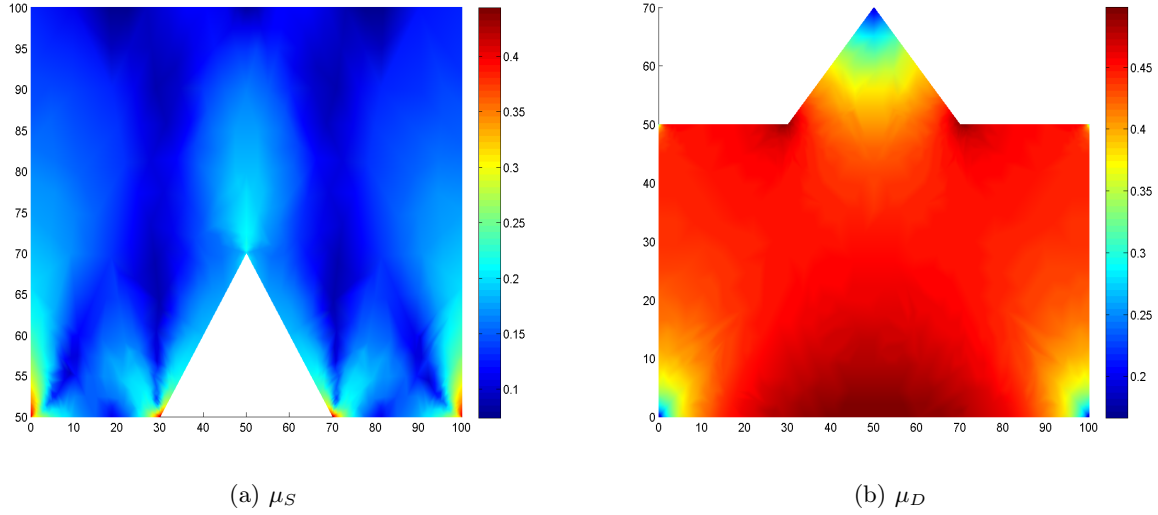
(b) refinement strategy II: 20-5 % marked

level	$\#T_D$	$\#T_S$	$\mathcal{F}_D$	$\mathcal{F}_S$	$\mathcal{F}_I$	$\theta_{lsf}$
0	118	97	3.1631e-001	1.8721e-001	1.5929e-001	
1	472	388	1.1278e-001	9.9640e-002	8.6361e-002	0.5748
2	1888	1552	2.9188e-002	4.9320e-002	2.4847e-002	0.7657
3	7552	6208	4.5486e-003	1.9322e-002	4.9042e-003	0.9224
4	30208	24832	5.8726e-004	7.3616e-003	9.7105e-004	0.8448
0 – 4						0.7769

(c) uniform refinement

Table 4.6: Example II (Cross model r=2.5): LSF and convergence rates

Figure 4.22: Example II (Cross:  $r=2.5$ ): Plots of the approximate solutions

Figure 4.23: Example II (Cross:  $r=2.5$ ): Viscosities

closer look at the maximal absolute value / the streamlines close to  $(50, 70)$ .

Again we see differences in the plots of  $|\boldsymbol{\sigma}_{S_h}|$ ,  $p_{S_h}$  and  $p_{D_h}$  compared to the other two cases. The opposite argument as in the case before can be applied regarding these differences.

For the plotted viscosity in figure 4.23 (a) we see the shear-thickening property close to the corners of high stress. Overall we can see that the viscosity plot is similar to the case of  $r = 1.5$  with respect to the changed role of shear rate/ absolute value of volumetric flux.

The triangulations are depicted in 4.24. They look similar to the other two cases and both strategies behave very similar.

### 4.3 Performance of the Gauß-Newton Method

In this section we take closer look at the performance of the Gauß-Newton method. We examine several examples and compare the necessary number of steps to reach a stopping criterion. Therefore we first note that a necessary condition for  $(\mathbf{u}_{S_h}^{(k)}, \boldsymbol{\sigma}_{S_h}^{(k)}, \mathbf{u}_{D_h}^{(k)}, p_{D_h}^{(k)})$  being a minimum is given by (compare (2.5)):

$$\left( \mathcal{R}(\boldsymbol{\sigma}_{S_h}^{(k)}, \mathbf{u}_{S_h}^{(k)}, \mathbf{u}_{D_h}^{(k)}, p_{D_h}^{(k)}, \mathbf{f}_S, f_D), \mathcal{L}(\delta \mathbf{v}_{S_h}, \delta \boldsymbol{\tau}_{S_h}, \delta \mathbf{v}_{D_h}, \delta q_{D_h}; \mathbf{u}_{S_h}^{(k)}, \mathbf{u}_{D_h}^{(k)}) \right)_{0, \Omega} = 0 \quad (4.24)$$

for all  $(\delta \mathbf{v}_{S_h}, \delta \boldsymbol{\tau}_{S_h}, \delta \mathbf{v}_{D_h}, \delta q_{D_h}) \in \mathcal{X}_{0_h}$ . Here

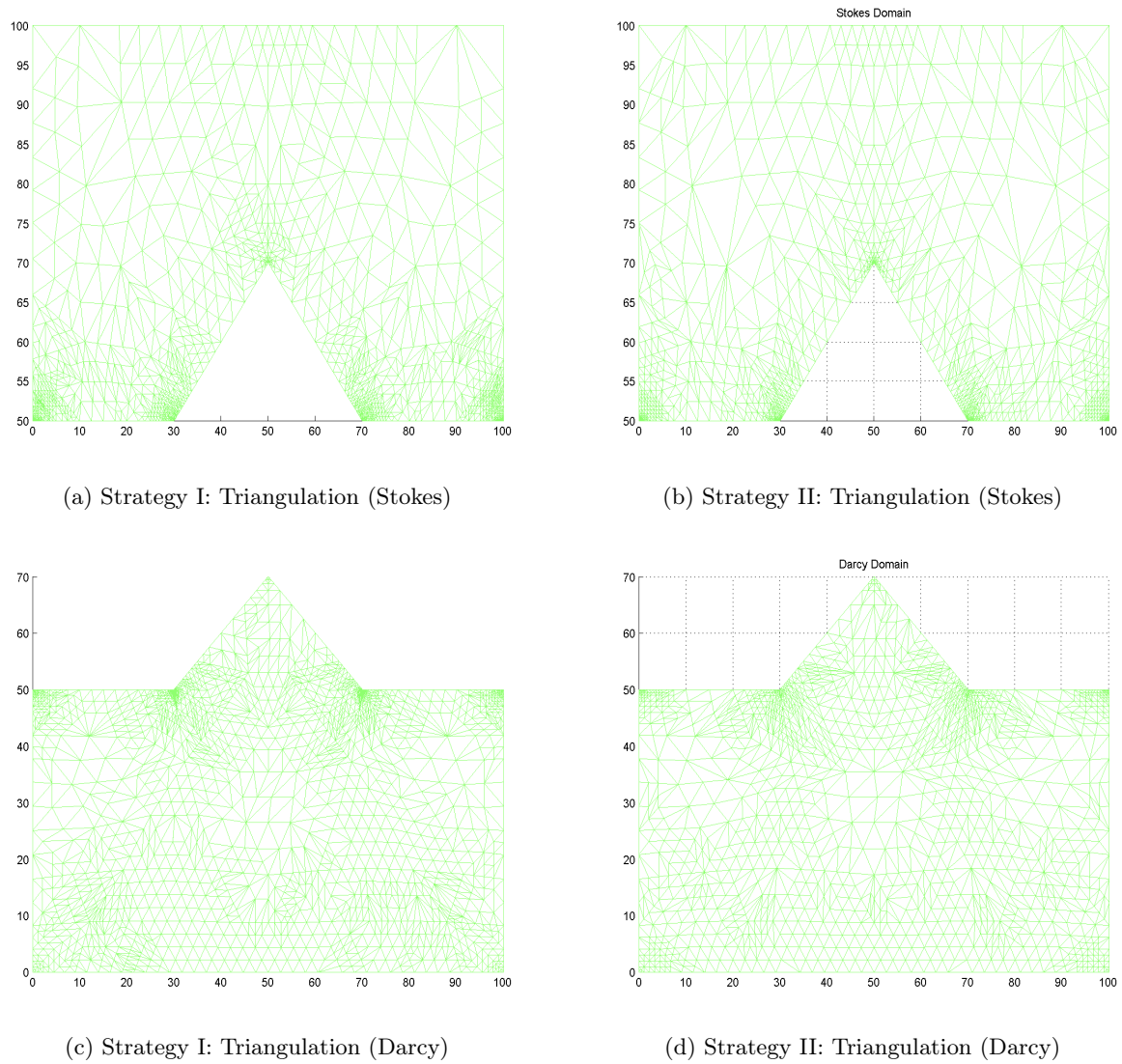
$$\mathcal{X}_{0_h} = (\mathcal{P}_2(\mathcal{T}_h(\Omega_S)))^2 \times (RT_1(\mathcal{T}_h(\Omega_S)))^2 \times RT_1(\mathcal{T}_h(\Omega_D)) \times \mathcal{P}_2(\mathcal{T}_h(\Omega_D))$$

denotes the finite dimensional FE spaces. By taking the basis functions  $\phi_i \in \mathcal{X}_{0_h}$  with  $i = 1, \dots, N$  with  $N = \dim(\mathcal{X}_{0_h})$  we can easily deduce the following necessary condition:

$$\mathbf{st}^{(k)} := \left( \left( \mathcal{R}(\boldsymbol{\sigma}_{S_h}^{(k)}, \mathbf{u}_{S_h}^{(k)}, \mathbf{u}_{D_h}^{(k)}, p_{D_h}^{(k)}, \mathbf{f}_S, f_D), \mathcal{L}(\phi_i; \mathbf{u}_{S_h}^{(k)}, \mathbf{u}_{D_h}^{(k)}) \right)_{0, \Omega} \right)_{i=1, \dots, N} = 0$$

This is used as a stopping criterion for our Gauß-Newton steps. In most cases we stop the iteration if  $\|\mathbf{st}^{(k)}\|_2 \leq 1e - 5$  if not noted otherwise.





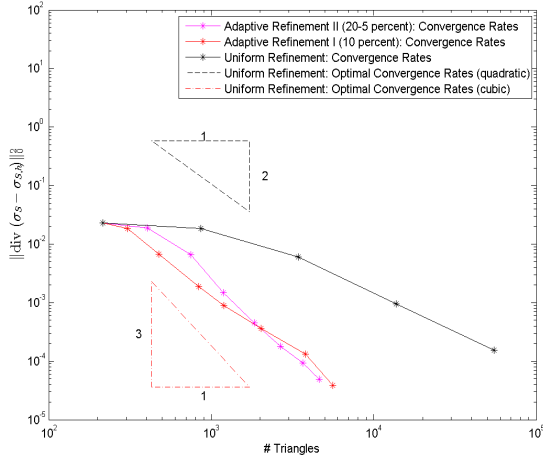
(a) Strategy I: Triangulation (Stokes)

(b) Strategy II: Triangulation (Stokes)

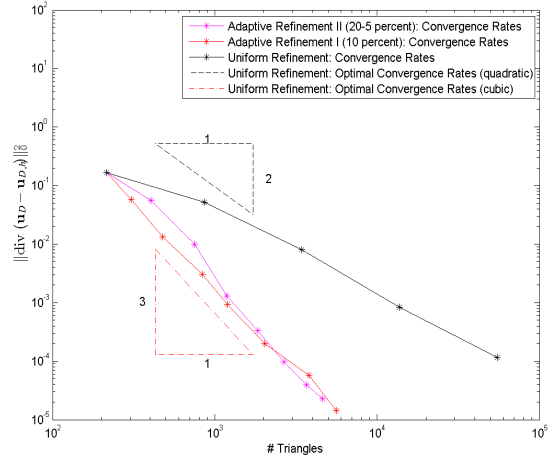
(c) Strategy I: Triangulation (Darcy)

(d) Strategy II: Triangulation (Darcy)

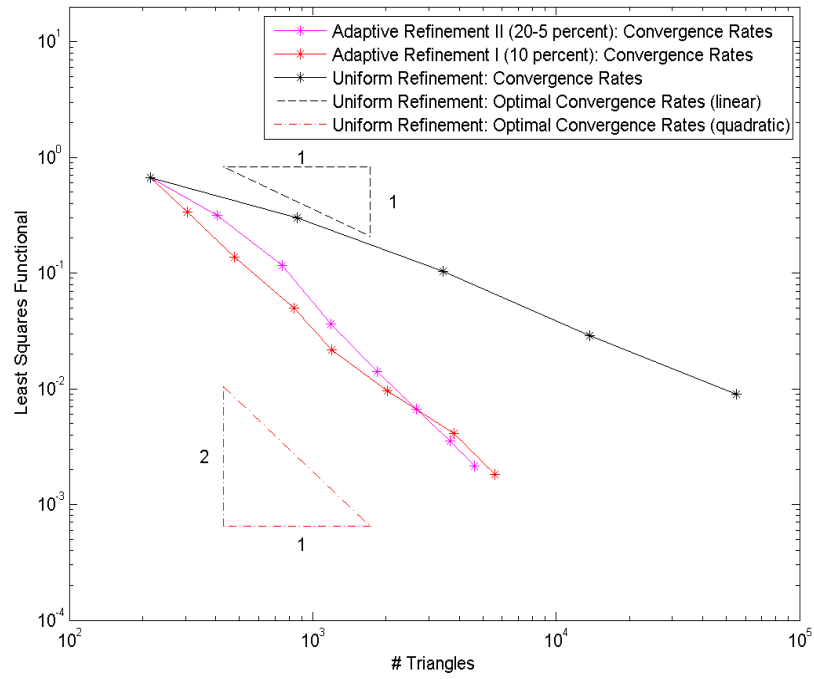
Figure 4.24: Example II (Cross:  $r=2.5$ ): Plots of both triangulation strategies



(a) Convergence rates:  $\|\text{div } \sigma_{D_h}\|_0^2$



(b) Convergence rates:  $\|\text{div } \mathbf{u}_{D_h}\|_0^2$



(c) Convergence rates:  $\mathcal{F}_C$

Figure 4.25: Example II (Cross:  $r=2.5$ ): Plots of convergence rates

**Remark:** It has to be noted that  $\mathbf{st}^{(k)}$  is given in step  $k + 1$  with no additional cost due to (4.23).

First we start by comparing several examples by the choice of starting conditions. The convergence of a Gauß-Newton method is like all Newton methods dependent on the choice of starting points. Therefore we compare two different starting points that might be considered a good choice

1. The solution of the linear problem with  $\mu_S = \frac{\mu_{0,S} + \mu_{\infty,S}}{2}$  and  $\mu_D = \frac{\mu_{0,D} + \mu_{\infty,D}}{2}$ .
2. The interpolated solution of the refinement step before if level  $> 0$  provided in [KS].

The nonlinearity is characterized by the four constants  $K, r, \mu_0$  and  $\mu_{\infty}$ . We take a closer look at the following examples where we take the same constants for both viscosities  $\mu_S$  and  $\mu_D$  :

- I  $K = 10, r = 1.01, \mu_0 = 1$  and  $\mu_{\infty} = 1e - 6$
  - II  $K = 50, r = 1.01, \mu_0 = 1$  and  $\mu_{\infty} = 1e - 6$
  - III  $K = 100, r = 1.01, \mu_0 = 1$  and  $\mu_{\infty} = 1e - 6$
  - IV  $K = 1, r = 1.5, \mu_0 = 1$  and  $\mu_{\infty} = 1e - 3$
  - V  $K = 50, r = 1.5, \mu_0 = 1$  and  $\mu_{\infty} = 1e - 3$
  - VI  $K = 100, r = 1.01, \mu_0 = 6e - 2$  and  $\mu_{\infty} = 2e - 2$
- and for the case  $r > 2$ :
- VII  $K = 1, r = 2.5, \mu_0 = 1$  and  $\mu_{\infty} = 1e - 3$
  - VIII  $K = 100, r = 5, \mu_0 = 1$  and  $\mu_{\infty} = 1e - 6$

Examples IV and VII are the ones given in chapter 4.2. For the adaptive refinement of all these example we chose strategy II of chapter 4.2.

We used a damped Gauß-Newton method where the dampening strategy considered the first Wolfe-condition (see [NW00] for example).

The comparison of the GN method with strategy 1 and 2 is given in table 4.7. For almost all examples strategy 2 works better. An exception is example IV where both strategies converge very fast indicating a weaker nonlinearity than the other examples. As strategy 1 converges very fast as well the advantage of the second strategy is not existent. In the case of example VI the small difference of  $\mu_0$  and  $\mu_{\infty}$  results in a weaker nonlinearity despite using constants that seem problematic for other examples.

It has to be noted that almost all examples show a decreasing number of necessary iterations to reach the stopping criterium for strategy 2. If we compare this to strategy 1 the computational cost is significantly smaller as most iterations will be done on the coarse meshes.

The results for example VIII are a special case: As the quadrature errors are not visible for the other examples (but still might have an effect) they are clearly visible in Example VIII. Therefore one has to be careful with overestimating the results of this example. What is shown by this example is the rather weak performance of strategy 2 compared to the other examples in the presence of large quadrature errors.

We now take a closer look at example II and IV. The viscosity / solution for example IV was already given in chapter 4.2. The performance of the Gauss-Newton method is given in figure 4.26. We clearly see that the method converges very fast: For level 7 the reduction of  $\mathcal{F}_C$  is  $\approx 1e - 8$  which is very small compared to the error  $\mathcal{F}_C \approx 5e - 3$ . The stopping criterium of  $\|\mathbf{st}^{(k)}\|_2 < 1e - 5$

level	0	1	2	3	4	5	6	7
GNsteps (strategy 1)	13	13	11	12	10	8	8	9
GNsteps (strategy 2)	13	11	9	8	8	8	8	8

(a) Example I

level	0	1	2	3	4	5	6	7
GNsteps (strategy 1)	52	31	19	15	19	17	18	36
GNsteps (strategy 2)	52	16	21	12	10	8	8	8

(b) Example II

level	0	1	2	3	4	5	6	7
GNsteps (strategy 1)	50	90	37	22	47	23	38	56
GNsteps (strategy 2)	50	41	26	17	22	11	12	9

(c) Example III

level	0	1	2	3	4	5	6	7
GNsteps (strategy 1)	6	5	5	4	4	4	4	4
GNsteps (strategy 2)	6	5	5	4	4	4	4	4

(d) Example IV

level	0	1	2	3	4	5	6	7
GNsteps (strategy 1)	17	19	50	16	8	6	7	7
GNsteps (strategy 2)	17	11	51	12	7	5	4	4

(e) Example V

level	0	1	2	3	4	5	6	7
GNsteps (strategy 1)	7	6	7	4	4	4	4	4
GNsteps (strategy 2)	7	5	5	5	4	5	3	3

(f) Example VI

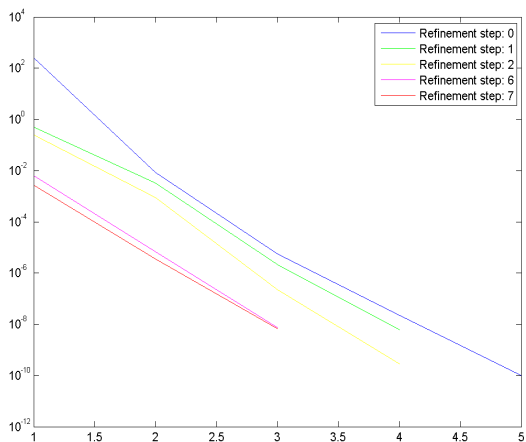
level	0	1	2	3	4	5	6	7
GNsteps (strategy 1)	9	9	8	7	5	5	5	5
GNsteps (strategy 2)	9	8	10	6	5	4	4	4

(g) Example VII

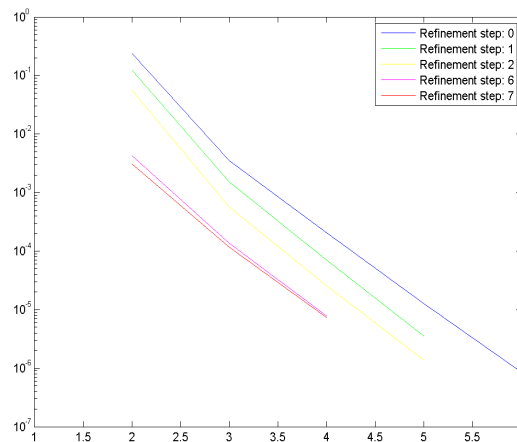
level	0	1	2	3	4	5	6	7
GNsteps (strategy 1)	54	62	25	48	52	54	49	20
GNsteps (strategy 2)	54	34	26	20	54	48	36	13

(h) Example VIII

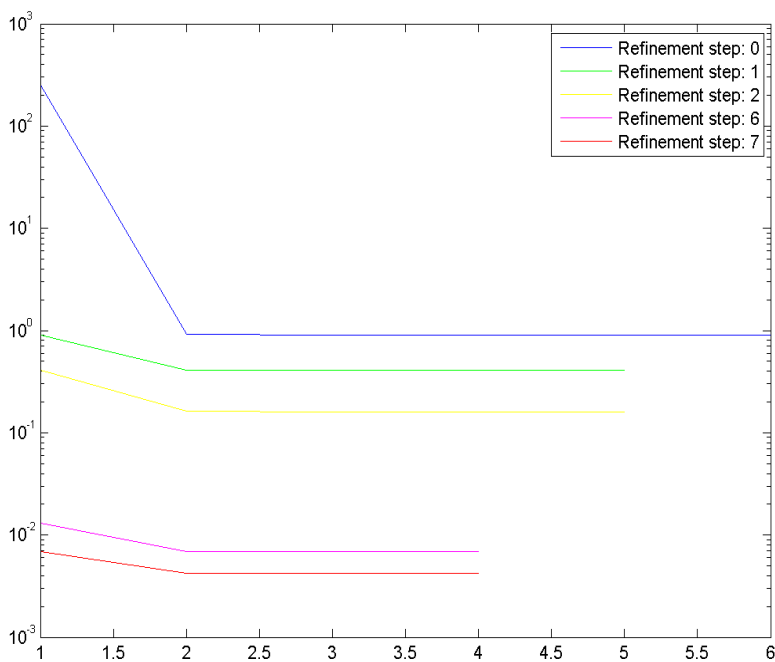
Table 4.7: Number of GN steps to reach stopping criterium



(a) reduction of  $\mathcal{F}_C$



(b) stopping criterium



(c)  $\mathcal{F}_C$

Figure 4.26: GN method: Example IV

seems to be good enough for this example and might even be chosen slightly larger to minimize the number of GN steps.

For example II we give the results of the LSFEM in table 4.8. The viscosities are given in figure 4.27. We clearly see the slightly reduced overall convergence rates. This is due to the very low viscosity / high shear rates close to the singularities. Due to the model the change in viscosity for the FE solutions is significant. Optimal convergence rates might be visible in later steps when the viscosity is close to the minimal value in proximity of the singularities. The actual value of the viscosity very close to the corners (30, 50) and (70, 30) is around  $1e-3$  which is hardly visible in the plot. The shear rates are very high in these corners compared to the other models used in section 4.2 as well. The performance of the Gauss-Newton method is depicted in figure 4.28. We clearly see the very fast convergence rates for step 6/7 in all three plots. Again the stopping criterion is good enough as the reduction of  $\mathcal{F}_C$  is small when the criterion is satisfied.

level	$\#T_D$	$\#T_S$	$\mathcal{F}_D$	$\mathcal{F}_S$	$\mathcal{F}_I$	$\theta_{lsf}$
0	118	97	1.0068e-002	2.9932e-002	6.5465e-003	
1	180	199	5.1858e-003	1.4590e-002	3.3327e-003	1.2352
2	296	374	1.8141e-003	7.8810e-003	1.4373e-003	1.2819
3	410	702	5.6024e-004	3.4332e-003	4.9495e-004	1.793
4	586	1191	2.3346e-004	1.6128e-003	1.5884e-004	1.7189
5	759	1892	1.0185e-004	7.4290e-004	4.5308e-005	2.0304
6	909	2752	6.8411e-005	4.1370e-004	1.5414e-005	1.8019
7	1078	3530	4.6640e-005	2.8570e-004	7.5572e-006	1.6561
0 – 7						1.6051

(a) refinement strategy II: 20-5 % marked

level	$\#T_D$	$\#T_S$	$\mathcal{F}_D$	$\mathcal{F}_S$	$\mathcal{F}_I$	$\theta_{lsf}$
0	118	97	1.0068e-002	2.9932e-002	6.5465e-003	
1	472	388	4.7023e-003	1.1900e-002	3.2180e-003	0.6158
2	1888	1552	1.3168e-003	5.7653e-003	1.3033e-003	0.6205
3	7552	6208	2.7727e-004	2.3073e-003	4.3301e-004	0.7372
4	30208	24832	4.1693e-005	7.8017e-004	1.2476e-004	0.8363
0 – 4						0.7025

(b) uniform refinement

Table 4.8: Example IV: LSF and convergence rates

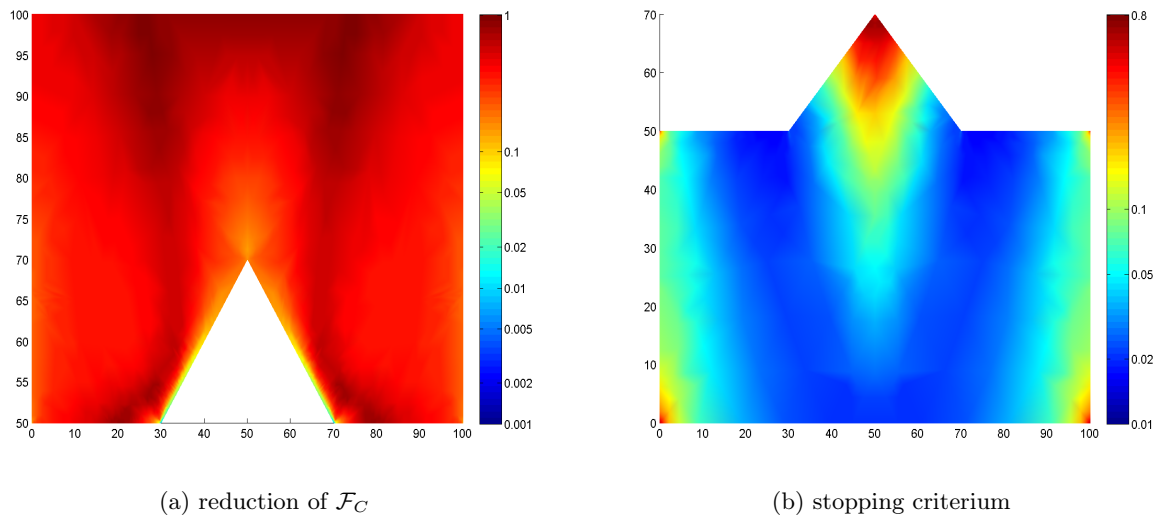
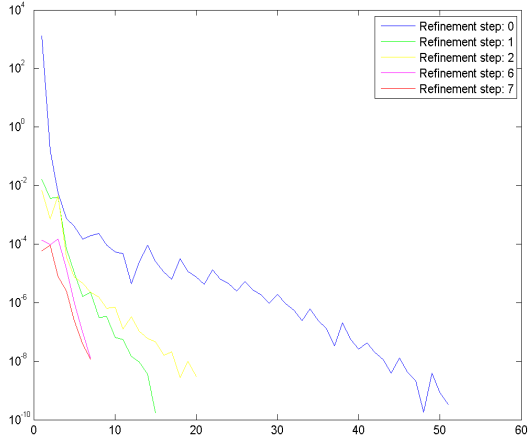
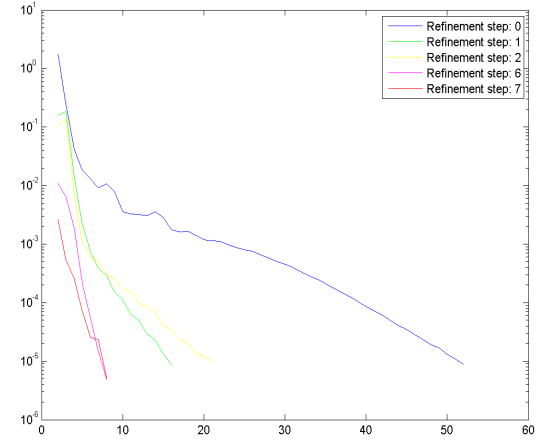


Figure 4.27: GN method: Viscosities for example II

(a) reduction of  $\mathcal{F}_C$ 

(b) stopping criterium

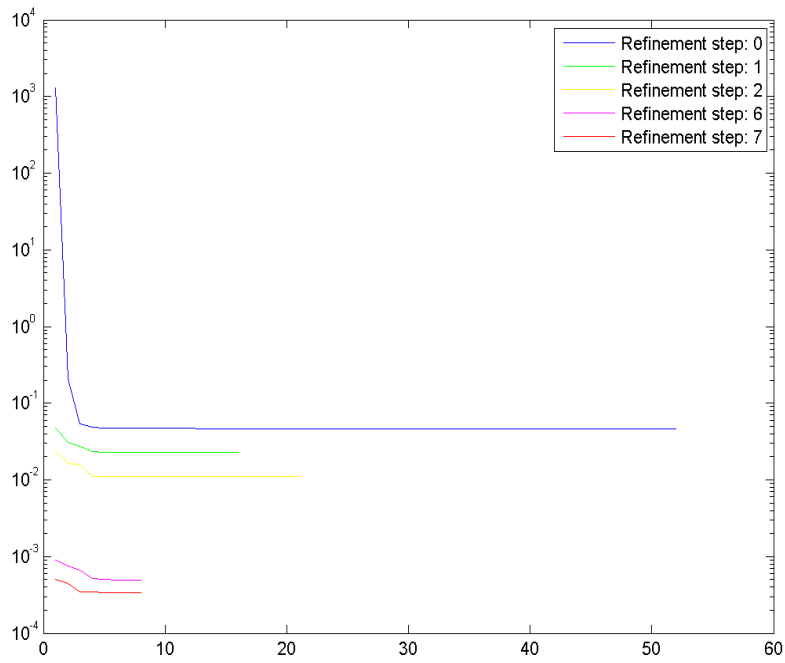
(c)  $\mathcal{F}_C$ 

Figure 4.28: GN method: Example II



# Chapter 5

## Outlook/Conclusion

### 5.1 Outlook

In this section we briefly discuss several open questions that arose in the course of this work. Furthermore we discuss additional steps that might be of interest for later research based on the results presented in this work.

#### 5.1.1 Free Boundary Problems

A field of interest is the numerical approximation of free boundary problems arising in two phase flows satisfying the Navier-Stokes equations. Typically Mixed FEM are used for these kinds of problems (see for example [GRR06]). The numerical solution of two phase flows involves level set functions. The least-squares finite element method can be used for free boundary problems as well (see [ABL<sup>+</sup>11]).

A motivation for the present work was the application of the least-squares finite element method to coupled problems arising in water-mud interaction. The equations for these problems are governed by Newtonian Stokes / generalized Newtonian Darcy flow as in [EM12].

The techniques applied to the nonlinearity in this thesis are not dependent on the coupling. Assuming the nonlinear problem to be a perturbation allows to reduce the problem to a linear problem in the analysis. The result was the independence of the viscosity models for both domains as long as the individual models met the independent assumptions for the viscosities. This should apply to free boundary problems as well and reduce the necessary analysis to linear problems.

The question how possibly nonlinear interface conditions have to be treated in a least-squares finite element method is still open for the model suggested in [EM12].

#### 5.1.2 Viscosity Models

Another open question was already mentioned in chapter 3. The viscosity models we used for our analysis are restricted by rather harsh assumptions. Models as the *Power law* in general and the *Carreau model* for shear thickening fluids do not meet these assumptions and the property of the least-squares functional being an error estimator is not established. Mixed finite element methods as in [BS08a, Kre12] for the Stokes problem and [EJS09] for the coupled problem can handle these models due to the choice of solution spaces. The use of these models for a (least-squares) mixed finite element methods requires quasi norms or similar constructions that have not been established in this thesis.

### 5.1.3 Conservation of Mass

The conservation of mass is essential in many applications. In the case of mixed finite element methods one gets local mass conservation for the Darcy equations and as a result improved convergence for local mass conservation in the case of least-squares finite element methods as stated before. This still has to be proven for the non-Newtonian case.

For the coupled problem the conservation of mass of the system is determined by the three parts of the functional  $\mathcal{F}_C$ :  $\|\operatorname{div} \mathbf{u}_S\|_{0,\Omega_S}^2$ ,  $\|\operatorname{div} \mathbf{u}_D\|_{0,\Omega_D}^2$  and  $\|\mathbf{u}_S \cdot \mathbf{n} - \mathbf{u}_D \cdot \mathbf{n}\|_{0,\Gamma_I}^2$ .

Especially example II of the coupled problem showed  $\|\operatorname{div} \mathbf{u}_S\|_{0,\Omega_S}^2$  to be the limiting factor for faster convergence. An approach to overcome this problem might be the use of Hybrid-FOSLS for the Stokes equations as introduced in [LMM<sup>+</sup>12]. The Hybrid-FOSLS method showed better mass conservation than standard FOSLS. Another approach for the velocity-vorticity-pressure system by using discontinuous velocities / stream-functions can be found in [BLO12]. Further research of this topic is necessary to see if these methods are applicable for the coupled problem.

### 5.1.4 Convergence of Gauss-Newton Methods

For our numerical examples the convergence of a damped Gauss-Newton method was achieved under the first Wolfe condition. We did not deliver theoretical results on the convergence of the method despite necessary parts as the full rank condition in the sense of variational equalities. Another goal would be to prove convergence in the respective Banach-spaces as it is done for Newton methods (see for example [Wan00]).

## 5.2 Conclusion

We have presented a least-squares approach for generalized Newtonian Stokes/Darcy flows as well as for the coupled problem along an interface. We have shown that the least-squares functional is an efficient and reliable error estimator for the separate problems and as a consequence for the coupled problem.

The reliability gives optimal asymptotic a-priori error bounds under standard regularity assumptions. Depending on the nonlinearities the asymptotic behavior might be reached very late which was seen in the examples of this work. This is due to the established efficiency/reliability constants being dependent on the nonlinearity.

The efficiency of the error estimator allowed for adaptive refinement which achieved better convergence rates than uniform refinement in the presence of singularities. For some examples the adaptive refinement was necessary to get a reasonable solution with computational costs that can be handled by current computers. To achieve the same estimate for the error with uniform refinement one would need very fast iterative solvers to handle memory problems /computational costs.

The Gauß-Newton method used in this thesis worked exceptionally well and performed even better on finer meshes. This might be due to quadrature errors as these are more present on coarse meshes. For reasonable viscosities the method converges very fast even if a not optimal starting point has been chosen. For more demanding problems a proper starting point is required. The interpolated solution on the coarse mesh has proven to be a good choice to keep cost intensive calculations on finer meshes small. Furthermore we established the well-posedness of the linearized problems resulting in a well defined sequence of approximates.

# Bibliography

- [ABL<sup>+</sup>11] J. H. Adler, J. Brannick, C. Liu, T. Manteuffel, and L. Zikatanov. First-order system least squares and the energetic variational approach for two-phase flow. *J. Comput. Phys.*, 230(17):6647–6663, July 2011.
- [ADG84] Douglas N. Arnold, Jim Douglas, Jr., and Chaitan P. Gupta. A family of higher order mixed finite element methods for plane elasticity. *Numer. Math.*, 45(1):1–22, 1984.
- [BCY06] Jan Brandts, Yanping Chen, and Julie Yang. A note on least-squares mixed finite elements in relation to standard and mixed finite elements. *IMA Journal of Numerical Analysis*, 26(4):779–789, October 2006.
- [BF91] Franco Brezzi and Michel Fortin. *Mixed and Hybrid Finite Element Methods*. Springer-Verlag New York, 1991.
- [BG09] Pavel B. Bochev and Max D. Gunzburger. *Least-Squares Finite Element Methods*. Springer, Berlin, 2009.
- [BJ67] G.S. Beavers and D.D. Joseph. Boundary conditions at a naturally permeable wall. *J. Fluid Mech.*, 30:197–207, 1967.
- [BL93] John W. Barrett and W. B. Liu. Finite element error analysis of a quasi-newtonian flow obeying the carreau or power law. *Numerische Mathematik*, 64:433–453, 1993. 10.1007/BF01388698.
- [BLO12] Pavel Bochev, James Lai, and Luke Olson. A locally conservative, discontinuous least-squares finite element method for the stokes equations. *International Journal for Numerical Methods in Fluids*, 68(6):782–804, 2012.
- [BMMS05] Markus Berndt, Thomas A. Manteuffel, Stephen F. McCormick, and Gerhard Starke. Analysis of first-order system least squares (fosl) for elliptic problems with discontinuous coefficients: Part i. *SIAM J. Numer. Anal.*, 43(1):386–408, January 2005.
- [BP07] Dieter Bothe and Jan Prüss.  $l_p$ -theory for a class of non-newtonian fluids. *SIAM Journal on Mathematical Analysis*, 39(2):379–421, 2007.
- [Bra92] Dietrich Braess. *Finite Elemente - Theorie, schnelle Löser und Anwendungen in der Elastizitätstheorie*. Springer, 1992.
- [BS94] Brent C. Bell and Karan S. Surana. p-version least squares finite element formulation for two-dimensional, incompressible, non-newtonian isothermal and non-isothermal fluid flow. *International Journal for Numerical Methods in Fluids*, 18(2):127–162, 1994.

- [BS08a] Stefano Berrone and Endre Süli. Two-sided a posteriori error bounds for incompressible quasi-newtonian flows. *IMA Journal of Numerical Analysis*, 28(2):382–421, 2008.
- [BS08b] S.C. Brenner and L.R. Scott. *The Mathematical Theory of Finite Element Methods*. Texts in Applied Mathematics. Springer, 2008.
- [Car72] Pierre J. Carreau. Rheological equations from molecular network theories. *Transactions of the Society of Rheology*, 16(1):99–127, 1972.
- [CB05] Hyo Won Choi and Abdul I Barakat. Numerical study of the impact of non-newtonian blood behavior on flow over a two-dimensional backward facing step. *Biorheology*, 42(6):493–509, 2005.
- [CBBH08] V. Calo, N. Brasher, Y. Bazilevs, and T. Hughes. Multiphysics model for blood flow and drug transport with application to patient-specific coronary artery flow. *Computational Mechanics*, 43:161–177, 2008. 10.1007/s00466-008-0321-z.
- [CCLT10] T. F. Chen, C. L. Cox, H. C. Lee, and K. L. Tung. Least-squares finite element methods for generalized newtonian and viscoelastic flows. *Appl. Numer. Math.*, 60:1024–1040, October 2010.
- [CGH<sup>+</sup>10] Yanzhao Cao, Max Gunzburger, Xiaolong Hu, Fei Hua, Xiaoming Wang, and Weidong Zhao. Finite element approximations for stokes-darcy flow with beavers-joseph interface conditions. *SIAM J. Numer. Anal.*, 47(6):4239–4256, January 2010.
- [Clé75] Ph Clément. Approximation by finite element functions using local regularization. *Rev. Française Automat. Informat. Recherche Opérationnelle Sér. Analyse Numérique*, 9:77–84, 1975.
- [Cro65] Malcolm M. Cross. Rheology of non-newtonian fluids: A new flow equation for pseudoplastic systems. *Journal of Colloid Science*, 20(5):417 – 437, 1965.
- [CS03] Zhiqiang Cai and Gerhard Starke. First-order system least squares for the stress-displacement formulation: Linear elasticity. *SIAM J. Numer. Anal.*, 41:715–730, 2003.
- [CTVW10] Zhiqiang Cai, Charles Tong, Panayot S. Vassilevski, and Chunbo Wang. Mixed finite element methods for incompressible flow: Stationary stokes equations. *Numerical Methods for Partial Differential Equations*, 26(4):957–978, 2010.
- [CW09] Z. Cai and C.R. Westphal. An adaptive mixed least-squares finite element method for viscoelastic fluids of oldroyd type. *J. Non-Newton. Fluid Mech.*, 159:72–80, 2009.
- [CWZ10] Zhiqiang Cai, Chunbo Wang, and Shun Zhang. Mixed finite element methods for incompressible flow: Stationary navier-stokes equations. *SIAM J. Numer. Anal.*, 48:79–94, April 2010.
- [Doe95] W. Doerfler. A robust adaptive strategy for the nonlinear poisson equation. *Computing*, 55(4):289–304, 1995.
- [DQ09] M. Discacciati and A. Quarteroni. Navier-Stokes/Darcy coupling: modeling, analysis and numerical approximation. *Revista Matematica Complutense*, 22(2):315–426, 2009.

- [DQM02] Marco Discacciati, Alfio Quarteroni, and Edie Miglio. Mathematical and numerical models for coupling surface and groundwater flows. *Elsevier Applied Numerical Mathematics*, 43:57–74, 2002.
- [EG04] A. Ern and J.-L. Guermond. *Theory and Practice of Finite Elements*. Springer, 2004.
- [EJS09] V. J. Ervin, E. W. Jenkins, and S. Sun. Coupled generalized nonlinear stokes flow with flow through a porous medium. *SIAM J. Numer. Anal.*, 47:929–952, February 2009.
- [EM09] Joachim Escher and Bogdan-Vasile Matioc. Multidimensional hele-shaw flows modelling stokesian fluids. *Mathematical Methods in the Applied Sciences*, 32(5):577–593, 2009.
- [EM12] Joachim Escher and Anca-Voichita Matioc. On the well-posedness of a mathematical model describing water-mud interaction. Submitted, 2012.
- [GMS11] Gabriel N. Gatica, Antonio Marquez, and Manuel A. Sanchez. A priori and a posteriori error analyses of a velocity-pseudostress formulation for a class of quasi-newtonian stokes flows. *Computer Methods in Applied Mechanics and Engineering*, 200(17-20):1619 – 1636, 2011.
- [GR86] V. Girault and P.A. Raviart. *Finite element methods for Navier-Stokes equations: theory and algorithms*. Springer series in computational mathematics. Springer-Verlag, 1986.
- [GRR06] S. Gross, V. Reichelt, and A. Reusken. A finite element based level set method for Two-Phase incompressible flows. *Comput. Vis. Sci*, 9(4):239–257, 2006.
- [HWNW06] N. Hanspal, A. Waghode, V. Nassehi, and R. Wakeman. Numerical analysis of coupled stokes/darcy flows in industrial filtrations. *Transport in Porous Media*, 64:73–101, 2006. 10.1007/s11242-005-1457-3.
- [JM00] Willi Jäger and Andro Mikelić. On the interface boundary condition of beavers, joseph, and saffman. *SIAM J. Appl. Math.*, 60:1111–1127, March 2000.
- [KA00] P. Knabner and L. Angermann. *Numerik partieller Differentialgleichungen*. Springer-Verlag Berlin Heidelberg, 2000.
- [KO87] N. Kikuchi and J.T. Oden. *Contact Problems in Elasticity: A Study of Variational Inequalities and Finite Element Methods*. SIAM studies in applied mathematics. Society for Industrial and Applied Mathematics, 1987.
- [Kre12] Christian Kreuzer. Analysis of an adaptive uzawa finite element method for the non-linear stokes problem. *Math. Comput.*, 81(277), 2012.
- [KS] Johannes Korsawe and Gerhard Starke. Ls-mfe toolbox.
- [LMM<sup>+</sup>12] K. Liu, T. A. Manteuffel, S. F. McCormick, J. W. Ruge, and L. Tang. Hybrid first-order system least squares (hybrid-fosl) finite element methods with application to stokes equations. submitted, 2012.
- [LSY02] William J. Layton, Friedhelm Schieweck, and Ivan Yotov. Coupling fluid flow with porous media flow. *SIAM J. NUMER. ANAL.*, 40:2195 – 2218, 2002.

- [Mat08] Tarek Mathew. *Domain Decomposition Methods for the Numerical Solution of Partial Differential Equations (Lecture Notes in Computational Science and Engineering)*. Springer Publishing Company, Incorporated, 2008.
- [MK10] Arif Masud and JaeHyuk Kwack. A stabilized mixed finite element method for the incompressible shear-rate dependent non-Newtonian fluids: Variational multiscale framework and consistent linearization. *Computer Methods in Applied Mechanics and Engineering*, September 2010.
- [MS11] Steffen Müntenmaier and Gerhard Starke. First-order system least squares for coupled stokes-darcy flow. *SIAM J. Numerical Analysis*, 49(1):387–404, 2011.
- [Mün08] Steffen Müntenmaier. Diplomarbeit: Finite-element-methoden für gekoppelte strömungsprozesse im untergrund und an der oberfläche. 2008.
- [Nec12] Jindrich Necas. *Direct Methods in the Theory of Elliptic Equations (Springer Monographs in Mathematics)*. Springer, 1st ed. 2012. corr. 3rd printing 2012 edition, March 2012.
- [NW00] Jorge Nocedal and Stephen J. Wright. *Numerical Optimization*. Springer, August 2000.
- [OP02] R.G. Owens and T.N. Phillips. *Computational Rheology*. Imperial College Press, 2002.
- [OR70] J.M. Ortega and W.C. Rheinboldt. *Iterative Solution of Nonlinear Equations in Several Variables*. Classics in Applied Mathematics. Society for Industrial and Applied Mathematics, 1970.
- [PS04] Per-olof Persson and Gilbert Strang. A simple mesh generator in matlab. *SIAM Review*, 46:2004, 2004.
- [Riv05] Béatrice Rivière. Analysis of a discontinuous finite element method for the coupled stokes and darcy problems. *J. Sci. Comput.*, 22-23:479–500, June 2005.
- [RY05] Béatrice Rivière and Ivan Yotov. Locally conservative coupling of stokes and darcy flows. *SIAM J. NUMER. ANAL.*, 42(5):50–292, 2005.
- [Saf71] P. Saffman. On the boundary condition at the surface of a porous media. *Stud. Appl. Math.*, 50:292–315, 1971.
- [Sta00] Gerhard Starke. Gauss–newton multilevel methods for least-squares finite element computations of variably saturated subsurface flow. *Computing*, 64:323–338, 2000. 10.1007/s006070070028.
- [Sta05] Gerhard Starke. A first order system least squares finite element method for the shallow water equations. *SIAM J. NUMER. ANAL.*, 42:2387–2407, 2005.
- [Sta07] Gerhard Starke. An adaptive least-squares mixed finite element method for elasto-plasticity. *SIAM J. Numer. Anal.*, 45:371–388, January 2007.
- [SWH<sup>+</sup>06] Nanfeng Sun, Nigel Wood, Alun Hughes, Simon Thom, and X. Xu. Fluid-wall modelling of mass transfer in an axisymmetric stenosis: Effects of shear-dependent transport properties. *Annals of Biomedical Engineering*, 34:1119–1128, 2006. 10.1007/s10439-006-9144-2.

- [Wan00] X Wang. Convergence of newton's method and uniqueness of the solution of equations in banach space. *IMA Journal of Numerical Analysis*, 20(1):123–134, 2000.





# Steffen Münzenmaier

---

## Diplomarbeit

Titel *Finite-Element-Methoden für gekoppelte Strömungsprozesse im Untergrund und an der Oberfläche*  
Betreuer Gerhard Starke  
Note 1,0

## Verlauf des Studiums

03/2008 **Abschluss: Diplom-Mathematiker**, Note: mit Auszeichnung.  
2001–2008 **Studium**, *Mathematik: Studienrichtung rechnergestützte Wissenschaften*, Leibniz Universität Hannover.  
7/2005–7/2006 **Auslandsstudium**, *Studium der angewandten Mathematik im Rahmen des „Study Abroad“ Programms der University of New South Wales, Sydney, 2 Urlaubssemester.*  
7/2005–7/2006 **Auslandsstipendium**, *Studienstiftung des deutschen Volkes.*  
03/2004 **Aufnahme in Studienstiftung des deutschen Volkes.**

## Berufstätigkeit

ab 04/2008 **Wissenschaftlicher Mitarbeiter**, *Institut für Angewandte Mathematik*, Leibniz Universität Hannover.  
2006–2008 **Wissenschaftliche Hilfskraft**, *Leibniz Universität Hannover.*  
2003–2005 **Wissenschaftliche Hilfskraft**, *Leibniz Universität Hannover.*  
2000–2001 **Ableistung des Zivildienstes**, *Sozialstation Lehrte (DRK Burgdorf).*

## Ausbildung und Schule

1993–2000 **Gymnasium Burgdorf**, *31303 Burgdorf, Abitur(2,2).*  
1991–1993 **Orientierungsstufe Garbsen**, *30823 Garbsen.*  
1987–1991 **Grundschule Osterberg**, *30823 Garbsen.*

## Veröffentlichungen

2011 **Steffen Münzenmaier, Gerhard Starke**, *First-Order System Least Squares for Coupled Stokes - Darcy Flow*, SIAM J. on Numerical Analysis Vol. 49 Issue 1, 2011.